Magnesium Hydride Reductions

Weetman, Catherine

Award date:
2015

Awarding institution:
University of Bath

UNIVERSITY OF BATH

Magnesium Hydride Reductions

Catherine Ellen Weetman

A thesis submitted for the degree of Doctor of Philosophy

University of Bath

Department of Chemistry

May 2015

Publications resulting from this thesis

'Magnesium hydrides and the dearomatisation of pyridine and quinoline derivatives' *Dalton trans*, 2011, 40 (46), 12500-12509.

'Magnesium-catalyzed hydroboration of pyridines' *Organometallics*, 2011, 30 (21), 5556-5559.

'Selective reduction of CO_2 to a methanol equivalent by $B(C_6F_5)_3$-activated alkaline earth catalysis' *Chemical Science*, 2014, 5, 2826.

'Kinetically Directed Reactivity of Magnesium Dihydropyridides with Organo-isocyanates' *Organometallics*, 2015, DOI: 10.1021/om5012374

Contents

Copyright

Declaration

The work described in this thesis was conducted by the author at the University of Bath between October 2011 and December 2014. It represents the author's original and independent work, except where specific reference is made to the contrary. Neither the whole nor any part of this thesis has been submitted previously in support of a degree at any other university.

Acknowledgements

Firstly I would like to thank my supervisor, Mike Hill, for the opportunity to carry out this PhD. Also for his constant enthusiasm for chemistry and continued support over the last few years, although I don't think I will ever trust the phrase 'a quick Hammett study' again.

I would also like to thank all the members of the Hill group over the last few years, in particular Merle Arrowsmith for helping me with various maths problems and to the rest of the Hill group in no particular order David, Pete, Mat, Amanda, Ben, Tom, Andy, Niall, and Dawkins, for entertaining chemistry discussions whether in the office or the pub.

Also this thesis would not have been possible if it wasn't for the various analytical support provided, special thanks to John Lowe for letting me have far more than my fair share of NMR time and to Mary Mahon for teaching me X-ray crystallography. Further thanks go to Gabriele Kociok-Köhn for X-ray crystallography and Anneke Lubben for mass spectrometry.

Finally I would like to thank my family for their continued support and attempts to understand what I have been doing over the last few years and to Ross for your encouragement throughout.

Abstract

Initial developments within group 2 chemistry led to the chemistry being described as 'lanthanide mimetic' however, over the last 10 years group 2 catalysis has emerged in its own right, making these comparisons unjustified. Development of this catalytic chemistry has, until now, largely focussed upon the use of protic reagents in order to achieve turnover. Reported in this thesis is the development of magnesium hydride chemistry for both stoichiometric and catalytic purposes.

Reported in chapter 2 of this thesis, is the use of the pharmaceutically relevant magnesium-dihydropyridide complexes and explores their use as hydride transfer reagents with respect to a representative ketone, benzophenone, whilst further study with various different isocyanate reagents with differing electronic and steric demands provides divergent reactivity. Extension of this chemistry with respect to carbodiimides provides a series of *N*-heterocyclic guanidinates in all but one case.

The chemistry described in chapters 3-6 investigates the use of magnesium hydrides in catalysis. Using the commercially available hydridic pinacol borane (HBpin) reagent a series of catalytic reactions with respect to pyridines (chapter 3), nitriles (chapter 4), *iso*-nitriles (chapter 5) and heterocumulenes (chapter 6) are investigated. In each case, studies have sought to underpin the catalytic reactivity by examining the single steps of the proposed catalytic cycle *via* a series of stoichiometric reactions which has allowed for the isolation and characterisation of numerous potential catalytic intermediates. Monitoring of these catalytic reactions *in situ* with NMR spectroscopy, combined with kinetic analysis, has allowed for further information to be obtained with regards to the mechanism and calculation of the activation energy parameters associated with each reaction.

Abbreviations

9-BBN	9-Borabicyclo(3.3.1)nonane
Ad	1-Adamantyl
Ae	Alkaline Earth
Ar	Aryl Group
BCF	tris(pentafluorophenyl)borane
br.	Broad NMR resonance
COSY	Correlation Spectroscopy
Cy	Cyclohexyl
DFT	Density Functional Theory
Dipp	2,6-di-*iso*-propylphenyl
DMAP	4-Dimethylaminopyridine
E	Heteroatom (E ≠ C, H)
E_a	Activation Energy
EDG	Electron Donating Group
eq.	Equivalents
EWG	Electron Withdrawing Group
FLP	Frustrated Lewis Pair
HBcat	Catechol Borane
HBpin	Pinacol Borane
Hrs	Hours
HSQC	Heteronuclear Single Quantum Correlation
***i*Quin**	*iso*-Quinoline
***iso*-Pr**	*iso*-Propyl
Ln	Lanthanide
M	Metal
Mes	2,4,6-trimethylphenyl
***n*-Bu**	*n*-Butyl
NCN	Carbodiimide
NCO	Isocyanate
NHC	*N*-heterocyclic carbene
NMR	Nuclear Magnetic Resonance
ORTEP	Oak Ridge Thermal Ellipsoid Plot
Ph	Phenyl
$PhSiH_3$	Phenyl Silane
Pyr	Pyridine
Quin	Quinoline
R	Alkyl or Aryl Group
RDS	Rate Determining Step
***t*-Bu**	*tert*-Butyl
THF	tetrahydrofuran
X	monoanionic-substituent
$\Delta G^{\neq}$	Gibbs Free Energy of Activation
$\Delta H^{\neq}$	Enthalpy of Activation
$\Delta S^{\neq}$	Entropy of Activation

List of literature compounds

Unless stated L = β-diketiminate

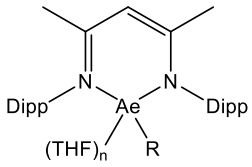

Ia Ib Ic Id Ie If Ig Ij
Ae = Mg, Mg Mg Mg Ca, Ca, Sr, Ca
R = Me, Bu, Bu, $N(SiMe_3)_2$, NPh_2
n = 0, 0, 1, 0, 0, 1, 1, 1

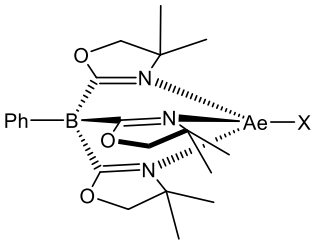

IIa IIb
Ae = Mg, Ca
R = Me, $N(SiMe_3)_2$

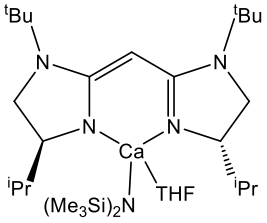

III

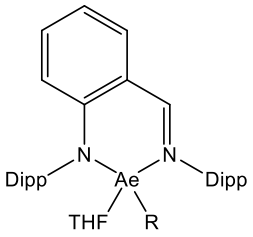

IVa IVb IVc
Ae = Ca, Sr, Ba
R = $N(SiMe_3)_2$
n = 1, 2, 2

$[Ae(N\{SiMe_3\}_2)_2]_2$

Va Vb Vc Vd
Ae = Mg, Ca, Sr, Ba

$[Ae(N\{SiMe_3\}_2)_2(THF)_2]$

VIa VIb VIc VId
Ae = Mg, Ca, Sr, Ba

$[Ae(CH\{SiMe_3\}_2)_2(THF)_2]$

VIIa VIIb VIIc VIId
Ae = Mg, Ca, Sr, Ba

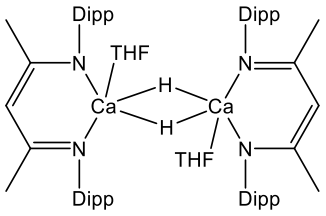

VIII

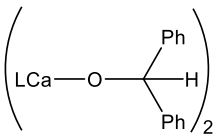

IX

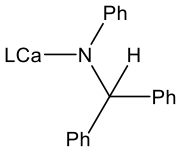

X

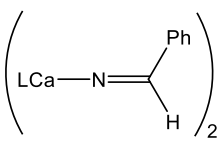

XI

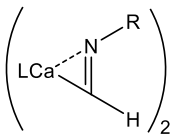

XII

R = ^{t}Bu, **XIIa**
R = Cy, **XIIb**

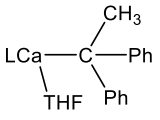

XIII

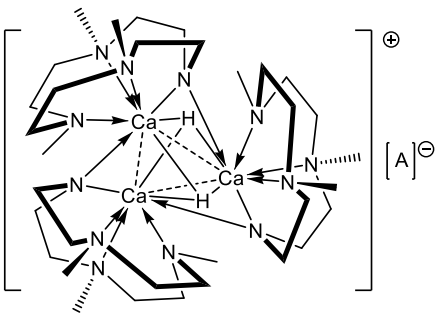

XIV

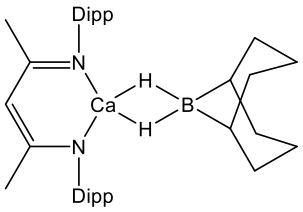

XV

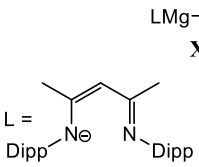

XVIa

XVI

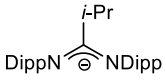

XVIb

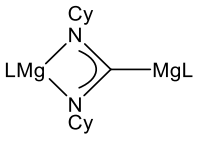

XVII

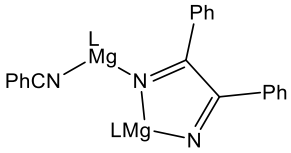

XVIII

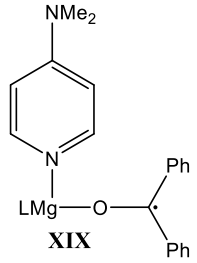

XIX

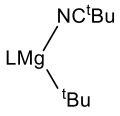

XXa

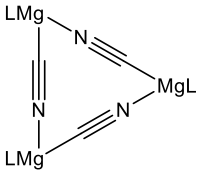

XXb

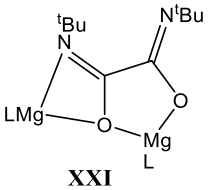

XXI

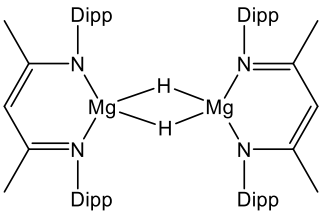

XXII

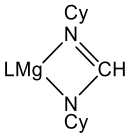

XXIII

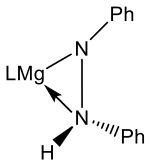

XXIV

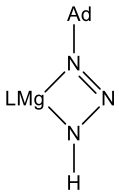

XXV

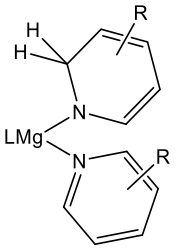

XXVI

R = H, **XXVIa**
R = 4-CH_3, **XXVIb**

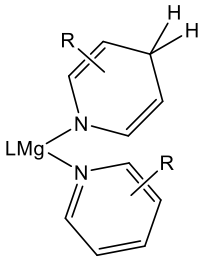

XXVII

R = H, **XXVIIa**
R = 2-CH_3, **XXVIIb**
R = 3-CH_3, **XXVIIc**
R = 3,5-CH_3, **XXVIId**
R = 4-$N(CH_3)_2$, **XXVIIe**

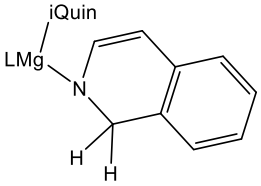

XXVIII

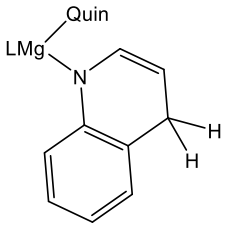

XXIX

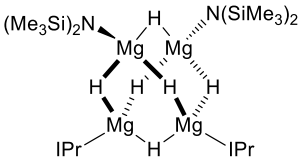

XXX

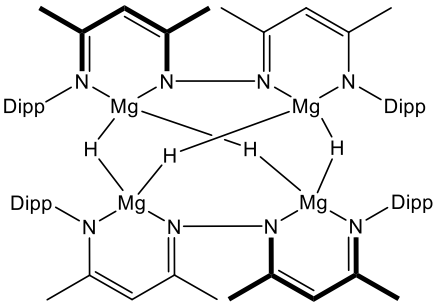

XXXI

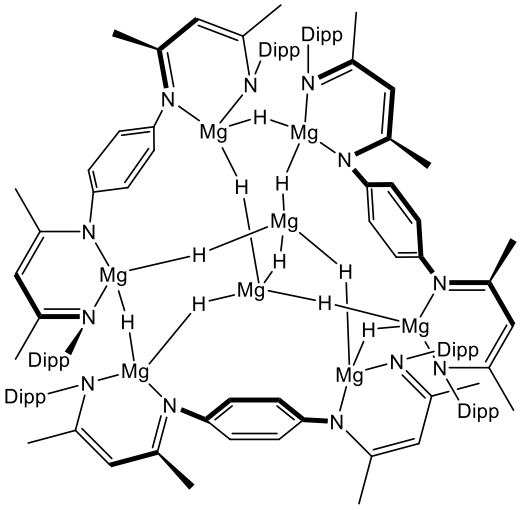

XXXII

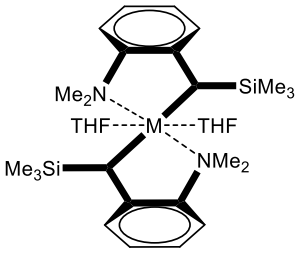

XXXIII

M = Ca, **XXXIIIa**
M = Sr, **XXXIIIb**

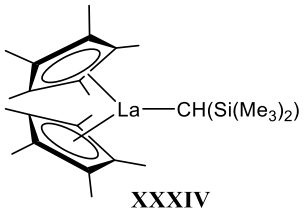

XXXIV

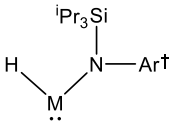

XXXV

M = Ge, **XXXVa**
M = Sn, **XXXVb**

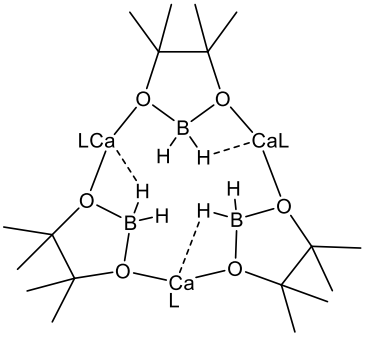

XXXVI

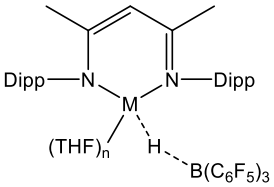

XXXVII

M = Mg, n = 0 **XXXVIIa**
M = Ca, n =1 **XXXVIIb**

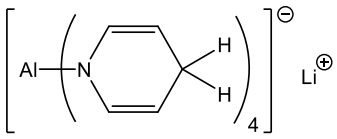

XXXVIII

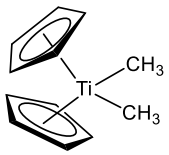

XXXIX

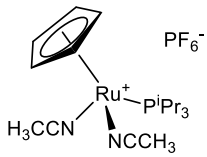

XL

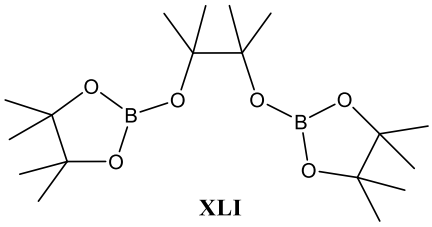

XLI

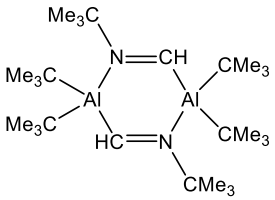

XLII

List of compounds reported in this thesis

Chapter 2.2 – *Reactivity of dihydropyridides with Isocyanates*

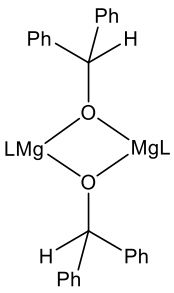

1

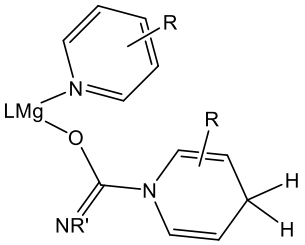

R = H; R' = Dipp (**2**), Mes (**3**), Ad (**4**)
R = 3-Me; R' = Dipp (**6**), Mes (**7**), Ad (**8**), *t*-Bu (**9**)
R = 3,5-Me; R' = Dipp (**10**), Mes (**11**), Ad (**12b**), *t*-Bu (**13**)
R = C_4H_4; R' = *iso*-Pr (**16**), Et (**17**)

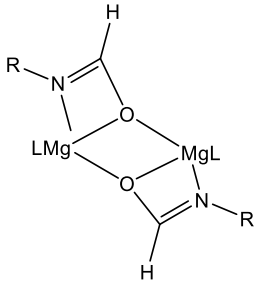

R = *t*-Bu (**5**)**,** Ad (**12a**)

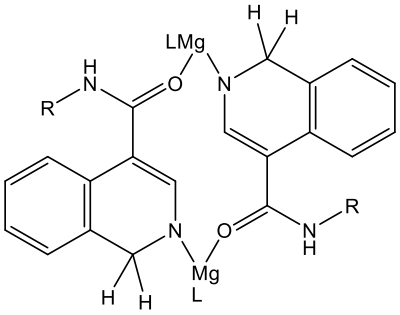

R = Ad (**14**), *tert*-Bu (**15**)

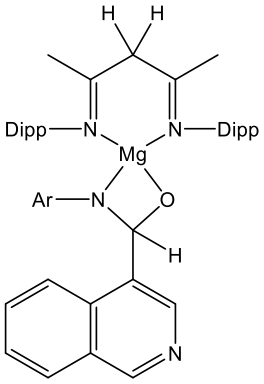

Ar = Dipp (**18**), Mes (**19**)

Chapter 2.3 – *Reactivity of dihydropyridides with carbodiimides*

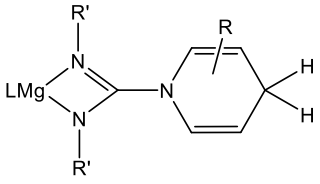

R = H; R' = iPr (**20**), Cy (**21**), *p*-Tol (**22**)
R = 3-Me; R' = iPr (**23**), Cy (**24**), *p*-Tol (**25**)
R = 3,5-Me; R' = iPr (**26**), Cy (**27**), *p*-Tol (**28**)
R = C_4H_4; R' = iPr (**29**), Cy (**30**), *p*-Tol (**31**)

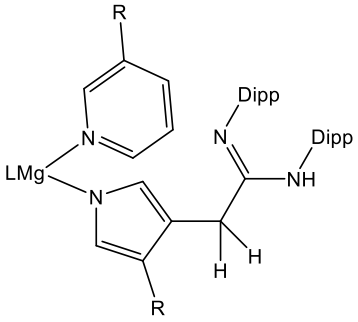

R = Me (**32**), MeO (**33**), Et (**34**)

Chapter 3 – *Hydroboration of Pyridines*

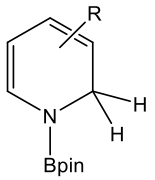

R = H (**35**), 3-Me (**38**), 3,5-Me (**40**), 4-Me (**42**), 4-Ph (**44**), C_4H_4 (**46**)

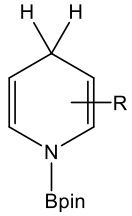

R = H (**36**), 2-Me (**37**), 3-Me (**39**), 3,5-Me (**41**), 4-Me (**43**), C_4H_4 (**45**)

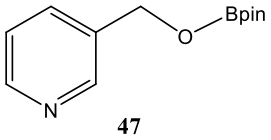

47

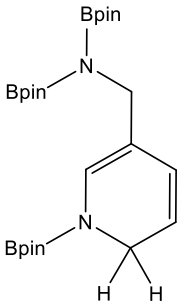

48

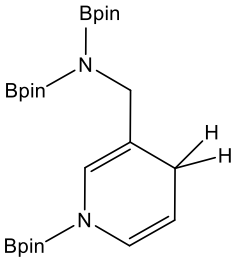

49

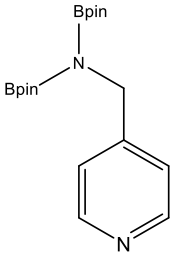

50

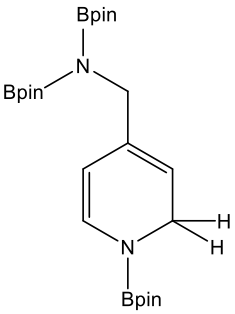

51

Chapter 4 – *Hydroboration of Nitriles*

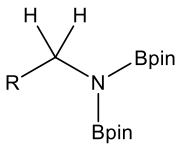

R = Pr (**53**), *iso*-Pr (**54**), *t*-Bu (**55**), Cy (**56**), Ph (**57**), *o*-(Me)Ph (**58**), *m*-(Me)Ph (**59**), *m*-(F)Ph (**60**), *m*-(MeO)Ph (**61**), *p*-(Me)Ph (**62**), *p*-(F)Ph (**63**), *p*-(Cl)Ph (**64**), *p*-(CF_3)Ph (**65**), *p*-(MeO)Ph (**66**), $(Ph)_2CH$ (**67**)

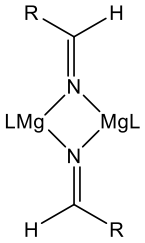

R = *t*-Bu (**68**), 3-(MeO)Ph (**69**), 4-(MeO)Ph (**70**)

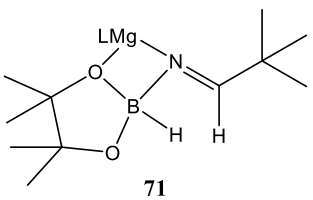

71

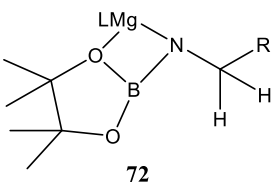

72

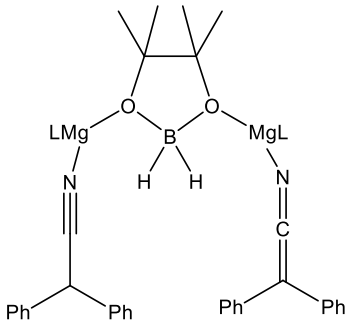

73

Chapter 5 – *Hydroboration of isonitriles*

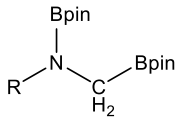

R = Cy (**74**), 1-C_5H_{11} (**75**), *t*-Bu (**76**), Bn (**77**), 2-$C_{10}H_7$ (**78**), 2,6-(Me)Ph (**79**)

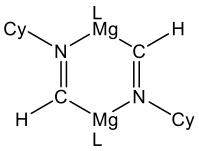

80

Chapter 6.2 – *Hydroboration of Carbodiimides*

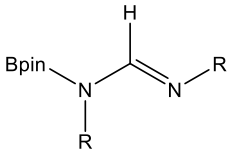

R = *i*-Pr (**81**), Cy (**82**), *t*-Bu (**83**), Dipp (**84**), *p*-Tolyl (**85**)

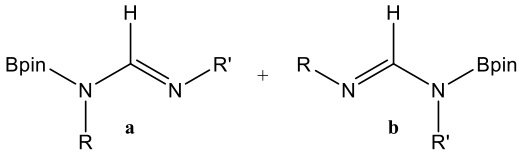

R, R' = *t*-Bu, Et (**86**); $PrNMe_2$, Et (**87**)

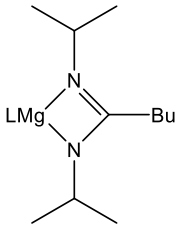

88

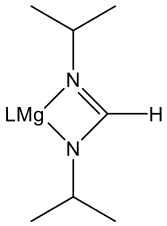

89

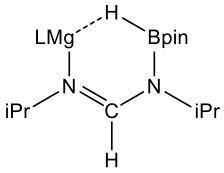

90

Chapter 6.3 – *Hydroboration of Isocyanates*

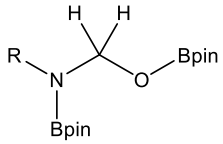

R = Mes (**91**), Dipp (**92**)

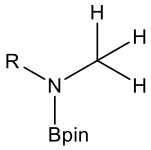

R = Ph (**93**), Et (**94**), Pr (**95**), *i*-Pr (**96**), *t*-Bu (**97**), Cy (**98**), Ad (**99**)

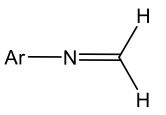

Ar = Mes (**100**), Dipp (**101**)

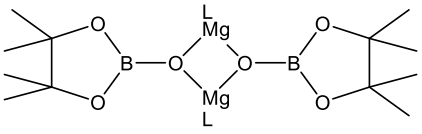

102

Chapter 1. Introduction

1.1 Group 2 Metals

In recent years main group chemistry has seen a resurgence in interest. This is not surprising considering the apparent need for more economically viable and 'eco-friendly' processes. Whilst the chemistry of the heavier transition metals is well developed in terms of catalysis, the major drawback is the cost of these naturally low abundant, toxic metals. On the other hand group 2 metals meet both of these criteria as they are cheap and environmentally benign; magnesium is the eighth most abundant element on the planet and calcium is the fifth. Until recently, however, there has been very little study of their application to catalysis and the most notable reactivity of the group 2 metals, specifically magnesium, has been in the form of stoichiometric Grignard reagents for organic synthesis.[1-3]

The chemistry of the alkaline earth (Ae) elements is largely determined by their redox inactive nature, as Ae cations in the 2+ oxidation state which also possess a d^0 electronic configuration. There are a few notable exceptions to the 2+ oxidation state. In 2007 Jones reported the first Mg-Mg bond,[4] with Mg formally in the +1 oxidation state. This has since been followed by work by Westerhausen for synthesis of a stable inverse sandwich Ca(I) complex.[5, 6]

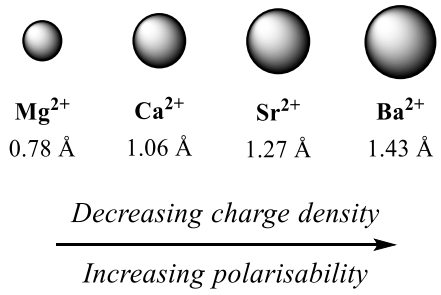

Figure 1-1. Variation in ionic radii upon descending group 2

The ionic radii of the Ae metals increase upon descending the group, whereas the Pauling electronegativity decreases (χ_p) leading to more electropositive character upon descending the group (Figure 1-1).[7] This combination lends magnesium a degree of covalency for metal-ligand binding whereas bonding to the heavier elements is dictated by ionic and even less directional interactions. This represented an initial issue for the development of well-defined reaction chemistry for the heavier group 2 elements due to the resultant propensity of the heteroleptic complexes, LMX (where L = monoanionic spectator ligand, X = monoanionic substituent eg. alkyl, amide, phosphide, hydride) to undergo Schlenk-type equilibria (Scheme 1-1) to form the

homoleptic compounds (L_2M and MX_2). This tendency to form the homoleptic species increases upon descending the group.

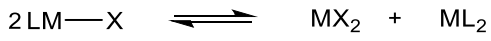

Scheme 1-1. Schlenk-equilibrium

To overcome this problem sterically demanding spectator ligands have been used to kinetically stabilise the heteroleptic in order species to suppress the rate of redistribution to the homoleptic species. Examples of stabilising ligands used in group 2 chemistry are summarised below in Figure 1-2. These include *β*-diketiminates (**Ia-g**),[8-13] borates (**II**),[14, 15] bis(imino)acenaphthenes,[16] bisimidazolinates (**III**),[17] aminotroponiminates,[18, 19] triazenides[20] and anilido-imines (**Va-c**).[21] Alternate approaches using homoleptic species have utilised bulky amide (**Va-d, VIa-d**)[22, 23] and alkyl (**VIIa-d**)[24, 25] groups.

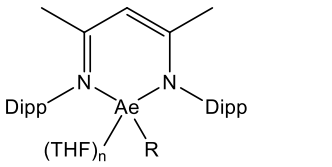

Ia Ib Ic Id Ie If Ig Ih
Ae = Mg, Mg Mg Mg Ca, Ca, Sr, Ca
R = Me, Bu, Bu, $N(SiMe_3)_2$, NPh_2
n = 0, 0, 1, 0, 0, 1, 1, 1

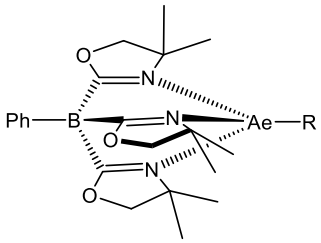

IIa IIb
Ae = Mg, Ca
R = Me, $N(SiMe_3)_2$

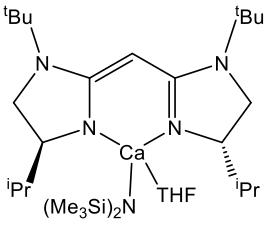

III

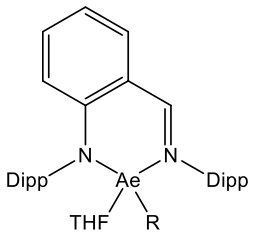

IVa IVb IVc
Ae = Ca, Sr, Ba
R = $N(SiMe_3)_2$
n = 1, 2, 2

$[Ae(N\{SiMe_3\}_2)_2]_2$

Va Vb Vc Vd
Ae = Mg, Ca, Sr, Ba

$[Ae(N\{SiMe_3\}_2)_2(THF)_2]$

VIa VIb VIc VId
Ae = Mg, Ca, Sr, Ba

$[Ae(CH\{SiMe_3\}_2)_2(THF)_2]$

VIIa VIIb VIIc VIId
Ae = Mg, Ca, Sr, Ba

Figure 1-2. A variety of stabilising ligands for group 2 complexes

Comparisons between the group 2 and lanthanide (Ln) metals can be drawn due to L_2LnX complexes containing similarly redox inactive, d^0 metal centres. Reactivity of the lanthanides can be described in two simple reaction mechanisms; σ-bond metathesis and the polarised insertion of unsaturated bonds (Scheme 1-2). By combination of these two steps it is possible to construct catalytic cycles as shown in the ground-breaking work of Marks *et al*.[26]

(a) σ-bond metathesis

(i) Protic

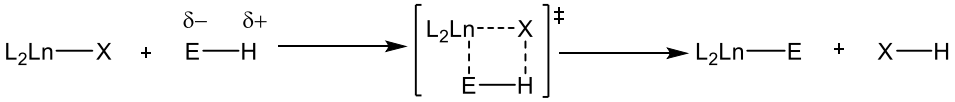

E = NR_2, OR, PR_2, SR

(ii) Hydridic

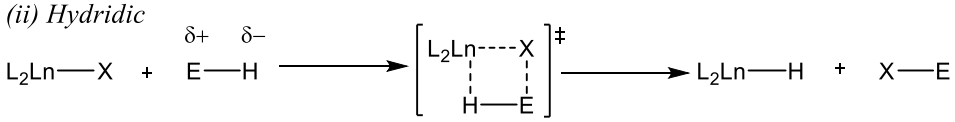

E = BR_2, SiR_3, AlR_2

(b) Insertion

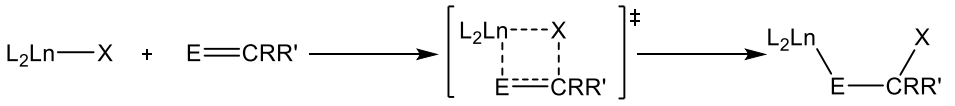

E = NR_2, OR, SR

Scheme 1-2. Series of key reaction steps in lanthanide-mediated catalysis: (**a**)i) σ-bond metathesis for substrate with protic E-H; (**a**)ii) σ-bond metathesis for a substrate with hydridic E-H; **b)** Insertion of unsaturated bond, E=C, into Ln-X bond. L = monoanionic spectator ligand.

Scheme 1-2 (**a**) shows the dependence on the polarity of the E-H bond in the outcome of the σ-bond metathesis reaction. In the case of protic substrates, (Scheme 1-2 (**a**)i), i.e. when E is more electronegative than H, protonolysis occurs. This leads to formation of a new M-E bond and protonation of substituent X. An example of this reactivity is the amination reaction, in which the lanthanide species, L_2LnX, reacts with an amine, R_2NH, to form a lanthanide amide, L_2LnNR_2.[27] Of particular relevance to the content of this thesis, is the opposite case, i.e. where H is more electronegative than E (Scheme 1-2 (**a**)ii). σ-bond metathesis reactions with substrates such as silanes, R_3SiH, and boranes, R_2BH, result in the formation of a metal-hydride species, L_2LnH, and a new X-E bond. The second type of reactivity observed is that of polarised insertion (Scheme 1-2 (**b**)). When the unsaturated substrate is not polarised, i.e. E=C (alkene or alkyne), polarisation is required to be induced by the Ln-X bond to enable insertion to occur. This possesses a necessarily higher energy barrier compared to when E ≠ C. When E = O or N (ketone and imine respectively), however, the substrate is already polarised across the unsaturated bond and a lower energy barrier to insertion is observed, allowing the synthesis of a wide range of complexes. These two steps (**a** + **b**) can be combined to construct catalytic cycles as shown in Scheme 1-3.

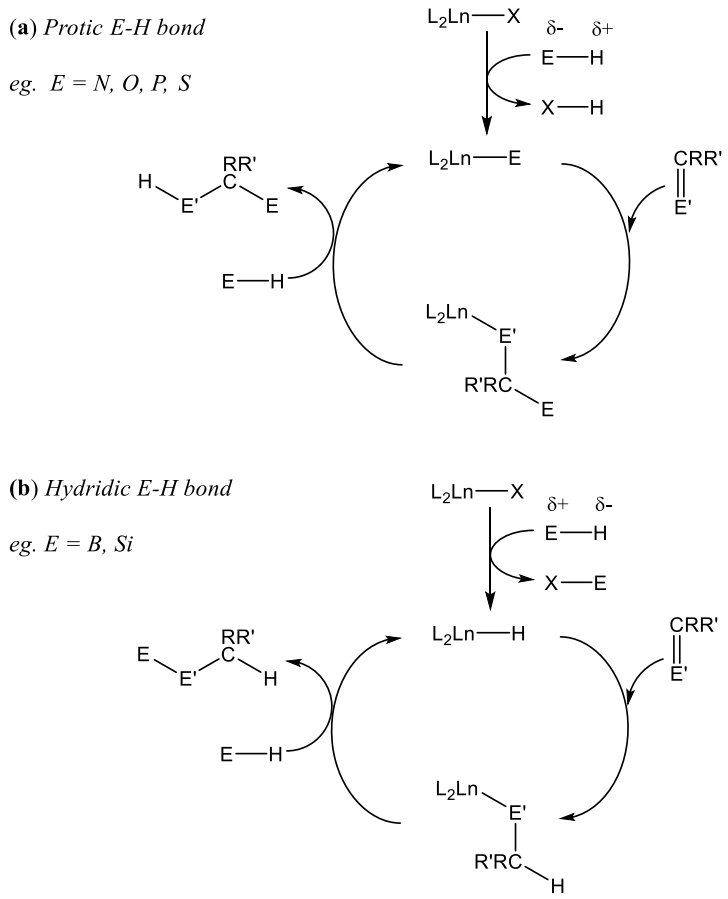

Scheme 1-3. Protic (**a**) and hydridic (**b**) catalytic cycles constructed from a series of σ -bond metathesis and insertion reactions at lanthanide metal centres. L = monoanionic spectator ligand.

Scheme 1-3 (**a**) shows the protic catalytic cycle in which the lanthanide precatalyst, L_2LnX, initially undergoes protonolysis *via* a σ-bond metathesis reaction to form the active catalyst. A similar dependence on an initial σ-bond metathesis step is also true of the hydridic catalytic cycle (Scheme 1-3 (**b**)). In this case, however, L_2LnH is formed as the active catalyst. Subsequent insertion of the unsaturated bond into this metal hydride results in formation of new Ln-E and C-H bonds. This complex then undergoes a final σ-bond metathesis reaction to form the product, whilst reforming the active L_2LnH catalyst. These proposed catalytic cycles have been applied to a wide range of synthetic reactions for lanthanide based catalysis such as; hydroamination,[28-39] carbostannylation,[40] hydroalkoxylation,[41-44] hydrogenation,[45, 46] hydrophosphination,[47-49] hydrothiolation,[50, 51] acylation,[52] amidation,[53] polymerisation,[54-57] and hydroboration.[58]

1.2 Group 2 Catalysis

As mentioned previously, comparisons between Ln^{3+} and Ae^{2+} centres can be drawn due to them both possessing a redox inactive d^0 configuration. These comparisons inspired the initial development of group 2 catalysis, leading to the chemistry being described as 'lanthanide mimetic' in the early years. Over the last 10 years, however, group 2 catalysis has emerged in its own right, making these comparisons unjustified.

The potential of group 2 chemistry was discovered through initial work focussing on the protonolysis step to yield catalytically relevant group 2 species. Reactions using group 2 amides and alkyls with alcohols, pyrroles, terminal alkynes, phosphines and C-H acidic heterocycles have been shown to yield alkoxide,[59-61] pyrrolide,[62] acetylide,[63-66] phosphide[67-70] and carbanion[71] fragments bound to the group 2 centre *via* σ-bond metathesis reactions. Scheme 1-4 shows the protonolysis of the group 2 amide (**Va-d**) with a protic reagent (E-H) forming the active Ae-E centre with subsequent formation of the protonated amine.

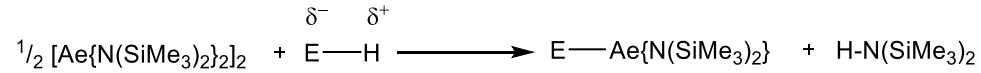

Scheme 1-4. Protonolysis of group 2 complexes *via* σ-bond metathesis yielding new Ae-E and H-($N(SiMe_3)_2$) species

Westerhausen *et al* observed the insertion of 1,4-diphenylbutadiyne into the Ae-P bond of the homoleptic group 2 phosphides, $[Ae\{P(SiMe_3)_2\}_2(THF)_4]$ (Ae = Ca, Sr, Ba). Benzonitrile was also observed to insert into the Ae-P bond of group 2 phosphides as well as the Ae-N bond of group 2 amides.[67, 72-76] Further evidence for the potential of group 2 mediated catalysis, was shown through the use of reactive group 2 benzyl complexes $[Ae(DMAT)_2(THF)_2]$ (Ae = Ca, Sr, Ba, DMAT = 2-dimethylamino-2-trimethylsilylbenzyl) for styrene polymerisation.[77-80]

The viability of the σ-bond metathesis to form catalytically active species and this facility for insertion reactions of unsaturated bonds into the newly formed Ae-X bonds indicated that the potential for this reactivity may be expanded into a catalytic regime. Using polarised substrates (when E ≠ C, E = O, N, X) allows for a wide range of heterofunctionalisation reactions to occur, as outlined in the following sections.

1.2.1 Group 2 mediated Hydroamination

The reaction which really initiated group 2 molecular catalysis was the intramolecular hydroamination of aminoalkenes and aminoalkynes.[81] The success of this reaction prompted in depth research from Hill and co-workers into the capabilities of these Ae catalytic systems based upon the type of reactivity seen in Scheme 1-3. This has provided access to a range of heterofunctionalisation reactions such as intermolecular hydroamination,[12, 82] hydroamination of heterocumulenes[83-85] and hydrophosphination.[86, 87] Extensive mechanistic and kinetic studies on the intramolecular hydroamination of aminoalkenes has provided further insight into the differences between the reactivity of the individual group 2 metals and will be discussed in this section.

The initial hydroamination reaction was based upon Chisholm's *β*-diketiminato calcium complex, **Ie**, which had been previously employed as an active catalyst for lactide polymerisation.[9] Reaction of this pre-catalyst with one equivalent of 1-aminohex-4-yne, provided the full consumption of the aminoalkene to form the 2-ethylpyrroline cyclisation product, within 30 minutes at room temperature.[81] Scheme 1-5 shows a general reaction scheme for the intramolecular hydroamination/cyclisation of aminoalkenes. Although a further stoichiometric reaction with 1-aminopent-4-ene highlighted issues with ligand redistribution as a competing side-reaction, the aminoalkene was completely consumed within 24 hours at room temperature to form the desired 2-methylpyrrolidine product. In subsequent work it was demonstrated that the homoleptic pre-catalyst $[Ca\{N(SiMe_3)_2\}_2(THF)_2]$, **VIb**, was similarly competent to previously employed $[Ln\{N(SiMe_3)_2\}_3]$ species for intramolecular hydroamination of aminoalkenes.[88] Since this initial discovery, a wide range of group 2 metal catalysts have been shown to catalyse this reaction. This includes the homoleptic group 2 bis(amides) (**VIa-d**) and bis(alkyls) (**VIIa-d)**, as well as the solvent free bis(amides) (**Va-d**) and the *β*-diketiminato ligated metal complexes (**Ia-g**).[8-10, 89, 90]

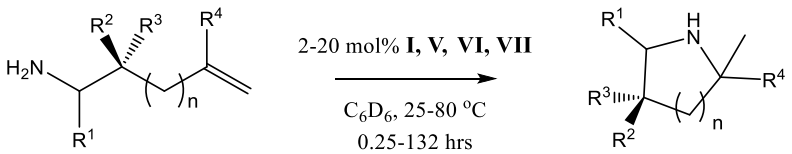

Scheme 1-5. Group 2 mediated intramolecular hydroamination of aminoalkenes

Although further studies revealed that substitution at the alkene moiety impeded the rate of reaction, and in some cases (terminal mono- or disubstitution) prevented the reaction completely, the use of bulky geminal groups in the *β*-position of the amine facilitated cyclisation. This was ascribed to a Thorpe-Ingold effect wherein an increase in the size of

substituent will create an angle compression between reactive sites, thus favouring reactivity.[91] This was also reflected in the synthesis of differing ring sizes as pyrrolidines could be formed easily in minutes at room temperature using 2-10 mol% of catalyst **Ie**, whereas (6-membered) piperidines and (7-membered) hexahydroazepines could take up to 5 days requiring temperatures up to 80 °C with 10-20 mol% catalyst (Scheme 1-5).[8-10, 90]

The mechanism for group 2-catalysed hydroamination (Scheme 1-6) is again similar to those previously seen with the lanthanide based catalysis,[26] as demonstrated by a series of stoichiometric reactions and deuterium labelling studies in order to observe intermediates present during catalysis.[90] Reaction of the pre-catalyst, **Ie**, with 2 equivalents of benzylamine provided the dimeric benzylamide product in equilibrium with the starting hexamethyldisilazide ($\Delta G_{(298K)}$ = -11.4 kJ mol^{-1}), indicating the potential for fast but reversible catalyst initiation. From these studies other modes of potential substrate inhibition became clear, wherein less acidic amines were found to displace the adducted THF and form amine adducts. Kinetic studies were subsequently carried out and further demonstrated both product and substrate inhibition, mirroring effects that had already been seen with analogous lanthanide systems.[92] Interestingly a non-linear activity trend was found: calcium was found to be the most active catalyst, followed by magnesium and then strontium, contrasting what has recently been reported for anilido imine derived catalysts (**IVa-c**) in which barium was the most active.[21]

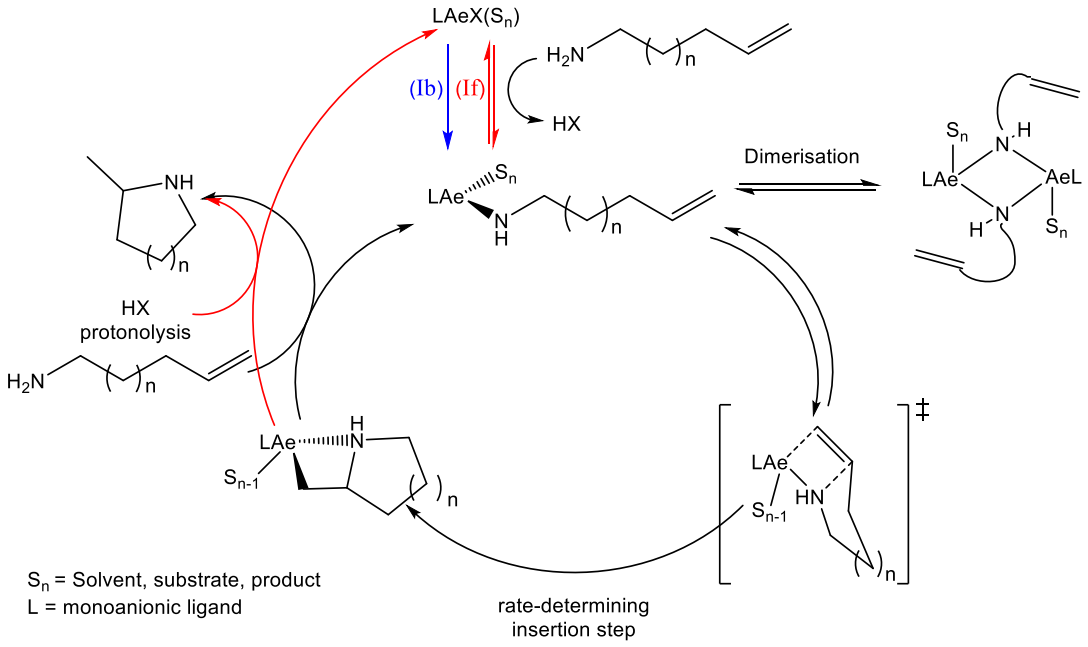

Scheme 1-6. Proposed catalytic cycle for the intramolecular hydroamination of aminoalkenes with reversible or irreversible catalyst initiation

This catalytic chemistry was further extended to the intermolecular hydroamination of various styrenes and conjugated dienes. Supported by DFT calculations, the rate determining step in

this reaction was suggested to be C=C insertion into the M-N bond *via* a four centred polarised transition state. Kinetic studies across the range of group 2 metals also showed the rate of reaction to be dependent upon the group 2 metal centre.[89] Upon descending the group a more pronounced change in charge density is observed for Ae^{2+} cations in comparison to the Ln^{3+} series. This results in a more complex trend upon descending the group. For the intermolecular hydroamination reaction this resulted in an entropic advantage for the larger strontium species due to a less constrained rate-determining alkene insertion transition state. This trend agrees with that observed in a recent report of the intermolecular hydroamination of vinyl arenes and isoprene, in this case employing the anilido-imine pre-catalyst (**IVa-c**), barium was found to be the most active followed by Sr > Ca > Mg.[21]

1.2.2 Further Group 2 Heterofunctionalisation reactions

This hydroamination catalysis was subsequently extended to a wide range of both protic E-H and C=E bonded substrates allowing the development of a series of heterofunctionalisation reactions. For example, Hill and co-workers reported the catalytic intermolecular hydrophosphination of activated alkenes using the *β*-diketiminato calcium complex (**If**) as shown below in Scheme 1-7.[86]

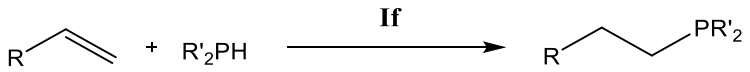

Scheme 1-7. Hydrophosphination of alkenes mediated by **If**

Further work in this area has shown this hydrophosphination reaction is also applicable to alkynes using homoleptic calcium phosphide pre-catalysts,[93] whilst Sarazin and co-workers have reported the use of the anilidoimine supported group 2 centres (**IVa-c**) for the hydrophosphination of alkenes. In this case the reported order of reactivity mirrors that seen for the hydroamination reactions (Ca < Sr < Ba) with the same ligands.[94] Further extension of this type of reactivity has moved beyond P(III)-H bonds, to include phosphite reagents for the hydrophophonylation catalysis of ketones and aldehydes mediated by **VIb-d**.[95]

Hill and co-workers have reported several examples of carbodiimide heterofunctionalisation reactions. **If**, **Vb-d** and **VIb-d** have all been shown to be effective pre-catalysts for the hydrophosphination[87] and hydroamination[83] of these substrates to form phosphaguanidines and guanidines. Metalloamination and metallophosphination reactions with **Va-c** have also been shown to be possible with carbodiimides.[96] Whilst extension of this reactivity to the isoelectronic isocyanates has proved more challenging, due to oligiomerisation reactions as shown by Harder *et al*.[97] Catalytic hydroamination of isocyanates to yield substituted ureas[84]

and hydrophosphorylation reactions with phosphines and phosphine oxides have also been reported.[98]

1.2.3 Group 2 mediated Dehydrocoupling

Whereas hydroamination reactions rely upon the use of protic substrates and combinations of σ-bond metathesis and insertion reactions to construct their catalytic cycles, dehydrocoupling reactions rely solely on σ-bond metathesis reactions and the use of a combination of protic and hydridic reagents. Using both E-H protic and E'-H hydridic reagents allows for the formation of new E-E' bonds with the elimination of hydrogen, as shown in Scheme 1-8 below.

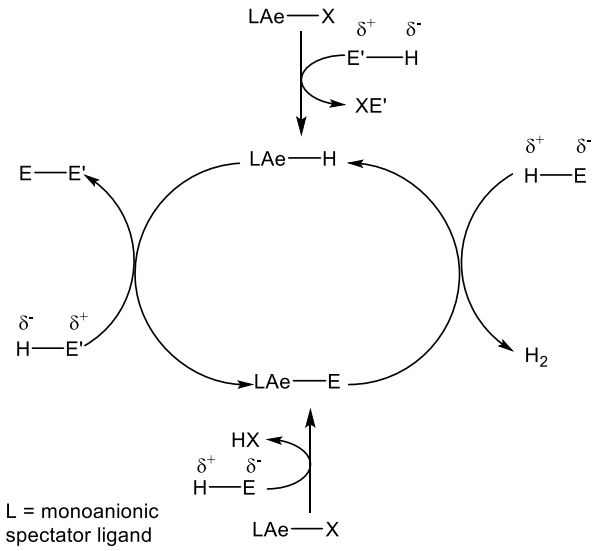

Scheme 1-8. Proposed generic mechanism for Group 2 catalysed dehydrogenative cross metathesis.

This type of reactivity with group 2 metals has largely focussed on silicon-nitrogen[15, 99] and amine-borane dehydrocoupling,[100-105] whilst Harder and co-workers have reported catalytic Si-C dehydrocoupling between a silane and terminal alkyne.[106]

Kinetic studies of the silicon-nitrogen dehydrocoupling reactions again showed a dependence upon the identity of the group 2 metal centre, reminiscent of that observed with the group 2 hydroamination catalysis described in Section 1.2.1. The calcium pre-catalyst (**Vb**) displayed the highest catalytic activity whilst rate laws derived for each metal centre outlined a clear difference in mechanism for the strontium-based catalysis. These apparent differences were again suggested to be due to the change in cation charge density and subsequent polarisability of the Ae^{2+} metal centre.

Hill *et al* have also shown that reactivity based upon this σ-bond cross metathesis system may be extended to E-E' species. The reaction of diphenylphosphine oxide with $PhSiH_3$,[107] mediated

by **If** and **VIb**, results in both reduction and dehydrocoupling to form the P(III)-P(V) compound $Ph_2P(O)PPh_2$ and its fully reduced counterpart Ph_2PPPh_2 (Scheme 1-9). It was also found that triarylphosphine oxides undergo similar cross-metathesis reactions to form new P-P bonds, a process which was postulated to occur *via* an additional P-C σ-bond metathesis reaction.

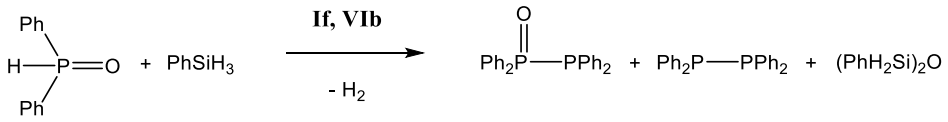

Scheme 1-9. Calcium-centred phosphine oxide reactivity: P–C metathesis, reduction and P–P coupling

1.3 Synthesis and reactivity of molecular Group 2 Hydrides

1.3.1 Synthesis and reactivity of Calcium (II) complexes

Harder and co-workers reported the first hydrocarbon soluble *β*-diketiminato-calcium hydride (**VIII**) which was synthesised through the σ-bond metathesis route outlined in Scheme 1-10.[108]

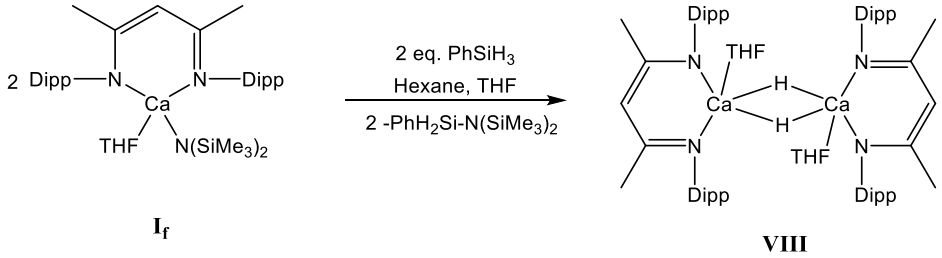

I_f **VIII**

Scheme 1-10. Synthesis of *β*-diketiminato calcium hydride complex

The approach utilised LCa–R complexes in which L is a bulky ligand and R a reactive group that could be converted into a hydride ligand. Initial attempts used (9-Me_3Si-fluorenyl)CaN^iPr_2 as the starting reagent, in the hope that heating the complex would result in decomposition of N^iPr_2 into $Me_2C{=}N^iPr$ and CaH in a similar manner to reactions with KN^iPr_2.[109, 110] No such decomposition, however, was observed in this case. Although the use of bulky tris(pyrazolyl)borate calcium amide complex (**IIb**) also failed to yield the desired hydride complex upon addition of $PhSiH_3$, reaction of the *β*-diketiminato calcium amide, **If**, with the silane reagent in hexanes yielded the desired heteroleptic *β*-diketiminato calcium hydride, **VIII** (Scheme 1-10).[108]

VIII was subsequently shown to take part in insertion reactions with a range of unsaturated substrates, [111-114] a few examples of which are shown in Scheme 1-11. The ability of this

soluble calcium hydride to react in a well-defined manner opened the door for a variety of new applications and contrasted with the primary function of calcium hydride (CaH_2) as a drying agent for organic solvents due to its lack of reactivity with organic functional groups.

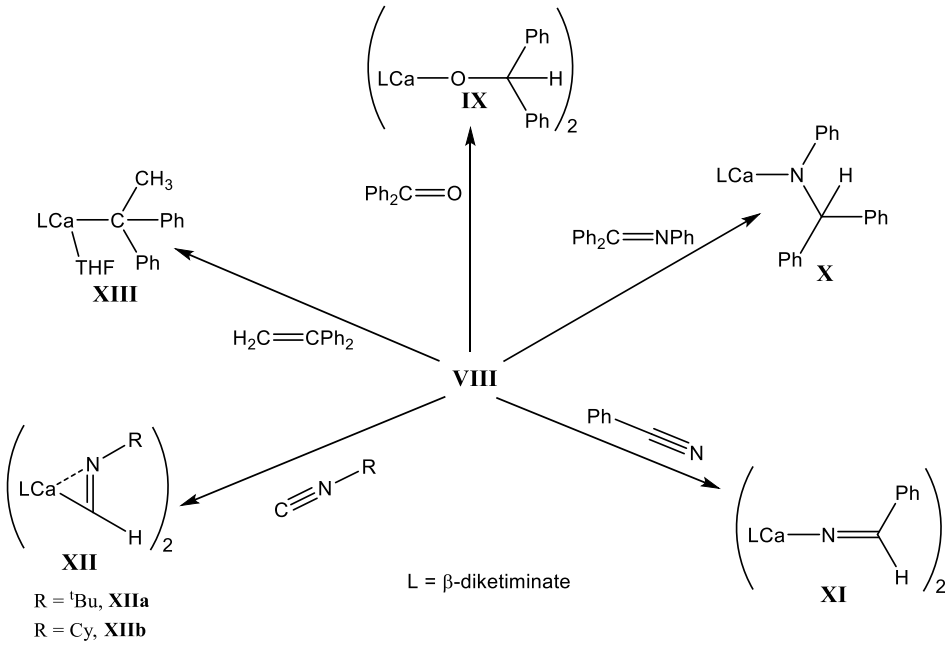

Scheme 1-11. Series of insertion reactions of E=C unsaturated bonds with β-diketiminato calcium hydride (**VIII**).

In all cases, apart from 1,1-diphenylethylene (Ph_2CCH_2), these stoichiometric reactions rely upon polarised unsaturated bonds, E=C, where E ≠ C. Reactions with benzophenone and imines provided easy access to calcium alkoxides (**IX**) and amides (**X**). Stoichiometric reactions of **VIII** were also shown to reduce C≡N triple bonds, to yield the first reported calcium aldimide (**XI**) from the reaction with benzonitrile, whilst isonitriles (R-N≡C) reacted in an umpolung fashion to also yield an isomeric calcium aldimide complex (**XII**). Addition of $Ph_2C{=}CH_2$ gave clean conversion to the calcium alkyl complex (**XIII**), unlike attempted reactions with other unsaturated C=C bonds such as norborene and styrene which either did not react or produced oligomeric products, respectively.

Since this initial report of the formation of a soluble calcium hydride, several further examples have been described, which were similarly reliant on the use of a silane as a hydride source. The use of a tetradentate cyclan- derived monoanionic ligand (Scheme 1-12) provided a cationic trimeric complex (**XIV**), in which the charge is balanced by an unusual silyl anion.[115]

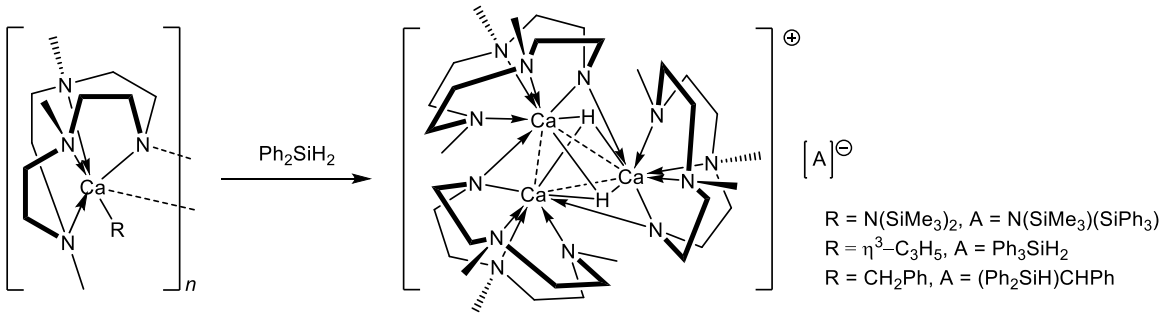

XIV

Scheme 1-12. Synthesis of trimeric calcium hydride

An alternative route to molecular calcium hydrides maybe achieved through the use of commercially available hydridic borane reagents. Reaction of 9-borabicyclo[3.3.1]nonane (9-BBN) with the *β*-diketiminato calcium diphenylamide (**Ih**) takes place *via* σ-bond metathesis to yield a new molecular calcium boro-hydride complex, **XV** (Scheme 1-13).[116]

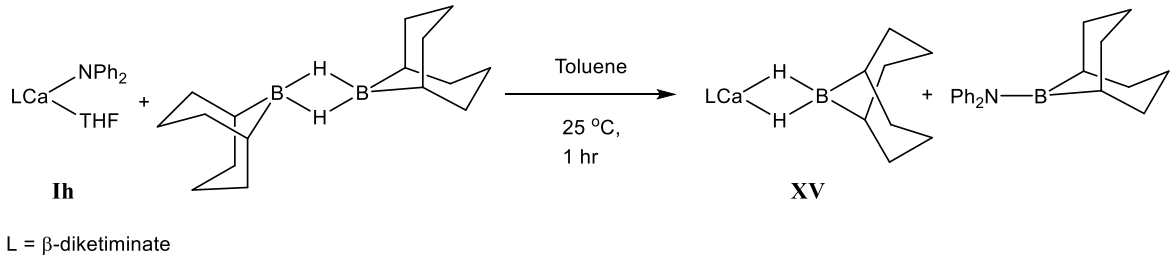

Ih **XV**

L = β-diketiminate

Scheme 1-13. Synthesis of Calcium borohydride, **XV**

1.3.2 Synthesis and reactivity of Magnesium (I) and (II) complexes

In a landmark study Jones and co-workers reported the extension of group 2 chemistry beyond the confines of the +2 oxidation state, by successful synthesis of the first Mg(I) complex. This was obtained through reduction of a *β*-diketiminate supported magnesium (II)iodo complex with potassium metal (Scheme 1-14), to yield the Mg(I) complex (**XVI**) which contains a direct Mg-Mg bond.[4, 117, 118]

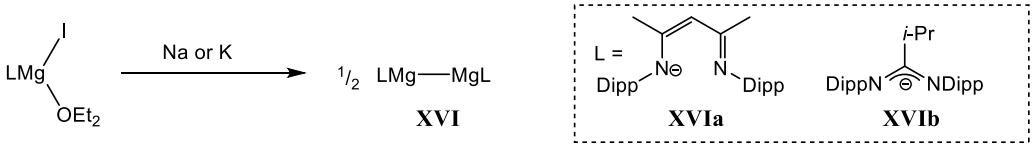

XVI **XVIa** **XVIb**

Scheme 1-14. Synthesis of Mg(I) dimer

Subsequent reactivity of the Mg(I) dimer (Scheme 1-15) demonstrates that Mg(I) is a powerful reducing reagent. It has also been used as a homogeneous reducing agent to yield a series of unusual stable NHC adducts of dimeric germanium (0)[119] and tin (0)[120] fragments as well as a monomeric germanium(I) radical[121] and an aluminium (II) hydride.[122]

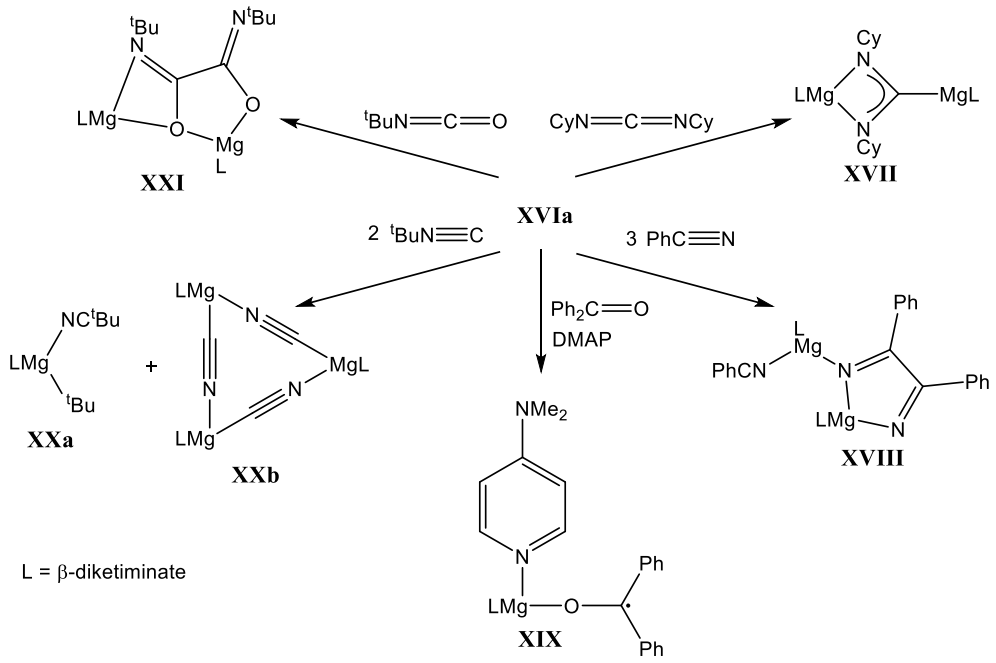

Scheme 1-15. Reactivity of *β*-diketiminate supported Mg(I) dimer, **XVIa**, with a variety of unsaturated organic fragments

Whilst the reduction potential of Mg(I) is of synthetic interest, this thesis focusses on the more readily synthesised magnesium hydride complex (**XXII**) as a tool for reduction chemistry and its application to catalysis. A similar route to that employed in the synthesis of the initial calcium hydride was applied; reaction of the *β*-diketiminato magnesium butyl complex (**Ib**) with $PhSiH_3$, yielded the *β*-diketiminato magnesium hydride (**XXII**, Scheme 1-16), as reported by Jones.[118]

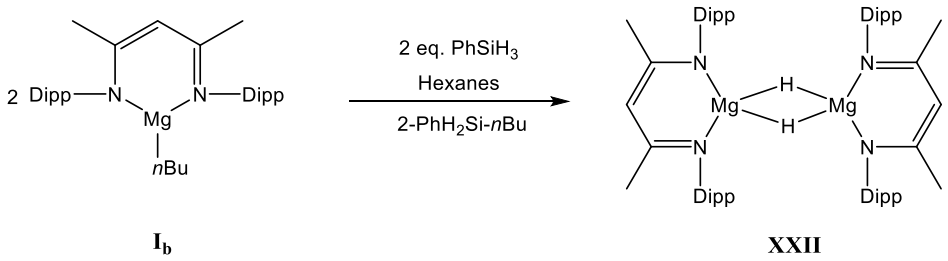

Scheme 1-16. Synthesis of *β*-diketiminato magnesium hydride, **XXII**

A few examples of insertion reactions have again been reported to provide smooth insertion of the unsaturated E=C unit into the Mg-H bond (Scheme 1-17).[117]

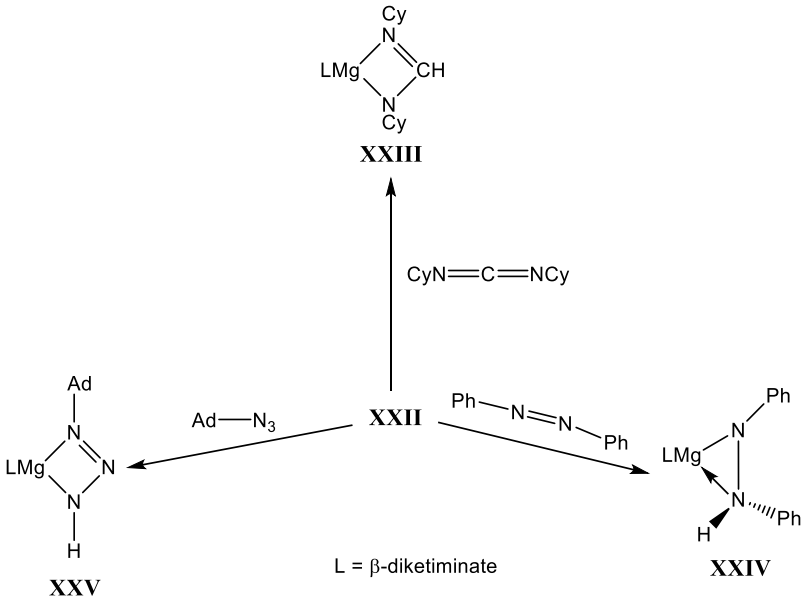

Scheme 1-17. Series of insertion reaction of E=C unsaturated bonds into *β*-diketiminato magnesium hydride, **XXII**

Reaction with *N,N'*-dicyclohexylcarbodiimide gave a clean reaction to form the formamidinate, **XXIII**, in a manner similar to that observed with the calcium hydride complex (**VIII**). Insertion of PhN=NPh resulted in the formation of a new magnesium species with an η^2 coordinated hydrazide ligand (**XXIV**), whilst reaction of AdN_3 yielded the expected singly reduced triazenide species (**XXV**) along with a very small amount (< 2%) of the fully reduced amide.

Further examples of the use of **XXII** have been reported by Hill and co-workers, for the stoichiometric dearomatisation of pyridines[123] and quinolines.[124] Using the magnesium *n*-butyl complex (**Ib**), the hydride can be generated *in situ* and subsequent addition of 2 equivalents of pyridine resulted in the formation of a kinetically favourable 1,2-dihydropyridide complex (**XXVI**). This reaction is proposed to occur through an unobserved coordinated *N*-heterocyclic magnesium hydride. Formation of the kinetically favoured 1,2-dihydropyridide results from hydride transfer from the magnesium centre. Over time, or with heating, the hydride then transfers to the more thermodynamically favoured 1,4-dihydropyridide, **XXVII** (Scheme 1-18).

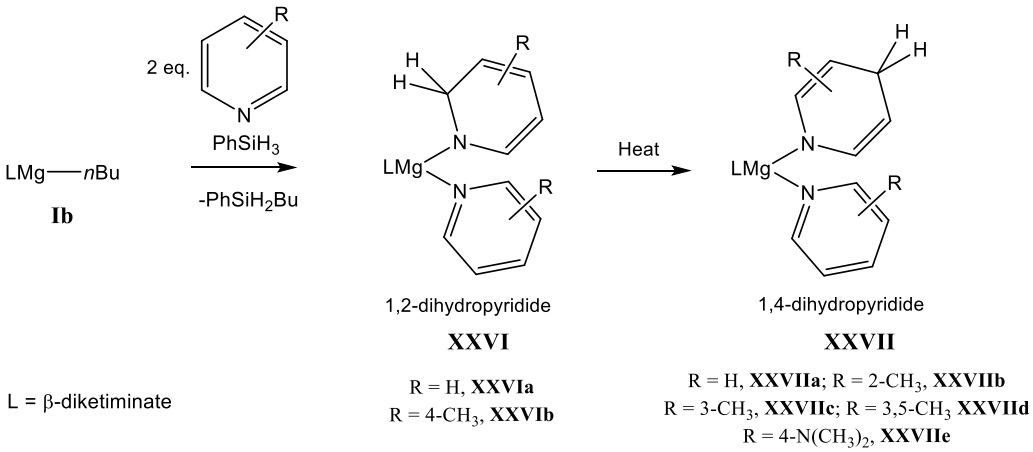

Scheme 1-18. Dearomatisation of a range of substituted pyridines *via* an *in situ* generated magnesium hydride

Scheme 1-18 shows that dearomatisation can be extended to a wide range of substitution patterns around the pyridine *N*-heterocycle. Similar reactions with 2,6-lutidine failed, however, supporting the proposed mechanism in which the reaction proceeds *via* the 2-positions which in this case are both blocked by methyl groups. This is also true of **XXVIb** in which dearomatisation at the 4-position is blocked leading to exclusive isolation of the 1,2-isomer. In contrast, hydride transfer to the 4-position was seen during the dearomatisation of 4-dimethylaminopyridine (DMAP) despite the presence of the 4-dimethylamino group. It was also possible to extend this type of reactivity to the fused ring quinoline and *iso*-quinoline reagents (Scheme 1-19).

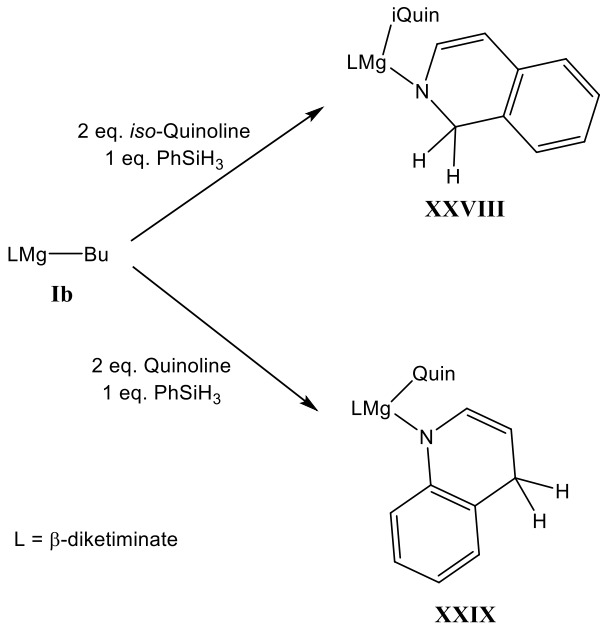

Scheme 1-19. Dearomatisation of quinolines *via* an *in situ* generated magnesium hydride

Again exclusive formation of the 1,2-dihydro-*iso*-quinolide (**XXVIII**) was observed as the 4-position is blocked by the fused-ring aromatic system. For quinoline, however, as expected the 1,4-quinolide complex (**XXIX**) was isolated in high yields. The reactivity of these dihydropyridide complexes will be discussed in detail in Chapter 2 of this thesis.

Further synthesis of magnesium hydrides has centred around the formation of hydride clusters. Hill and co-workers reported the first hydride-rich magnesium cluster supported by bulky amides and a *N*-heterocyclic carbene ligand (Scheme 1-20).[125]

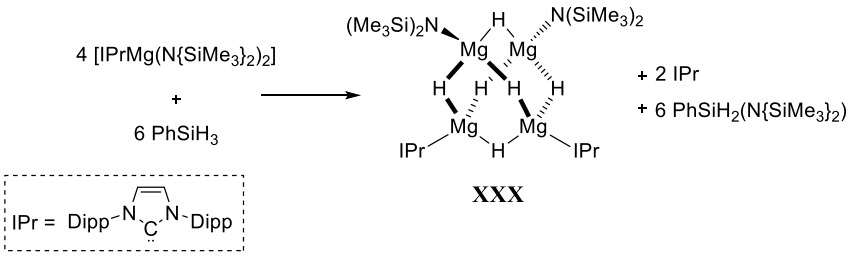

Scheme 1-20. Synthesis of a hydride rich magnesium cluster

As seen in Scheme 1-20, **XXX** is again formed *via* σ-bond metathesis with a silane to yield the hydride cluster which contains a 1:1.5 ratio of magnesium centres to hydrides. Subsequent work by Hill and co-workers yielded a range of bimetallic polyhydride aggregates, this time from σ-bond metathesis between $PhSiH_3$ and alkali-metal (diamino)alkylmagnesiates ($[M\{N(SiMe_3)_2\}_2MgBu]$, M=Li, Na, K). The nature of the polyhydride complexes was dependent upon the identity of the group 1 metal. For example reaction of $PhSiH_3$ with $[Na\{N(SiMe_3)_2\}_2MgBu]$ led to the formation of an unprecedented dodecametallic decahydride

cluster.[126] Whilst interesting compounds for potential hydrogen storage applications, these hydride clusters have not yet been employed in defined reaction chemistry.

Harder and co-workers have also employed *β*-diketiminate ligands in the formation of higher nuclearity magnesium hydrides. Synthesis of tethered bis-*β*-diketiminate complexes led to the formation of tetra- (**XXXI**) and octanuclear (**XXXII**) magnesium hydride clusters (Figure 1-3).[127, 128] The application of these compounds to catalysis will be discussed in section 1.4.1.

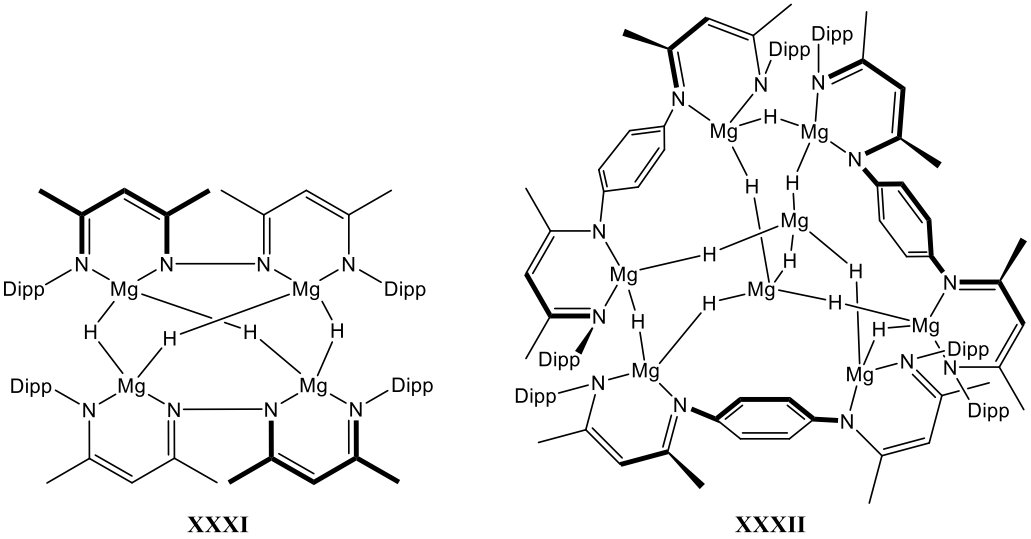

Figure 1-3. Bis-*β*-diketiminate supported magnesium hydrides

1.3.3 Group 2 mediated Hydrosilylation

The application of group 2 hydrides in catalysis, based upon catalytic cycles proposed in Scheme 1-3 (b), has been more limited in comparison to those cycles based upon protic substrates. The first reported example of such a 'hydridic' E-H type catalytic system was the hydrosilylation of alkenes and dienes.[129] Here the homoleptic calcium and strontium dibenzyl catalysts, **XXXIIIa** and **XXXIIIb**, respectively, previously employed in the living polymerisation of styrene,[80] were utilised for the reaction of $PhSiH_3$ and activated alkenes with resultant addition of H-Si across an unsaturated C=C bond. These reactions proceeded under mild conditions (0.5 – 10 mol % catalyst, 25 – 50 °C and 0.1 – 48 hours) to afford both the Markovnikov and *anti*-Markovnikov products (Scheme 1-21).

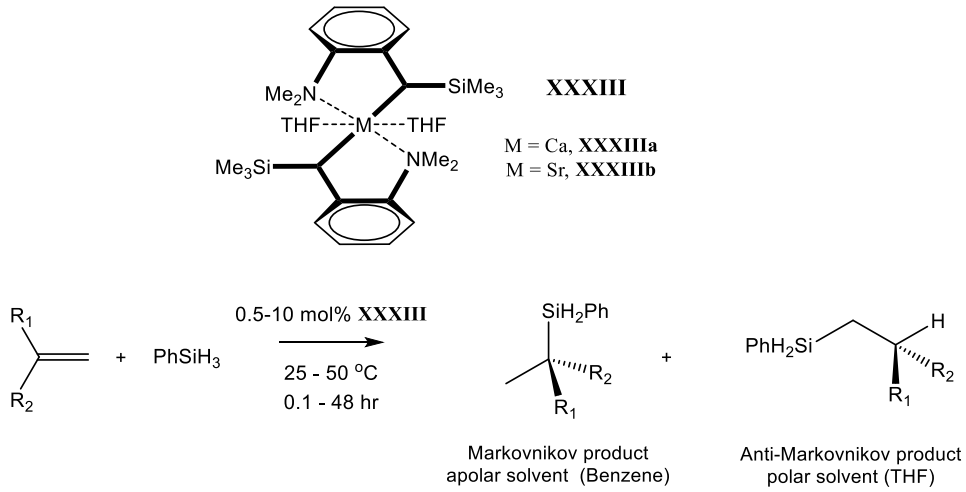

Scheme 1-21. Hydrosilylation of activated alkenes

The regioselectivity of the product could be controlled by the choice of solvent. The Markovnikov product was observed in apolar solvents whereas the *anti*-Markovnikov product was obtained from polar solvents such as THF. The reaction is thought to proceed *via* a metal-hydride species formed from σ-bond metathesis of compound **XXXIII** with $PhSiH_3$. Although never directly observed in this catalytic cycle, the subsequent isolation of the *β*-diketiminate calcium hydride complex, **VIII**, provided sufficient evidence for the likelihood of this intermediate.

Due to the solvent dependency on the outcome of the reaction, Harder proposed two catalytic cycles for the hydrosilylation of alkenes (Scheme 1-22). The Markovnikov product was suggested to be formed *via* the 'lanthanide mimetic' cycle (**A**) where the alkene inserts into the metal-hydride and subsequent σ-bond metathesis with a further equivalent of $PhSiH_3$ produces the desired product whilst regenerating the hydride. In order to generate the *anti*-Markovnikov product in polar solvents Harder suggested cycle (**B**), which is accessed *via* a charge-separated ion pair of the form $[LM]^+[PhSiH_4]^-$. This then converts into a group 2 silyl complex with formation of H_2. The steric demands of this complex would thus favour the *anti*-Markovnikov product.

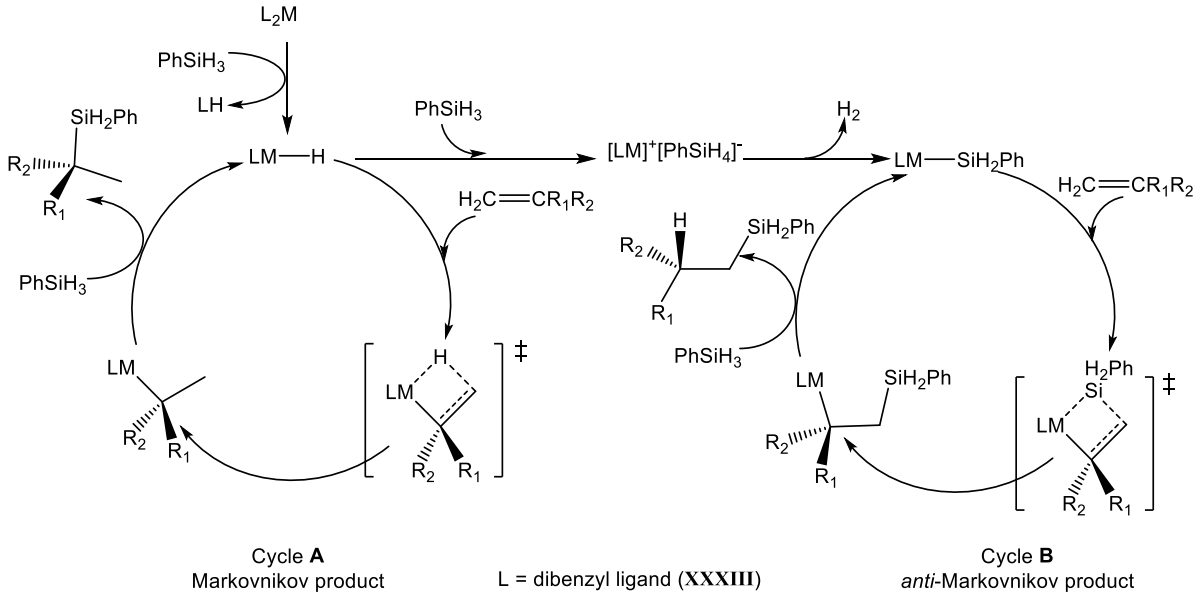

Scheme 1-22. Proposed mechanistic cycles for the hydrosilylation of alkenes

Application of this catalytic regime to the hydrosilylation of styrene, mediated by **XXXIII**, was largely unsuccessful. A subsequent report by Okuda and co-workers, however, demonstrated that the homoleptic calcium silyl complex, $[Ca(SiPh_3)_2(THF)_4]$, provided efficient turnover for the hydrosilylation of α-phenyl- and α-methylstyrene with triphenylsilane. The regioselectivity of the product was suggested to provide further support to the alternate mechanism postulated by Harder *via* the calcium silyl intermediate.[130]

Extension of this hydrosilylation catalysis has shown **XXXIIIa** and **VIII** to be successful for the hydrosilylation of ketones.[114] These reactions proceeded under mild conditions (1-5 mol % catalyst loading, 20-50 °C, 0.2-54 hours) to produce dialkoxysilane products (Scheme 1-23) rather than the expected alkoxysilane. Attempts to form the monosubstituted silane product by varying the starting ratio between ketone and $PhSiH_3$ were unsuccessful.

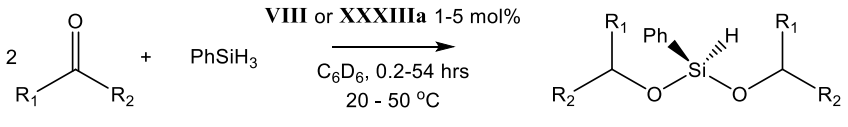

Scheme 1-23. Calcium-mediated hydrosilylation of ketones to form dialkoxysilanes

Stoichiometric reactions were carried out to try and isolate intermediates in this cycle; each attempt, however, yielded calcium alkoxide species which failed to react with further equivalents of $PhSiH_3$, thus suggesting this species is catalytically inactive and cannot be an intermediate in this hydrosilylation cycle. It was again proposed that the mechanism occurs

through a charge separated ion pair, despite the reaction being carried out in apolar benzene, with the reaction taking place at the hypervalent silicon centre.

1.4 Hydroboration Catalysis

Organoboranes have over the years shown themselves to be valuable synthons for numerous bond-forming processes, such as carbon-oxygen, carbon-carbon, boron-carbon, boron-chlorine, carbon-nitrogen bond forming reactions (Figure 1-4).[131] Classical methods for the synthesis of organoboron compounds are based on the reaction of trialkyl borates with Grignard or lithium reagents (transmetalation) or the addition of H–B reagents to alkenes or alkynes (hydroboration).[132]

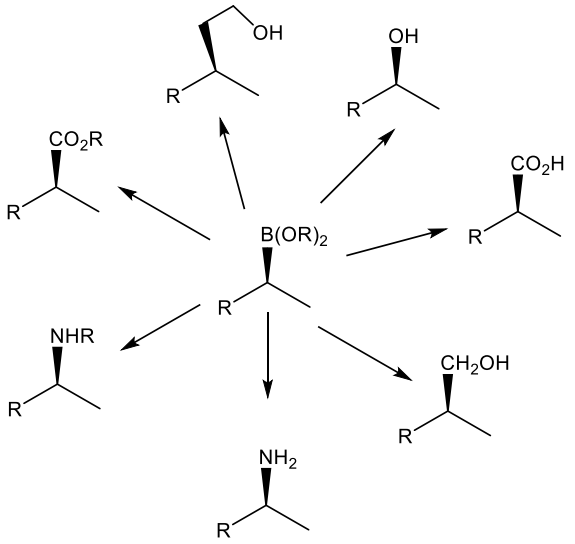

Figure 1-4. Transformations of the Boron-Carbon bond

The pioneering work of Brown, which earned him a Nobel Prize in 1979, paved the way for the use of borane and borohydrides as reducing agents. It was found that diborane (B_2H_6) reacted with aldehydes and ketones to produce dialkoxyboranes, which subsequently underwent hydrolysis with water to produce alcohols.[133] Although this discovery provided a feasible method for the reduction of carbonyls, it was limited by its reliance upon the use of the pyrophoric diborane reagent. The reaction of sodium hydride and tri-methyl borate at 250 °C was later found to produce sodium borohydride and sodium methoxide,[134] which was also able to reduce aldehydes and ketones.[135] In subsequent work, simply changing the metal ion (lithium, magnesium, or aluminium) produced a variety of mild reducing agents of differing reducing strength, which also proved successful for the reduction of carbonyl functional groups (Figure 1-5).[136]

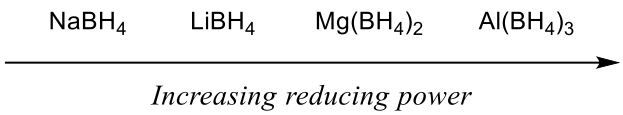

Figure 1-5. A variety of metal borohydride reducing agents

It was during the course of these studies, that a minor anomaly resulted in the discovery of hydroboration. It was observed that in the presence of aluminium chloride, sodium borohydride reduced ethyl oleate to the corresponding organoborane by addition of H-B across the carbon-carbon double bond.[137] Further exploration of this newly discovered reactivity focussed upon improving reaction conditions. Most notably the reaction of diborane with alkenes was catalysed in organic ether solvents and in some cases was found to be instantaneous and quantitative.[138]

Since the work by Brown and co-workers, further catalytic systems have been developed using a variety of hydroboration reagents. This has largely focussed upon the use of catechol borane (HBcat) with transition metal catalysts, in particular rhodium. Männig and Nöth in 1985 reported that using as little as 0.5 mol% of Wilkinson's complex [$RhCl(PPh_3)_3$] catalysed the addition of HBcat to alkenes or alkynes. This was the first example of a metal catalysed hydroboration reaction which, unlike the uncatalysed reaction, gave the *anti*-Markovnikov derivative as the major product (Scheme 1-24).[139]

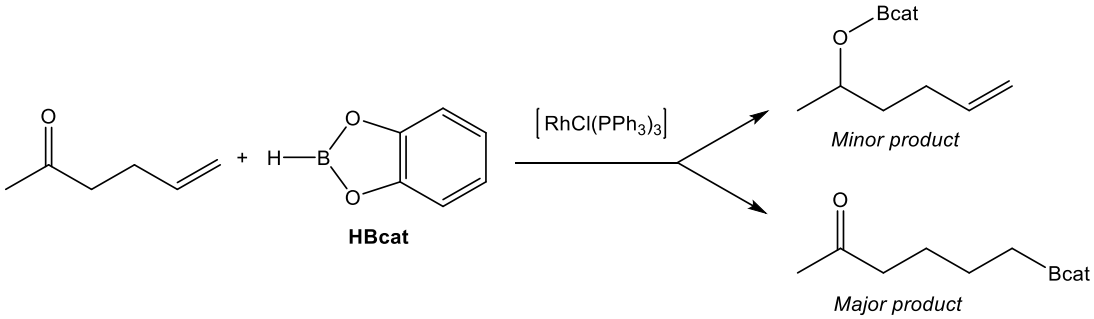

Scheme 1-24. First example of metal catalysed hydroboration of alkenes

The mechanism of this rhodium-catalysed hydroboration reaction is thought to depend on the nature of the substrate, the catalyst, the ligand used and the reaction conditions employed.[140] Dissociation of the triphenylphosphine ligand produces the active 14 electron Rh(I) species which undergoes oxidative addition with HBcat to form the active Rh(III) species. Migratory insertion of the alkene into the Rh-H bond leads to reductive elimination to give either the *anti*-Markovnikov or Markovnikov products whilst regenerating the active 14 electron rhodium(I) complex (Scheme 1-25).

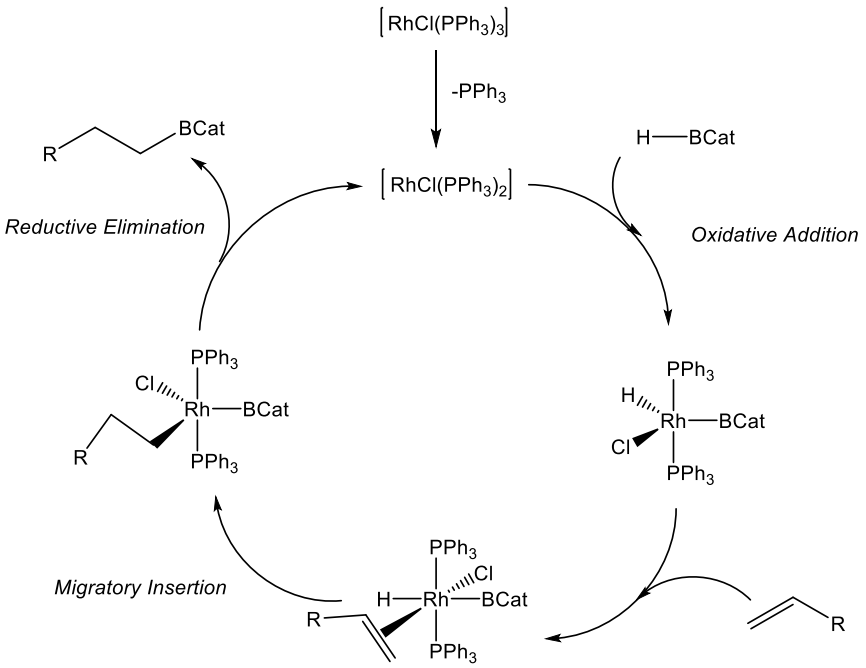

Scheme 1-25. Mechanism for the hydroboration of alkenes mediated by Wilkinson's catalyst

Relevant to this thesis, a recent study by Suginome and co-workers has described the rhodium-catalysed hydroboration of pyridines which exclusively yields the *N*-boryl-1,2-dihydropyridides (Scheme 1-26). Even at temperatures of 50 °C, no signs of the *N*-boryl-1,4-dihydropyridide were observed. This selectivity for the 1,2-dihydropyridide product was also observed over a range of substituted pyridines.[141]

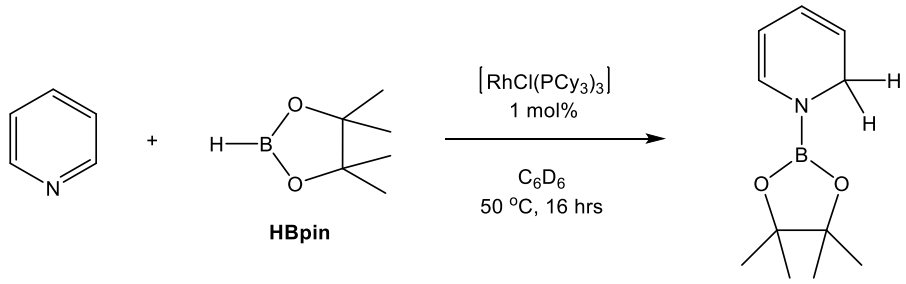

Scheme 1-26. Rhodium-catalysed hydroboration of pyridines

The proposed catalytic cycle for this reaction was again based upon a general redox mechanism similar to that outlined in Scheme 1-25, for the rhodium-catalysed hydroboration of alkynes and alkenes. The driving force of the reaction is believed to be provided by the formation of a strong B-N bond. It was also reported that the *N*-boryl-1,2-dihydropyridides underwent further transformations in a Diels-Alder type reaction and acylation of the B-N bond, in each case the dihydropyridide fragment was retained.

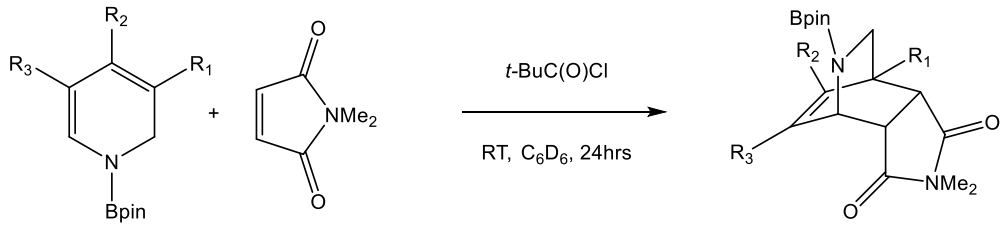

Scheme 1-27. Diels-Alder reactions of *N*-boryl-1,2-dihydropyridides

Whilst a large amount of research into transition metal catalysed hydroboration reactions has thus been undertaken, the nature of the redox mechanism is not applicable to group 2 chemistry. The first lanthanide-based hydroboration catalysis was reported by Marks and co-workers for the hydroboration of olefins using a lanthanum(III) catalyst (**XXXIV**).[142] This system proved efficient for the hydroboration of a variety of substituted olefins with HBcat, all of which showed high regioselectivity for the *anti*-Markovnikov products (Scheme 1-28).

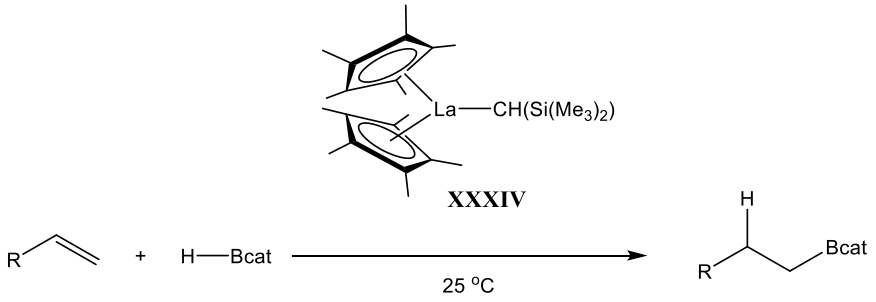

Scheme 1-28. Lanthanum-catalysed hydroboration of olefins

This protocol was applied to a variety of substrates including terminal, internal di-substituted and tri-substituted olefins but could not be extended to tetra-substituted olefins. The reaction rates determined for the various substituted olefins, were found to decrease with increasing olefin substitution, which was rationalised as a consequence of the increasing steric congestion at the lanthanum centre during catalytic turnover (Figure 1-6).

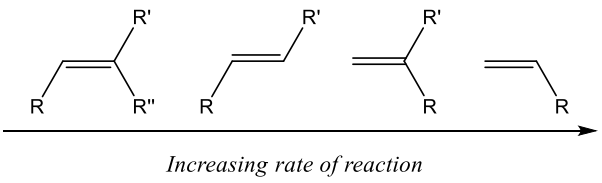

Figure 1-6. Influence of sterics on the rate of reaction for lanthanum-catalysed hydroboration of olefins

The proposed mechanism was suggested to proceed *via* a series of σ-bond metathesis and insertion reactions as shown in Scheme 1-29.

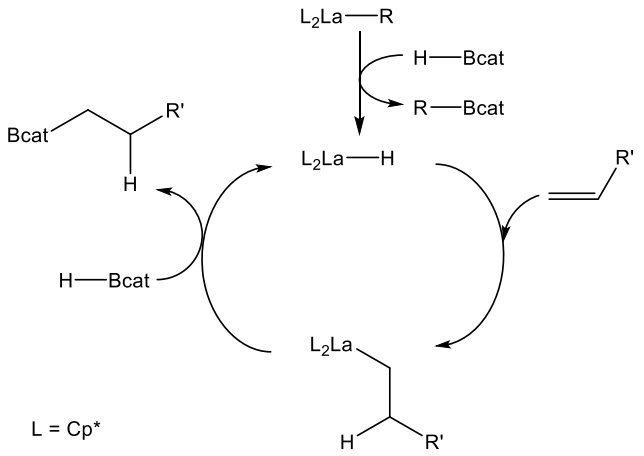

Scheme 1-29. Lanthanum-mediated hydroboration of olefins

Subsequent deuterium labelling studies showed clean addition of the deuterium to the olefin *β*-position compared to previous studies with rhodium, in which scrambling was observed due to reversible olefin insertion-extrusion.[143-146]

A recent report by Marks and co-workers showed that lanthanum-mediated hydroboration catalysis can also be extended to carbon-heteroatom (C=E) hydroboration, more specifically pyridines.[58] Using as little as 1 mol% of **XXXIV** with a 1:1 ratio of pinacol borane (HBpin) to pyridine, provided exclusive formation of *N*-boryl-1,2-dihydropyridide after 11 hours at the optimum temperature of 35 °C. No sign of any of formation of the 1,4-dearomatised species was observed even after 48 hours at 100 °C.

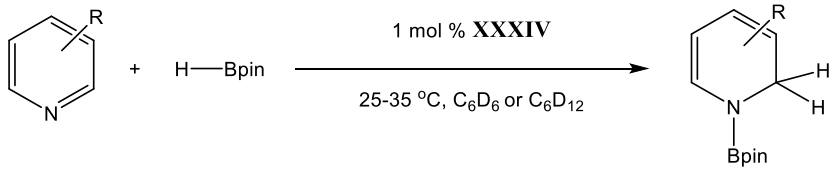

Scheme 1-30. Lanthanum-mediated hydroboration of pyridines

A wide variety of pyridines were found to undergo efficient hydroboration. A notable effect on the rate of reaction was observed for various electron withdrawing groups (EWG) and donating groups (EDG). EWGs in the 4-position were found to enhance the rate of reaction whereas the inclusion of an EDG in the 3-position slowed the reaction down. Also noted was this catalytic system's tolerance towards halogenated pyridines. This is particularly problematic for transition metal based systems due to competing C-X oxidative addition reactions.[147] The hydroboration of fused ring quinolines also proceeded rapidly.

Detailed mechanistic studies were also carried out, initially *via* a series of stoichiometric reactions. The catalytic reaction pathway followed that of the hydroboration of olefins, with

insertion of the pyridine into the lanthanum-hydride followed by σ-bond metathesis to yield the *N*-borylated-dihydropyridide with reformation of the lanthanum hydride. A zwitterionic complex was also identified through crystallographic techniques (Figure 1-7), synthesised from the reaction of Cp^*_2LaH with 1 equivalent of HBpin. Whilst an interesting complex, it was found that this species was catalytically inactive and represents a potential deactivation mechanism.

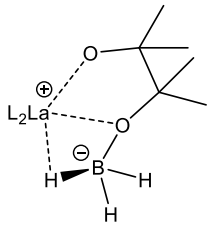

Figure 1-7. Zwitterionic complex, from the reaction of Cp^*_2LaH and HBpin

Kinetic studies provided the rate law (Equation 1-1) which was first order in [catalyst], inverse first order in [HBpin] but concentration dependant on [pyridine]. At low concentrations (less than 0.2 M) x was found to be first order, but approaching zero order at higher concentrations.

$$Rate = k_{obs} \frac{[La]^1[Pyr]^x}{[HBpin]^1}; x = 0 - 1$$

Equation 1-1. Experimentally derived rate law for the lanthanum-catalysed hydroboration of pyridines

This was interpreted to suggest a $Cp^*_2LaH(Pyr)_n$ resting state, with turnover limiting intramolecular C=N insertion, whilst the inverse dependence on HBpin implies a competing turnover-limiting-step with potential for irreversible catalyst deactivation (Scheme 1-31).

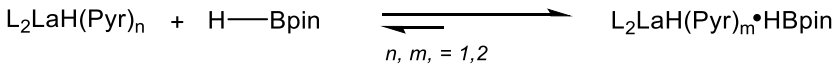

Scheme 1-31. Proposed inhibition by HBpin

Activation energy parameters were also calculated and provided a large negative $\Delta S^{\neq}$ which is characteristic of d^0 f^n centred hydroelementation reactions.[148, 149] A detailed computational study using DFT methods, which was then verified using the recently developed energetic span model was carried out.[150, 151] This suggested a similar catalyst resting state of $Cp^*_2LaH(Pyr)(HBpin)$ whilst identifying two rate-determining transition states (RDS). Firstly the dissociation of HBpin from the $Cp^*_2LaH(Pyr)$ active catalyst and secondly insertion of the pyridine C=N bond into the La-H bond, in agreement with experimental observations. Combination of these key steps leads to the following proposed mechanistic cycle (Scheme 1-32).

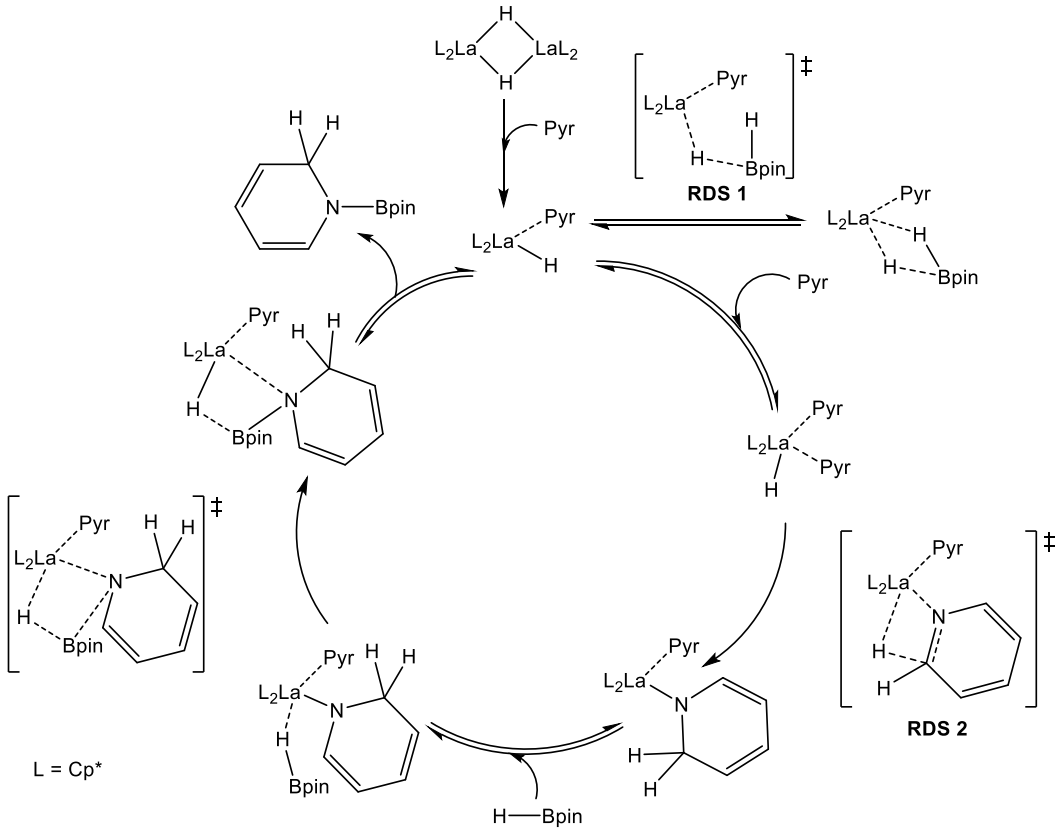

Scheme 1-32. Proposed mechanism for the lanthanum-mediated hydroboration of pyridines

The proposed mechanism is in agreement with the DFT-derived energetics of the system. Coordination of a pyridine causes break-up of the hydride dimer at which point HBpin can coordinate leading to an off cycle resting state which is catalytically inactive. Alternatively a further equivalent of pyridine can coordinate which then undergoes an intramolecular hydride transfer to yield the coordinated 1,2-dihydropyridide complex. Both of these steps are considered rate-determining but only one persists depending on the concentration of pyridine. At low pyridine concentration x = 1, RDS 1 prevails and HBpin has to dissociate in order to allow for the incoming pyridine molecule to insert into the metal hydride. At high pyridine concentration x = 0, insertion of the C=N bond into the metal-hydride is rate determining (RDS 2), as the high concentration of pyridine will shift the equilibrium for RDS 1 over to the left, thus, favouring the active catalyst ($Cp^*_2LaH(Pyr)$) and ruling out this pathway. Addition of HBpin to the complexed 1,2-dihyrdopyridide again proceeds *via* coordination/σ-bond metathesis to yield the desired product with regeneration of the active catalyst.

The first reported use of a well-defined low valent *p*-block metal hydride in catalytic synthesis was reported by Jones and co-workers.[152] Utilising very sterically demanding ligands (Figure 1-8) allowed for the synthesis of two coordinate, monomeric germanium (**XXXVa**) and tin

(**XXXVb**) hydrides which were efficient catalysts for the hydroboration of carbonyls. Fast turnover was observed using as little as 0.05 mol% with HBpin as the borane source.

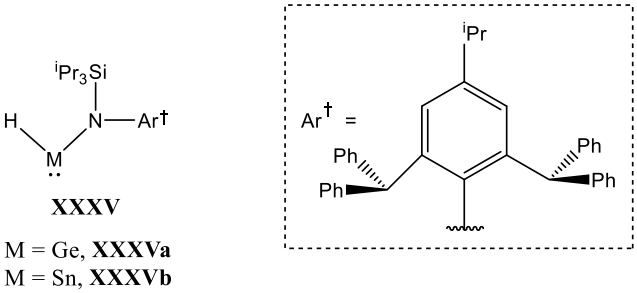

Figure 1-8. Low valent *p*-block monomeric metal hydrides used for the hydroboration of carbonyls

1.4.1 Group 2 mediated Hydroboration

As mentioned previously well-defined hydrocarbon soluble group 2 hydrides maybe synthesised from commercially available hydridic reagents (Scheme 1-13).[116] Harder *et al* reported the attempted hydroboration of alkenes, using 3 different calcium catalysts (**If, XV, XXXIIIa**) with HBcat. In each case, however, several products were observed in the ^{11}B NMR spectrum, which further analysis identified as BH_3 and B_2Cat_3, leading to the suggestion that calcium catalyses the decomposition of HBcat.[153] This has also been seen previously for lanthanide-based systems.[29] A stoichiometric reaction between the *β*-diketiminate supported calcium hydride (**VIII**) and HBpin provided an unusual trimeric calcium complex (**XXXVI**, Figure 1-9) with bridging $[H_2Bpin]^-$ anions which interact with the metal centre through both Ca-O and Ca-H bonds.

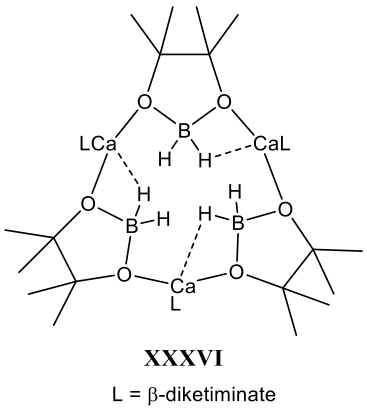

Figure 1-9. $[LCa(H_2Bpin)]_3$, isolated from the stoichiometric reaction of **VIII** and HBpin

Similar decomposition of HBcat in the presence of group 2 complexes was also noted by Hill and co-workers, leading them to turn their attention to the less electron withdrawing pinacol borane (HBpin). The latter showed efficient turnover with magnesium precatalyst (**Ib**) for the hydroboration of aldehydes and ketones.[154] Using as little as 0.05 mol% of **Ib** complete conversion of aldehydes to the fully reduced boron ester was observed in less than 1 hour (by NMR). This extremely active catalyst also provided high reactivity for ketone hydroboration whilst using 0.1 mol% of **Ib** enabled complete conversion in 2 hrs (Scheme 1-33).

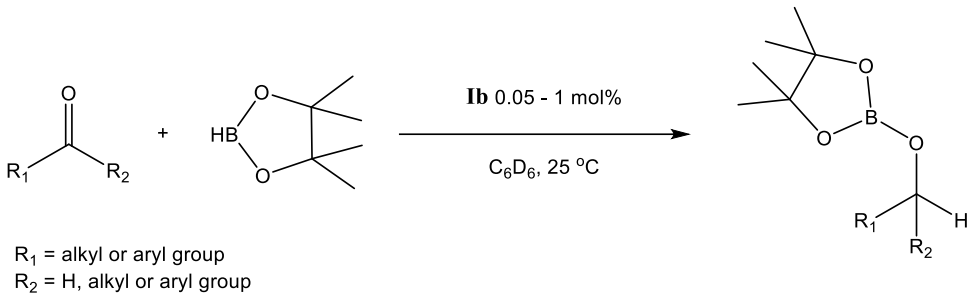

Scheme 1-33. Magnesium-catalysed hydroboration of aldehydes and ketones

After the success of the hydroboration of unsaturated C=O bonds the study was extended to unsaturated C=N bonds.[155] A variety of aldehyde- and ketone-derived imines were synthesised and then tested with regards to hydroboration. Reactions typically required 5 mol % of **Ib** and at room temperature near full conversion was observed (by NMR) in 2 hours for the aldehyde-derived imines. The bulkier ketone-derived imine substrates required mild heating (50 °C) and extended reaction times (up to 24 hours) to reach approximately 80% conversion.

The magnesium-catalysed hydroboration of both C=O and C=N bonds was suggested to proceed *via* mechanisms similar to those previously proposed for the hydridic lanthanide systems (Scheme 1-3 (b)). As seen below (Scheme 1-34) this proposed catalytic cycle is again based upon a series of σ-bond metathesis steps involving the B-H fragment and subsequent insertion reaction into the Mg-H bond.

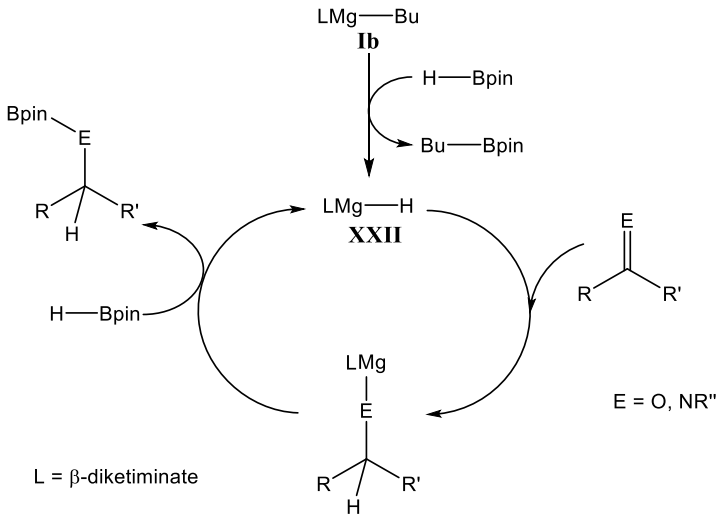

Scheme 1-34. Proposed mechanistic cycle for the magnesium-catalysed hydroboration of E=C unsaturated bonds

This proposed mechanism was supported by a series of stoichiometric reactions. Formation of **XXII** from **Ib** was found to occur readily as observed in both the ^{1}H and ^{11}B NMR spectra. Subsequent addition of PhCH=NPh provided an instant colour change to a bright-orange solution which faded over a period of three hours at room temperature. Analysis of the resulting ^{1}H NMR spectrum revealed the disappearance of the LMg*H* and aldimide signals at δ 4.00 ppm and δ 8.12 ppm respectively, to yield quantitative conversion to the amido complex. Addition of a further equivalent of HBpin for the final σ-bond metathesis step yielded the desired product ($PhCH_2N(Bpin)Ph$) as observed by NMR spectroscopy, however only ~10% of **XXII** was found to have regenerated. Further analysis of the NMR spectrum showed a complex splitting pattern in the *iso*-propyl C*H* region in the ^{1}H NMR spectrum, as well as a further singlet at δ 2.87 ppm which was suggested to be a result of adduct formation between the magnesium hydride and product. This was further confirmed by an additional signal in the ^{11}B NMR spectrum at δ 1.6 ppm compared to the product peak at δ 28.4 ppm.

Kinetic studies of this catalytic system also supported the proposed mechanism (Scheme 1-34). Reactions with both substrates consistently displayed second-order kinetics up to a period of three half-lives (80%). It was found to be first order with respect to [catalyst], thus supporting the monomeric nature of the magnesium centre during catalysis. Using a 10-fold excess of HBpin was found to inhibit the rate of reaction, thought to be a consequence of reversible borane coordination/de-coordination and consequently catalyst inhibition. A second order dependence was found with respect to imine concentration, suggesting that two molecules of imine are needed to facilitate turnover. The overall experimentally derived rate law is shown in Equation 1-2. It was proposed that the rate-determining Mg-H insertion is facilitated by the

ability of a secondary imine molecule to displace the HBpin from the coordination sphere of the active magnesium centre.

$$Rate = k' \frac{[cat][imine]^2}{[HBpin]_0}$$

Equation 1-2. Experimentally derived rate law for the magnesium-catalysed hydroboration of imines

A recent report by Harder *et al* has demonstrated the use of the bis-*β*-diketiminate magnesium complexes, **XXXI** and **XXXII**, for the catalytic hydroboration of pyridines.[156] Initial reactivity of these two complexes for the stoichiometric dearomatisation of pyridines mirrored that observed by Hill *et al*.[123, 124] In this case, however, the use of **XXXII** showed exclusive formation of 1,2-dihydropyridides. Although extension of this stoichiometric reactivity to catalytic hydroboration of pyridines, with HBpin, provided efficient turnover using **XXXI**, the previous regioselectivity of the stoichiometric reactions did not translate to the catalytic regime. **XXXII** was found to be inactive towards hydroboration of pyridines; this was thought to be due to the rigid nature of this hydride cluster. The explanation for this apparent lack of selectivity in the catalytic regime was proposed to be the result of an alternate mechanistic pathway which circumvents the magnesium hydride intermediate (Scheme 1-35).

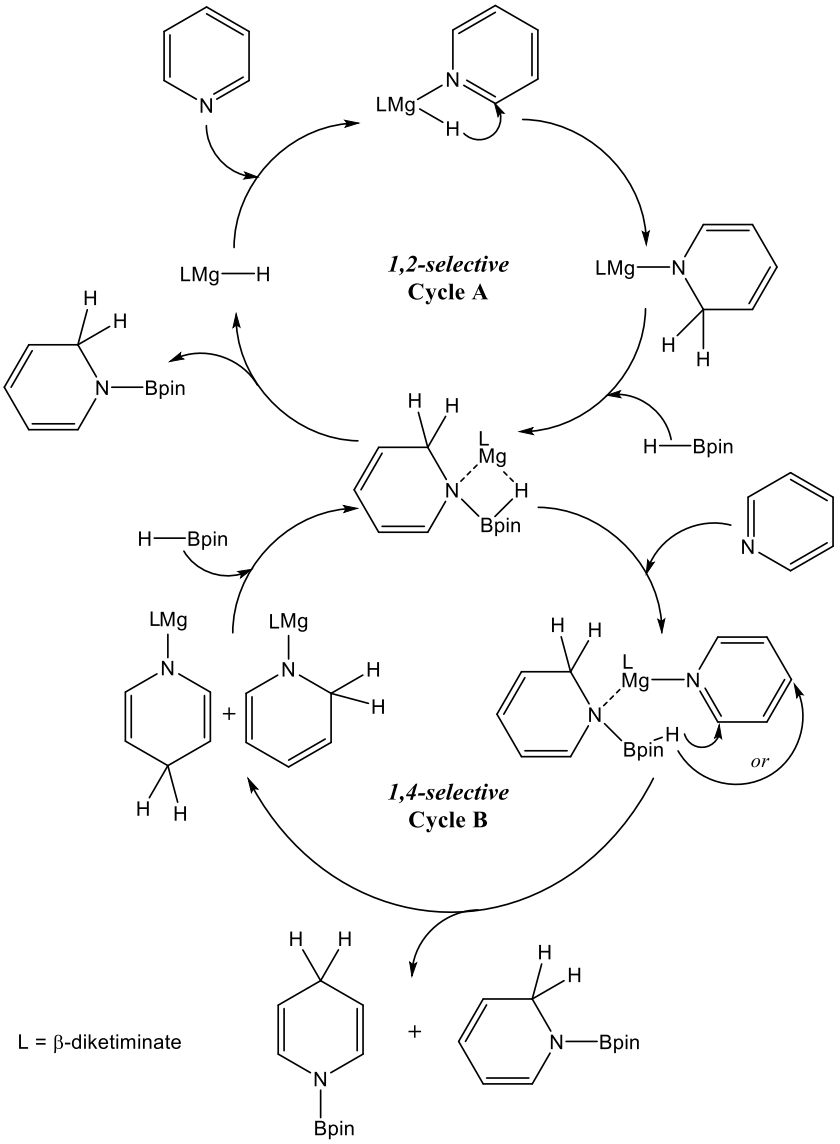

Scheme 1-35. Proposed mechanism accounting for the difference in regioselectivity observed with the magnesium-catalysed (**XXXI**) hydroboration of pyridines

The common intermediate in both of these cycles is a magnesium borate species, which was proposed to undergo σ-bond metathesis to yield the 1,2-isomer whilst regenerating the magnesium hydride (cycle A). Alternatively a subsequent pyridine molecule can coordinate to the magnesium centre allowing the hydride to transfer directly from the boron to either the 2- or 4- position. Subsequent σ-bond metathesis reactions complete the cycle and regenerate the borate intermediate (cycle B). It was also suggested that simple isomerisation of the initially formed 1,2-isomers could occur at the temperature of the catalysis (60 °C).

In related work Sadow and co-workers reported the use of magnesium catalyst, **IIa**, for the hydroboration of esters.[157] With two equivalents of HBpin this was found to be highly efficient and resulted in cleavage of the C-O bond to yield two alkoxyborane products in the presence of 0.5-5 mol% **IIa** at room temperature (Scheme 1-36).

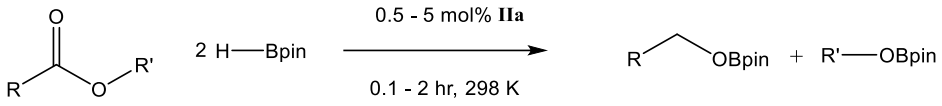

Scheme 1-36. Magnesium-catalysed hydroboration of esters

This system was also found to be tolerant to a series of functional groups such as cyano-, nitro-, cyclopropyl- and conjugated olefins showing selectivity for the ester group over 1,4-addition. To study the initiation step, **IIa** and 1 equivalent of HBpin reacted readily to generate MeBpin and an unstable magnesium hydride species. It was possible to isolate $LMgH_2Bpin$ through slow addition of **IIa** to 15 equivalents of HBpin. Alternatively, addition of EtOAc to **IIa** resulted in the formation of LMgOEt with production of acetone through a series of insertion and β-ethoxide elimination reactions. This was initially thought to provide a model for the C-O cleavage observed during the catalysis subsequent kinetic studies, however, ruled out this pathway. Initiation of **IIa** to give the magnesium hydride complex was found to be 20 times faster than LMgOEt formation. Kinetic studies provided the following rate law (Equation 1-3).

$$Rate = k'[Mg]^1[EtOAc]^{1/2}[HBpin]^0$$

Equation 1-3. Experimentally derived rate law for the magnesium-catalysed hydroboration of esters

Several mechanistic possibilities are ruled out by this rate law. Most importantly, neither of the σ-bond metathesis reactions is turnover limiting thus ruling out an insertion/ σ-bond metathesis pathway. According to the overall order of the reaction, turnover limiting reactions between either substrate and **IIa** would provide an overall second-order rate law rather than the observed overall 1/2 order rate law.

The half-order dependence on [EtOAc] indicated a reversible interaction of catalyst and ester to give ester cleavage prior to the turnover-limiting step. The ability of **IIa** to break the C-O bond was further supported by a series of cross-ester metathesis reactions. Sadow and co-workers provided evidence of the presence of LMg{EtO(H)Bpin} from *in situ* monitoring of a series of catalytic reactions. This was identified as the catalytic resting state as the only magnesium-containing species during the catalysis. Upon addition of EtOAc to this compound, product formation was observed, thus explaining the zero-order dependence on [HBpin] as the hydride reducing equivalent is already present in the catalyst resting state.

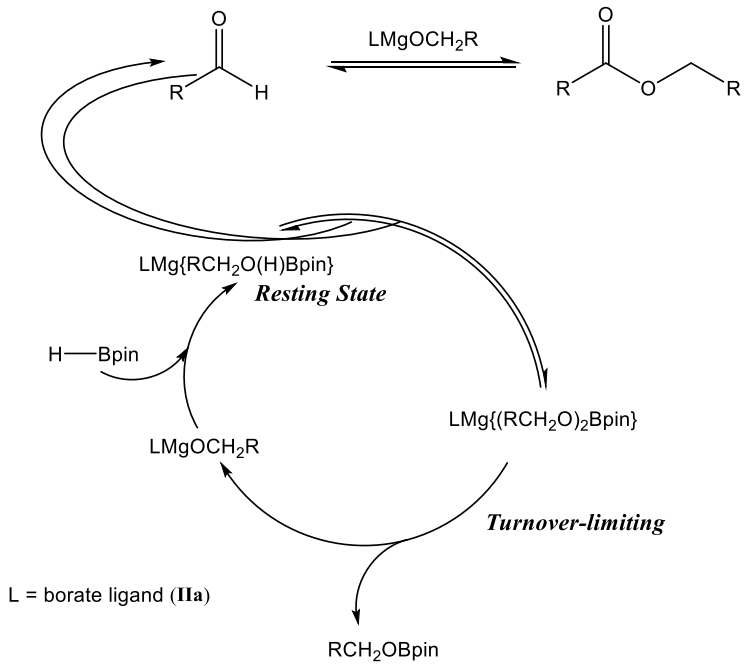

Scheme 1-37. Proposed mechanism for the magnesium-catalysed hydroboration of esters

Scheme 1-37 illustrates the proposed mechanism based on the experimentally derived rate law, and shows that the σ-bond metathesis and insertion reaction pathway proposed previously for group 2 catalysis is not followed in this reaction. Instead a 'zwitterionic' mechanism is proposed which highlights other bond making and bond-breaking pathways available in main group system.

Similar C-O cleavage reactions were observed by Hill and co-workers during the group 2 mediated hydroboration of CO_2. Using a strong Lewis acidic tris(pentafluorophenyl)boron (BCF) reagent to access *β*-diketiminate supported magnesium and calcium borohydrides, CO_2 was found to undergo selective reduction to a methanol equivalent, MeOBpin (Scheme 1-38).[158]

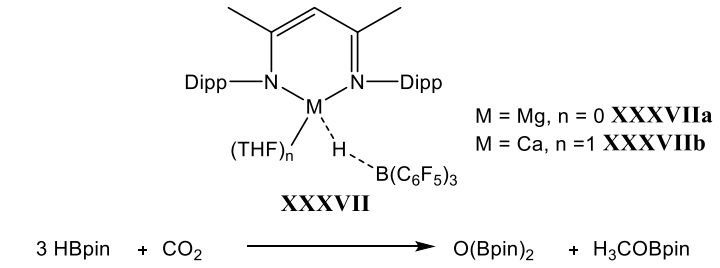

Scheme 1-38. BCF activated group 2 catalysts for the hydroboration of carbon dioxide

This initial report of the highly selective reduction of CO_2, is comparable to work by Piers and co-workers, in which BCF was shown to increase the reactivity of lanthanide hydrides.[159] Further mechanistic work on this system is ongoing, to understand the role in which BCF plays in activating the metal centre.

1.5 Aims of this thesis

Previous group 2 mediated heterofunctionalisation catalysis has largely focussed on using 'protic' reagents and extensive mechanistic studies have been undertaken in particular on hydroamination reactions. The research presented in this thesis aims to investigate the potential of the 'hydridic' type heterofunctionalisation catalyses using *β*-diketiminate supported magnesium hydride for the reduction of a range of unsaturated E=C bonds. This research was undertaken *via* a combination of synthetic and mechanistic investigations utilising NMR analysis for *in situ* reaction monitoring and kinetic investigations of both stoichiometric and catalytic reactions. Single crystal X-ray studies will also aim to provide evidence for catalytic resting states and the structural viability of catalytic intermediates.

Chapter 2 aims to explore the reactivity of a series of magnesium dihydropyridide complexes (**XXVII** and **XXVIII**) and their use as hydride transfer reagents. A series of stoichiometric reactions with a representative ketone, isocyanates and carbodiimides aim to assess the viability of this class of compounds for hydride reduction chemistry.

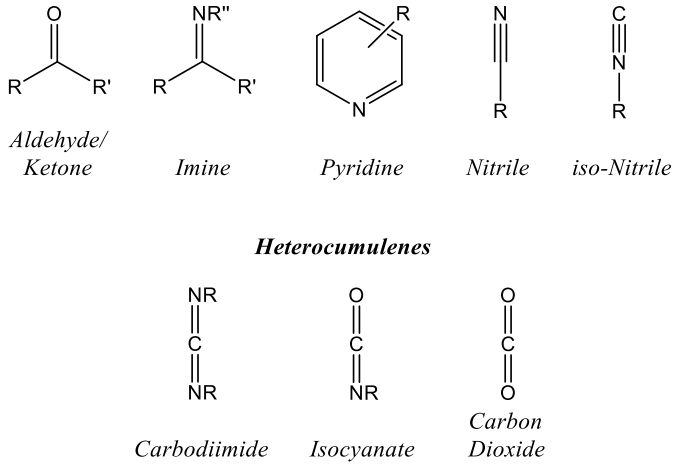

Figure 1-10. Variety of unsaturated organic substrates investigated

The subsequent chapters of this thesis focus upon the magnesium-catalysed hydroboration of a variety of unsaturated substrates (Figure 1-10), mediated by the pre-catalyst **Ib**. Building upon knowledge gained from the previously reported aldehyde/ketone and imine hydroboration studies this will be applied to a range of substrates, with the end goal being the reduction of CO_2. Furthermore studies into nitrile and *iso*-nitrile reagents aim to investigate the potential of this catalytic system for the complete reduction and double functionalization of C≡E triple bonds. The knowledge gained from these reduction studies will then be applied to heterocumulenes.

Chapter 2. Reactivity of Magnesium dihydropyridides with heterocumulenes

2.1 Introduction

Dihydropyridines are an important class of compound, as they are building blocks in a variety of natural products which makes them of great pharmaceutical interest. For example, dihydronicotinamide adenine dinucleotide (NADH) (Figure 2-1) and its phosphorylated analogue dihydronicotinamide adenine dinucleotide phosphate (NAD(P)H) are the primary biological reducing reagents for carbohydrate synthesis during the dark reactions of photosynthesis.[160, 161] The majority of bio-inspired and organocatalytic NADH analogues are based upon Hantzsch esters (HEH).[162]

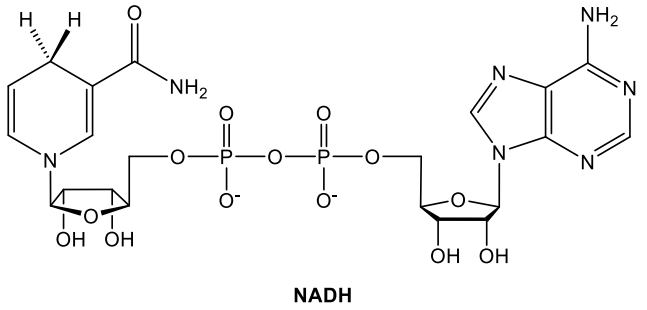

Figure 2-1. Naturally occurring dihydropyridine, NADH

Hantzsch reported that a mixture of aldehyde, a *β*-ketoester and ammonia in ethanol, heated under reflux for several hours, resulted in ring closure to produce the target dihydropyridine in good yields (Scheme 2-1). This multi-component synthesis allows for the synthesis of a large variety of dihydropyridine compounds, and has since been utilised to afford a wide range of active pharmaceutical reagents for the treatment of hypertension[163], calcium channel blockers in chemotherapy[164] and various anti-inflammatory,[165] anti-convulsant[166] and anti-tubercular agents.[167, 168]

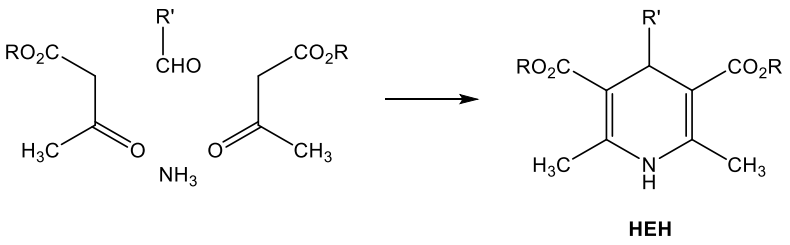

Scheme 2-1. Synthesis of Hantzsch esters (HEH) from multicomponent ring closure reactions

Alternate synthetic routes to dihydropyridines have been developed from metal based reduction reactions of pyridines affording the dearomatised metal-dihydropyridide complexes. This has subsequently led to further studies into the coordination and reaction chemistry of these dihydropyridide complexes which in some cases have shown them to act as hydride donors.[169-174] The most notable main group organohydride donor, Lansbury's reagent (Figure 2-2, **XXXVIII**), has been shown to selectively reduce ketones in the presence of carboxylic acid and ester groups.[175-179] These reactions are seemingly driven by the favourable re-aromatisation of the pyridine ring system; the propensity for re-aromatisation is shown by the limited number of examples of reaction chemistry in which the reduced fragment is retained.

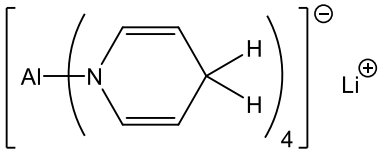

XXXVIII

Figure 2-2. Lansbury's Reagent

As shown in Scheme 1-15, using **Ib** with 2 equivalents of pyridine and a stoichiometric amount of $PhSiH_3$, affords two distinct magnesium 1,2 and 1,4-dihydropyridide complexes, **XXVI** and **XXVII** respectively. It is to be expected that these dihydropyridide complexes behave in a similar manner to **XXXVIII**. It has also recently been observed in studies of similarly d^0 and electropositive group 3 elements, scandium and yttrium, that heterocycle C-H activation and dearomatisation can be combined to give C-C coupling between the two heterocycles (Scheme 2-2).[180-182]

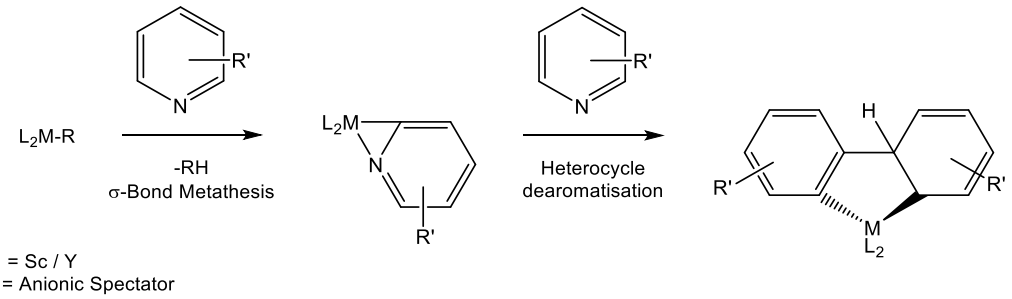

Scheme 2-2. Stoichiometric C-H activation and dearomatisation by group 3 complexes leading to C-C coupling of two pyridines

The ability of dihydropyridides to potentially undergo further reactivity as hydride transfer reagents is of great interest. The reactivity of a series of magnesium derivatives of monocyclic 1,4-dihydropyridides and the fused ring 1,2-isoquinolide with a range of polarised unsaturations and heterocumulenes was, thus, undertaken. Compounds **XXVIIa** (pyridine), **XXVIIc** (3-

picoline) and **XXVIId** (3,5-lutidine) were chosen due to their diagnostic ^{1}H NMR spectra and gradual adjustment of the pyridine steric demands.

2.2 Reactions with Carbonyl Functions

The ability of the magnesium-1,4-dihydropyridide complexes, **XXVIIa,c,d** and **XXVIII**, to act as hydride transfer reagents to electrophilic carbon centres, was demonstrated through an initial series of reactions with benzophenone (Scheme 2-3).

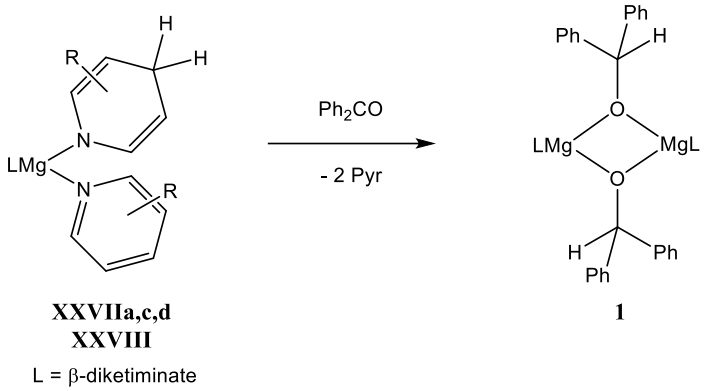

Scheme 2-3. Dihydropyridide complexes displaying hydride transfer to benzophenone

In all cases clean and efficient transfer of the hydride was observed to form the new magnesium diphenylmethoxide species (**1**). In each case rearomatisation of the corresponding pyridine was also identified in the ^{1}H NMR spectrum due to the loss of the alkenyl NC*H*=CH and NCH=C*H* resonances at ca. δ 6.5 and 4.5 ppm and subsequent increase in the intensity of the aromatic pyridine resonances ca. δ 8.5 and 7.5 ppm. Further evidence of the hydride transfer was given by the downfield shift of the protons of the dihydropyridide 4-positions from ca. δ 2.6 ppm to 6.15 ppm. Subsequent HSQC analysis showed a corresponding ^{13}C NMR resonance at δ 78.6 ppm characteristic of an α-alkoxide sp^3 carbon.

After the success of these hydride transfer reactions, a wider scope of reactivity with regards to aryl and alkyl isocyanates was undertaken with the expectation that similar hydride transfer to the central carbon of the isocyanate functional group and reduction to the formamidinate, may be observed. Using DippNCO (Dipp = 2,6-di-*iso*-propylphenyl) and MesNCO (Mes = 2,4,6-trimethylphenyl) as the aryl reagents of choice due to their clearly identifiable NMR resonances and differing steric demands, using AdNCO (Ad = 1-adamantyl) and *tert*-ButylNCO as representative alkyl reagents, again for their diagnostic NMR resonances, a series of stoichiometric reactions was carried out.

2.2.1 Reactivity of 1,4-dihydropyridides and substituted 1,4-dihydropyridides

Further reactivity of magnesium-1,4-dihydropyridides initially focussed upon the use of the non-substituted pyridine substrate, **XXVIIa**. Addition of a stoichiometric amount of DippNCO to solution of **XXVIIa** resulted in immediate decolouration of the bright yellow solution to provide a pale yellow solution. Analysis of the resultant ^{1}H NMR spectrum indicated the retention of the dearomatised fragment suggesting insertion of the isocyanate into the Mg-N bond of the coordinated dihydropyridide anion had occurred. This was confirmed through the observation in the ^{13}C NMR spectrum of a new resonance at δ 115.2 ppm which was shown through corresponding HSQC analysis not to correlate to any proton, thus confirming the presence of the N_2CO ureide core (Scheme 2-4, compound **2**).

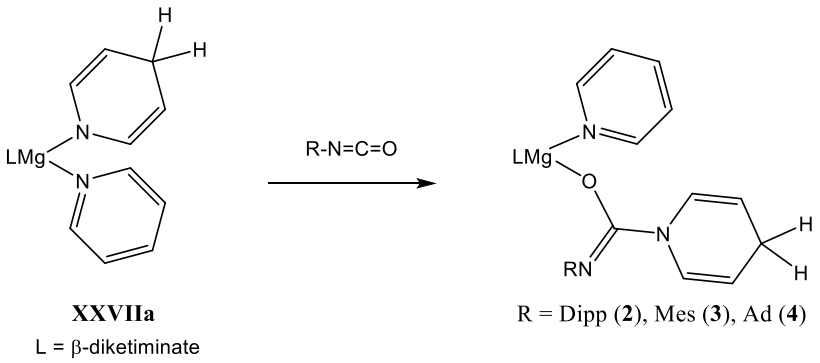

Scheme 2-4. Insertion of RNCO into magnesium-dihydropyridide complex **XXVIIa**

Similar reactions using MesNCO and AdNCO also provided instantaneous decolouration of the NMR scale reaction upon addition of the isocyanates, and the corresponding NMR spectra were again indicative of isocyanate insertion to form new ureide complexes (**3** and **4**) respectively. The respective ^{1}H NMR spectrum also confirmed that the dearomatised dihydropyridide anion had been retained through observation of the sp^3 hybridised CH_2 multiplet at ca. δ 2.6 ppm.

Subsequent scale up reactions enabled the isolation of single crystals of compound **2** from a toluene solution, whereupon crystallographic analysis confirmed the proposed identity of the product (Figure 2-3).

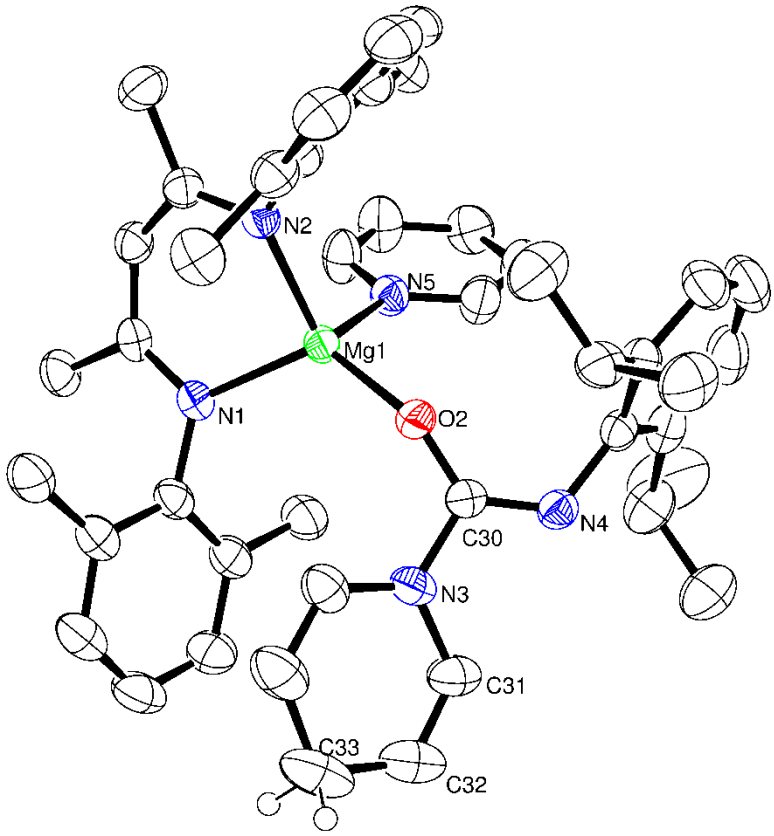

Figure 2-3. ORTEP representation of compound **2** with thermal ellipsoids set at 25% level of probability. Hydrogen atoms except those attached to C(33) and the methyl groups of the *β*-diketiminate 2,6-di-*iso*-propylphenyl substituents are removed for clarity. Selected bond lengths (Å) and angles (°): Mg(1)-N(1) 2.0528(15), Mg(1)-N(2) 2.0545(16), Mg(1)-O(2) 1.8921(13), Mg(1)-N(5) 2.1341(16), N(3)-C(30) 1.414(2), N(4)-C(30) 1.285(2), O(2)-C(30) 1.296(2), O(2)-Mg(1)-N(1) 121.70(6), O(2)-Mg(1)-N(2) 124.70(6), N(1)-Mg(1)-N(2) 94.34(6), O(2)-Mg(1)-N(5) 105.38(6), N(1)-Mg(1)-N(5) 106.86(6), N(2)-Mg(1)-N(5) 101.35(6), C(30)-O(2)-Mg(1) 147.97(11).

Figure 2-3 shows the 4-coordinate magnesium complex, **2**. The magnesium coordination sphere comprises the bidentate *β*-diketiminate ligand, a neutral pyridine molecule and the ureide ligand resulting from DippNCO insertion which binds exclusively through the oxygen donor atom. The Mg-O distance [1.8921(13) Å] is comparable to that reported by Chisholm for a terminal *β*-diketiminato magnesium *tert*-butoxide complex [1.844(2) Å][183] and Fedushkin's series of terminally oxygen-bound magnesium enolates supported by a 1,2-bis{(2,6-diisopropylphenyl)imino}acenaphthene ligand [range, 1.8902(19) – 1.9212(18) Å] in which the magnesium centres are five-coordinate.[184] Although formally the bonds between the dihydropyridide anion and isocyanate are consistent with single (C(30)-N(3) [1.414(2) Å]) and double bonds (C(30)-N(4) [1.285(2) Å]) respectively, the co-planarity of the O(2), N(3) and N(4) with the sp^2 hybridised C(30) carbon centre [$\Sigma_{(angles)}$ = 360°] are indicative of significant delocalisation across the ureide CON_2 unit.

In contrast to these observations, the reaction of **XXVIIa** with 1 equivalent of *tert*-BuNCO gave no immediate colour change and subsequent NMR analysis indicated that no reaction had occurred at room temperature. After heating at 80 °C for 12 hours, decolouration of the solution was observed and conversion to a new single product (compound **5**) was observed in the corresponding NMR spectrum. This was identified as the desired hydride transfer product due to the loss of all NMR resonances corresponding to the 1,4-dihydropyridide anion and subsequent increase in intensity of the rearomatised pyridine signals (Scheme 2-5). Also observed in the ^{1}H NMR spectrum was a singlet at δ 7.03 ppm corresponding to the formamidate species.

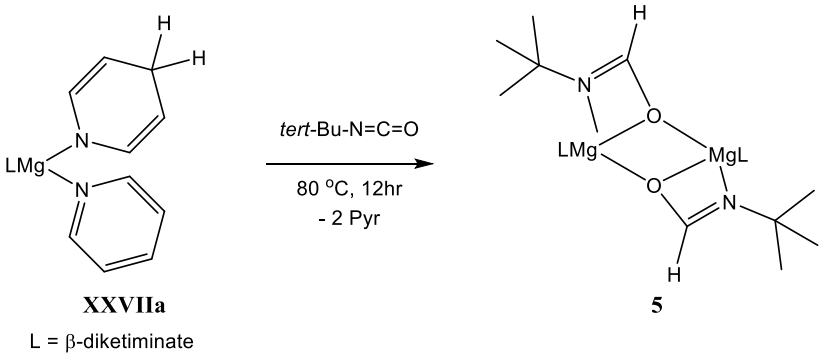

Scheme 2-5. Hydride transfer from **XXVIIa** to *tert*-BuNCO

Extension of this reactivity to substituted monocyclic pyridide complexes, specifically 1,4-dihydro-3-picoline (**XXVIIc**), with the same range of isocyanates provided insertion into the Mg-N bond to form the ureide species in all cases (Scheme 2-6). In each case the retention of the dihydropyridide anion could clearly be seen in the ^{1}H NMR spectrum due to retention of the alkenyl resonances of the NC*H*=CH (ca. δ 6.8 ppm) and NCH=C*H* (ca. δ 4.5 ppm) units along with observation of a new sp^2 ^{13}C{^{1}H} NMR resonance at ca. δ 115 ppm in the NMR spectrum. Further confirmation of the formation of the ureide complexes for DippNCO (compound **6**) and MesNCO (compound **7**) was gained from mass spectrometry. In both cases the $[M]^+$ parent cation was observed for the corresponding hydrolysed product.

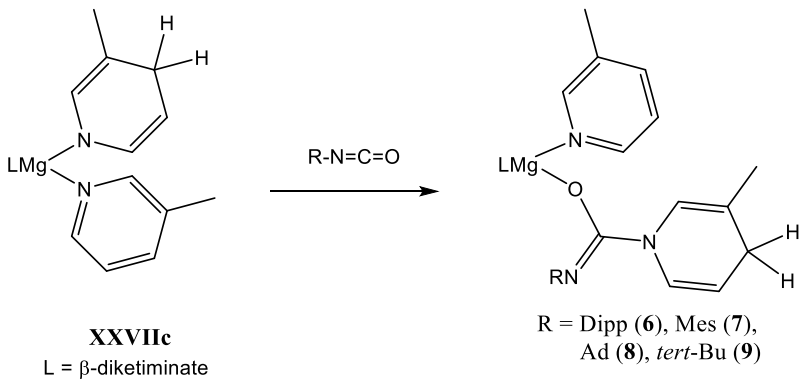

Scheme 2-6. Isocyanate insertion reactions with **XXVIIc**

The steric demands of the pyridide substrate were increased through use of the 1,4-dihydro-3,5-lutidide complex (**XXVIId**). Again instant decolouration of the bright orange solution was observed upon addition of each isocyanate. DippNCO (compound **10**), MesNCO (compound **11**), and *tert*-BuNCO (compound **13**) were all observed to insert into the Mg-N bond to form the ureide species (Scheme 2-7) as identified by NMR analysis and mass spectrometry.

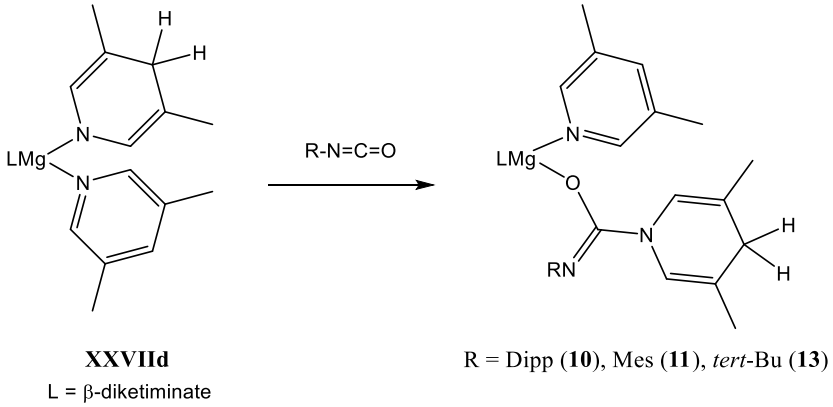

Scheme 2-7. Isocyanate insertion reactions with **XXVIId**

Confirmation of the formation of the insertion products was provided through crystallographic analysis of single crystals isolated from the scale up reaction of **XXVIId** with *tert*-BuNCO (Figure 2-4). Whilst an instant colour change was also observed upon addition of AdNCO to a solution of **XXVIId** (Scheme 2-8), 2 products were identified in the resulting ^{1}H NMR spectrum, in an approximate 70:30 ratio. The major product, compound **12a**, was identified as the formamidate species due to the observed rearomatisation of 1,4-dihydro-3,5-lutidide, and a NC*H*O 1H singlet resonance (δ 6.19 ppm) in the ^{1}H NMR spectrum comparable to that observed for compound **5** (δ 7.03 ppm). Compound **12b** was identified as the Mg-N insertion product from the retention of the dearomatised 1,4-dihydropyridide fragment. The constitution of the major product was confirmed, after fractional crystallisation, by single crystal X-ray diffraction analysis, as the formamidinate resulting from hydride transfer to the central carbon of the isocyanate functional group (Figure 2-5).

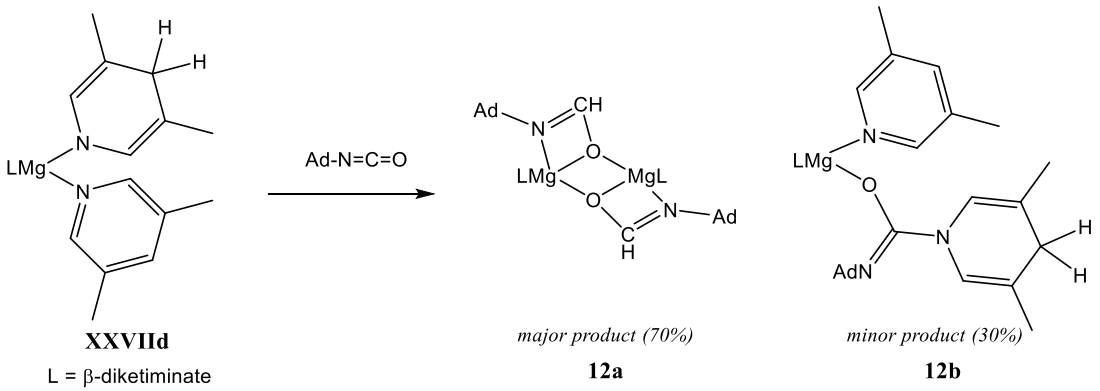

Scheme 2-8. 1-Adamantyl isocyanate insertion with **XXVIId**

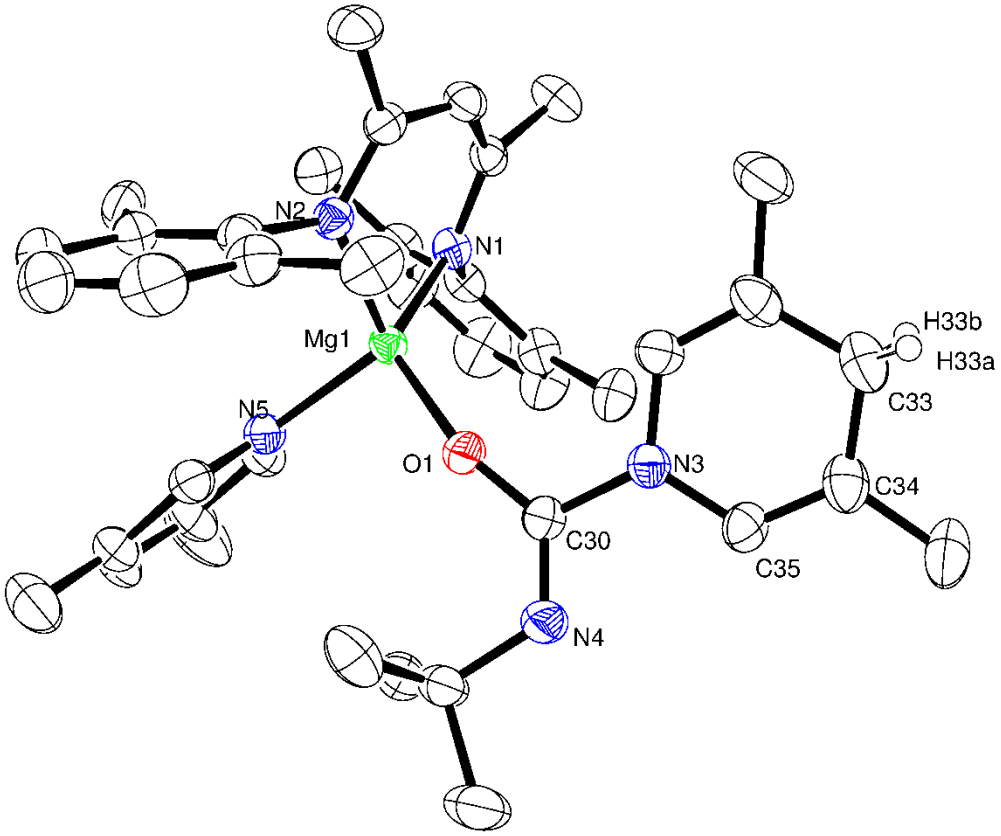

Figure 2-4. ORTEP representation of compound **13** with thermal ellipsoids set at 25% level of probability. Hydrogen atoms except those attached to C(33) and the methyl groups of the *β*-diketiminate 2,6-di-*iso*-propylphenyl substituents are removed for clarity. Selected bond lengths (Å) and angles (°): Mg(1)-N(1) 2.0442(15), Mg(1)-N(2) 2.0406(15), Mg(1)-O(1) 1.8804(12), Mg(1)-N(5) 2.1033(15), N(3)-C(30) 1.437(2), N(4)-C(30) 1.275(2), O(1)-C(30) 1.296(2), O(1)-Mg(1)-N(2) 114.99(6), O(1)-Mg(1)-N(1) 124.81(6), N(2)-Mg(1)-N(1) 93.29(6), O(1)-Mg(1)-N(5) 100.07(6), N(2)-Mg(1)-N(5) 111.93(6), N(1)-Mg(1)-N(5) 112.24(6), C(30)-O(1)-Mg(1) 158.59(12).

Compound **13** is structurally similar to compound **2**. A 4-coordinate magnesium centre is again observed which is bound by the *β*-diketiminate ligand, a neutral 3,5-lutidine molecule and the ureide anion. Key bond lengths are also comparable between the two complexes; Mg-O [**2** 1.8921(13); **13** 1.8804(12) Å], C(30)-N(3) [**2** 1.414(2), **13** 1.437(2) Å], C(30)-N(4) [**2** 1.285(2), **13** 1.275(2) Å]. Retention of the dihydropyridide anion is also confirmed due to the easily identifiable sp^3 carbon (C33) leading to a noticeable puckering of the ring system.

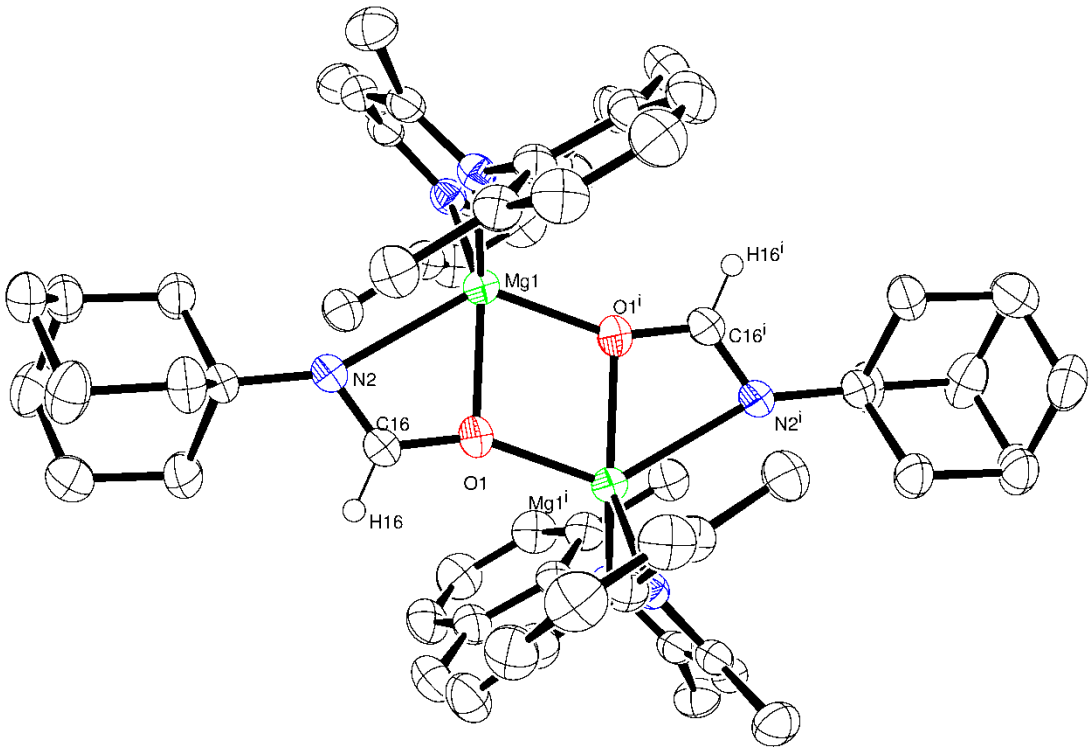

Figure 2-5. ORTEP representation compound **12a** with thermal ellipsoids set at 25% level of probability. Hydrogen atoms except those attached to C(16) and the methyl groups of the *β*-diketiminate 2,6-di-*iso*-propylphenyl substituents are removed for clarity. Selected bond lengths (Å) and angles (°), Mg(1)-O(1)^{i} 2.0013(18), Mg(1)-O(1) 2.0785(18), Mg(1)-N(1)^{ii} 2.0839(13), Mg(1)-N(1) 2.0839(13), Mg(1)-N(2) 2.4344(18), O(1)-C(16) 1.312(3), O(1)^{i}-Mg(1)-N(1)^{ii} 110.49(5), O(1)-Mg(1)-N(1)^{ii} 132.46(4), O(1)^{i}-Mg(1)-N(1) 110.49(5), O(1)-Mg(1)-N(1) 132.46(4), N(1)^{ii}-Mg(1)-N(1) 92.29(7), O(1)^{i}-Mg(1)-N(2) 130.69(7), O(1)-Mg(1)-N(2) 58.02(6), N(1)^{ii}-Mg(1)-N(2) 103.01(5), N(1)-Mg(1)-N(2) 103.01(5). Symmetry transformations used to generate equivalent atoms: ^{i} -x+2,-y,-z+1, ^{ii} x,-y,z, ^{iii} -x+2,y,-z+1.

The dimeric *N*-adamantyl formamidate complex **12a** contains two five-coordinate magnesium centres, each coordinated by a *β*-diketiminate ligand, and a *N*,*O*-chelating formamidate ligand, with dimer formation *via* μ^2-O bridging interactions. The asymmetric unit of compound **12a** contains one quarter of the dimer molecule with Mg(1), O(1), N(2), C(16), H(16) and C(17) located on a mirror plane which combined with an inversion centre proximate to Mg(1), generates the equivalent atoms. Additional problems caused by the high symmetry resulted in disordering of the adamantane cage over 2 sites, with the exception of C(17). The central Mg_2O_2 ring within **12a** displays similar Mg-O bond lengths Mg(1)-O(1)' [2.0013(18) Å] and Mg(1)-O(1) [2.0785(18) Å] and the C(16)-N(2) distance [1.250(3) Å] is indicative of significant localised imine character within the amidate ligand structure. The bridging motif is reminiscent of that observed in the only previously reported magnesium amidate complex, the heterobimetallic acetamidate $[Me_2Al(i\text{-}Et_2N)_2Mg\{(Ph)NC(CH_3)O\}]_2$ and in the bridging R_2NCO^{2-} ligands of several magnesium carbamate structures.[185, 186]

2.2.2 Reactivity of fused ring 1,2-isoquinolides

The thermodynamically preferred 1,4-dihydropyridide ligands have been utilised for all reported organocatalytic and biologically occurring organohydride donors, eg. NADH (Figure 2-1),[187] implying that 1,4-dearomatisation is necessary for hydrogen transfer reactivity. Conversely Diaconescu and co-workers reported the use of 1,2-dearomatised *iso*-quinolides, in which the 1,4-position is blocked by a fused aromatic system, for the reduction of ketones to the corresponding alkoxide.[188]

In a similar manner, the previously reported *iso*-quinolide complex (**XXVIII**) was reacted with 1 equivalent of benzophenone. Observations consistent with those associated with formal hydride transfer to form the alkoxide were noted, similar to those identified in Scheme 2-3 for complexes **XXVIIa,c,d**. This observation confirmed that 1,2-dearomatised complexes can still act as hydride transfer reagents, and the study was thus extended to an investigation of the reactivity of **XXVIII** with isocyanates.

The reactivity of **XXVIII** was examined with AdNCO and *tert*-ButylNCO. In these cases, a different course of reaction was observed compared to the previous reactions with **XXVIIa,c,d** producing complexes **14** (AdNCO) and **15** (*tert*-BuNCO). In both cases analysis of the resulting NMR spectra after addition indicated retention of the 1,2-dihydro-*iso*-quinolide methylene signals at δ 3.54 ppm and δ 4.12 ppm respectively. The AB doublet system at δ 6.4 ppm and δ 5.6 ppm, however, arising from the dearomatised methine NCH=CH protons were no longer observed in the ^{1}H NMR spectrum. Rather a singlet resonance corresponding to 1H, by integration, was observed at δ 6.63 ppm (**14**) and δ 5.86 ppm (**15**). In addition, a broad N*H* singlet resonance, also integrating to 1H, was observed at δ 4.14 ppm for complex **15**.

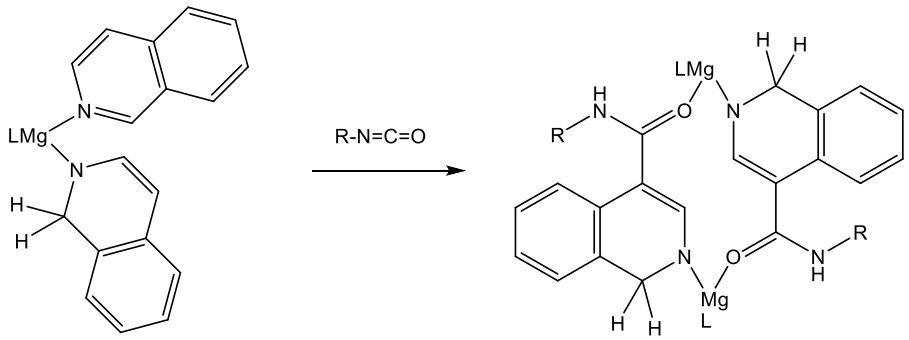

XXVIII
L = β-diketiminate

R = Ad (**14**), *tert*-Bu (**15**)

Scheme 2-9. Addition reactions of **XXVIII** with bulky alkyl isocyanates to form C-C coupled products **14** & **15**

These observations were confirmed through analysis of single crystals of **14** suitable for X-ray crystallography, the results of which are illustrated in Figure 2-6. Compound **14** consists of a

dimeric magnesium complex containing a dodecameric heterocyclic centre. In each case the 4-coordinate magnesium is coordinated by the bidentate *β*-diketiminate ligand, a formally covalent bond to the *iso*-quinolide ring [Mg(1)-N(3) 2.0627(15), Mg(2)-N(7) 2.0593(15) Å] and a formally dative covalent Mg-O interaction [Mg(1)-O(1) 1.9670(12), Mg(2)-O(2) 1.9530(12) Å] to the carbonyl group of the adamantyl amide substituent.

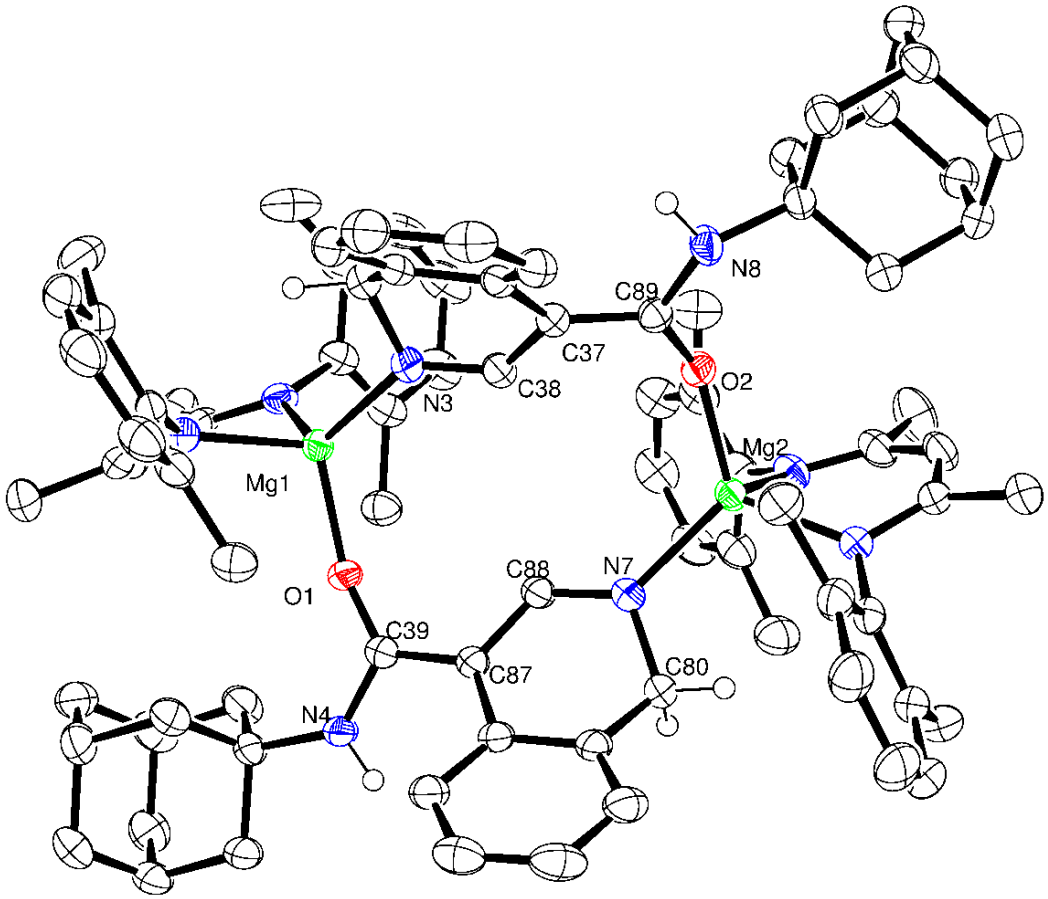

Figure 2-6. ORTEP representation of compound **14** with thermal ellipsoids set at 25% level of probability. Hydrogen atoms except those attached to C(30), C(80), N(4) and N(8) and the methyl groups of the *β*-diketiminate 2,6-di-*iso*-propylphenyl substituents are removed for clarity. Selected bond lengths (Å) and angles (°), Mg(1)-N(1) 2.0547(15), Mg(1)-N(2) 2.0703(14), Mg(1)-O(1) 1.9670(12), Mg(1)-N(3) 2.0627(15), N(3)-C(30) 1.483(2), N(4)-C(39) 1.348(2), O(1)-C(39) 1.2722(19), O(1)-Mg(1)-N(1) 108.94(6), O(1)-Mg(1)-N(3) 120.92(6), N(1)-Mg(1)-N(3) 109.17(6), O(1)-Mg(1)-N(2) 102.46(5), N(1)-Mg(1)-N(2) 92.81(6), N(3)-Mg(1)-N(2) 118.77(6), O(2)-Mg(2)-N(6) 105.94(6), O(2)-Mg(2)-N(5) 111.15(6), N(6)-Mg(2)-N(5) 92.49(6), O(2)-Mg(2)-N(7) 117.35(6), N(6)-Mg(2)-N(7) 115.62(6), N(5)-Mg(2)-N(7) 111.51(6).

Comparison with the X-ray structure of the isolated dearomatised *iso*-quinolide species (**XXVIII**) showed similar bond lengths for the dearomatised ring (Figure 2-7); N(3)-C(30) [1.468(3) Å] and N(7)-C(80) [1.480(2) Å]; C(30)-C(31) [1.502(3) Å] and C(80)-C(81) [1.500(2) Å]; and C(31)-C(32) [1.422(4) Å] and C(81)-C(86) [1.407(2) Å].

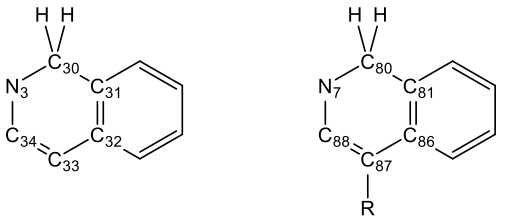

XXVIII **14**
1,3 addition

Figure 2-7. Comparison of *iso*-quinolide fragments for the starting complex, **XXVIII**, and the 1,3-addition product, **14**

Elongation of the C(88)-C(87) [1.393(2) Å] and C(87)-C(86) [1.468(2) Å] bonds was observed compared to C(34)-C(33) [1.366(3) Å] and C(33)-C(32) [1.431(4) Å] for **XXVIII**. This is likely a consequence of the removal of electron density from the double bond towards the N*C*O unit of the addition product. As a consequence of this N(7)-C(88) [1.321(2) Å] is slightly shorter in the addition product compared to the **XXVIII**, N(3)-C(34) [1.356(3) Å]. The retention of the dearomatised nature of compound **14** is also confirmed through the *pseudo*-tetrahedral geometry around the C(30) and C(80) methylene carbon centres.

Reactivity using less sterically demanding alkyl isocyanates was also investigated to further assess the implications of the variation in RNCO steric demands on this system. Using *i*-PrNCO and EtNCO, immediate decolouration of the reaction mixture was observed. Subsequent NMR analysis identified full retention of the dearomatised fragment, indicating insertion of the isocyanate to form the ureide complexes (*i*Pr **16**, Et **17**) had likely occurred. These observations were further confirmed by single crystal X-ray diffraction analysis performed on compound **16** (Figure 2-8).

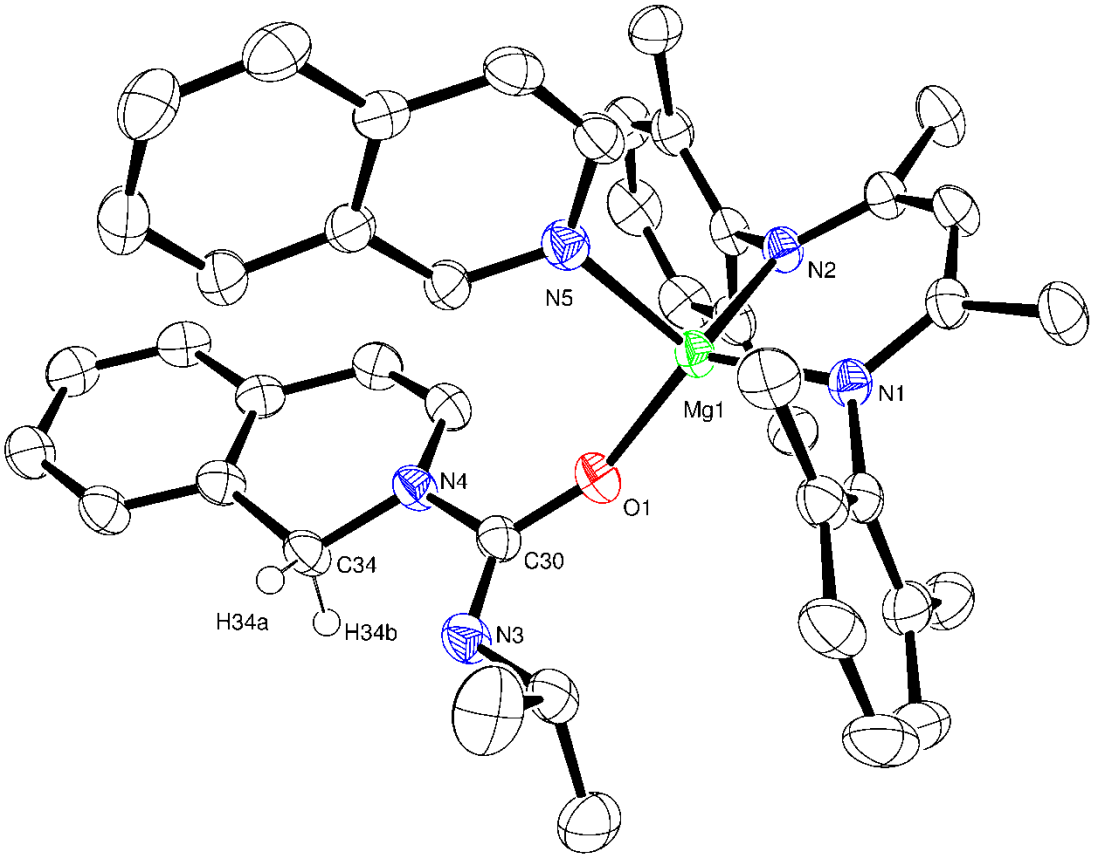

Figure 2-8. ORTEP representation of compound **16** with thermal ellipsoids set at 25% level of probability. Hydrogen atoms except those attached to C(34) and the methyl groups groups of the *β*-diketiminate 2,6-di-*iso*-propylphenyl substituents are removed for clarity. Selected bond lengths (Å) and angles (°), Mg(1)-N(1) 2.0344(14), Mg(1)-N(2) 2.0368(14), Mg(1)-O(1) 1.8787(12), Mg(1)-N(5) 2.1129(15), N(3)-C(30) 1.283(2), N(4)-C(30) 1.421(2), O(1)-C(30) 1.3013(2), O(1)-Mg(1)-N(1) 123.84(6), O(1)-Mg(1)-N(2) 118.24(6), N(1)-Mg(1)-N(2) 94.25(6), O(1)-Mg(1)-N(5) 102.39(6), N(1)-Mg(1)-N(5) 107.62(6), N(2)-Mg(1)-N(5) 110.10(6), C(30)-O(1)-Mg(1) 151.91(11), C(2)-N(1)-C(18) 118.51(13), C(2)-N(1)-Mg(1) 121.16(11), C(18)-N(1)-Mg(1) 120.28(10).

Figure 2-8 shows the ureide complex **16**, which is structurally similar to compounds **2** and **13**. Again the 4-coordinate magnesium centre is coordinated by the bidentate *β*-diketiminate ligand, a neutral *iso*-quinoline molecule and the ureide anion which confirms the insertion of the C=O bond into the Mg-N bond of the *iso*-quinolide ligand. Key bond lengths are also comparable across the 3 complexes (Table 2-1).

Table 2-1. Comparison of bond lengths (Å) for compounds **2, 13** & **16**

Compound	**2**	**13**	**16**
Mg-O	1.8921(13)	1.8804(12)	1.8787(12)
C(30)-N(3)	1.414(2)	1.437(2)	1.283(2)
C(30)-N(4)	1.285(2)	1.275(2)	1.421(2)

Reactions of **XXVIII** with aryl isocyanates provided immediate decolouration of the red wine colour to a pale red solution with both DippNCO and MesNCO. Although immediate NMR analysis evidenced the loss of *iso*-quinolide methine NC*H*=CH and NCH=C*H* resonances, the *iso*-quinolide methylene resonance at δ 4.2 ppm was still observed. Upon leaving the solution at room temperature overnight the pale red solution became colourless and subsequent NMR analysis showed loss of the 1,2-dihydro resonance as well as loss of the *β*-diketiminate backbone methine resonance (ca. δ 5.0 ppm) in the ^{1}H NMR spectrum. Also noted was a new 2H singlet, by integration, at ca. δ 3.3 ppm.

Monitoring the reaction of **XXVIII** with 1 equivalent of MesNCO over a period of 12 hrs at room temperature with ^{1}H NMR spectra recorded at set time intervals (Figure 2-9) revealed that the disappearance of the *β*-diketiminate methine singlet was coincident with the increase in intensity of a new 2H singlet at δ 3.3 ppm, concomitant with simplification of the two distinct 2H *iso*-propyl methine resonances to one 4H septet. This is proposed to result from protonolysis of the *β*-diketiminate ligand, which remains bound to the magnesium centre as the neutral bis(imine) form of the ligand.

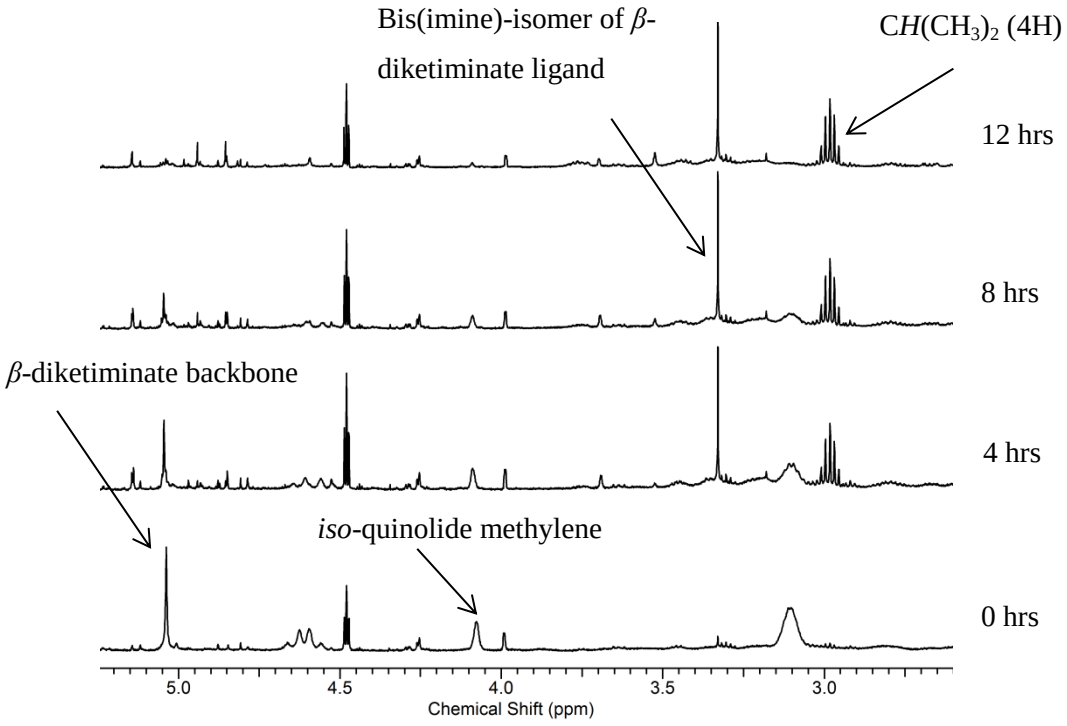

Figure 2-9. Series of stacked ^{1}H NMR spectra, in d_8-Tol, for the room temperature reaction of **XXVIII** and MesNCO

Further ^{13}C{^{1}H} NMR analysis of both the DippNCO- and MesNCO-based reactions identified a resonance shift in the central carbon of the isocyanate functional group from ca. δ 125 ppm to ca. δ 53 ppm, indicating a reaction with the isocyanate had occurred. HSQC analysis found the resonance at δ 53 ppm in the ^{13}C NMR spectrum to correlate with a 1H singlet at ca. δ 3.70

ppm, suggesting that hydride transfer had occurred in a manner similar to that observed in the reaction of **XXVIIa,c,d** with benzophenone. Upon comparison with the previous formamide species (**5** & **12a**), however, in this case the NC*H*O resonance was found to be considerably shifted upfield (δ 7.03 ppm and δ 6.19 ppm, respectively).

Subsequent analysis by mass spectrometry of the hydrolysed product found the parent ion to correspond to the proposed formulae $C_{22}H_{25}N_2O$ (335.2123 *m/z*) and $C_{19}H_{21}N_2O$ (293.1654 *m/z*) for the DippNCO and MesNCO products, respectively. This suggested that the product contained both the aryl isocyanate and *iso*-quinoline molecules. Based upon these findings and the NMR analysis, it is thus tentatively suggested that the magnesium centre is coordinated to the neutral diimine ligand, with the charge of the dication being balanced through *N*,*O*-chelation from a hemiaminalate dianion. The rearomatisation of the *iso*-quinoline molecule is proposed to arise from a similar C-C coupling process to that observed with **XXVIII** and Ad- and *t*-BuNCO, with subsequent proton transfer from the dihydroquinolide to the central carbon atom of the isocyanate fragment and rearomatisation (Scheme 2-10).

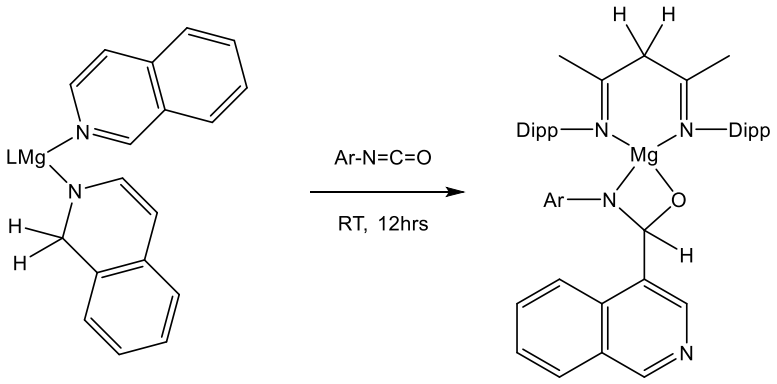

XXVIII
L = β-diketiminate

Ar = Dipp (**18**), Mes (**19**)

Scheme 2-10. Reaction of **XXVIII** with aryl isocyanates to give the proposed products **18** & **19**

Synthesis of **XXVIII-d$_7$** was carried out using d_7-*iso*-quinoline and $PhSiH_3$, to yield the desired complex with a CDH methylene unit in the 2 position of the 1,2-dihydroquinolide. This species was then reacted with 1 eq. of MesNCO and monitored at regular intervals in order to follow the course of the hydride, to determine whether or not this protonates the ligand or reduces the isocyanate. Unfortunately this procedure yielded inconclusive results, with broad overlapping signals observed in the resulting NMR spectrum. It is, however, proposed that the reaction of **XXVIII** with ArNCO proceeds as depicted in Scheme 2-11, *via* a C-C coupling reaction at the C4-position to form the aryl amide, which is sufficiently acidic to protonate the *β*-diketiminate ligand. This may be further driven by concomitant rearomatisation of the *iso*-quinoline fragment.

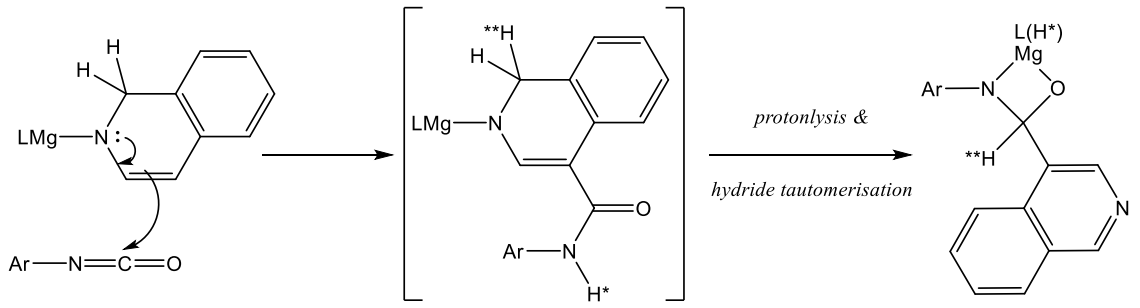

Scheme 2-11. Proposed mechanism for the reaction of **XXVIII** with ArNCO

These observations of the reactivity of **XXVIII** indicate that the outcome of the reactions is dependent upon the electronic nature and steric demands of the *N*-substituent of the isocyanate. Variations in *N*-substituent identity have been reported to provide only minor inductive modulation of the basicity of organic isocyanates.[189] Both aryl and bulky R groups undergo C-C coupling reactions at the C^4 position, with subsequent ligand protonolysis in the case of the aryl isocyanates. A kinetic preference depending on the alkyl isocyanate reagent is observed, with the ability of the isocyanate to pre-coordinate to the Mg centre likely to be the major contributing factor to the outcome of the reaction. It has previously been demonstrated that this pre-coordination step is vital for the related catalytic guanylation reactions of carbodiimides with lithium or aluminium amides.[190] The less sterically demanding substrates *N*-ethyl and *N*-*iso*-propyl isocyanate are therefore able to pre-coordinate to the magnesium centre with subsequent intramolecular N-C bond formation through migration of the nucleophilic *iso*-quinolide to the central *sp* carbon of the isocyanate.

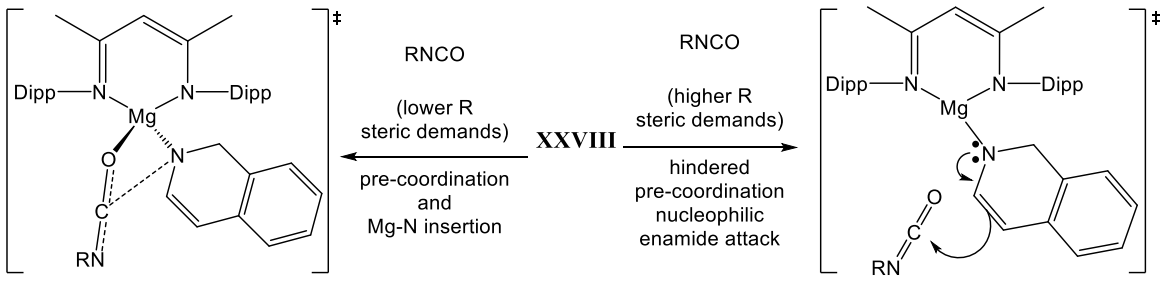

Scheme 2-12. Different reaction products from the reaction of **XXVIII** with alkyl isocyanates of different steric demands

In the case where R is bulky (*N*-adamantyl and *N*-*tert*-butyl) this pre-coordination to the magnesium centre is hindered, leading to the more kinetically favoured nucleophilic attack of the enamide C=C double bond at the electrophilic isocyanate carbon centre (Scheme 2-12). In support of this hypothesis enamines and enamide derivatives are known to behave as potent carbon-based nucleophiles,[191] which may be employed in a host of C-C bond forming processes through reactions with carbonyl-containing reagents.[192]

2.3 Reactions with Carbodiimides

The reactivity of magnesium dihydropyridides with organic isocyanates was expanded to include isoelectronic carbodiimides. It was again thought that hydride transfer may occur to the central carbon of the carbodiimide functional group to yield the formamidinate product. All reactions of a range of commercially available *N,N'*-substituted carbodiimides (*iso*-propyl (iPr), cyclohexyl (Cy) and *para*-tolyl (*p*-Tol)) with a stoichiometric amount of the magnesium dihydropyridide complexes (**XXVIIa,c,d** and **XXVIII)** were found to insert cleanly to form guanidinate complexes at room temperature within minutes (compounds **20**-**31**, Scheme 2-13). Similar insertion reactions with carbodiimides have been previously reported with magnesium complexes to yield amidinates, from insertion into Mg-H[118] or Mg-C[193-195] bonds.

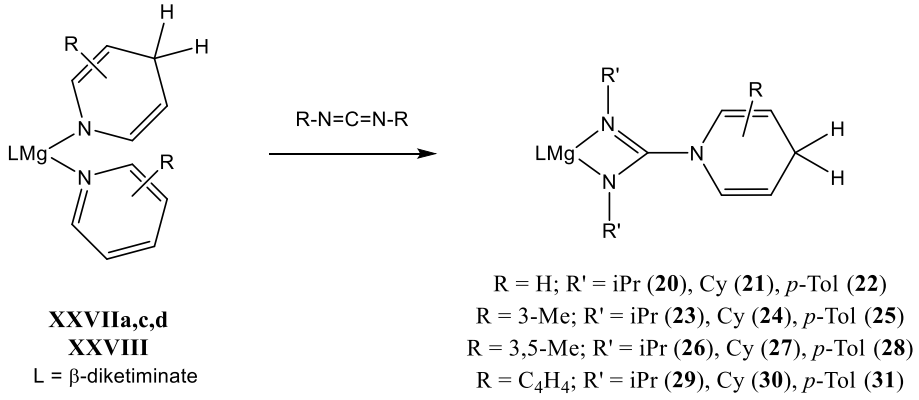

XXVIIa,c,d
XXVIII
L = β-diketiminate

R = H; R' = iPr (**20**), Cy (**21**), *p*-Tol (**22**)
R = 3-Me; R' = iPr (**23**), Cy (**24**), *p*-Tol (**25**)
R = 3,5-Me; R' = iPr (**26**), Cy (**27**), *p*-Tol (**28**)
R = C_4H_4; R' = iPr (**29**), Cy (**30**), *p*-Tol (**31**)

Scheme 2-13. Insertion reactions of carbodiimides into magnesium-dihydropyridide complexes

In each case a downfield shift of ca. 0.5 ppm was noted in the ^{1}H NMR spectra for the *ortho*-C*H* protons of the dearomatised ring. This occurred in addition to an upfield shift of the dihydro-CH_2 proton resonances of ca. 0.7 ppm, indicating Mg-N insertion had likely occurred. A characteristic ^{1}H NMR spectrum is shown in Figure 2-10, which illustrates the product of the insertion of *i*PrNCN*i*Pr into **XXVIId** (top spectrum) in comparison to the starting complex (bottom spectrum). Also observed is a small shift in the *β*-diketiminate ligand methine singlet as well as a simplification of the C*H iso*-propyl methine septets of this **XXVIId**, indicating a likely higher symmetry of the resulting complex (compound **26**).

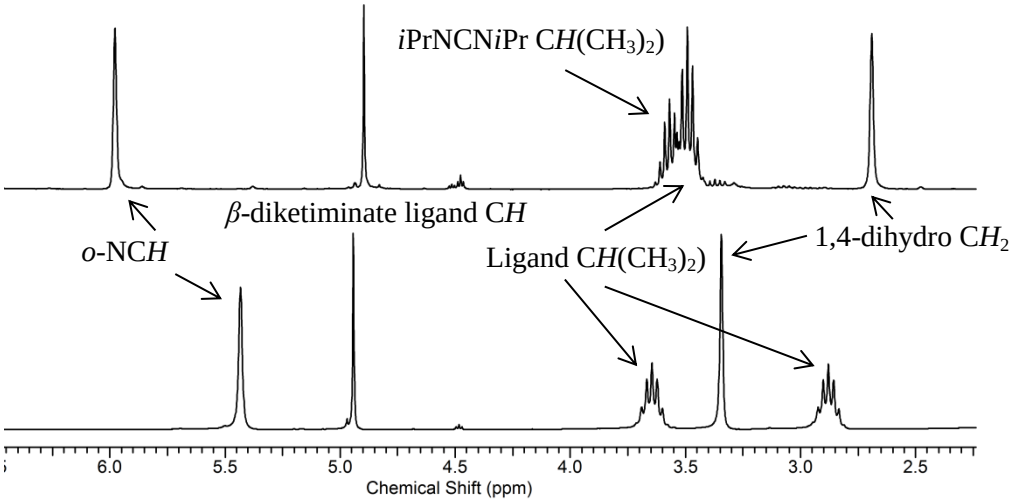

Figure 2-10. Stacked ^{1}H NMR spectra, in C_6D_6, showing **XXVIId** (bottom) and the resulting spectrum from the insertion of *N,N'*-di-*iso*-propylcarbodiimide to give compound **26** (top)

Although several attempts were made to isolate single crystals of compounds **20**-**31**, none suitable for crystallographic analysis could be obtained. Further confirmation of guanidinate formation was obtained by mass spectrometry performed on the hydrolysed product where, in most cases, the parent ion or the sodium adduct was observed. Interestingly, no divergent reactivity was observed with the *iso*-quinolide complex as seen previously with the isocyanate reactions.

Most attempted reactions between **XXVIIa,c,d** and **XXVIII** with bulkier carbodiimides (*tert*-butyl and Dipp), failed to provide any evidence of reaction even upon extended heating at 80 °C. It is suggested that the pre-coordination step (Figure 2-11) required for the insertion to occur is prevented by the substituent steric demands in these cases.

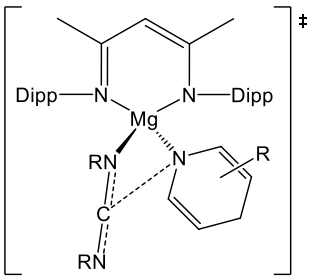

Figure 2-11. Proposed intermediate for the insertion of carbodiimides into magnesium-dihydropyridide complexes

The reaction between DippNCNDipp and compound **XXVIIc**, bearing the 3-methyl-1,4-dihydropyridide ligand provided a different course of reaction. Since no immediate reaction was observed at room temperature, this solution was then heated at 60 °C for 12 hrs to try and force the substrate to insert. The resultant ^{1}H NMR spectrum (Figure 2-12) indicated a complete loss

of those resonances associated with the dearomatised dihydropicolide. Instead five singlet resonances, each integrating as 1H, were observed. A subsequent ^{1}H-^{1}H COSY NMR experiment showed that none of these resonances coupled to each other, whilst a ^{1}H-^{13}C HSQC correlation showed that the singlet at δ 4.01 ppm did not arise from a proton attached to a carbon atom.

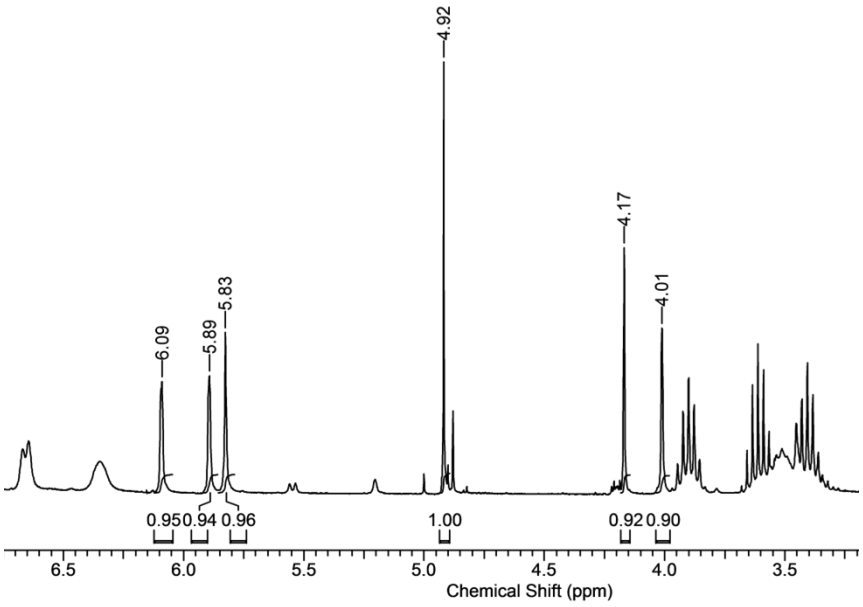

Figure 2-12. ^{1}H NMR spectrum, in C_6D_6, for compound **32**

The origin of these observations was resolved through the use of single crystal X-ray analysis performed on compound **32**. Single crystals were grown by slow evaporation of a toluene solution at room temperature, to yield large diamond shaped single crystals (Figure 2-13). This analysis showed **XXVIIc** had undergone an unexpected ring contraction to form a coordinated pyrrollide with the remaining carbon (C(35)), now external to the ring system as a methylene group which forms a new C-C bond to the central carbon of the carbodiimide-derived fragment. The carbodiimide has also been protonated into an amidine, accounting for the singlet resonance observed at δ 4.01 ppm in the ^{1}H NMR spectrum, which does not couple to any ^{13}C carbon resonance.

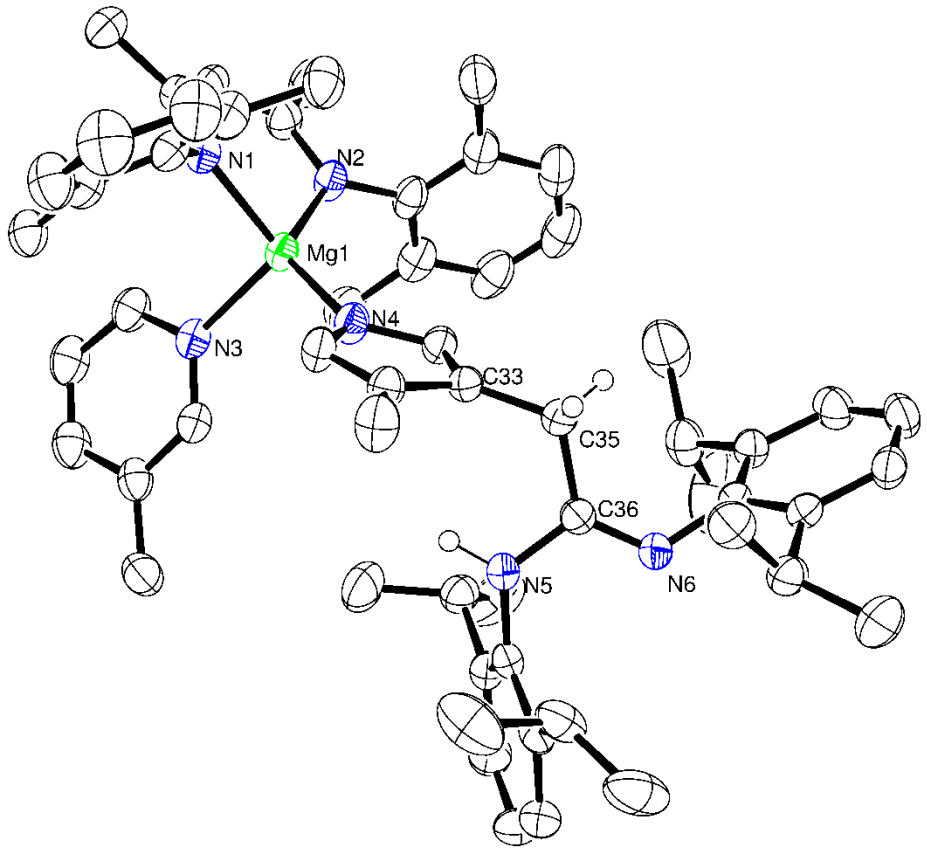

Figure 2-13. ORTEP representation of compound **32** with thermal ellipsoids set at 25% level of probability. Hydrogen atoms except those attached to C(35), N(5) and the methyl groups of the *β*-diketiminate 2,6-di-iso-propylphenyl substituents are removed for clarity. Selected bond lengths (Å) and angles (°): Mg(1)-N(1) 2.0500(18), Mg(1)-N(2) 2.0438(18), Mg(1)-N(3) 2.1290(19), Mg(1)-N(4) 2.0042(18), N(4)-C(34) 1.371(3), C(34)-C(33) 1.381(3), C(33)-C(35) 1.505(3), C(35)-C(36) 1.517(3), C(36)-N(5) 1.374(3), C(36)-N(6) 1.285(2), C(33)-C(35)-C(36) 116.06(17), N(5)-C(36)-N(6) 118.69(18), C(36)-N(5)-C(49) 121.00(17).

Compound **32** contains a 4-coordinate magnesium centre, in which 2 of the coordination sites are bound to the bidentate *β*-diketiminate ligand, a neutral 3-picoline molecule and the resulting ring contracted pyrrollide anion. The pyrrollide fragment is delocalised around the *N*-heterocycle [N(4)-C(30) 1.337(3) Å, C(30)-C(31) 1.376(3) Å, C(31)-C(33) 1.417 (3) Å, C(33)-C(34) 1.381(3) Å, C(34)-N(4) 1.371(3) Å], while the remaining carbon centre, C(35), arising from the original dihydro-3-picolide ligand, displays sp^3 hybridisation from the tetrahedral geometry observed. The formation of the new C-C bond is confirmed to have single bond character [C(35)-C(36) 1.517(3) Å], whilst the reduced carbodiimide contains both a localised single [N(5)-C(36) 1.374(3) Å] and double carbon-nitrogen bond [N(6)-C(36) 1.285(2) Å].

Information about the mechanism of this unusual ring contraction reaction was obtained through monitoring the reaction of **XXVIIc** with 1 equivalent of DippNCNDipp by NMR spectroscopy. ^{1}H NMR spectra, acquired at set time intervals over the course of the 12 hour reaction period,

showed the loss of the dearomatised proton resonances of **XXVIIc** with simultaneous increase in the new singlet resonances of compound **32**, which grew in at the same rate. This suggests a concerted mechanism in which any intermediate that forms is unstable and rapidly rearranges to the ring-contracted pyrrolide. It is proposed that, in a similar fashion to that observed earlier with the reactions of **XXVIII** and bulky alkyl isocyanates, the steric demands of the bis(2,6-di-*iso*-propylphenyl)carbodiimide substrate hinder pre-coordination to the magnesium centre, thus, preventing Mg-N insertion. Although a similar nucleophilic enamide attack on the carbodiimide maybe envisaged, in this case the resulting intermediate (Figure 2-14) is unstable and undergoes onward reactivity driven by rearomatisation to a 5-membered *N*-heterocycle.

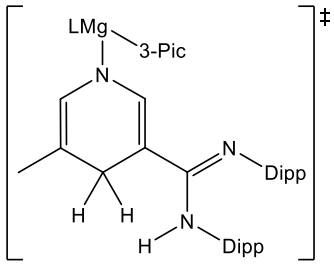

Figure 2-14. Proposed intermediate in the ring contraction reaction of **XXVIIc** with *N,N'*-bis(2,6-di-*iso*-propylphenyl)carbodiimide

Further information about the mechanism of this reaction was obtained from deuterium labelling studies. Reaction of 3-Picoline-(d_7) with a stoichiometric amount of $PhSiH_3$ yielded the 1,4-hydro-3-picolide(d_7) complex (**XXVIIc-d$_7$**), which then reacted *in situ* with 1 equivalent of DippNCNDipp at 60 °C for 24 hrs (Scheme 2-14). The resulting ^{1}H NMR spectrum comprised one singlet at δ 4.00 ppm (Figure 2-15), which was identified as the proton transferred to the amidine N-*H* bond, by comparison to the analogous spectrum obtained from the previous protio experiment (Figure 2-12).

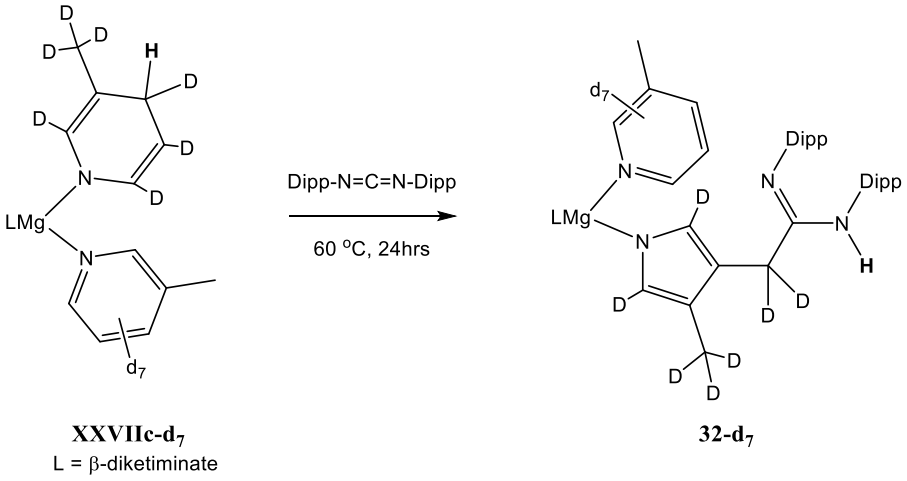

XXVIIc-d$_7$
L = β-diketiminate

32-d$_7$

Scheme 2-14. Deuterium labelling reaction to observe the proton transfer in the ring contraction reaction

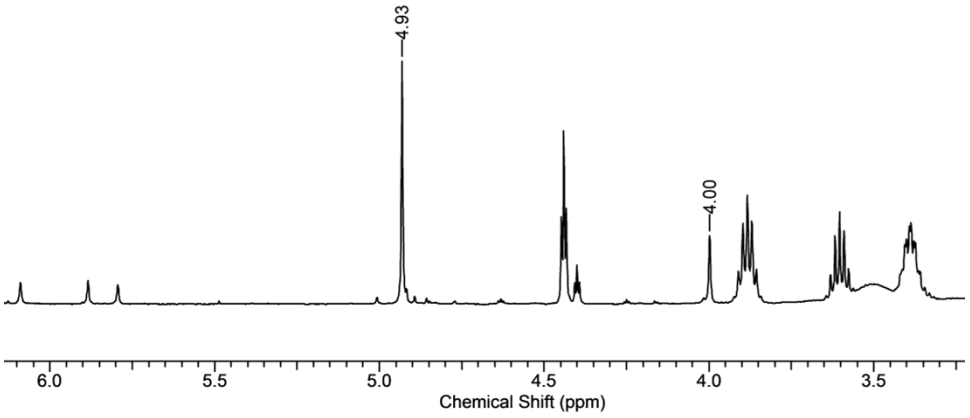

Figure 2-15. ^{1}H NMR spectrum, in C_6D_6, of the reaction of **XXVIIc-d$_7$** with DippNCNDipp to form compound **32-d$_7$**

Further confirmation that this was indeed an N-H and not a C-H environment, was gained from ^{1}H-^{14}N HSQC NMR experiment (Figure 2-16), which demonstrated a clear correlation between the singlet at δ 4.00 ppm in the ^{1}H NMR spectrum and that of the nitrogen in the carbodiimide-derived amidine moiety at δ 70 ppm in the ^{14}N NMR spectrum.

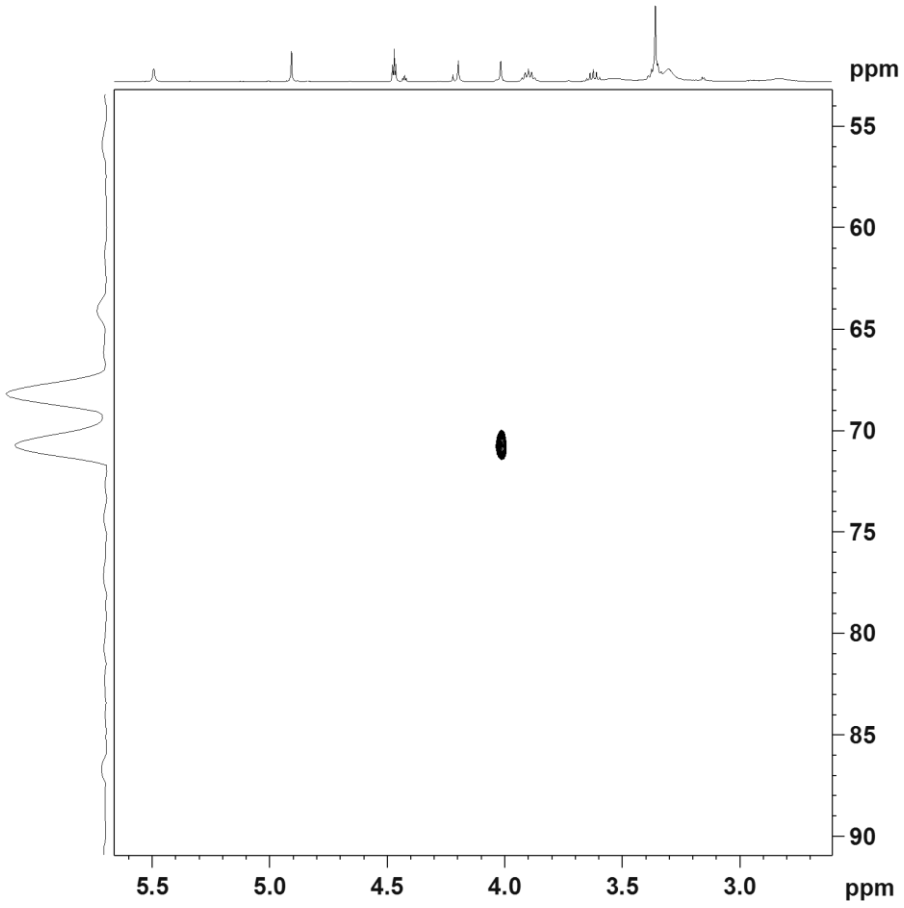

Figure 2-16. ^{1}H-^{14}N HSQC, in C_6D_6, for compound **32-d$_7$**

The observation that no reactivity is seen with *t*-BuNCN*t*-Bu suggests that this ring contraction may not be completely sterically induced and that the electronic nature of the substrate may also be important. The effect of varying electronics on this system was examined by using an electron withdrawing group instead of the methyl group on the pyridine ring. *In situ* generation of the 3-methoxy-1,4-dihydropyridide magnesium complex and subsequent addition of 1 eq. of DippNCNDipp again provided no immediate evidence of reaction. Heating the reaction at 60 °C for 12 hrs, however, again resulted in the characteristic loss of the dearomatised fragment and the formation of 5 new singlet resonances in the ^{1}H NMR spectrum consistent with those observed for compound **32** and suggesting that ring contraction had again occurred (Compound **33**, Scheme 2-15).

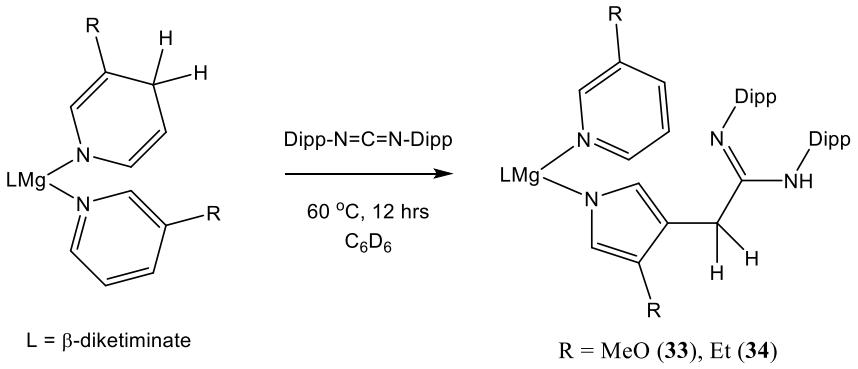

Scheme 2-15. Extension of study to contain different R groups in 3-position

Variation of the steric demands of the 3 position whilst incurring only minimal adjustment to the electronic nature of the pyridine ring was achieved by using 3-ethyl pyridine to generate *in situ* the 3-ethyl-1,4-dihydropyridide magnesium complex. This compound also provided analogous ring contraction to cleanly afford the pyrrollide complex (compound **34**), again after heating for 12 hrs at 60 °C.

The proposed mechanism for the ring contraction of magnesium-supported 3-substituted-1,4-dihydropyridides upon reacting with DippNCNDipp, is shown in Scheme 2-16. This is suggested to proceed *via* initial nucleophilic enamide attack at the central electrophilic carbon of the carbodiimide substrate. This intermediate undergoes subsequent ring contraction to form a cyclopropanamidate species either directly or *via* a 6π electron cyclisation. Further rearrangement to form the pyrrolide ring, yields the more stable methylene pyrrolide complexes (compounds **32**-**34**).

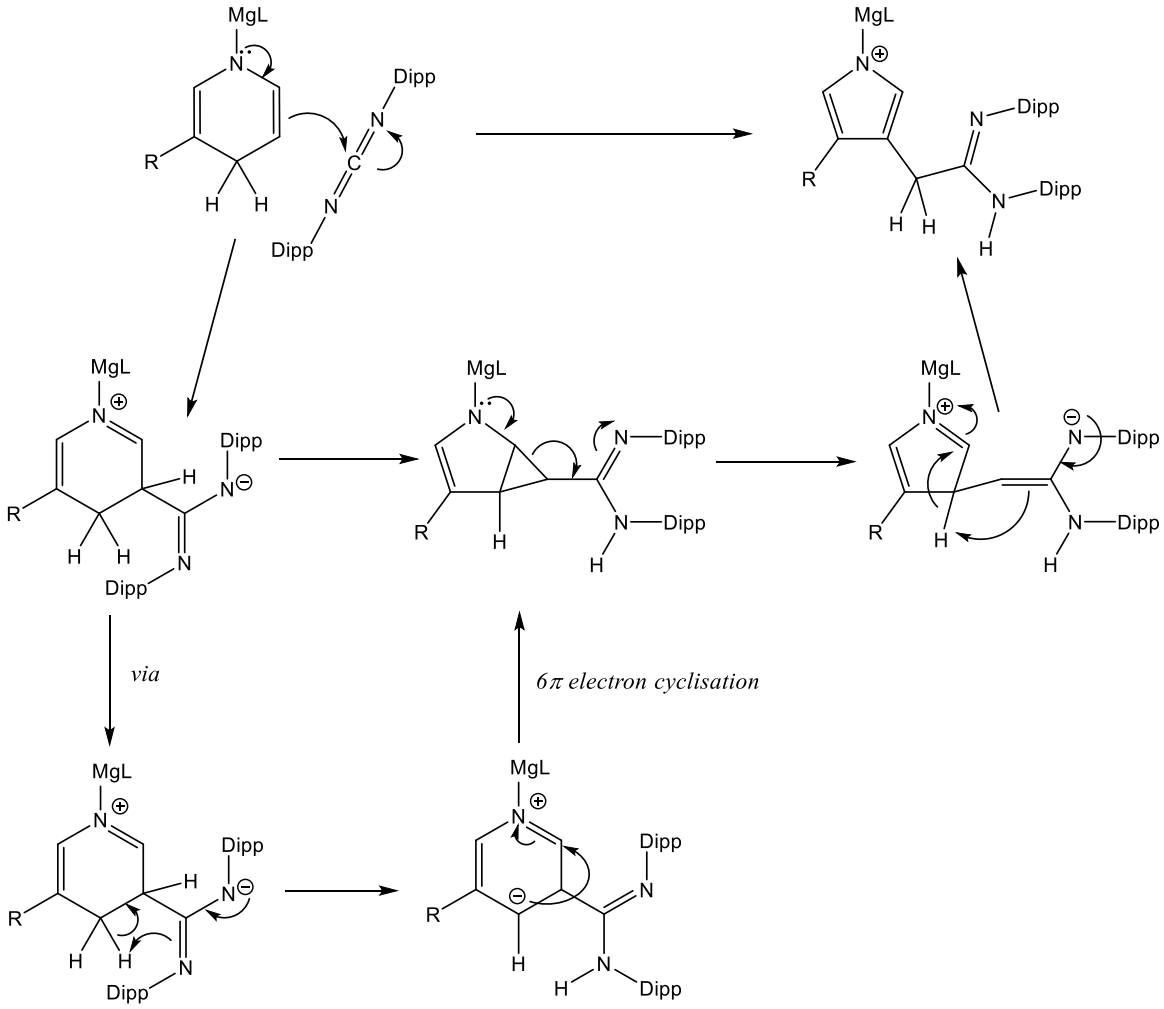

Scheme 2-16. Proposed mechanism for the ring contraction to form compounds **32**-**34**

2.4 Conclusions

In conclusion, although magnesium dihydropyridides have been shown to act as effective hydride transfer reagents upon reaction with a representative ketone, benzophenone, reactions of 1,4-dihydropyridide (**XXVIIa,c,d**) species with organic isocyanates provided insertion into the Mg-N bond to afford the *O*-bound ureide complexes in the majority of cases. Attempts to yield the hydride transfer product of these isolated complexes by extended heating was unsuccessful. In 2 cases, however, formal hydride transfer to yield the formamidate species was identified. In contrast to this relatively straightforward insertion behaviour of the 1,4-dihydropyridides, reactions with the 1,2-dihydro-*iso*-quinolide (**XXVIII**) complex displayed a distinct dependence upon the nature of the isocyanate *N*-substituent. Reactions with smaller alkyl groups provided insertion into the Mg-N bond to again yield the *O*-bound ureide complexes. Increasing the steric demands of the substituent, however, is suggested to prevent pre-coordination to the magnesium centre, resulting in unusual enamide C-C coupling reactions. Similar C-C coupling

reactions were observed using aryl isocyanates; the resulting more acidic aryl amide complexes, however, continued to react and resulted in protonation of the *β*-diketiminate ligand.

Extension of this study to include the isoelectronic carbodiimides resulted in insertion into the Mg-N bond to form a series of guanidinates which retained the dearomatised heterocycle. Attempted reactions using more bulky substituents resulted in no observed reaction, except for the reaction of a 1,4-dihydro-3-picolide (**XXVIIc**) with DippNCNDipp which resulted in an unexpected ring contraction to yield a pyrrolide complex with C-C coupling to the central carbon of the subsequently protonated carbodiimide fragment. Further studies have shown this reactivity may be expanded to other 3-substituted-1,4-dihydropyridide complexes.

Chapter 3. Hydroboration of Pyridines

3.1 Introduction

As described in the previous chapter selective dearomatisation of pyridines is of high importance to the pharmaceutical industry. Whilst the stoichiometric reactions outlined previously successfully accessed a wide variety of functionalised dihydropyridides, this system requires the use of a stoichiometric amount of magnesium. Although magnesium is considerably cheaper and more environmentally benign than transition metals, it will still be advantageous for this reactivity to be rendered catalytic.

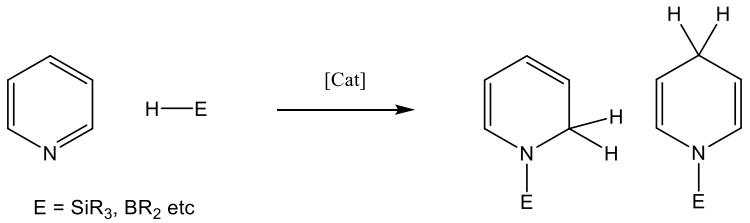

Scheme 3-1. Catalytic heterofunctionalisation of pyridines

Prior to this work, very little homogeneous catalytic heterofunctionalisation reactivity of pyridines had been reported (Scheme 3-1). The hydrosilylation of pyridines was initially described by Harrod[196] using Cp_2TiMe_2 (**XXXIX**) whilst a more recent report by Nikonov[148] based similar reactivity upon a ruthenium (**XL**) catalyst system. Both of these systems showed the hydride insertion step to proceed through initial formation of a 1,2-dihydropyridide reminiscent of the stoichiometric reactivity seen with magnesium. Both systems showed tolerance to some functional groups and to substitution around the *N*-heterocyclic ring.

XXXIX **XL**

Figure 3-1. Selection of pre-catalysts for the heterofunctionalisation of pyridines

Since publication of the following work, several more examples of hydroboration of pyridines have been noted in the literature. Suginome[141] reported the first transition metal catalysed hydroboration of pyridines, whilst Marks[58] reported the use of the lanthanum catalyst (**XXXIV**) both of which allowed the selective formation of *N*-boryl-1,2-dihydropyridines whilst showing tolerance towards a variety of functional groups. The most recent work, by Harder[156] has also

shown a bis(magnesium) hydride supported by a bis(-*β*-diketiminate) ligand (**XXXI**) to allow the efficient hydroboration of pyridines.

3.2 Catalyst Scope

In an attempt to extend the reactivity described in Chapter 2 to the catalytic hydrosilylation of pyridines, the reaction of pyridine and $PhSiH_3$ was attempted in the presence of 10 mol% of **Ib**. Heating at the elevated temperature of 80 °C provided no sign of reactivity (Scheme 3-2).

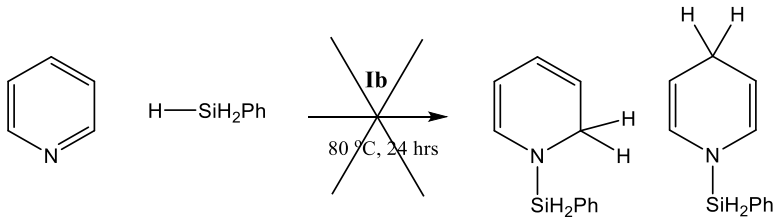

Scheme 3-2. Attempted magnesium-catalysed hydrosilylation of pyridines

No reaction was also observed between the isolated magnesium-dihydropyridide (**XXVIIa**) and a stoichiometric amount of $PhSiH_3$, in the hope of providing a stoichiometric approach to the hydrosilylation of pyridines. This apparent lack of reactivity is thought to be due to the low basicity of the silane which is insufficient to allow the formation of the necessary polarised Si-H/Mg-N transition state required in order to produce the *N*-silylated-dihydropyridine.

A similar catalytic reaction performed with HBpin, instead of $PhSiH_3$, provided facile conversion to the desired heterofunctionalised pyridine, which in this case yielded both the *N*-borylated 1,2- and 1,4-dihydropyridine products. Due to the success of this initial reaction, a series of stoichiometric reactions were undertaken to assess potential mechanistic steps in this reaction.

3.3 Stoichiometric Reactivity

In a similar manner to that reported by Marks for the hydroboration of olefins,[142] initial catalyst activation proceeds *via* a σ-bond metathesis reaction between the metal alkyl and borane reagent. Due to the hydridic nature of HBpin this results in formation of the active magnesium hydride species (**XXII**) and an equivalent of *n*-butyl borane. This is clearly observed in the ^{11}B NMR spectrum due to the disappearance of the HBpin doublet at δ 32.0 ppm and the appearance of a new singlet resonance at δ 37.5 ppm indicative of a new B-C bond. This could also be clearly identified in the ^{1}H NMR spectrum due to a noticeable upfield shift of the methine singlet of the *β*-diketiminate backbone, from δ 4.99 ppm to δ 4.71 ppm. Also noted was a new

singlet at δ 3.9 ppm, which was assigned as the hydride resonance through comparison to the molecular hydride complex (**XXII**) previsouly reported by Jones (Mg*H* δ 4.01 ppm).[117]

Addition of a stoichiometric equivalent of pyridine to a solution of **XXII** provided the C=N insertion product after heating the solution to 60 °C for 12 hours (Scheme 3-3). The 1,4-dihydropyridide complex (**XXVIIa**) was identified as the major product from this reaction, as confirmed through comparison of the previously reported NMR resonances.[124]

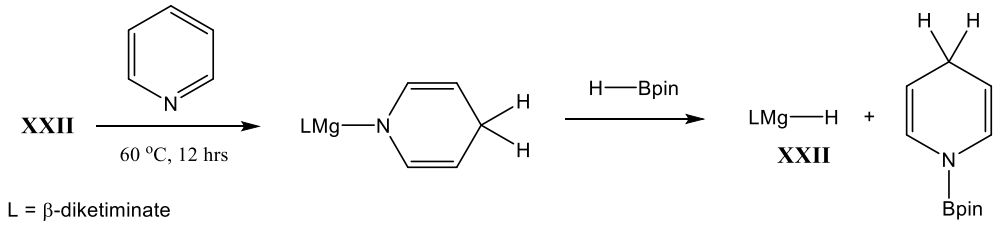

Scheme 3-3. Stoichiometric formation of *N*-borylated-1,4-dihydropyridines

Subsequent addition of HBpin to this solution provided clean formation of the desired product (Scheme 3-3), as observed by NMR spectroscopy. In the ^{1}H NMR spectrum the dearomatised pyridine ring could be identified by the alkenic resonances in the δ 5.5 to δ 7.0 ppm region for the 1,4-dihydropyridide isomer, as well as the corresponding dihydro methylene resonance at δ 2.8 ppm. The ^{11}B NMR spectrum displayed a singlet at δ 27.0 ppm indicating formation of a new B-N bond, with regeneration of the magnesium hydride complex completing the catalytic cycle. Combination of these σ-bond metathesis and insertion steps can be used to construct the following catalytic cycle for the hydroboration of pyridines (Scheme 3-4).

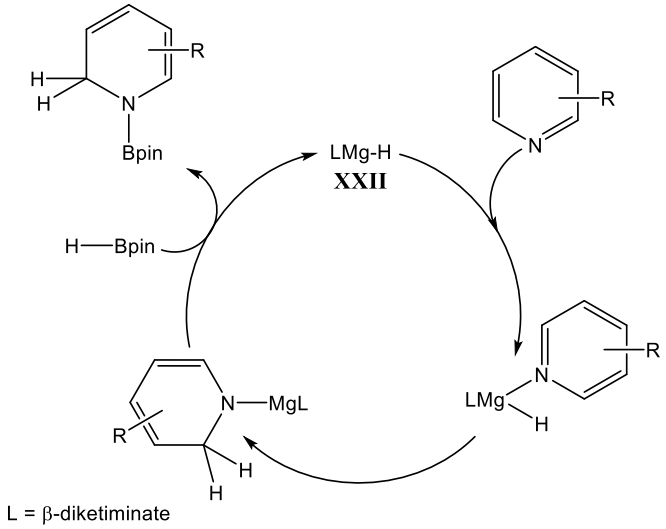

Scheme 3-4. Proposed catalytic cycle for the magnesium-catalysed hydroboration of pyridines

3.4 Catalysis

Previous stoichiometric reactions resulting from the $PhSiH_3$ derived dearomatisation of pyridine showed that heating at 70 °C for 2 days resulted in exclusive 1,4-dihydropyridide formation whereas room temperature reactions yielded the kinetic 1,2-dihydropyridide derivative. Initial catalytic runs for the hydroboration of pyridine used 10 mol% of **Ib** (Table 3-1).

Table 3-1. Temperature optimisation for the magnesium-catalysed hydroboration of pyridines

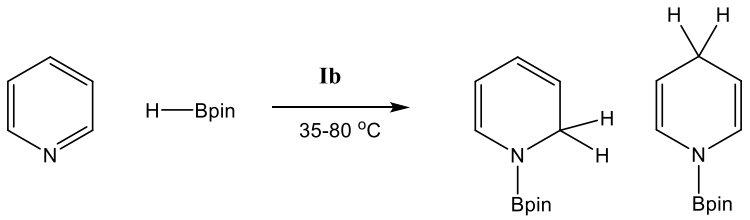

35 **36**

Entry	Catalyst (mol %)	Time (hr)	Temp (°C)	NMR yield (%)	1,2-:1,4-ratio
3-1	10	16	80	90	5:95
3-2	10	17	70	92	37:63
3-3	10	2 d	50	90	45:55
3-4	10	4 d	35	81	49:51
3-5	0	24	70	0	0

These reactions were, thus, carried out at different temperatures to assess whether the formation of the 1,2- vs 1,4-dihydropyridine isomer could be controlled. Heating at 80 °C (entry 3-1) resulted in 90% conversion by NMR and a 5:95 ratio of 1,2-:1,4-*N*-boryl-dihydropyridine. This again shows the system's thermodynamic preference for the 1,4 isomer. Reducing the temperature to 70 °C (entry 3-2) resulted in a reduction of the proportion of the 1,4- product, which was enhanced through reduction of the temperature to 50 °C (entry 3-3) and 35 °C (entry 3-4). It was not possible, however, to exclusively form the 1,2-*N*-boryl-dihydropyridine as the reduction in temperature also resulted in increased reaction times leading to the formation of the thermodynamic 1,4-product by isomerisation. A reaction of a 1:1 solution of pyridine and HBpin, containing no catalyst, was placed at 70 °C for 24 hours (entry 3-5). No indication of dearomatisation/borylation was observed in either the ^{1}H or ^{11}B NMR spectra indicating that the magnesium catalyst is necessary for the reaction to produce the hydroborated product.

Following the success of this pyridine hydroboration, a variety of 2-,3- and 4,-substituted pyridines were examined under similar conditions (Table 3-2). Inclusion of 10 mol% **Ib** at 70 – 80 °C provided clean formation of a variety of substituted *N*-boryl-dihydropyridines.

Table 3-2. Hydroboration of various substituted pyridines

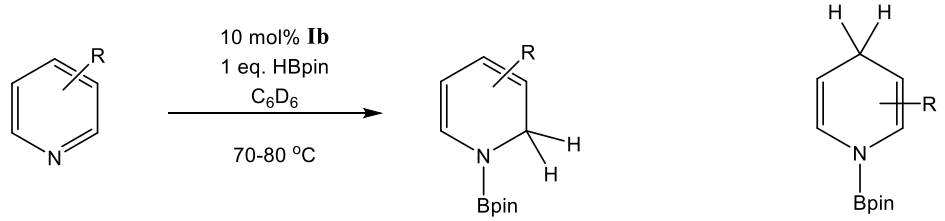

R = H (**35**), 3-Me (**38**), 3,5-Me (**40**), 4-Me (**42**), 4-Ph (**44**)

R = H (**36**), 2-Me (**37**), 3-Me (**39**), 3,5-Me (**41**), 4-Me (**43**)

Entry	Pyridine	Time (hrs)	Temp (°C)	NMR yield (%)	1,2-:1,4-ratio
3-6	2-picoline	4 d	70	51	0:100
3-7	3-picoline	3.5	70	91	48:52
3-8	4-picoline	23	70	91	81:19
3-9	2,6-lutidine	21	80	0	-
3-10	3,5-lutidine	21	70	92	40:60
3-11	2-phenylpyridine	3 d	80	0	-
3-12	4-phenylpyridine	8	70	95	100:0
3-13	4-dimethylaminopyridine	3 d	80	<5	100:0

NMR experiments were carried out in C_6D_6, whereas large scale experiments were carried out in hexanes. For full scale up procedure and isolated yields see experimental section 7.3.

Comparison of the differences in yield and 1,2-:1,4-isomer ratio provided some insight into the mechanistic factors controlling this reaction. For example, the hydroboration of 2-picoline (entry 3-6) proceeded slowly and after 4 days at 70 °C had only reached 51% conversion. This further supports an initial insertion step proceeding *via* 1,2-hydride transfer. This is further supported in the case of 2,6-lutidine (entry 3-9) and 2-phenylpyridine (entry 3-11) where no reactivity is seen, presumably as the 2-position is blocked by a methyl and phenyl group respectively. Attempts to force these reactions to turn over at increased temperatures up to 100 °C, and in the presence of a further equivalent of HBpin were also unsuccessful. New boron containing species were, however, observed in the ^{11}B NMR spectrum: a singlet at δ 25.7 ppm and a quartet at δ -9.0 ppm which was identified as a pyridine-BH_3 adduct. Crystallographic analysis carried out on isolated single crystals from this reaction mixture identified the species at δ 25.7 ppm through comparison to the known unit cell, as the redistribution product, tris(pinacolato)diboron (**XLI**, B_2pin_3) (Figure 3-2).[197]

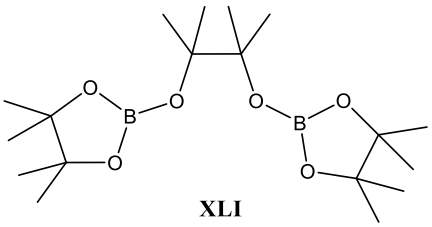

XLI

Figure 3-2. B_2pin_3 decomposition product

The hydroboration of 3-picoline (entry 3-7) provided a high yield in the shortest reaction time, but provided no preferential formation of either the 1,2 or 1,4 isomer. A similar lack of selectivity was also observed for 3,5-lutidine (entry 3-10), but with extended reaction times. In the case of 4-picoline (entry 3-8) it was expected that no 1,4-isomer would be observed due to the 4-position being blocked by a methyl group, as was the case with the stoichiometric $PhSiH_3$ derived dearomatisation reactions. Whilst the 1,2- isomer was the major product, 20% conversion to the 1,4-isomer was still observed. Replacement of the methyl group in the 4-position with a phenyl group (entry 3-12), however, resulted in exclusive formation of the 1,2-dihydropyridine with a notably decreased reaction time, which is likely due to the influence of a strong inductive effect upon the pyridine ring by the phenyl substituent. In contrast, use of 4-dimethylaminopyridine (DMAP) (entry 3-13) provided almost no hydroboration (<5%), unlike the stoichiometric $PhSiH_3$ reactions where the 1,4-isomer was observed as the major product. Further inspection of the ^{11}B NMR spectrum for the DMAP hydroboration also indicated consumption of the HBpin substrate and through the formation of **XLI** and BH_3. Formation of these decomposition products could be reduced by avoiding temperatures above 70 °C. Prolonged reaction times at this temperature also appeared to favour the formation of a variety of decomposition products which inhibit catalysis.

Table 3-3. Hydroboration of fused ring pyridines and bipyridines

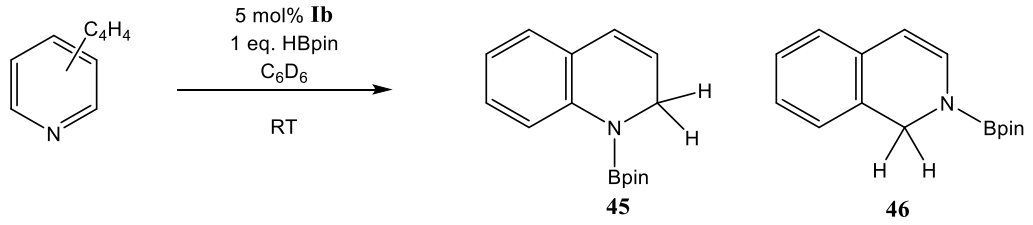

45 **46**

Entry	Pyridine	Catalyst (mol %)	Time (hrs)	Temp (°C)	NMR yield (%)	1,2-:1,4-ratio
3-14	quinoline	5	5	25	90	100:0
3-15	*iso*-quinoline	5	3	25	>99	100:0
3-16	2,2'-bipyridine	10	2 d	70	<5	-

Reactions using fused ring pyridines, unlike substituted pyridines, proceeded at room temperature with only 5 mol% catalyst loading (Table 3-3). Reaction of quinoline (entry 3-14) provided exclusive formation of the 1,2-isomer (**45**) despite the system being able to isomerise to the 1,4-isomer as seen with the stoichiometric $PhSiH_3$-derived dearomatisation reaction. Room temperature formation of the 1,2-isomer (**46**) was also cleanly observed in high yields from the reaction with *iso*-quinoline (entry 3-15). Expanding this work to include polypyridines proved unsuccessful; upon addition of 2,2'-bipyridine (bipy) (entry 3-16) an instant colour change was observed from pale yellow to a dark red/purple. It is thought that due to the chelating nature of bipy this has undergone insertion into either the Mg-H or Mg-C bond and resulted in stoichiometric dearomatisation similar to that reported for dearomatisation reactions of 2,2';6'.2"-terpyridine using a lutetium(III) alkyl complex.[198]

Attempts to gain crystals suitable for crystallographic characterisation resulted in the isolation of the bis(boryl)oxide, $O(Bpin)_2$, which co-crystallised with *N*H-1,2-dihydroquinoline, compound $\mathbf{46_H}$, (Figure 3-3), confirming the products are indeed highly air- and moisture-sensitive. Such hydrolysis was also observed upon monitoring a NMR sample of *N*-boryl-1,2-dihydroquinoline: upon exposure to moisture the rapid formation of *N*H-1,2-dihydroquinoline was observed in the ^{1}H NMR spectrum by the appearance of a broad 1H N*H* singlet at δ 2.61 ppm. Over time this slowly decomposed to the rearomatised *iso*-quinoline starting material.

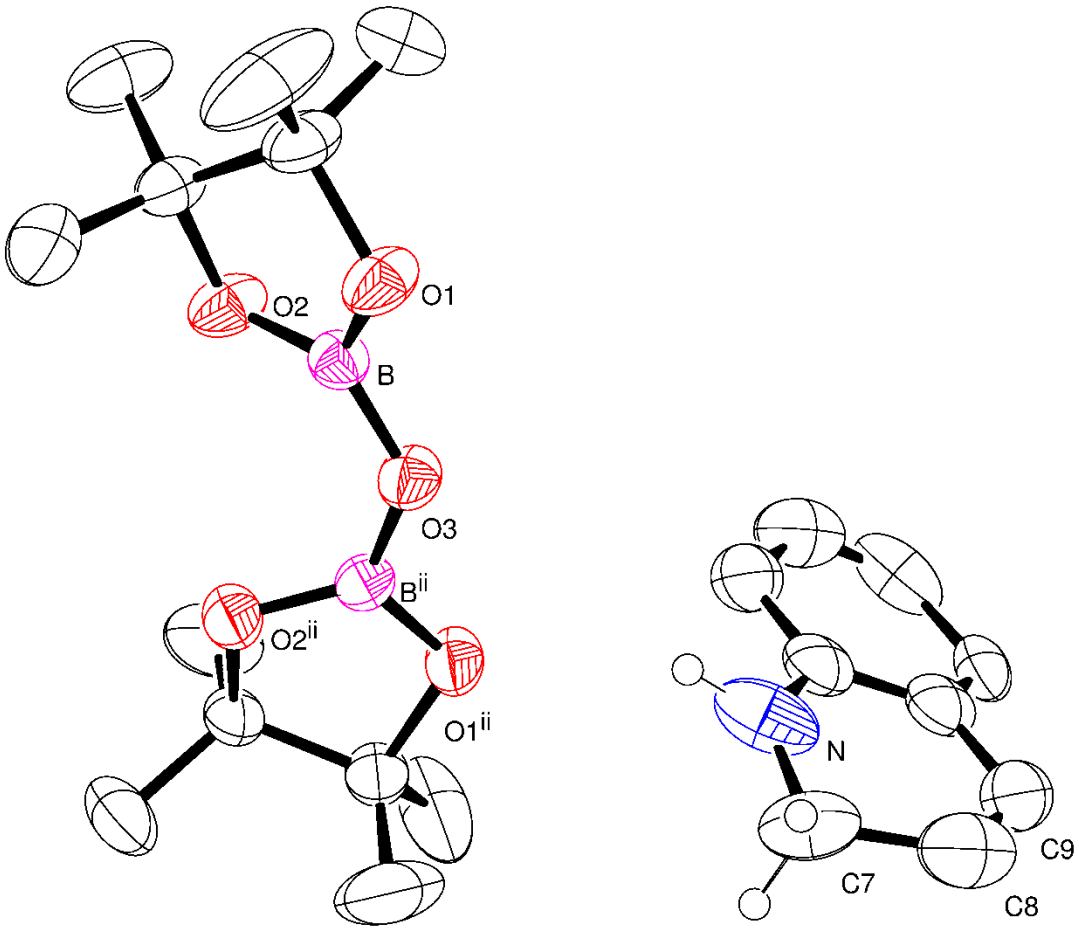

Figure 3-3. ORTEP representation of bis(boryl)oxide and *N*H-1,2-dihydroquinoline (**46$_H$**), ellipsoids are set to 30%. Hydrogen atoms except H7a, H7b and H11^{i} have been removed for clarity. Selected bond lengths (Å) and angles (°): B-O(3) 1.3627(19), N-C(7) 1.31(2), C(7)-C(8) 1.618(11), C(8)-C(9) 1.360(4), B-O(3)-B^{ii} 128.8(2), N-C(7)-C(8) 109.1(9), C(7)-C(8)-C(9) 121.9(5). Symmetry transformations used to generate equivalent atoms: #1 -x,y,-z+1/2, #2 -x,-y+2,-z+1.

Consideration of selected bond lengths and angles confirmed the maintenance of the dearomatised, but protonated 1,2-dihydro-*iso*-quinoline (**46$_H$**). C(7) in the 2-position displays sp^3 hybridisation as shown by a N-C(7)-C(8) bond angle of 109.1 (9)°. Similarly, the elongation of C(7)-C(8) [1.618 Å] compared to C(8)-C(9) [1.360 Å] indicates more single bond character corresponding to the maintained reduction of this molecule upon hydrolysis. This bis(boryl)oxide product is likely to have formed *via* hydrolysis of *N*-Bpin-1,2-dihydroquinoline and subsequent condensation of the molecules of Bpin(OH). This was also apparent in the ^{11}B NMR spectrum through the observation of a new singlet at δ 25.0 ppm for the bis(boryl)oxide product.

3.4.1 Functional Group Tolerance

In order to assess the robustness of this hydroboration system for synthetic application, a series of functionalised pyridines were tested (Table 3-4). Upon reaction with 3-pyridinecarboxaldehyde (entry 3-17) rapid hydroboration of the aldehyde C=O fragment was observed. This increased rate of reaction is consistent with that observed for the hydroboration of aldehydes and ketones, where aldehyde hydroboration proceeds rapidly with as little as 0.1 mol% catalyst at room temperature.[154] Attempts to further reduce the product, specifically the pyridine ring, failed. This system's preference for B-O formation was also noted upon reaction with 3-methylnicotinate (entry 3-18), in which the C=O bond was again reduced in preference to the pyridine ring. In this case, however, stoichiometric cleavage of the methoxy group was also observed.

Table 3-4. Hydroboration of a series of functionalised pyridines

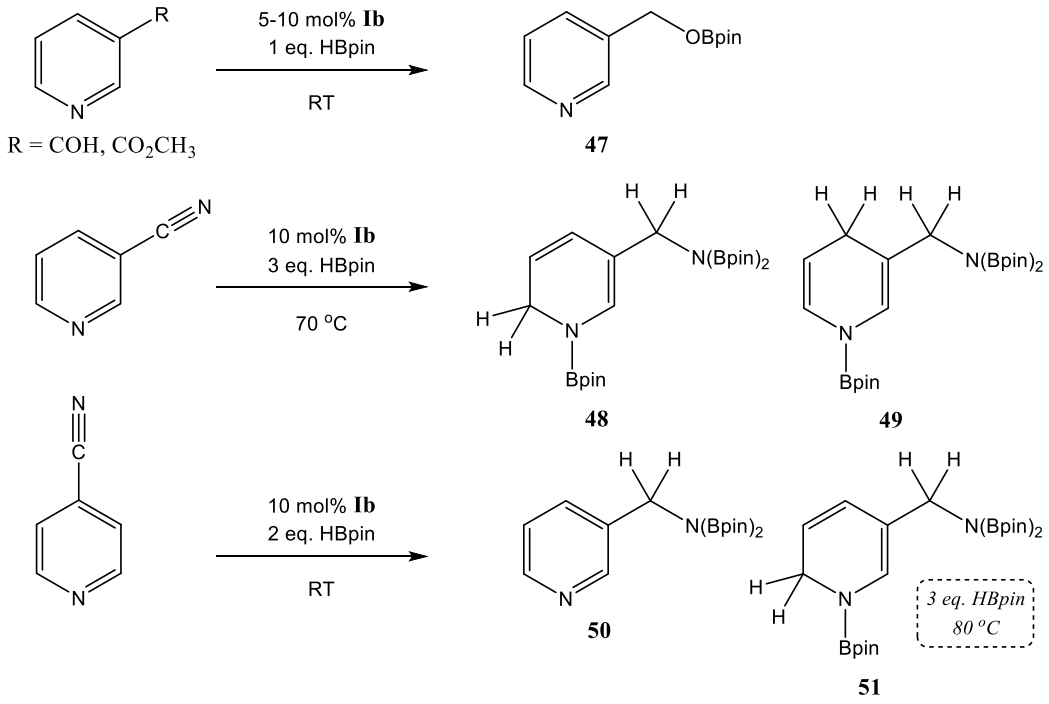

Entry	Pyridine	Catalyst (mol %)	Time (hrs)	Temp (°C)	NMR yield (%)	1,2-:1,4-ratio
3-17	3-pyridinecarboxaldehyde	5	0.2	25	>99	-
3-18	3-methylnicotinate	10	0.5	25	50	-
3-19	3-cyanopyridine	10	8	70	88	5:95
3-20	4-cyanopyridine	10	1	25	>99	-
3-21	4-cyanopyridine	10	16 d	80	53	90:10

NMR experiments were carried out in C_6D_6, whereas large scale experiments were carried out in hexanes. For full scale up procedure and isolated yields see experimental section 7.3.

Similar reactivity was observed with 3- and 4-cyanopyridine. In both cases 3 equivalents of HBpin were added in order to fully reduce the C≡N triple bond and the pyridine fragment. In the case of 3-cyanopyridine (entry 3-19) complete reduction was observed to give the desired *N,N'N'*-{Bpin}$_3$-3-aminomethyl-1,4-dihydropyridine (**49**) as the major product. The reaction with 4-cyanopyridine proceeded at room temperature to fully reduce the cyano fragment within 1 hr (entry 3-20). Addition of a further equivalent of HBpin (entry 3-21) and prolonged heating, however, only afforded 54% conversion to the 1,2-dihydropyridine product.

3.5 Kinetic Studies

To further investigate the mechanism of this reaction kinetic experiments into the magnesium catalysed hydroboration of pyridines were undertaken. The hydroboration of *iso*-quinoline (iQuin) was selected for this study as the reaction proceeded to completion within a few hours at room temperature. This substrate is also restricted to the formation of the 1,2-dearomatised isomer and therefore potential secondary kinetics from isomerisation to the 1,4 isomer can be eliminated from the study.

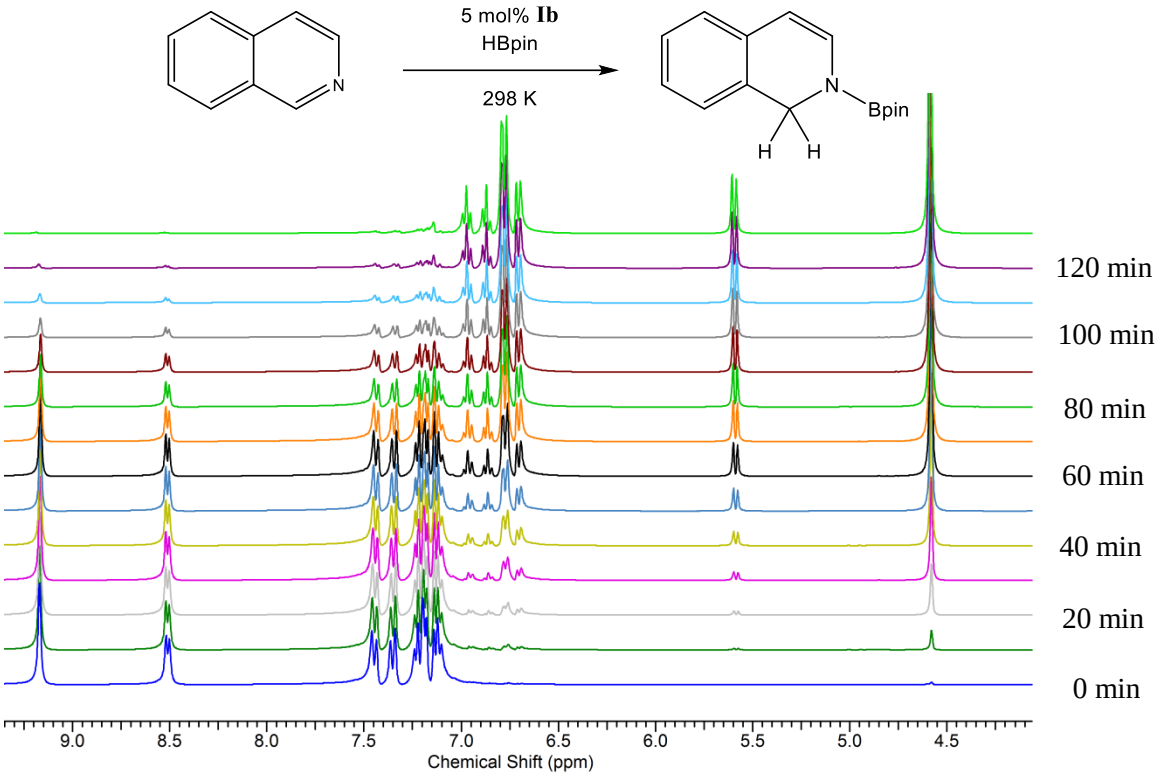

Figure 3-4. Stack plot of ^{1}H NMR spectra, in C_6D_6, for the hydroboration of iQuin, showing the consumption of the iQuin starting reagent (δ 9.2 and δ 8.5 ppm) and subsequent formation of iQuin(H)-Bpin (δ 5.6 and δ 4.6 ppm). Spectra acquired every 10 minutes.

All reactions were carried out at 298 K unless stated otherwise and were monitored by ^{1}H NMR spectroscopy to three half-lives (80% product conversion). Figure 3-4 shows a series of stacked spectra for the standard reaction of 5 mol% **Ib** (0.04 M) with 0.8 M iQuin to 0.84 M of HBpin.

A small excess of HBpin is used in order to form the initial magnesium hydride species *in situ*. Activation of the precatalyst occurs rapidly and it is therefore assumed that the active catalyst is present at t = 0. Using the above standard reaction, the overall reaction order could be determined by comparison of a series of zero, first and second order rate plots (Figure 3-5). This indicated that the reaction conformed to overall zero order kinetics.

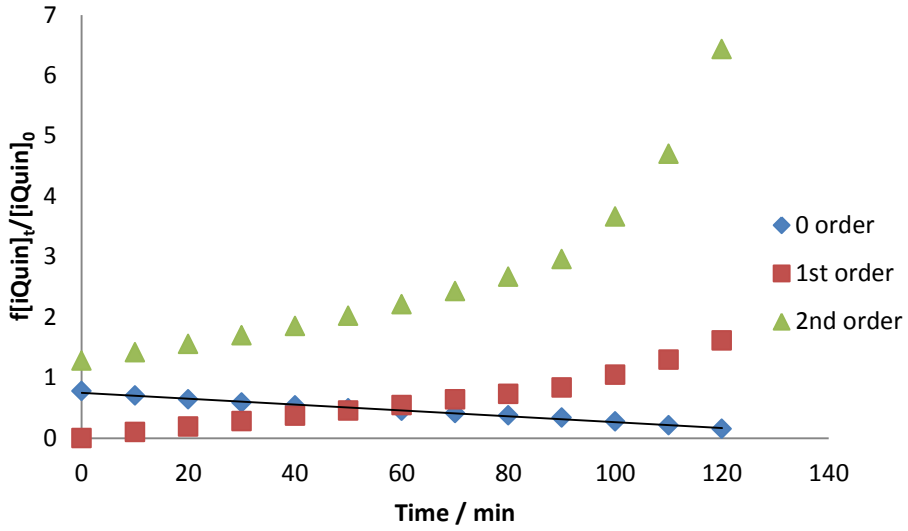

Figure 3-5. Series of different zero, first and second order rate plots as a function of [iQuin] vs time

3.5.1 Determination of order in [Catalyst]

In order to determine the order with respect to [Mg], a series of reactions were carried out using variable catalyst loadings whilst keeping [iQuin] and [HBpin] constant (Figure 3-6).

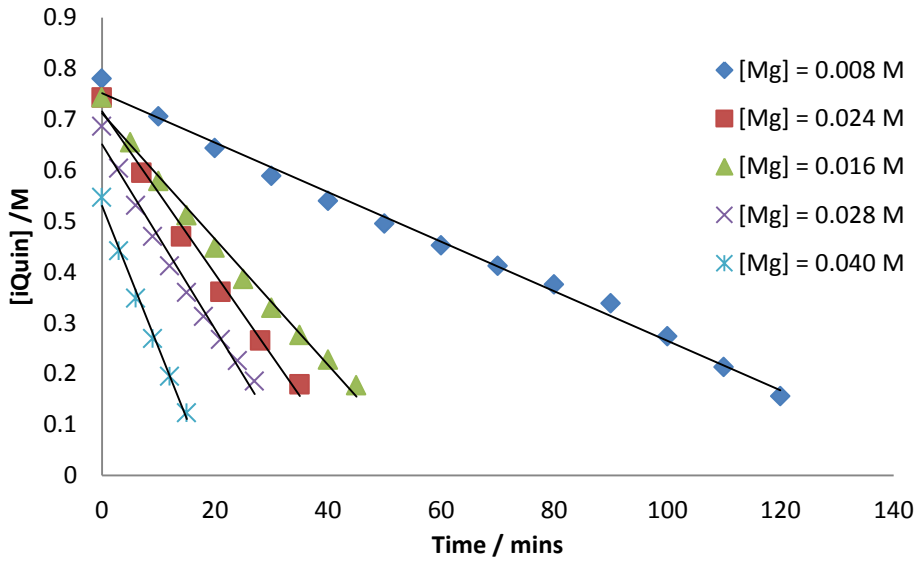

Figure 3-6. Plot of [iQuin] vs time for variable catalyst loadings

Least squares error calculations are provided in supplementary Figure S 3-1

The amount of active catalyst in solution was calculated based on NMR integrals against an added standard of tetramethylsilane. Figure 3-6 shows a series of zero order plots for five different concentrations of catalyst. As expected, increasing the catalyst concentration increased the observed rate of reaction, indicating the order with respect to magnesium is likely to be 1. This was confirmed by taking the observed rate constants from Figure 3-6 and plotting them directly against the concentration of magnesium (Figure 3-7).

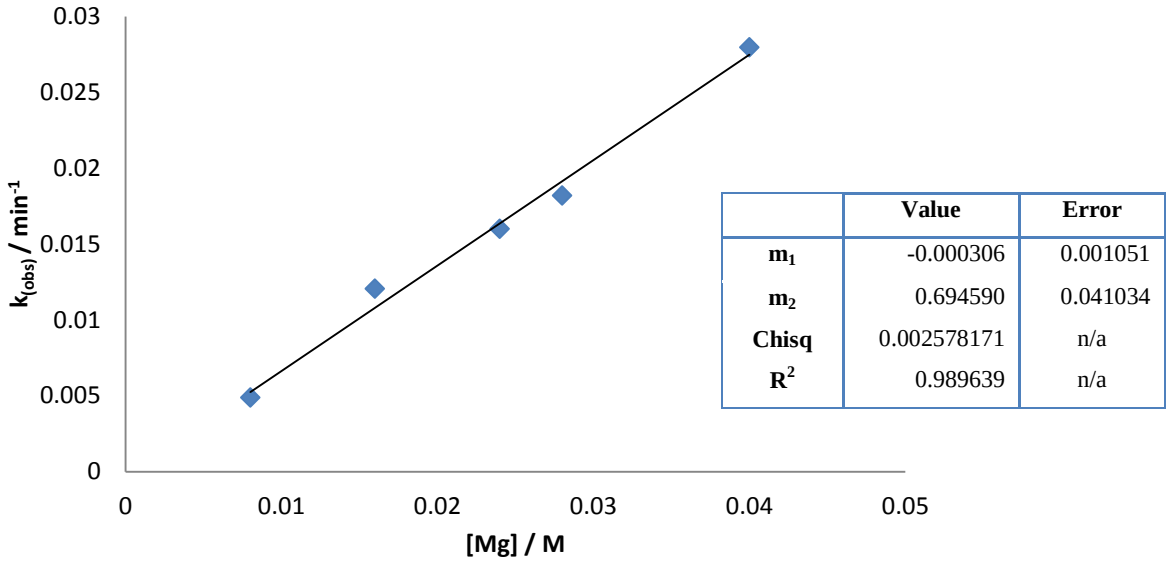

	Value	Error
m_1	-0.000306	0.001051
m_2	0.694590	0.041034
Chisq	0.002578171	n/a
R^2	0.989639	n/a

Figure 3-7. Plot of observed rate constants $k_{(obs)}$ vs [Mg] and least squares error calculations

This observation is consistent with other magnesium and calcium catalysed reactions with in which the Ae^{2+} centre is coordinated by a β-diketiminate ligand. It is thus suggested that this is indicative of reaction of a mononuclear rate-determining step during the course of the catalysis.

3.5.2 Determination of order in [iQuin]

The reaction order in [iQuin] was obtained using *pseudo* first order methods employing a large excess of HBpin (8.0 M) and varying the starting concentration of iQuin whilst keeping the catalyst concentration invariant (0.04 M).

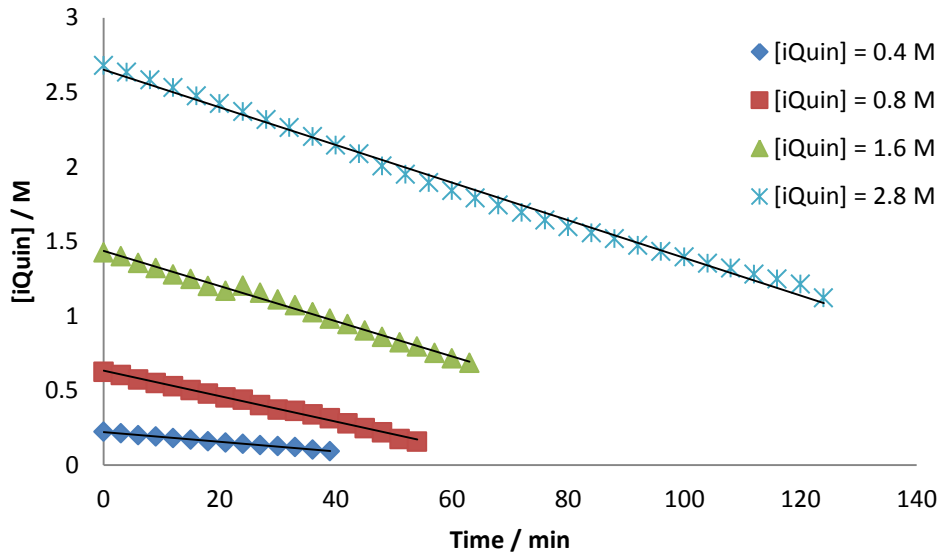

Figure 3-8. Plot of [iQuin] vs time for variable starting concentrations of iQuin, under *pseudo*-first order conditions in [HBpin]. Least squares error calculations are provided in supplementary Figure S 3-5.

Figure 3-8 again shows a series of zero order plots for the consumption of iQuin vs time under *pseudo*-first order conditions in [HBpin]. This shows that increasing concentration of iQuin provides a seemingly negative impact on the observed rate of reaction, an observation that was confirmed by plotting the deduced rate constants for the series of zero order plots against $[iQuin]^{-1}$ (Figure 3-9).

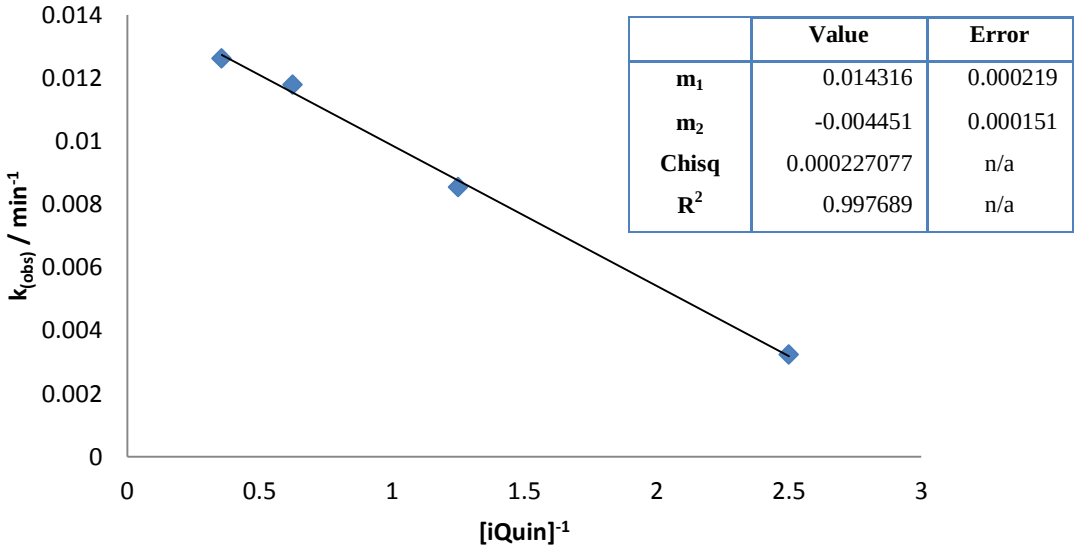

	Value	Error
m_1	0.014316	0.000219
m_2	-0.004451	0.000151
Chisq	0.000227077	n/a
R^2	0.997689	n/a

Figure 3-9. Plot of $k_{(obs)}$ vs $[iQuin]^{-1}$ and least squares error calculations

Figure 3-9 illustrates an inverse first order dependence on [iQuin]. Initial attempts to fit data to a plot of $k_{(obs)}$ vs [iQuin] failed to provide a linear fit (Figure S 3-9), which matches the trend observed in Figure 3-8, of rate decreasing upon increasing [iQuin].

3.5.3 Determination of order in [HBpin]

The use of similar *pseudo*-first order methods employing a large excess of iQuin (8.0 M) and varying the starting concentration of HBpin, whilst keeping catalyst concentration invariant, also allowed deduction of the reaction order with respect to changing concentration of HBpin.

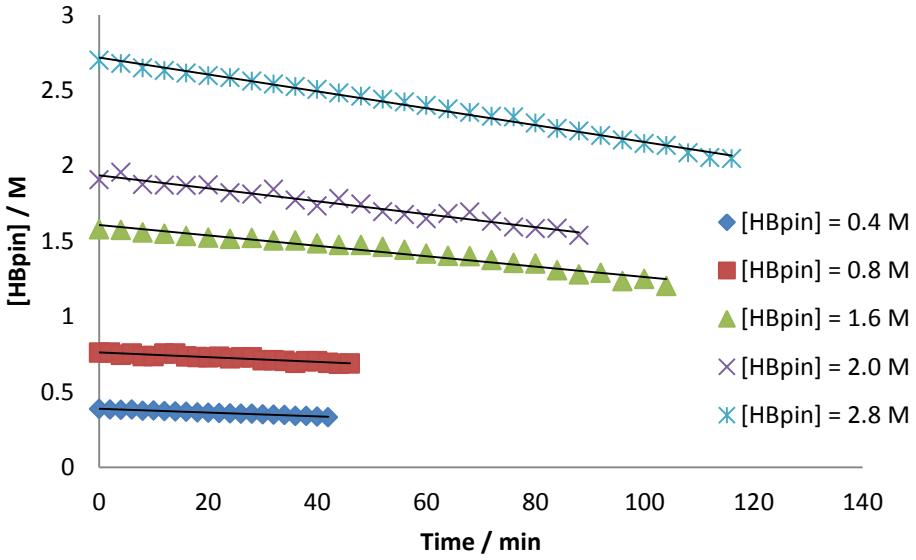

Figure 3-10. Series of zero order plots [HBpin] vs time for variable HBpin starting concentrations. Least square error calculations are provided in supplementary Figure S 3-10.

Figure 3-10 shows a series of overall zero order plots for the consumption of [HBpin] vs time for a series of variable starting HBpin concentrations. In this case a plot of the observed rate constants ($k_{(obs)}$) against [HBpin] (Figure 3-11) indicated a first order dependence on [HBpin].

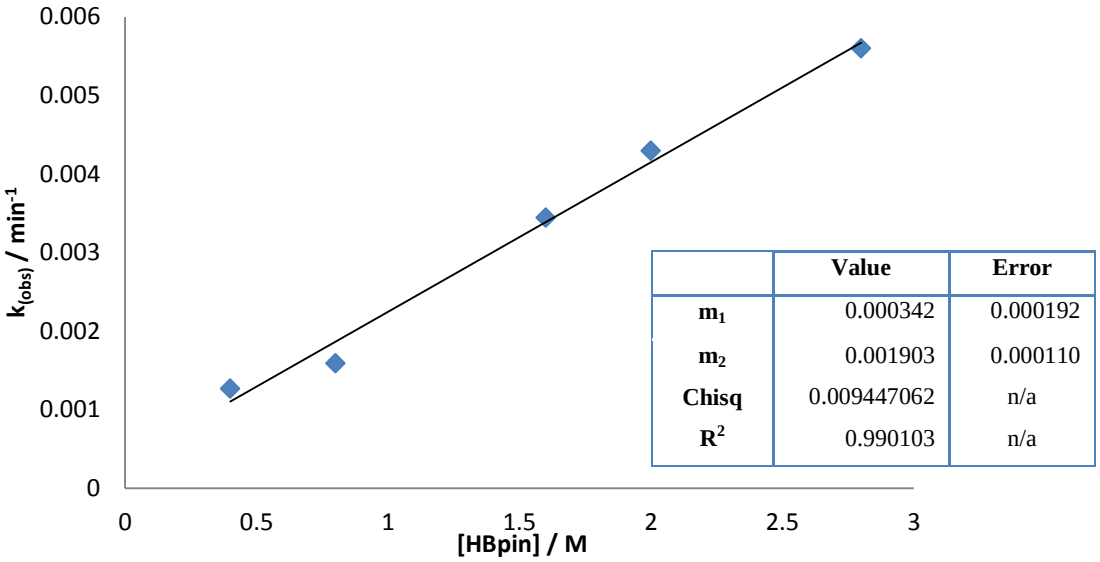

Figure 3-11. Plot of $k_{(obs)}$ vs [HBpin] and least squares error calculations

Combination of the experimentally determined orders of reagent provides the following rate law:

$$Rate = k[Mg]^1[iQuin]^{-1}[HBpin]^1$$

The catalyst concentration remains constant throughout the course of the reaction, and can thus be incorporated into $k_{(obs)}$ providing a rate law which correlates with the overall zero order rate of reaction.

$$Rate = k_{obs}[iQuin]^{-1}[HBpin]^1$$

The inverse dependence on [iQuin] may be attributed to the ability of the iQuin molecule to coordinate to the magnesium centre as a neutral donor, thus impeding the ability of the HBpin molecule to enter the coordination sphere of the magnesium for subsequent B-H/N-Mg metathesis and hydroboration reactivity, as depicted on the left hand of Scheme 3-5. This is further supported by the first order dependence on [HBpin], wherein increasing the concentration above the standard 1:1 ratio increases the displacement of the neutral iQuin molecule allowing subsequent catalytic turnover.

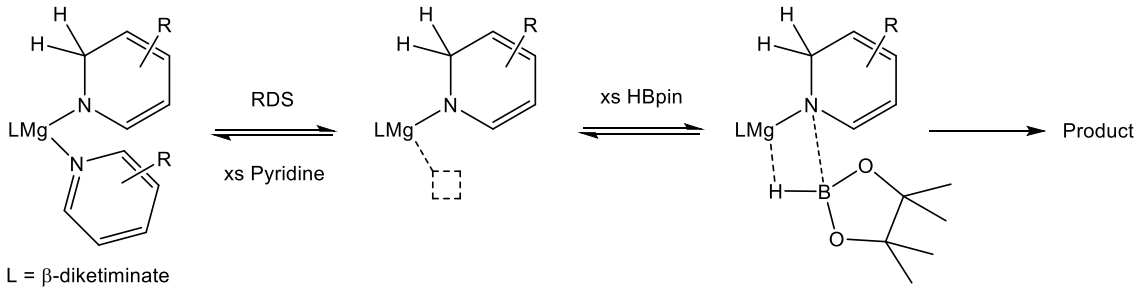

Scheme 3-5. Proposed mechanism for the rate determining step in the hydroboration of pyridines

It is therefore suggested that the rate determining step (RDS) involves dissociation of the neutral pyridine molecule which subsequently allows the HBpin molecule to undergo the final σ-bond metathesis step to form the product whilst regenerating the active magnesium hydride species.

3.5.4 Eyring and Arrhenius Analyses

Further insight into the nature of this mechanism was obtained through variable temperature kinetic studies, used to provide activation parameters for the hydroboration of pyridines. Again using iQuin as the pyridine of choice, reactions under the standard conditions of 5 mol% **Ib** (0.04 M) with a 1:1.05 ratio of iQuin to HBpin (0.8 M and 0.84 M respectively) were carried out over a range of 5 different temperatures (288 K – 308 K). Temperatures above 308 K were not studied due to the rate of reaction becoming too fast to monitor. Extraction of the observed rate constants from plots of [iQuin] vs time (supplementary Figure S 3-14) allowed the construction of Eyring (Figure 3-12) and Arrhenius plots (Figure 3-13).

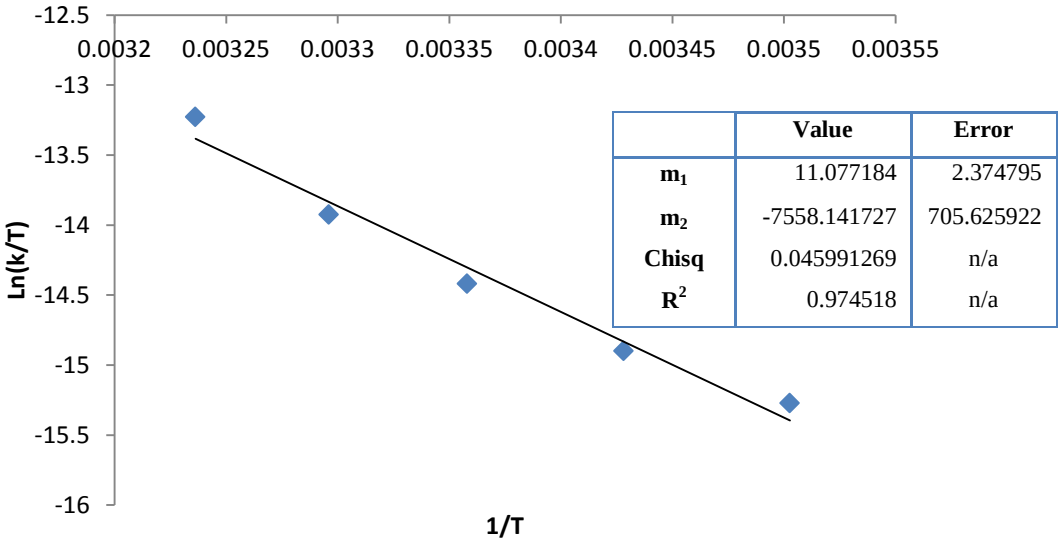

	Value	Error
m_1	11.077184	2.374795
m_2	-7558.141727	705.625922
Chisq	0.045991269	n/a
R^2	0.974518	n/a

Figure 3-12. Eyring plot and least squares error calculations

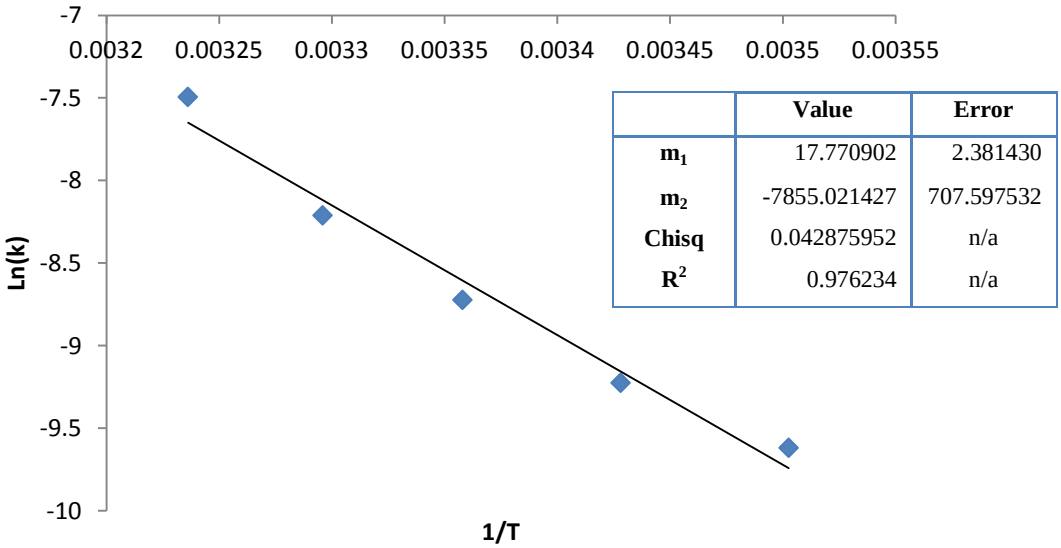

	Value	Error
m_1	17.770902	2.381430
m_2	-7855.021427	707.597532
Chisq	0.042875952	n/a
R^2	0.976234	n/a

Figure 3-13. Arrhenius plot and least squares error calculations

Using Eyring and Arrhenius techniques it was possible to deduce a number of key parameters involved in the rate determining step. These values are outlined in Table 3-5. Standard errors were calculated using the least squares method for linear regression.

Table 3-5. Kinetic activation parameters for the magnesium-catalysed hydroboration of iQuin

	Value	**Error**
Ea	65.3 kJ mol^{-1}	± 7.4
$\mathbf{\Delta H^{\neq}}$	62.8 kJ mol^{-1}	± 7.4
$\mathbf{\Delta S^{\neq}}$	-105.5 J k^{-1} mol^{-1}	± 24.7
$\mathbf{\Delta G^{\neq}_{298}}$	94.3 kJ mol^{-1}	n/a

As expected, the value for $\Delta H^{\neq}$ closely resembles that of the activation energy. These values suggest a concerted transition state with significant bond making to compensate for bond breaking (B-N vs B-H respectively). The large negative $\Delta S^{\neq}$ indicates a significant entropic contribution to the observed reaction kinetics and supports the assembly of a highly organised rate determining transition state.

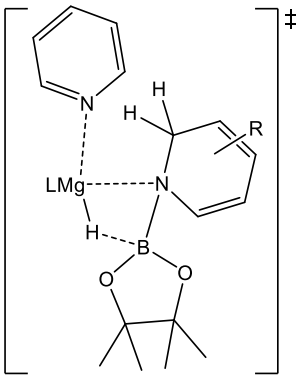

Figure 3-14. Proposed pre-assembled transition state

Figure 3-14 illustrates a proposed pre-assembled transition state, in which the neutral pyridine molecule must be displaced as the HBpin substrate enters the coordination sphere of the magnesium centre, leading to the necessary breakage of the B-H bond. The driving force of the reaction is thus the formation of the B-N bond. Previous group 2 catalysed hydroamination studies have highlighted a pronounced entropic influence on both intra- and intermolecular hydroamination reactions. Similar intermediates have also been identified in a recent DFT study on the lanthanide-catalysed hydroboration of pyridines reported by Marks.[58] Although in this case the experimentally derived rate law indicated inhibition by HBpin, it was noted that the overall driving force of the reaction was again the σ-bond metathesis step and resultant B-N bond formation. Another direct comparison to this lanthanide based catalysis was noted by the surprisingly similar experimentally derived activation parameters ($\Delta H^{\neq}$ = 65.7 (± 2.1) kJ mol^{-1},

$\Delta S^{\neq}$ = -113.8 (±1.3) J K^{-1} mol^{-1} and Ea = 68.2 (±1.7) kJ mol^{-1}) which are again indicative of an organised rate determining transition state.

3.6 Conclusions

In conclusion, the hydroboration of pyridines using a magnesium *β*-diketiminate catalyst (**Ib**) allows an extension of previous stoichiometric silane-based reactivity to a catalytic regime. Although selective formation of *N*-borylated-1,2-dihydropyridines or *N*-borylated-1,4-dihydropyridines can be somewhat controlled by temperature, with increased temperatures favouring the 1,4-dihydropyridine isomer, extended heating can lead to the redistribution of HBpin reagent preventing catalysis. This system also works well for a variety of methyl-substituted and fused-ring pyridines, but falls short in functional group tolerance tests, where heteronuclear multiple bonds react preferentially to the pyridine ring.

Kinetic studies showed the reaction to be zero order overall, with observed inhibition in [iQuin] due to the ability of the pyridine molecule to coordinate as a neutral donor thus blocking the vacant coordination site for the incoming HBpin molecule. It is therefore postulated that the rate determining step requires the dissociation of the pyridine molecule in a reaction which is subject to considerable entropic control.

Chapter 4. Hydroboration of Nitriles

4.1 Introduction

The reduction of nitriles to form primary amines is an essential component of many industrial processes such as the production of dyes, plastics, agrochemicals and precursors for pharmaceutical applications.[199] Typically in industry hydrogenation is employed to reduce nitriles to afford the desired amine, however this often results in the formation of unwanted secondary or tertiary amines whilst also requiring high temperatures and expensive and toxic transition metal catalysts.[200-205] It is also possible to stoichiometrically reduce nitriles using main group reducing agents, such as $LiAlH_4$ and $NaBH_4$,[206-208] which also allows some chemoselective and regioselective control over the formation of the product compared to transition metal hydrogenation. Again this system is not ideal, however, due to the use of large amounts of pyrophoric reagents, whilst also requiring transition metal salts to improve reaction efficiency. Recent efforts in the literature have shown reduction mediated by more easily handled amine borane reagents,[209] whilst other new hydrogenation methods have involved the use of 'frustrated Lewis pairs' to provide the first metal free catalyst to reduce nitriles under relatively mild reaction conditions.[210, 211]

Whilst hydrogenation may be a more direct route to the desired amine, hydroelementation reactions such as hydrosilylation or hydroboration can be advantageous due to their introduction of further functionality to the amine to create aminosilane or -borane compounds. For the hydroboration of nitriles there is only a handful of examples in the literature and all but one are non-catalysed.[212-214] Nikonov recently reported the first catalytic example of hydroboration of nitriles.[215] Using 5 mol% of an imido-hydrido Mo(IV) complex with HBcat acetonitrile and benzonitrile were reduced within 12 hours at room temperature to the bis(boryl)amine product. Again the reliance upon transition metals for hydroboration is evident despite their high cost and toxicity.

As noted in Chapter 3.4 both 3- and 4-substituted cyanopyridines underwent double hydroboration of the cyano group to form the bis(boryl)amino pyridines, in preference to the reduction of the pyridine moiety. This chapter continues this theme and describes the magnesium-catalysed hydroboration of nitriles.

4.2 Catalysis

An initial catalytic reaction using 10 mol% of **Ib** with 2 equivalents of HBpin and propionitrile at room temperature yielded slow conversion to the desired bis(borylated)amine product. A direct repeat of this reaction, at 60 °C, showed quantitative conversion within 30 mins to the bis(boryl)amine as confirmed by the new 2H methylene triplet seen in the ^{1}H NMR spectrum at δ 3.42 ppm as well as the new singlet in the ^{11}B spectrum at δ 29.5 ppm. Based on this encouraging result the study was extended to include a range of alkyl and aryl nitriles. These reactions were all carried out at 60 °C with 10 mol% of **Ib** and the results are outlined below in Table 4-1.

Table 4-1. Catalytic di-hydroboration of nitriles with HBpin and 10 mol% **Ib**

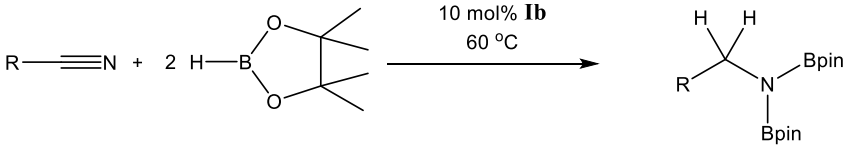

R = Pr (**53**), *iso*-Pr (**54**), *t*-Bu (**55**), Cy (**56**), Ph (**57**), *o*-(Me)Ph (**58**), *m*-(Me)Ph (**59**), *m*-(F)Ph (**60**), *m*-(MeO)Ph (**61**), *p*-(Me)Ph (**62**), *p*-(F)Ph (**63**), *p*-(Cl)Ph (**64**), *p*-(CF_3)Ph (**65**), *p*-(MeO)Ph (**66**), $(Ph)_2CH$ (**67**)

Entry	Nitrile	Time (hr)	NMR yield (%)	Isolated yield (%)
4-1	propionitrile	0.5	>99	70
4-2	*iso*-butyronitrile	1	93	96
4-3	trimethylacetonitrile	5.5	97	54
4-4	cyclohexylnitrile	1	94	75
4-5	benzonitrile	12	92	56
4-6	*o*-tolunitrile	15	86	73
4-7	*m*-tolunitrile	15	87	81
4-8	3-(fluoro)benzonitrile	14	88	57
4-9	3-(methoxy)benzonitrile	15	90	60
4-10	*p*-tolunitrile	13	91	72
4-11	4-(fluoro)benzonitrile	12	94	61
4-12	4-(chloro)benzonitrile	12	93	59
4-13	4-(trifluoromethyl)benzonitrile	12.5	89	76
4-14	4-(methoxy)benzonitrile	13.5	88	58
4-15	diphenylacetonitrile	30	75	43

NMR experiments were carried out in C_6D_6, whereas large scale experiments were carried out in toluene. For full scale up procedure and isolated yields see experimental section 7.4.

Mirroring the results found with the hydroboration of aldehydes, ketones and imines, increased steric bulk at the α-position of the nitrile led to increased reaction times. This is most readily appreciated through consideration of the effects of increasing steric demands upon substitution of the C≡N-bound carbon centre of aliphatic nitriles wherein a 10-fold increase in reaction time was required across the transition from propionitrile (entry 4-1) to *iso*-propylnitrile (entry 4-2) to *tert*-butylnitrile (entry 4-3). This also had an impact on the isolated yield of the reaction with the faster reactions reaching near quantitative yields.

Aryl nitriles (entries 4-5 to 4-15) also provided clean reactions with no side products, but with notably slower reaction times. Initially it was thought that these may produce faster reactions due to the more electropositive nature of the nitrile carbon, rendering it more susceptible to nucleophilic attack from the hydride. Different reaction rates were also observed within varying substitution patterns around the aryl rings, with *ortho*- and *meta*-substitutions providing the longest reaction times along with subsequent lower isolated yields. Although in the case of *o*-tolunitrile (entry 4-6) the slower reaction may again be attributed to an increase in substituent steric hindrance proximal to the reaction centre. Any minor variability across the range of *meta*- and *para*-substituted arylnitriles is more realistically attributed to electronic adjustments across the pi-conjugated substrate or intermediate structure.

The identities of the products from this catalysis were confirmed by ^{1}H, ^{11}B and ^{13}C NMR spectroscopy and a single crystal X-ray diffraction analysis performed upon the product isolated from the catalytic dihydroboration of propionitrile, compound **53**, (Figure 4-1). The N-C(1) bond length of 1.497(2) Å is consistent with the expected double reduction of the nitrile. Further evidence for the product is provided by the bond angle between N-C(1)-C(2) of 109.1^{o} in which the carbon atom is now sp^3 hybridised and no longer linear as in the nitrile functionality.

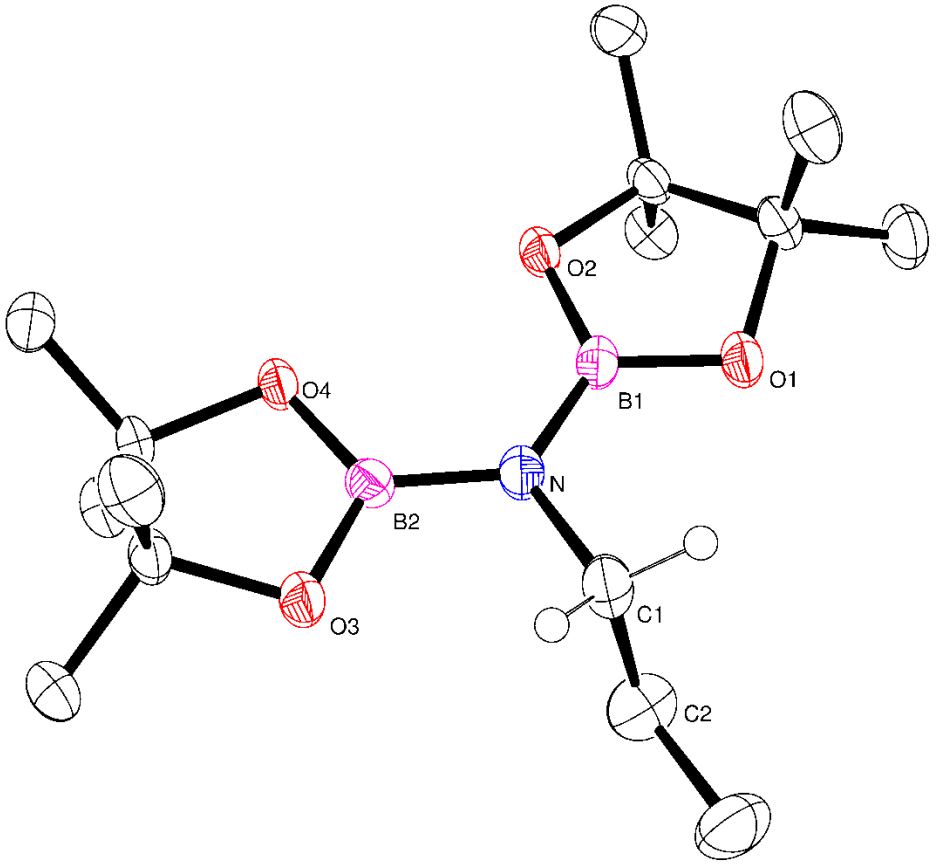

Figure 4-1. ORTEP representation of the structure of the bis(borylated) propionitrile reduction product, compound **53** (30% probability ellipsoid). Hydrogen atoms, except for those attached to the C(1) methylene carbon centre, are omitted for clarity. Selected bond lengths (Å) and angles (°): N-C(1) 1.497(2), N-B(1) 1.423(2), N-B(2) 1.430(2), C(1)-C(2) 1.490(3), B(1)-N-B(2) 126.15(15), B(1)-N-C(1) 117.15(14), N-C(1)-C(2) 112.55(16).

Based upon previous magnesium hydroboration catalysis the reaction sequence depicted in Scheme 4-1 was constructed as a rational means to effect the bis(borylation) of organic nitriles. This again combines the two types of reactivity seen for Ae metals, insertion and σ-bond metathesis steps. In this case the production of the final bis(boryl)amine product (**F**) requires the consumption of two molecules of HBpin and the intermediacy of an initial magnesium-bound imide (**A**), a borylated imine (**B**) as the product of initial B-H/Mg-N metathesis and an amide species (**D**) formed by formal Mg-H insertion of the borylimine (**B**). Irrespective of the likely formation of borate intermediates such as **C** and **E**, the additional complexity introduced by the requirement for two-fold nitrogen functionalisation raises a number of issues: specifically the nature of the rate determining processes, the (potentially multiple) catalytic resting states and the overall validity of the single manifold mechanism exemplified by Scheme 4-1

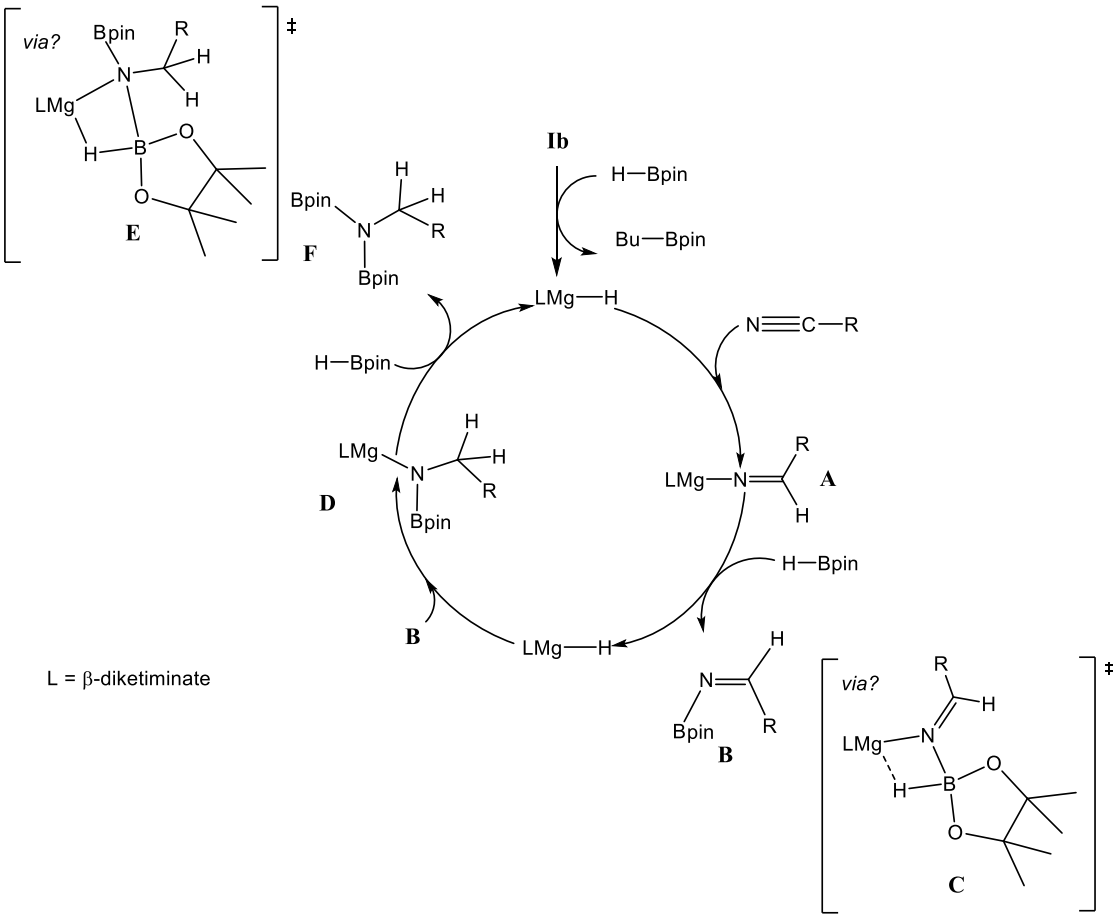

Scheme 4-1. Proposed mechanism for the magnesium-catalysed di-hydroboration of nitriles

4.3 Stoichiometric reactions

To provide further insight into the course of these successful catalytic reactions and the viability of intermediate species such as those shown in Scheme 4-1 (**A**-**E**), a series of stoichiometric reactions were undertaken. The reaction of *tert*-butyl nitrile (*t*-BuCN) was chosen due to the diagnostic *tert*-butyl group in the ^{1}H NMR spectrum. Addition of 1 equivalent of *t*-BuCN to the *in situ* generated magnesium hydride, which was obtained through the reaction of 1 equivalent of HBpin with the precatalyst **Ib**, showed complete insertion into the magnesium hydride bond after heating for 12 hours at 60 °C (Scheme 4-2).

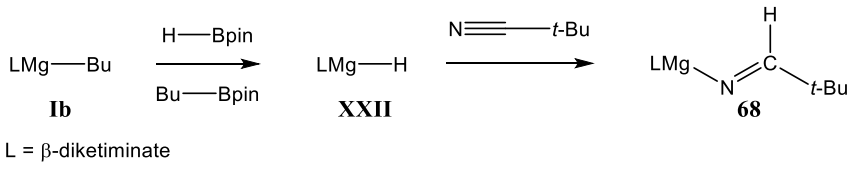

Scheme 4-2. Insertion of *t*-BuCN into the *in situ* generated magnesium hydride

The formation of this aldimide derivative (compound **68**), analogous to species **A** in Scheme 4-1 was observed in the ^{1}H NMR spectrum by a new downfield singlet at δ 7.84 ppm (1H by integration) which was assigned as the aldimide methine proton, as well as a single new *β*-

diketiminate ligand environment (see also Figure 4-5 – i). Attempts to isolate single crystals suitable for X-ray diffraction of this aliphatic aldimide species were unsuccessful, however analogous reactions performed with *m*- and *p*-(MeO)C_6H_4CN (yielding compounds **69** and **70**, respectively) again showed the characteristic aldimide methine singlet resonances (**69** δ 8.63; **70** δ 8.58 ppm) in their respective ^{1}H NMR spectra, as well as providing suitable single crystals for X-ray diffraction analysis from toluene solutions. Results of these analyses are shown below in Figure 4-2 and Figure 4-3, while selected bond lengths and angles are provided in the figure captions.

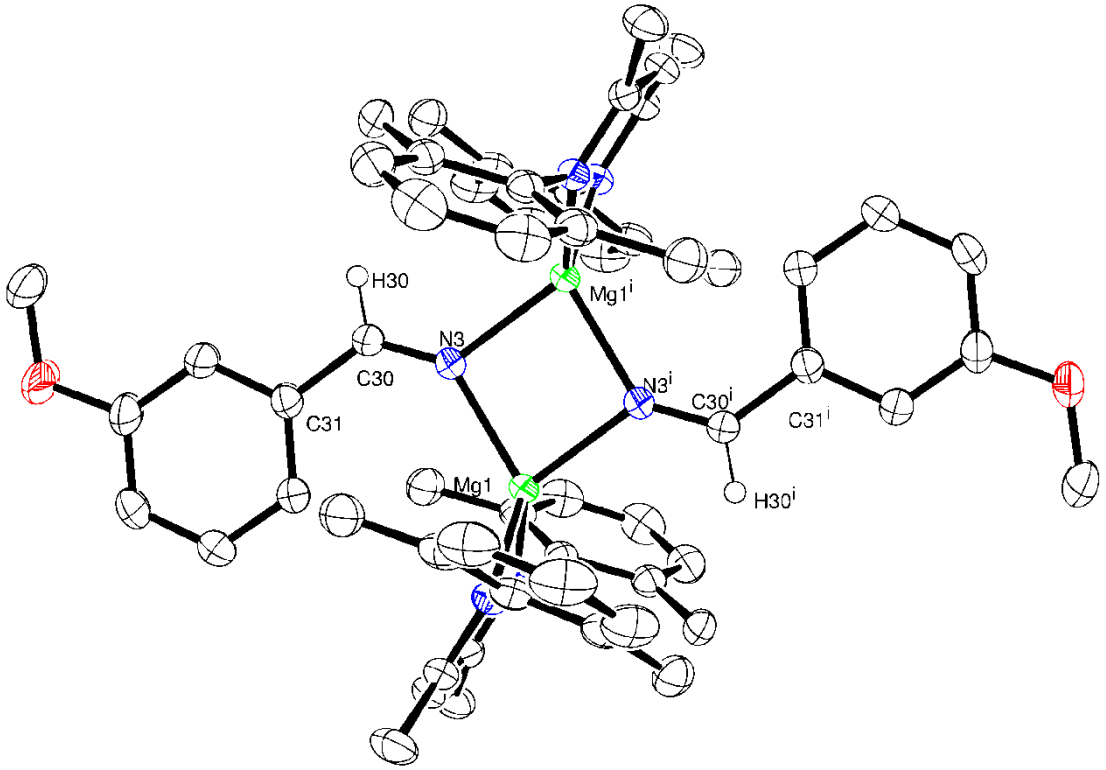

Figure 4-2. ORTEP representation of compound **69** thermal ellipsoids set at a 30% level of probability. Hydrogen atoms, except for those attached to the C(30) and C(30)^i aldimide carbon centre and the methyl groups of the *β*-diketiminate 2,6-di-*iso*-propylphenyl substituents are removed for clarity. Selected bond lengths (Å) and angles (°): Mg(1)-N(3) 2.1062(16), Mg(1)-N(3)^i 2.0918(16), Mg(1)^i-N(3) 2.0918(16), N(3)-C(30) 1.263(2), C(30)-C(31) 1.494(3); Mg(1)-N(3)-Mg(1)^i 95.51(6), Mg(1)-N(3)-C(30) 136.56(13), N(3)-C(30)-C(31) 127.97(18). Symmetry transformations used to generate equivalent atoms: -x+1,-y+1,-z+1.

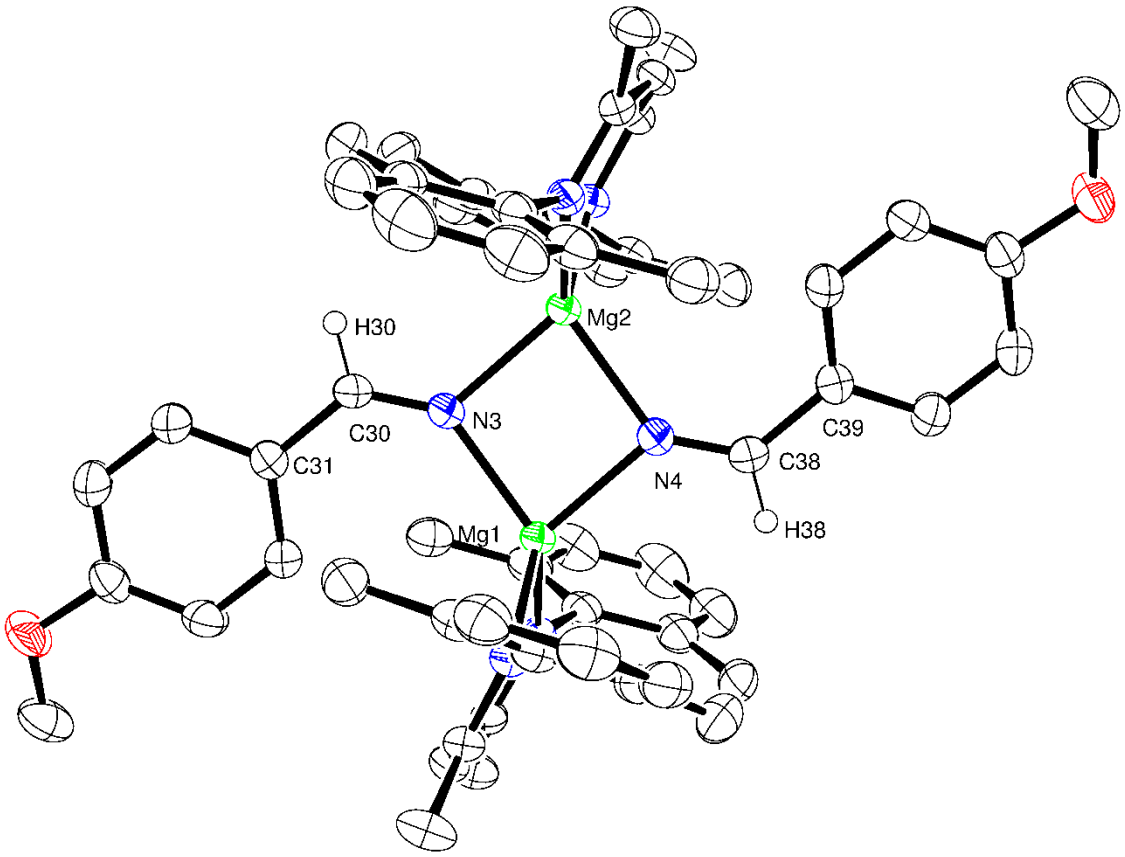

Figure 4-3. ORTEP representation of compound **70** with thermal ellipsoids set at a 30% level of probability. Hydrogen atoms, except for those attached to the C(30) and C(38) aldimide carbon centre and the methyl groups of the *β*-diketiminate 2,6-di-*iso*-propylphenyl substituents are removed for clarity. Selected bond lengths (Å) and angles (°): Mg(1)-N(3) 2.0951(16), Mg(1)-N(4) 2.0882(16), Mg(2)-N(3) 2.0909(16), Mg(2)-N(4) 2.0974(16), N(3)-C(30) 1.271(2), N(4)-C(38) 1.262(2), C(30)-C(31) 1.489(3), C(38)-C(39) 1.485(3); Mg(1)-N(3)-Mg(2) 95.26(6), Mg(1)-N(4)-Mg(2) 95.27(6), Mg(1)-N(3)-C(30) 137.55(13), Mg(2)-N(3)-C(30) 127.18(13), Mg(1)-N(4)-C(38) 127.64(13), Mg(2)-N(4)-C(38) 136.74(14), N(3)-C(30)-C(31) 128.81(17), N(4)-C(38)-C(39) 128.23(18).

Although compounds **69** and **70** are the first magnesium aldimide complexes to be characterised in the solid state, their structures are analogous to the previously described calcium benzaldimide (**XI**) reported by Harder and co-workers, which is also supported by the *β*-diketiminate ligand.[111] The structures of compounds **69** and **70** are dimeric with bridging Mg-N-Mg interactions provided by the aldimide ligands. The asymmetric unit of compound **69** comprises of half a dimer which straddles a crystallographic inversion centre, whereas each half of the dimeric unit of compound **70** is unique. Regardless of this, the gross features of both structures are very similar in the fact that both magnesium centres are bridged by unsymmetrical Mg-N-Mg interactions. The magnesium to aldimide nitrogen Mg-N bond lengths in **69** and **70** [**69**: 2.1062(16), 2.0918(16); **70**: 2.0840(16), 2.0882(16), 2.0951(16), 2.0974(16) Å] are shorter

than the magnesium to amide contacts observed within topologically related dimeric magnesium benzylamide and pyrrolidide derivatives [2.1251 and 2.117(2) Å respectively], both of which contain four-coordinate magnesium centres supported by the identical *β*-diketiminate ligand. Also noted is the transition from formal sp^3 to sp^2 hybridisation at the bridging nitrogen centres in comparison to these previously described compounds as reflected by the increased Mg-N-Mg bond angles [90.73(6) and 91.58(9)° *versus* (**69**) 95.51(6)°, (**70**) 95.26(6) and 95.27(6)°] within compounds **69** and **70**.

The methoxyphenyl rings of both compounds **69** and **70** are virtually co-planar with the planes formed by the magnesium and the aldimide nitrogen and sp^2 carbon centres; this was also observed in the discussion of the calcium benzaldimide species (**XI**) by Harder and co-workers. This in-plane conformation is also a common feature for the dimeric diorganoaluminum benzaldimide species, $[R_2AlN{=}C(Ph)H]_2$,[216] and has been calculated for the model lithium compound, $[LiN{=}CH_2]_2$,[217] to lie some 17 kcal mol^{-1} lower in energy than the alternative conformation in which the methylene unit is perpendicular to the Li_2N_2 plane. In the case of compounds **69** and **70** the angles observed by the aryl ring and the various Mg-N-C(Ar)H planes [(**69**) 0.66°; (**70**) 11.34, 10.88°] indicate that this stabilisation is further enhanced by delocalisation across the aryl substituents: this data should, however, be treated with caution due to the possibility of solid-state crystal packing and dispersion effects. The enhanced co-planarity of **69** in comparison to **70** is thought to be due to the mesomeric influence of the respectively stabilising 3-methoxy and destabilising 4-methoxyphenyl substituents. Whilst the differences in the potential for through-bond conjugation within compounds **69** and **70** has little observable effect upon the magnesium coordination environment between the two solid-state structures, the variations in the additional resonance stabilisation by the various electron withdrawing and electron donating substitution patterns across the aryl nitrile substrates listed in Table 4-1 (entries 5-14) impart a substantial effect on the overall course of the catalysis.

Continuation of the series of stoichiometric reactions by addition of 1 equivalent of HBpin to the imide product did not yield the expected borylated imine derivative (shown as species **B** in Scheme 4-1), mitigating against the proposed B-H/Mg-N metathesis step *via* intermediate **C**. Further attempts to yield the borylated imine derivative, *via* catalysis with 10 mol% **Ib** and 1 equivalent of HBpin also failed. The resulting product from the stoichiometric reaction (Figure 4-5 – ii) was assigned as a magnesium aldimidoborohydride. This was identified upon inspection of the ^{11}B NMR spectrum as a new doublet at δ 9.27 ppm ($^1J_{BH}$ = 105 Hz) indicative of a 4-coordinate boron species compared to the 3-coordinate HBpin reagent (δ 32 ppm, $^1J_{BH}$ = 175 Hz). Subsequent scale up of this reaction in hexane and storage at -30 °C, allowed for the isolation of the aldimidoborohydride derivative, compound **71**, which was fully characterised by multinuclear NMR spectroscopy and single crystal X-ray diffraction analysis (Figure 4-4).

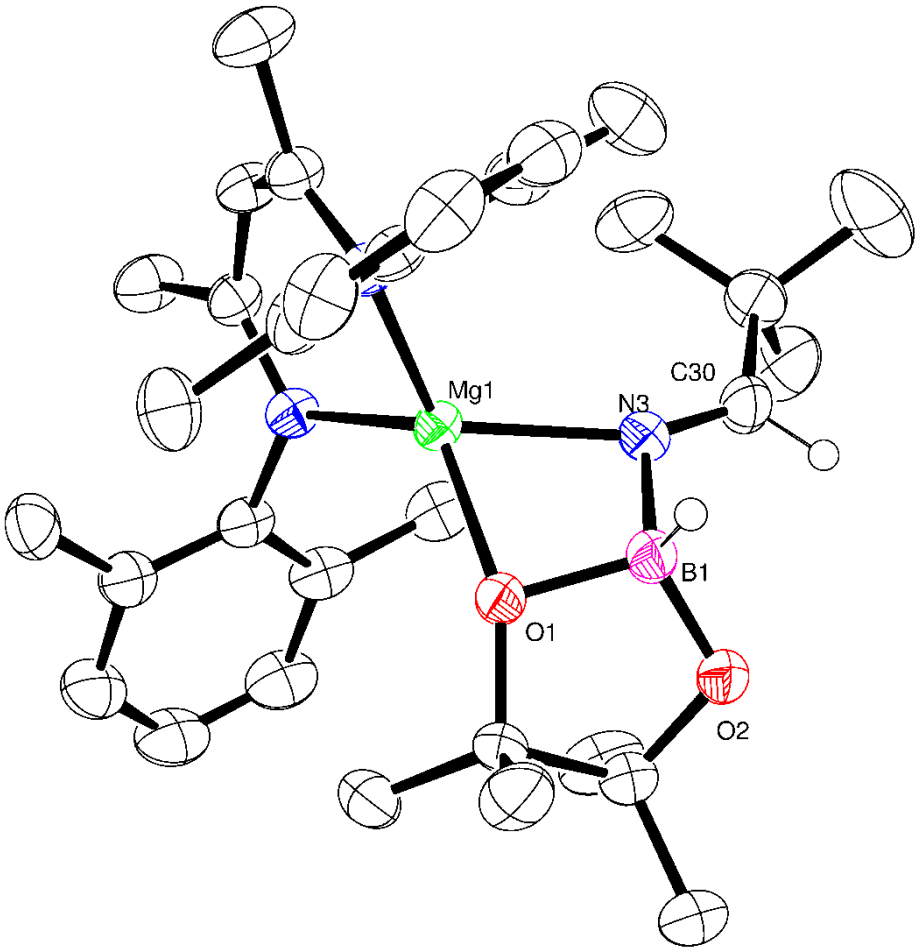

Figure 4-4. ORTEP representation of compound **71**. with thermal ellipsoids set at a 30% level of probability. Hydrogen atoms, except for those attached to B(1) and C(30) and the methyl groups of the *β*-diketiminate 2,6-di-*iso*-propylphenyl substituents are removed for clarity. Selected bond lengths (Å) and angles (°): Mg(1)-N(3) 2.0825(13), Mg(1)-O(1) 1.9714(11), N(3)-C(30) 1.266(2), N(3)-B(1) 1.572(2), B(1)-O(1) 1.529(2), B(1)-O(2) 1.441(2), B(1)-H(1) 1.157(17); O(1)-Mg(1)-N(3) 71.91(5), Mg(1)-N(3)-C(30) 150.55(12), N(3)-C(30)-C(31) 127.56(15), B(1)-N(3)-C(30) 120.10(13), O(1)-B(1)-N(3) 100.34(11).

Compound **71** comprises a monomeric species containing a distorted tetrahedral geometry about the magnesium centre. Coordination to the aldimidoborohydride ligand occurs *via* the imide nitrogen centre and one of the oxygen atoms of the pinacolate unit of the anion. Compound **71** provides the first crystallographic evidence for the intermediacy of borohydride intermediates during any magnesium-mediated hydroboration catalysis, as previous studies of both carbonyl and imine hydroboration by Hill and co-workers and Sadow's ester reduction catalysis only implied such intermediates from NMR studies. The retention of the imide moiety is evident upon comparison of the N=C bond length to the previously described magnesium aldimide compounds **69** and **70** [(**71**) 1.226(2); (**69**) 1.263(2); (**70**) 1.262(2), 1.271(2) Å]. Although shorter than in compounds **69** and **70**, this distance is closely comparable to exclusively transition metal-coordinated imine-derived borate anions.[218-220]

Upon monitoring samples in d_8-toluene, **71** was observed to undergo continued reaction on standing at room temperature over a period of 12 hours. This was observed by monitoring of the ^{1}H NMR spectra through the disappearance of the downfield 1H aldimido proton singlet and the simultaneous appearance of a new 2H resonance, by integration, at δ 3.35 ppm (Figure 4-5 – iii). The corresponding ^{11}B NMR spectrum also indicated reactivity of the aldimidoborohydride through a small downfield shift to δ 6.3 ppm with the loss of the doublet signal multiplicity. These observations are suggestive of an intramolecular hydride shift resulting in the reduction of the aldimide moiety to yield a magnesium borylamide derivative (compound **72**) analogous to that proposed as species **D** in Scheme 4-1.

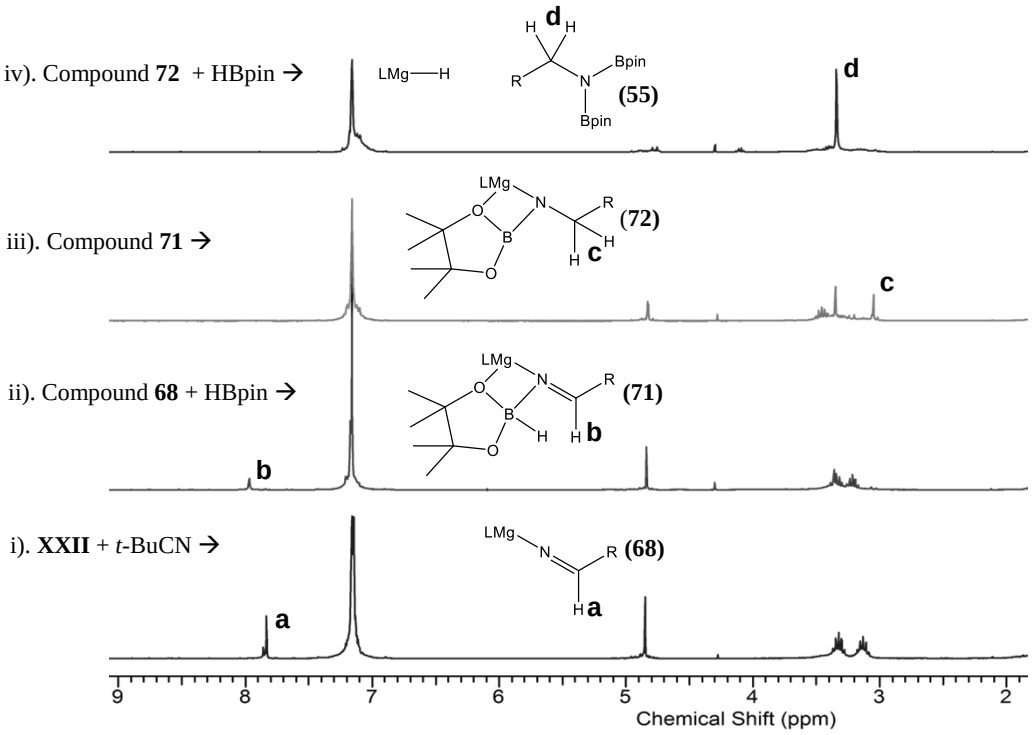

Figure 4-5. Series of stacked ^{1}H NMR spectra, in C_6D_6, for the stoichiometric reduction of *t*-BuCN with HBpin and the *in situ* generated **XXII**.

Addition of a final equivalent of HBpin (Figure 4-5 – iv) yielded the desired dihydroboration product, depicted as species **F** in Scheme 4-1. This final B-H/Mg-N σ-bond metathesis step in the proposed catalytic cycle required heating at 60 °C in order to yield the desired product (compound **55**) with regeneration of the initial magnesium hydride species. Due to the required elevated temperatures of this final step, observation of any intermediates similar to that proposed (species **E**, Scheme 4-1) were unsuccessful.

Further stoichiometric reactions with compounds **69** and **70** by addition of one equivalent of HBpin provided no evidence for similar borohydride formation. DOSY NMR analysis of these

reactions showed no change in the solution diffusion coefficient attributed to the dimeric species even with elevated temperatures and addition of further equivalents of HBpin. This is suggested to be due to the additional conjugation providing increased stability to the dimeric unit by the co-planarity of the 3- and 4-methoxyphenyl substituent and the C-N-Mg linkage.

A similar stoichiometric reaction performed through the addition of 2 equivalents of Ph_2CHCN to the *in situ* generated magnesium hydride and a further equivalent of HBpin highlighted the potential for more complex behaviour. Upon addition of the reagents, bubbles of gas were observed and single crystals of a new compound (**73**) were isolated from the unstirred reaction mixture. Whilst the single crystals were suitable for X-ray analysis (Figure 4-6), the compound was insufficiently soluble to allow for characterisation by solution-state NMR spectroscopy.

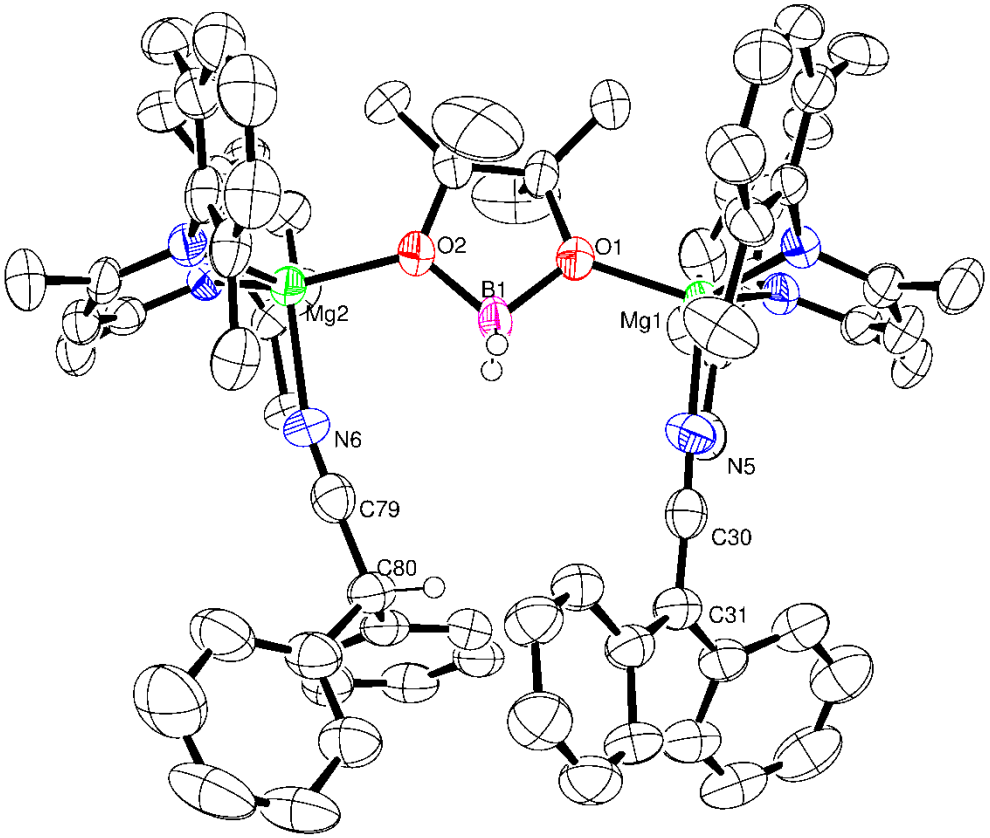

Figure 4-6. ORTEP representation of compound **73** with thermal ellipsoids set at a 30% level of probability. Hydrogen atoms, except for those attached to B(1) and C(80) and the methyl groups of the *β*-diketiminate 2,6-di-*iso*-propylphenyl substituents are removed for clarity. Selected bond lengths (Å) and angles (°): Mg(1)-O(1) 1.974(4), Mg(2)-O(2) 1.953(4), Mg(1)-N(5) 1.996(6), Mg(2)-N(6) 2.117(6), N(5)-C(30) 1.188(8), C(30)-C(31) 1.395(9), N(6)-C(79) 1.114(7), C(79)-C(80) 1.496(10); O(1)-Mg(1)-N(5) 103.31(19), Mg(1)-N(5)-C(30) 175.3(5), N(5)-C(30)-C(31) 177.7(6), O(2)-Mg(2)-N(6) 97.01(19), Mg(2)-N(6)-C(79) 166.9(5), N(6)-C(79)-C(80) 177.4(6), C(79)-C(80)-C(81) 112.6(5).

The 4-coordinate magnesium centres of compound **73** are both connected through bridging interactions provided by both oxygen atoms of a $[H_2Bpin]^-$ anion, in a manner reminiscent of the recently reported trimeric calcium species, $[HC\{C(Me)N(Dipp)\}_2Ca(H_2Bpin)]_3$ (**XXXVI**), which also contains identical β-diketiminate ligands.[153] Whilst each magnesium centre displays a similar *pseudo*-tetrahedral N_3O coordination sphere (2 sites occupied by the β-diketiminate anion and the other by the bridging borate anion), the nature of the fourth nitrogen centred ligand differs across the two Mg atoms of the molecule. Mg(1) is coordinated to the deprotonated nitrile species yielding a diphenylketeniminate anion, whilst Mg(2) binds to the neutral diphenylacetonitrile substrate. Magnesium and barium derivatives with the same diphenylketeniminate anion have been seen previously wherein the alkaline earth centres are coordinated to the sterically demanding bis(imino)acenaphthene (Dipp-BIAN) radical anions. The magnesium complex was prepared by deprotonation of the diphenylacetonitrile by Dipp-BIANMgMe.[184, 221] It is therefore suggested that the diphenylketeniminate derivative of compound **73** is formed in a similar manner. This competitive reactivity may explain the reduced yields and increased reaction times observed during the catalytic hydroboration of diphenylacetonitrile (Table 4-1, entry 15).

In combination with the results from the stoichiometric reactions it is possible to construct a new proposed catalytic cycle for the magnesium-catalysed di-hydroboration of nitriles (Scheme 4-3). This again combines a series of insertion and σ-bond metathesis steps, as well as a proposed intramolecular hydride transfer similar to that observed in isolated samples of compound **71**.

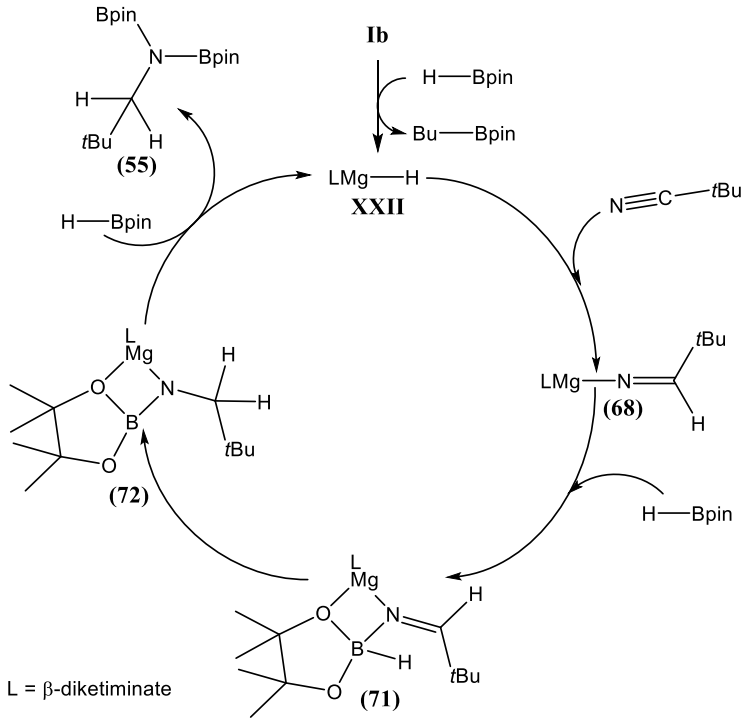

Scheme 4-3. Proposed mechanism for the magnesium-catalysed di-hydroboration of *t*-BuCN based upon findings from a series of stoichiometric reactions

4.4 Kinetic Studies

4.4.1 Alkyl Nitrile Kinetics

To further assess the mechanistic implications of these observations, a kinetic investigation into the magnesium-catalysed hydroboration of nitriles was undertaken. Propionitrile (EtCN) was selected as the representative alkyl nitrile substrate due to its provision of opportune reaction rates and clearly observed starting material and product resonances in the ^{1}H NMR spectrum. All reactions were carried out at 323 K and were monitored by ^{1}H NMR spectroscopy to three half-lives (80% product conversion), using the standard catalytic reaction of 10 mol% of the pre-catalyst **Ib** in conjunction with a 1:2.1 ratio of EtCN (0.4 M) to HBpin (0.82 M). Using the above standard reaction, the overall reaction order could be determined by comparison of a series of zero, first and second order rate plots (Figure 4-7), which indicated the reaction displays overall zero order kinetics.

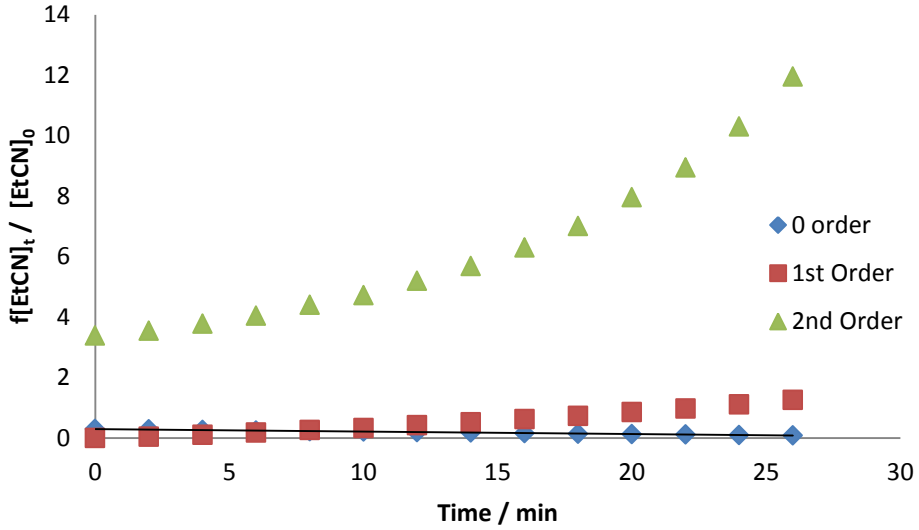

Figure 4-7. Series of different zero, first and second order plots as a function of [EtCN] vs time

While the reactions displayed overall zero order kinetic behaviour (Figure 4-7), a first order dependence on [**Ib**] was deduced through variation of the catalyst loading (Figure S 4-1) with maintenance of the same concentrations of EtCN and HBpin (Figure 4-8). This observation is consistent with other magnesium- and calcium-catalysed reactions in which the Ae centre is coordinated by a *β*-diketiminate ligand and it is suggested that this is indicative of the involvement of an isolated magnesium centre during the rate determining process of the catalysis.

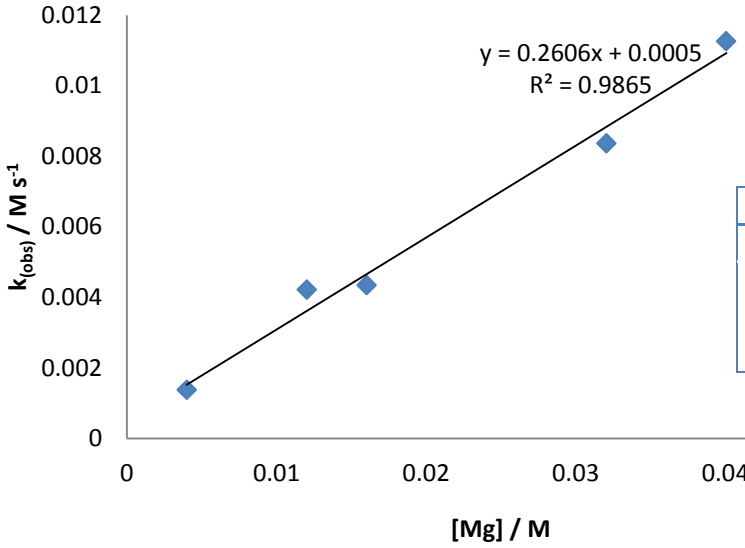

	Value	Error
m_1	0.000477	0.000435
m_2	0.260600	0.017616
Chisq	0.018455	n/a
R^2	0.9865	n/a

Figure 4-8. Plot of the observed rate constants $k_{(obs)}$ vs [Mg] and least squares error calculations

Further experiments under *pseudo*-first order conditions employing a large excess of EtCN (8.0 M) were consistent with a first order dependence on [HBpin] (Figure S 4-5) and a clear inverse

dependence of the reaction rate of EtCN dihydroboration on [EtCN] allowing deduction of the rate law (Equation 4-1).

$$Rate = k_{obs}\,[HBpin]^{1}[EtCN]^{-1}$$

Equation 4-1. Experimentally derived rate law for magnesium-catalysed alkyl nitrile kinetics

This inverse dependence on [EtCN] is thought to be due to the ability of the nitrile to coordinate to the metal centre as a neutral donor, blocking free coordination sites and impeding the approach of incoming molecules of HBpin. This is further supported by the observed first order dependence on HBpin wherein increasing the concentration will favour the displacement of the neutral nitrile from the magnesium coordination sphere allowing formation of intermediate aldimidoborohydride species similar to compound **71**.

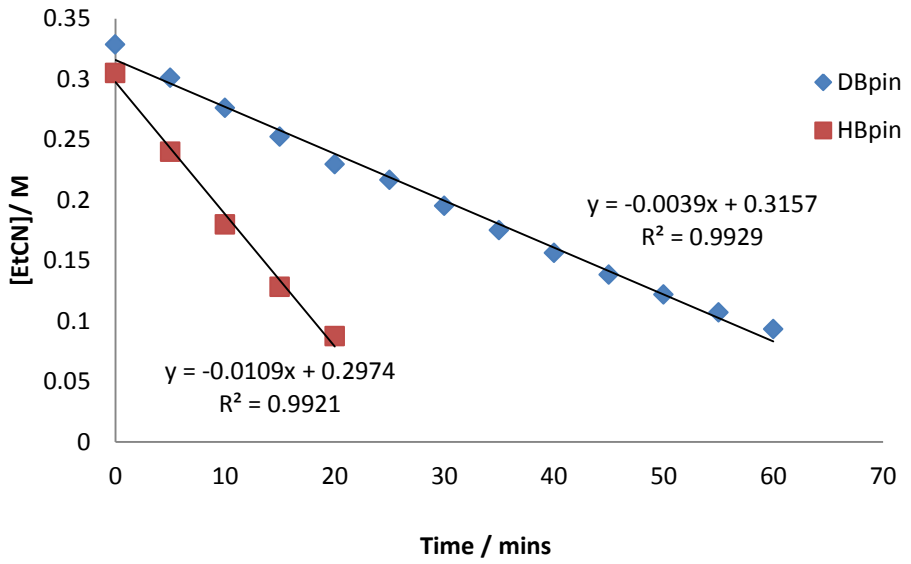

	HBpin	
	Value	Error
m_1	0.315705	0.003927
m_2	-0.003880	0.000495
Chisq	0.052852	n/a
R^2	0.992897	n/a

	DBpin	
	Value	Error
m_1	0.297389	0.006899
m_2	-0.010935	0.000563
Chisq	0.009358	n/a
R^2	0.992101	n/a

Figure 4-9. Plot of [EtCN] vs time for both HBpin and DBpin reactions

Utilising DBpin and comparison of the subsequent zero order rate constants provided a kinetic isotope effect (KIE, k_H/k_D) of 2.79 (Figure 4-9). Whilst this is relatively small, it constitutes a very large secondary effect and is significantly in excess of comparable results (k_H/k_D = 1.62) reported by Hartwig *et al* during studies of HBcat metathesis at ruthenium(II) alkyl centres, in which B-H bond breaking processes are integral to the progress of the reaction.[222] It is therefore suggested that compounds analogous to compound **71** do not persist under catalytic conditions,

but are consumed by intramolecular hydride transfer from HBpin to the metal-bound aldimide fragment.

4.4.2 Hammett Study

In order to probe the difference in observed reaction times between alkyl and aryl nitriles (Table 4-1), a Hammett study was undertaken. In all cases, reactions conformed to unambiguous first order kinetic behaviour (Figure 4-10) and the observed rate constants varied internally across the range of aryl substitution patterns employed.

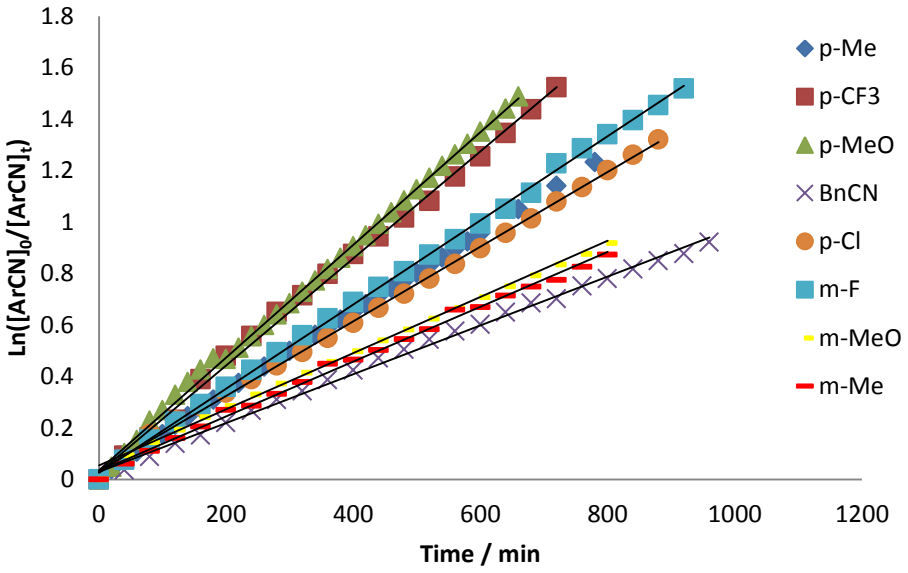

Figure 4-10. A plot of $Ln([ArCN]_0/[ArCN]_t)$ vs time for varying substitution patterns around the aryl ring. Least squares error calculations are provided in Figure S 4-8.

A Hammett plot was constructed using the observed first order rate constants against the original Hammett parameter, σ (Figure 4-11). This provided a chevron-shaped plot, with the minimum centred at 0, which indicates a change in mechanism from the transition from overall electron donating (Ar(EDG)CN), to electron withdrawing (Ar(EWG)CN) aryl nitrile substitution. A similar chevron-shaped Hammett plot has been reported for the rhodium-catalysed hydroboration of vinyl arenes, however, no further discussion about the nature of the change in mechanism was reported.[223]

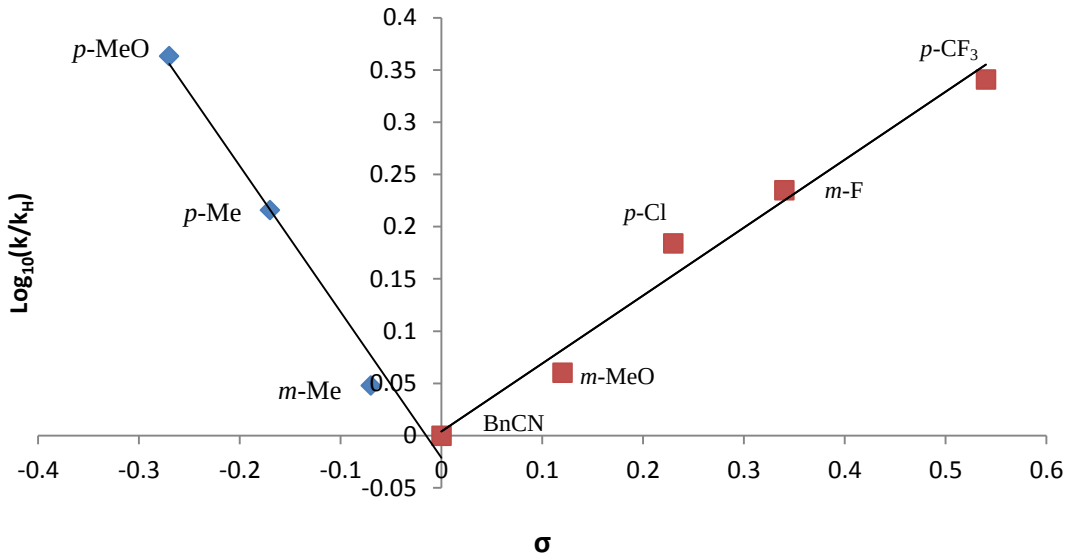

	Ar(EDG)CN	
	Value	Error
m_1	-0.021180	0.020524
m_2	-1.395670	0.125666
Chisq	0.021751	n/a
R^2	0.98404	n/a

	Ar(EWG)CN	
	Value	Error
m_1	0.004090	0.017839
m_2	0.650020	0.057909
Chisq	0.001125	n/a
R^2	0.97674	n/a

Figure 4-11. Hammett plot and least squares error calculations

Although the resultant ρ values [ρ(EDG) = –1.46; ρ(EWG) = +0.68] are relatively small and must be interpreted with caution,[224] the change in sign is indicative of minor, yet mechanistically significant, adjustments to the redistribution of electronic charge during the traversal of the rate determining transition state(s). To probe this apparent change in mechanism, rate laws for both EDG and EWG aryl nitriles will be studied.

4.4.3 Electron Donating Aryl Nitriles

Using the same reaction conditions as the alkyl nitrile kinetics, with the representative Ar(EDG)CN (*p*-(MeO)C_6H_4CN) a series of reactions were carried out to determine the order with respect to each reagent. Again a first order dependence on catalyst concentration was found (Figure 4-12), consistent with a rate determining catalytic step that is mediated by a single magnesium centre ($k_{(obs)}$ values taken from Figure S 4-12).

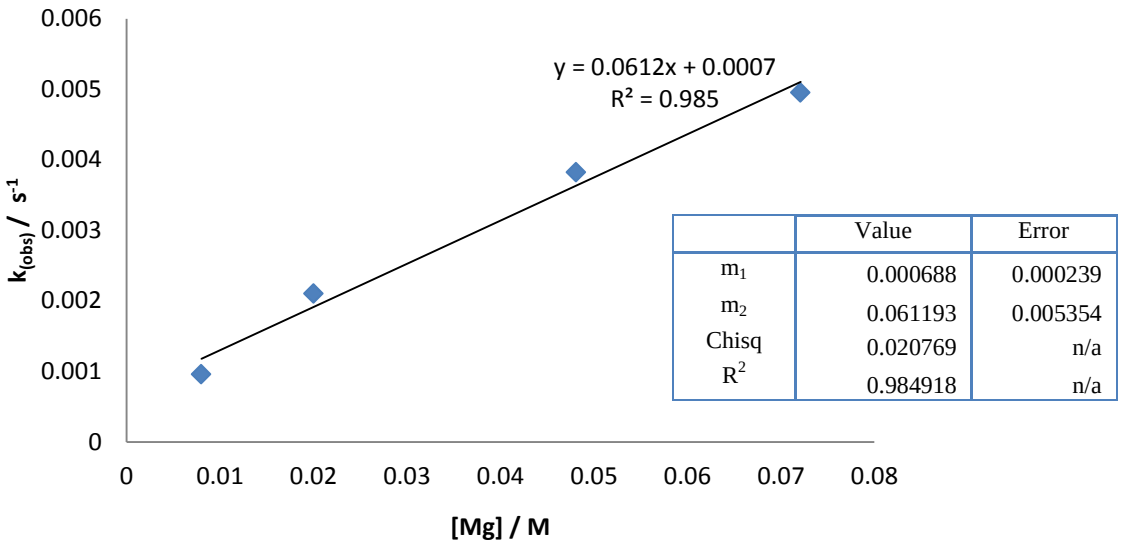

Figure 4-12. Plot of the observed rate constants $k_{(obs)}$ against [Mg]. Least squares error calculations are also provided.

Utilising *pseudo*-first order conditions to deduce the order with respect to [Ar(EDG)CN] and [HBpin], again showed an inverse dependence on [Ar(EDG)CN], however, consistent with the overall 1st order reaction kinetics, a second order dependence on [HBpin] was observed (Figure S 4-15). This provides the following rate law (Equation 4-2):

$$Rate = k_{obs}\,[HBpin]^2[Ar(EDG)CN]^{-1}$$

Equation 4-2. Experimentally derived rate law for the magnesium-catalysed hydroboration of EDG aryl nitriles

The observed inverse dependence on [Ar(EDG)CN] indicates nitrile inhibition as a key influence on the observed reaction rate. An assumption that the experimental reaction order in [HBpin] reflects the molecularity of the rate determining process, however, implicates two molecules of the borane substrate for rate determining catalytic turnover. Similar KIE values to the alkyl nitriles were observed for reactions performed with Ar(EDG)CN providing k_H/k_D = 2.44 (Figure S 4-16).

4.4.4 Electron Withdrawing Aryl Nitriles

Analogous kinetic reactions using the representative Ar(EWG)CN (*m*-(MeO)C_6H_4CN), indicated divergent reactivity despite similar overall first order rate behaviour. Reactions to identify the order of reaction with respect to [Mg] revealed an unexpected second order dependence (Figure 4-13).

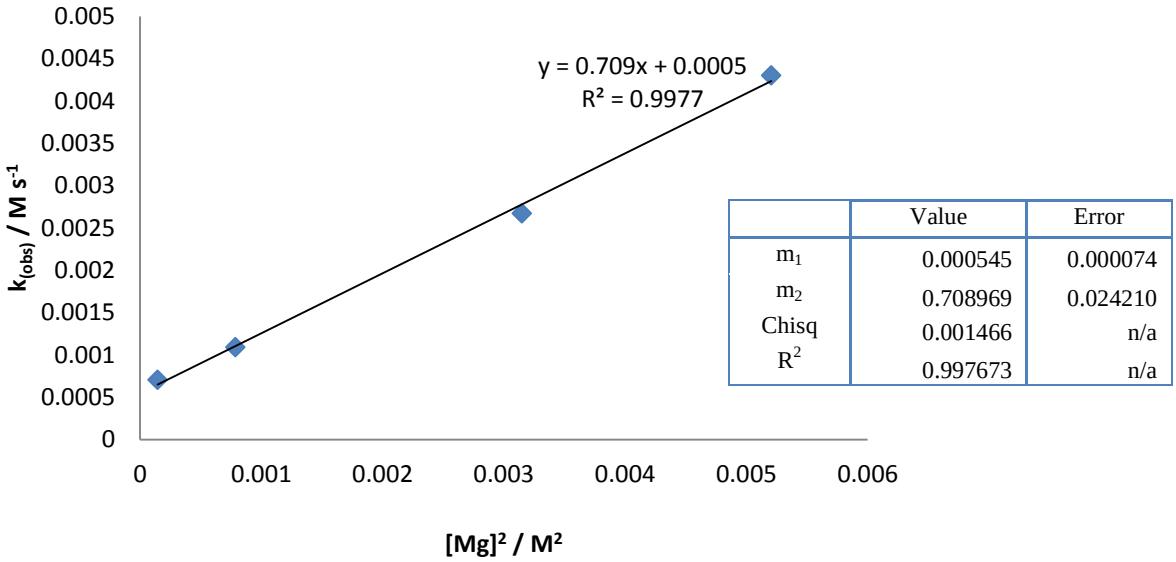

	Value	Error
m_1	0.000545	0.000074
m_2	0.708969	0.024210
Chisq	0.001466	n/a
R^2	0.997673	n/a

Figure 4-13. Plot of observed rate constants $k_{(obs)}$ vs $[Mg]^2$. Least square error calculations are also provided

Deduction of the rate law (Equation 4-3) was again carried out *via pseudo*-first order methods, which found the reaction to be independent of [HBpin] (Figure S 4-23) and provided a first order dependence on [Ar(EWG)CN].

$$Rate = k_{obs}\,[HBpin]^0[Ar(EWG)CN]^1$$

Equation 4-3. Experimentally derived rate law for magnesium-catalysed hydroboration of Ar(EWG)CN

This zero order dependence on [HBpin] was further supported by the corresponding reactions performed with DBpin, whereupon no acceleration or retardation of the reaction was observed, thus providing a KIE (k_H/k_D) of 1.00 (Figure S 4-25). This indicates HBpin has no influence on the rate determining step during the course of the magnesium-catalysed hydroboration of electron poor nitrile substrates.

Derivation of the experimentally determined rate law *via pseudo*-first order methods does provide an efficient route for gathering further information about the catalytic reaction. It was found, however, that whilst a self-consistent rate law could be determined in each case further study showed that this may not be reflective of the true catalytic conditions. Under *pseudo*-first

order conditions employing a large excess of HBpin, varying the catalyst concentration (Figure S 4-28) identified a change in the order with respect to [Mg]. Figure 4-14 shows a plot of the observed rate constants taken from a series of first order plots for varying [Mg] under the large excess of HBpin. A linear plot is obtained against the cube of [Mg] indicating a third order dependence on catalyst concentration.

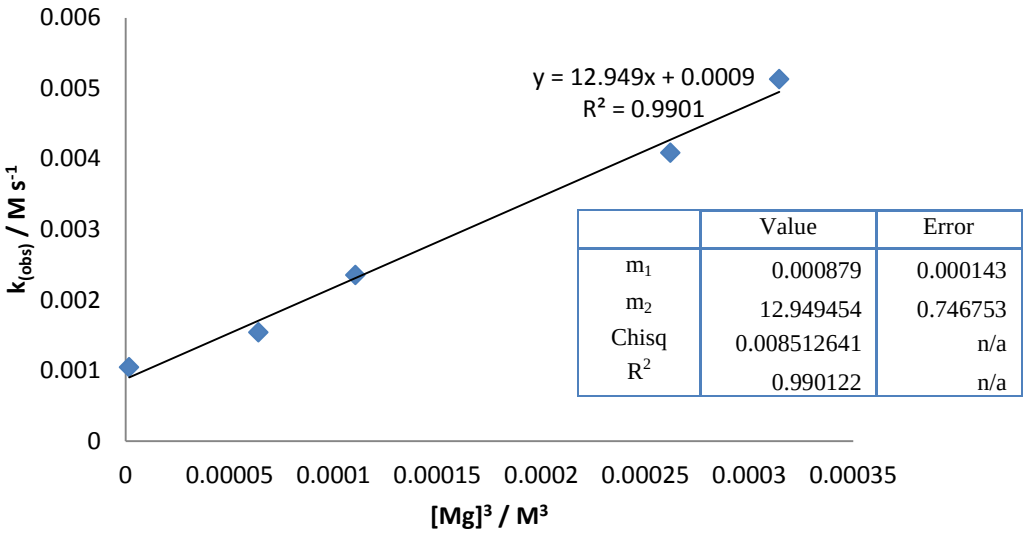

Figure 4-14. Plot of observed rate constants $k_{(obs)}$ vs $[Mg]^3$. Least squares error calculations are also provided

Analogous change in catalyst rate dependence was also observed for both the alkyl and Ar(EDG)CN substrate cases, indicating a different mechanism is operant under *pseudo*-first conditions in HBpin. It is a proposed that a trimeric magnesium species is the active catalyst under these conditions (Figure 4-15), similar to a calcium species identified by Harder and co-workers for during their study of calcium-mediated hydroboration of alkenes (**XXXVI**, Figure 1-9).[153]

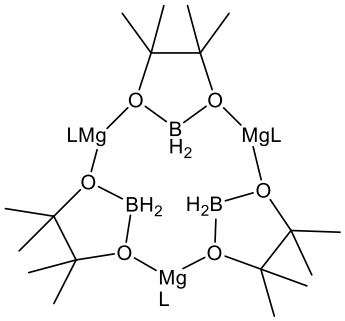

Figure 4-15. Proposed active catalyst under *pseudo*-first order conditions in HBpin

Although attempts to isolate this species failed to provide crystals suitable for single crystal X-ray analysis, this apparent change in the active catalyst species indicates that such *pseudo*-first order conditions in [HBpin] are not reflective of the catalysis performed under the correct 2:1

(HBpin: RCN) stoichiometry of the hydroboration reaction. Further experiments were also carried out under *pseudo*-first order conditions employing a large excess of nitrile. These experiments provided no change in the order with respect to [catalyst]. The observation of such a change in catalyst rate dependence at high [HBpin] indicates that, while three classes of nitrile rate laws may be deduced for the three classes of nitrile studied, this data must be interpreted with caution. With this provision in place, however, it remains instructive to consider the possible mechanistic implications of the apparent variations across equations 4-1, 4-2 and 4-3.

4.4.5 Variable Temperature Studies

Further insight into the nature of these mechanistic discontinuities was provided by variable temperature kinetic studies of all three reaction types. The macro- and microscopic activation parameters for the hydroboration of EtCN, *p*-(MeO)C_6H_4CN, *m*-(MeO)C_6H_4CN mediated by 10 mol % of **Ib** were determined through Eyring (Figure 4-16 (Alkyl), Figure S 4-41 (EDG) and Figure S 4-46 (EWG)) and Arrhenius analyses (Figure 4-17 (Alkyl), Figure S 4-42 (EDG) and Figure S 4-47 (EWG))) performed at four different temperatures, with standard errors calculated using the least squares method for linear regression (Table 4-2).

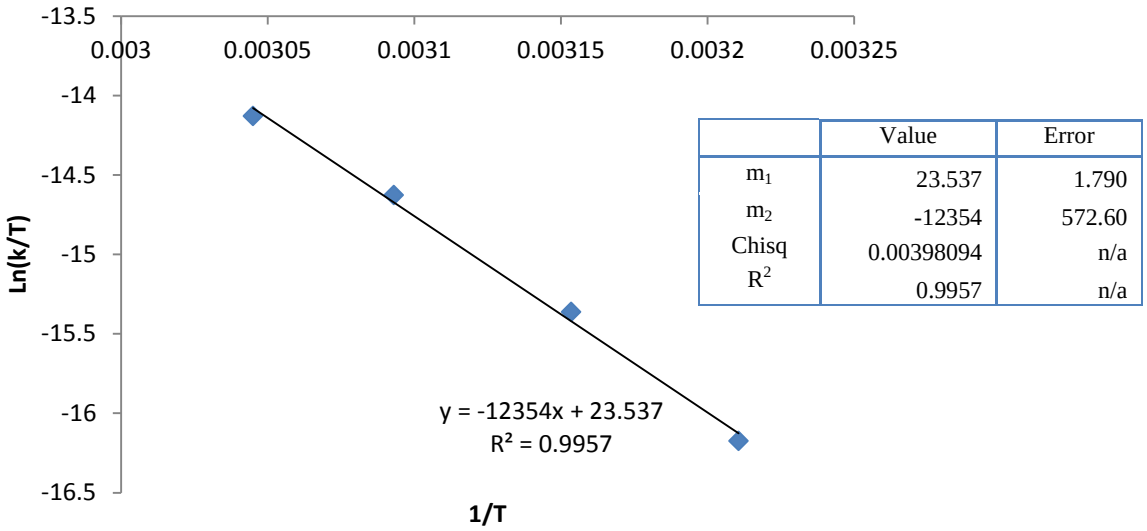

Figure 4-16. Eyring Plot for magnesium-catalysed alkyl nitrile hydroboration

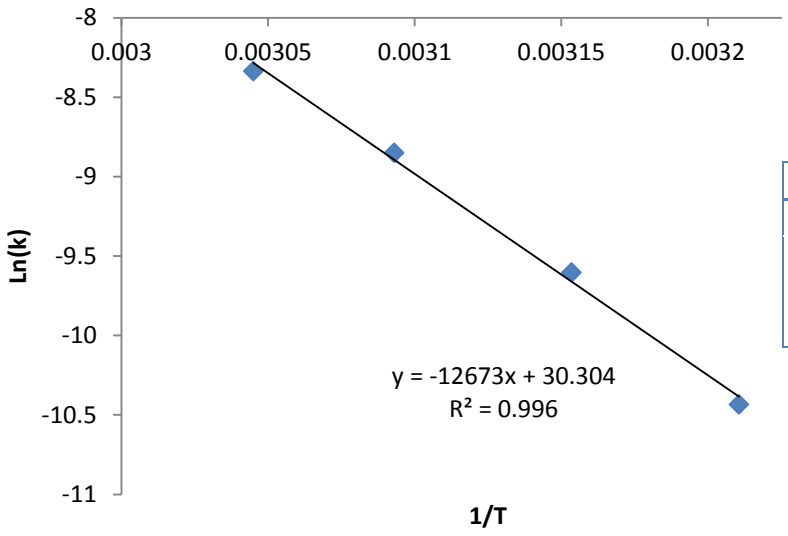

	Value	Error
m_1	30.304	1.785
m_2	-12673	570.876
Chisq	0.004023456	n/a
R^2	0.9960	n/a

Figure 4-17. Arrhenius Plot for the magnesium-catalysed alkyl nitriles hydroboration

Table 4-2. Kinetic activation parameters for the hydroboration of EtCN, *p*-(MeO)C_6H_4CN and *m*-(MeO)C_6H_4CN mediated by 10 mol% **Ib**.

Nitrile	E_a (kJ mol^{-1})	$\Delta H^{\neq}$ (kJ mol^{-1})	$\Delta S^{\neq}$ (J K^{-1} mol^{-1})
EtCN	105.4 (±4.8)	102.7 (±4.8)	-1.9 (±14.9)
***p*-(MeO)C_6H_4CN**	52.6 (±7.0)	49.9 (±7.0)	-176.3 (±21.9)
***m*-(MeO)C_6H_4CN**	48.4 (±3.4)	45.8 (±3.4)	-190.8 (±10.6)

The data presented in Table 4-2 again indicates considerable variability and strongly indicates different rate determining and bond breaking and forming processes across the three substrate classes. While the hydroboration of EtCN is enthalpically disadvantaged and the catalysis benefits from a markedly less negative (effectively zero) activation entropy than that deduced for either aryl substrate. This observation and the observed rate law presented in Equation 4-1, along with the significant KIE value implicates a combination of borane and nitrile substrates which are pre-assembled at the magnesium centre prior to B-H bond breakage. It is thus suggested that compound **71** provides a viable solid-state model for the assembled rate determining step during the hydroboration of alkyl nitriles prior to the intramolecular B-N bond forming and B-H bond breaking process to form the magnesium borylamido species which is then rapidly consumed by facile Mg-N/B-H metathesis with a further equivalent of HBpin.

In comparison the $\Delta H^{\neq}$ and $\Delta S^{\neq}$ values for both the aryl nitrile substrates are notably dictated by entropic rather than enthalpic contributions. In each case the enthalpic contribution to the microscopic activation free energies are ca. 50% of that deduced for EtCN. The significantly negative activation entropy of ca. -180 J K^{-1} mol^{-1} is, in both cases, indicative of the associative

formation of activated complexes through the assembly of two or more reaction components and must be accounted for in any mechanistic rationale.

4.5 Mechanistic Considerations

Whilst a series of different rate laws were found (Equation 4-1-3), and a clear change in mechanism was indicated between electron donating and electron withdrawing groups, as illustrated by the Hammett Plot (Figure 4-11), it is proposed that each reaction type conforms to a common mechanism. The differing kinetic profiles for the three substrate classes simply indicate a substrate-dependent adjustment to the individual kinetic barrier heights of a delicately poised, multi-step reaction during the traversal of a relatively shallow potential energy surface.

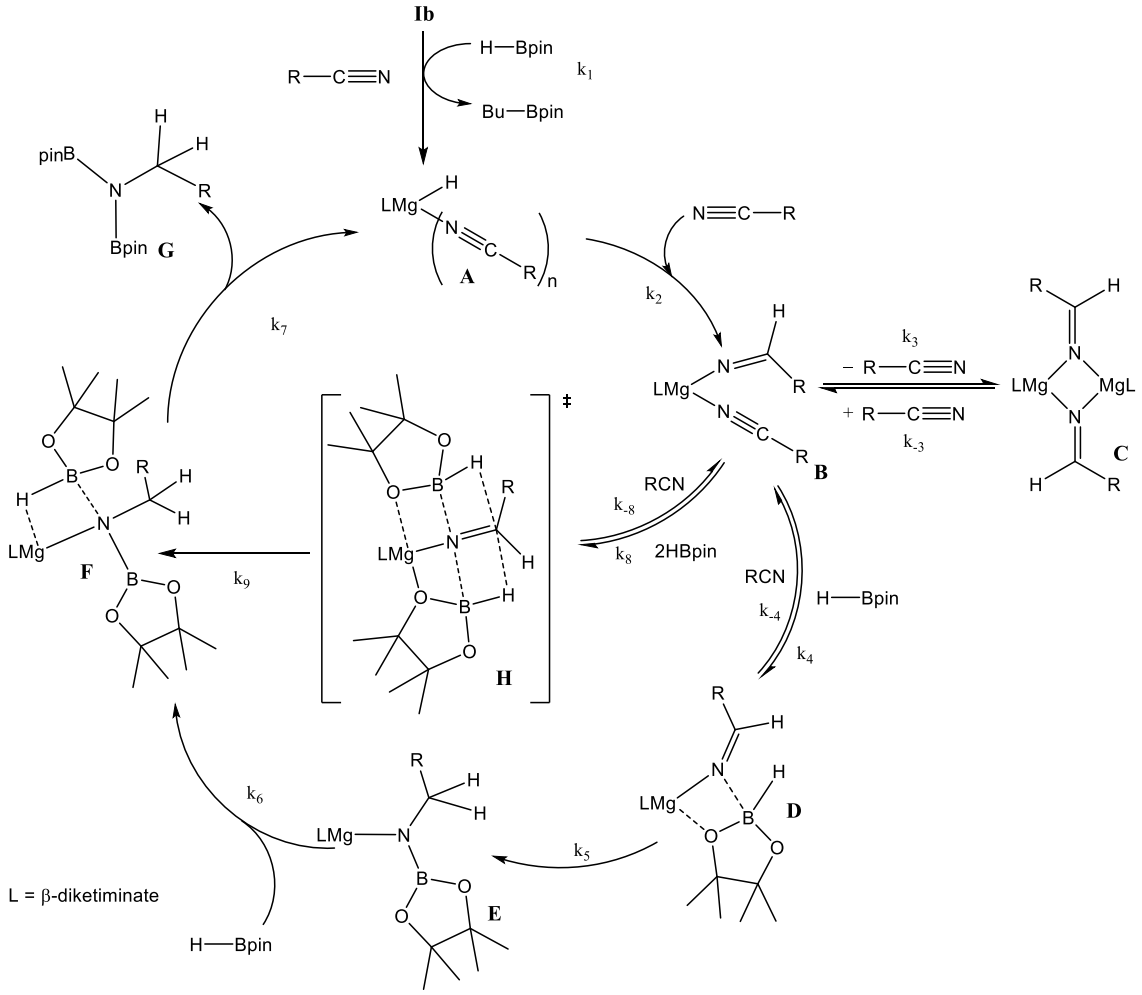

Scheme 4-4. Proposed mechanism for the magnesium-catalysed hydroboration of nitriles

Scheme 4-4 outlines a catalytic mechanism that, although common to each substrate, identifies the discrepancies between the various rate determining steps for (a) alkyl nitriles (RCN), (b) electron donating aryl nitriles (Ar(EDG)CN) and (c) electron withdrawing aryl nitriles (Ar(EWG)CN). A common initiation step, conversion of the magnesium pre-catalyst (**Ib**) into

the active hydride species (**A**) through σ-bond metathesis of the magnesium-butyl bond with HBpin, is proposed. Insertion of the nitrile substrate into the Mg-H bond is also observed for all substrates, as confirmed by the isolation of compounds **69** and **70** and the NMR observation of **68**. Although the activation of organonitriles towards different nucleophiles (e.g. water, alcohols, amines,[225-228] mercaptans,[229] phosphines,[230, 231] oximes[232, 233]) by coordination to transition metal centres is well known and has been rationalised by an increase of the effective positive charge induced on the nitrile *sp* carbon centre.[234, 235] This process is, however, observed to have little overall impact on the facility for catalytic turnover. It is therefore proposed that the rate determining processes of the catalytic reaction depend upon a series of differing pre-equilibria, which are dictated by variations in nitrile basicity and magnesium aldimide stability. Whilst only minor variations in experimental and calculated gas-phase basicities and proton affinities have been reported across a variety of organic nitriles,[236-240] it is suggested that even the slight changes in basicity induced by the relative stabilising influence of the *N*-alkyl or *N*-aryl residue will affect the access of HBpin to the magnesium centre, and the consequent formation of borate species similar to compound **71**, which is necessary for subsequent catalytic turnover. From this perspective, the variation in rate law across the three substrate classes (a) – (c) may be discriminated.

4.5.1 Alkyl Nitriles, case (a)

As identified during the kinetic studies, an isolated magnesium centre is likely to be involved in the rate determining step. The more basic nature of the alkyl nitriles ensures that the monomer/dimer equilibrium shown in Scheme 4-5 favours the monomeric species, **B** (i.e. $k_{-4} >> k_4$). The formation of aldimidohydridoborate anions (compound **71**, depicted as species **D** in Scheme 4-4) requires the displacement of pre-coordinated nitrile by the HBpin substrate. This equilibrium process is inhibited by increasing nitrile concentration reflecting the inverse order dependence identified in Equation 4-1. Once formed, subsequent imine reduction by intramolecular boron-carbon hydride transfer to form the borylamide intermediate **E**, is facile and dictated by the relative stability of the aldimide fragment and subsequent Mg-N metathesis and the second equivalent of HBpin to provide the ultimate bis(boryl)amine product (**G**) *via* the assembly of a further borate intermediate (**F**). The aldimide group in this case is inductively destabilised by alkyl substitution, and therefore this process is suggested to be relatively facile and occurs immediately upon borane coordination under catalytic conditions with $k_5 > k_{-4}$ (Scheme 4-5). This is further supported by the effectively zero entropic component (-1.9 (±14.9) J K^{-1} mol^{-1}) of the free energy of activation for this process.

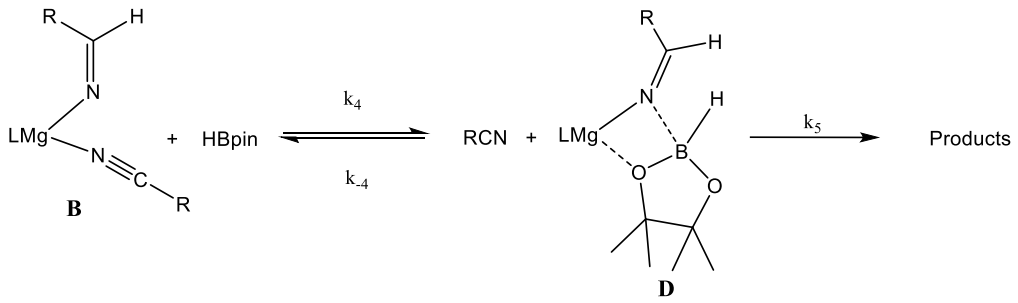

Scheme 4-5. Proposed rate determining pre-equilibrium step for alkyl nitriles

$$\frac{d[Prod]}{dt} = k_5[\boldsymbol{D}]$$

At equilibrium: $K_{BD} = \frac{[\boldsymbol{D}][RCN]}{[\boldsymbol{B}][HBpin]} = \frac{k_4}{k_{-4}}$

$$\frac{d[Prod]}{dt} = \frac{k_5 k_4[\boldsymbol{B}][HBpin]}{k_{-4}[RCN]} = \frac{k_{obs}[\boldsymbol{B}][HBpin]}{[RCN]}$$

Under catalytic conditions [**B**] is constant, thus: Rate $= \frac{k_{obs}[HBpin]}{[RCN]}$

Equation 4-4. Derivation of RDS by steady state approximations

The catalytic hydroboration of alkyl nitriles is consequently determined by the pre-equilibration of **B** to **D** and its subsequent rapid consumption through B-H transfer to the coordinated aldimide fragment in a sequence of reactions described by Equation 4-4, which corresponds to the experimentally derived rate law Equation 4-1. It is therefore proposed that the observed rate of catalysis for the alkyl nitrile hydroboration is, thus, dictated by the ability of HBpin to replace the nitrile in the magnesium coordination sphere.

4.5.2 Electron Donating Aryl Nitriles, case (b)

Aryl nitriles containing electron donating groups are disfavoured with respect to more electron withdrawing substitution; however the aldimide derivatives formed through their reduction benefit from considerably enhanced conjugative stability in comparison to those bearing alkyl groups of comparable steric demands. In this case, it is suggested that the kinetic profile summarised by Equation 4-2 reflects the resistance to intramolecular hydride transfer of an aldimidoborate species analogous to compound **71** (species **D** in Scheme 4-4). The inverse dependence on [Ar(EDG)CN] in Equation 4-2, implies the ease of formation of such species is again dictated by the ability of HBpin to displace the magnesium-coordinated nitrile. In this case the additional stability of the resultant aldimidoborate towards intramolecular C=N reduction suggested the sequence of reactions derived from species **D** in Scheme 4-4 is inoperable for these more conjugatively-stabilised intermediates. It is thus suggested that

hydride transfer and consequent catalytic turnover occurs *via* the formation of transition state **H** under the assistance of a second molecule of HBpin (Scheme 4-6), which destabilises the aldimide linkage towards hydride transfer.

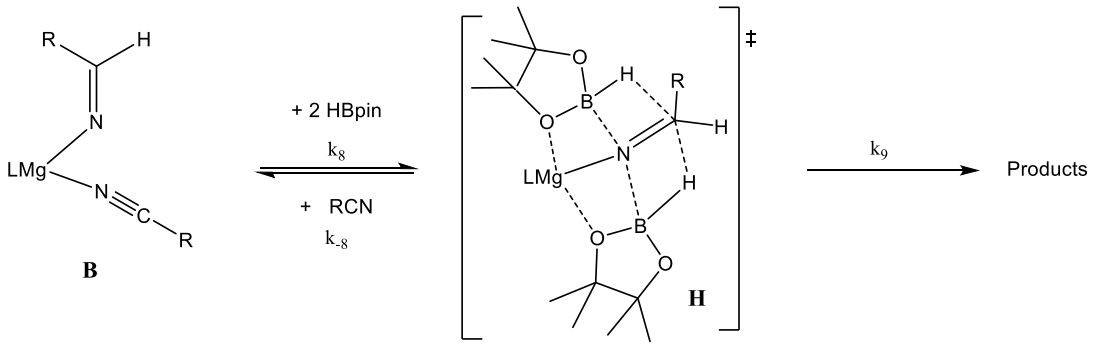

Scheme 4-6. Proposed rate determining pre-equilibrium step for Ar(EDG)CN

$$\frac{d[Prod]}{dt} = k_9[\boldsymbol{H}]$$

$$K_{BH} = \frac{[\boldsymbol{H}][Ar(EDG)CN]}{[\boldsymbol{B}][HBpin]^2} = \frac{k_8}{k_{-8}}$$

$$\text{Hence: } \frac{d[Prod]}{dt} = \frac{k_9 k_8\,[\boldsymbol{B}][HBpin]^2}{k_{-4}[Ar(EDG)CN]} = k_{obs}\frac{[\boldsymbol{B}][HBpin]^2}{[Ar(EDG)CN]}$$

Under catalytic conditions [**B**] is constant, thus:

$$Rate = k_{obs}\frac{[HBpin]^2}{[Ar(EDG)CN]}$$

Equation 4-5. Derivation of RDS by steady state approximations for Ar(EDG)CN

Although this circumvents the formation of a borylamide analogous to species **E**, the KIE (2.44) associated with this process is comparable to that observed for alkyl nitrile hydroboration and it is therefore suggested that this occurs as a stepwise process rather than an alternative pathway involving simultaneous aldimide reduction and Mg-N/B-H metathesis. The pre-equilibrium of Ar(EDG)CN and HBpin and the involvement of a second molecule of HBpin to provide the activated complex represented by transition state **H**, is reflective of the notably negative activation entropy resulting from this process ($\Delta S^{\neq}$ = -176.3 (±21.9) J K^{-1} mol^{-1}). Consideration of the entire process (Scheme 4-6), allows for the deduction of a rate law (Equation 4-5) which corresponds with the experimentally derived rate law and predicts the second order dependence on [HBpin], whilst also accounting for the inhibitory effects of increasing nitrile concentration and a first order reliance of [Mg].

4.5.3 Electron Withdrawing Aryl Nitriles, case (c)

Insertion of the representative (EWG) aryl nitrile, 3-methoxybenzonitrile into the Mg-H bond provides a dimeric aldimide (**C**) with a solution structure similar to that depicted for compound **69** (Figure 4-2) as the catalytic resting state. The zero order dependence in Equation 4-3 on [HBpin] in equation 4-3 suggests HBpin is not involved in the rate determining step, a deduction which is further supported by the absence of a KIE upon replacement with DBpin. The pre-equilibrium depicted in Scheme 4-7 is, thus, entirely dependent on the ability of the weakly basic nitrile to coordinate to magnesium with rupture of the dimeric resting state to form the intermediate **B***. Use of the steady state approximation (Equation 4-6) allows for the derivation of a rate law that is independent of [HBpin] and predicts the rate determining process in hydroboration catalysis in which $k_3 >> k_{-3} < k_4$.

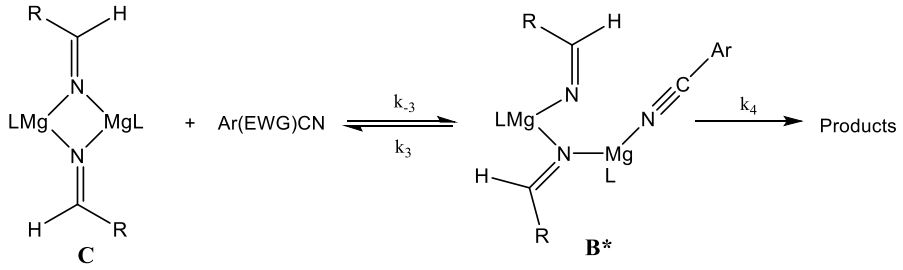

Scheme 4-7. Proposed rate determining pre-equilibrium step for Ar(EWG)CN

$$\frac{d[Prod]}{dt} = k_4[\boldsymbol{B}^*]$$

$$\frac{d[\boldsymbol{B}^*]}{dt} = k_{-3}[\mathbf{C}][Ar(EWG)CN] - k_3[\boldsymbol{B}^*] - k_4[\boldsymbol{B}^*] = 0$$

$$[\boldsymbol{B}^*] = \frac{k_{-3}[\boldsymbol{C}][Ar(EWG)CN]}{k_3 + k_4}$$

$$\frac{d[Prod]}{dt} = \frac{k_4 k_{-3}[\boldsymbol{C}][Ar(EWG)CN]}{k_3 + k_4} = k_{obs}[\boldsymbol{C}][Ar(EWG)CN]$$

Under conditions of the catalysis [**C**] is constant, thus:

$$Rate = k_{obs}[Ar(EWG)CN]$$

Equation 4-6. Derivation of RDS by steady state approximations for Ar(EWG)CN

The ability of the dimeric aldimide units to dissociate into monomeric units (**B** in Scheme 4-4) conflicts with the identification of a second order dependence on [Mg] and the notably negative activation entropy deduced for this reaction ($\Delta S^{\neq}$ = -190.8 (±10.6) $J.K^{-1}.mol^{-1}$). It is suggested, therefore, that this occurs with only partial rupture of the dimeric unit as illustrated in Scheme

4-7, whereupon subsequent reaction with HBpin can only take place at the terminal aldimide to magnesium bond of the unsymmetrical dimeric intermediate (**B***). Under this regime the experimentally deduced second order dependence on initial pre-catalyst concentration (**Ib**) is reflective of the involvement of two magnesium centres in the formation of **B***.

4.5 Conclusions

In conclusion, the *β*-diketiminato magnesium species, **Ib**, is an active precatalyst for the HBpin-derived hydroboration of a range of alkyl and aryl nitriles with HBpin to form bis(boryl)amines. Catalysis occurs readily under mild conditions, with reasonable catalyst loadings and is proposed to occur through a series of magnesium-mediated insertion and metathesis steps. Whilst a common catalytic manifold may be applied to describe the reduction of every nitrile assessed, subtle variations in the structure of the substrate results in different rate determining steps which are proposed to be a consequence of minor changes in substrate basicity and the stability of mono- and dimeric intermediates. These observations indicate that, somewhat counter to historical prejudice, there is likely to be considerable variation across even superficially identical reactions when catalysed by alkaline earth metals.

Chapter 5. Hydroboration of Isonitriles

5.1 Introduction

Isonitriles are a delicately poised chemical entities capable of being coaxed to react as nucleophiles or electrophiles. Directing this tunable reactivity with metal and non-metal catalysts provides rapid access to a large array of complex nitrogenous structures ideally functionalised for medicinal applications.[241] The majority of isonitrile reactivity observed in synthesis has been in the form of multicomponent reactions most notably the Passerini and Ugi[242] reactions (Figure 5-1). Whilst isoelectronic to CO, analogous insertion and subsequent catalytic activity is significantly less common in the literature. This is thought to be due to the stronger σ-donation from the lone pair on the carbon, in comparison with CO, which leads to particularly strong complexes with metals in high oxidation states.[243] This presents its own challenges during catalysis such as preventing multiple insertions, which could lead to oligomers and polymers, as well as irreversible complexation to the catalyst.

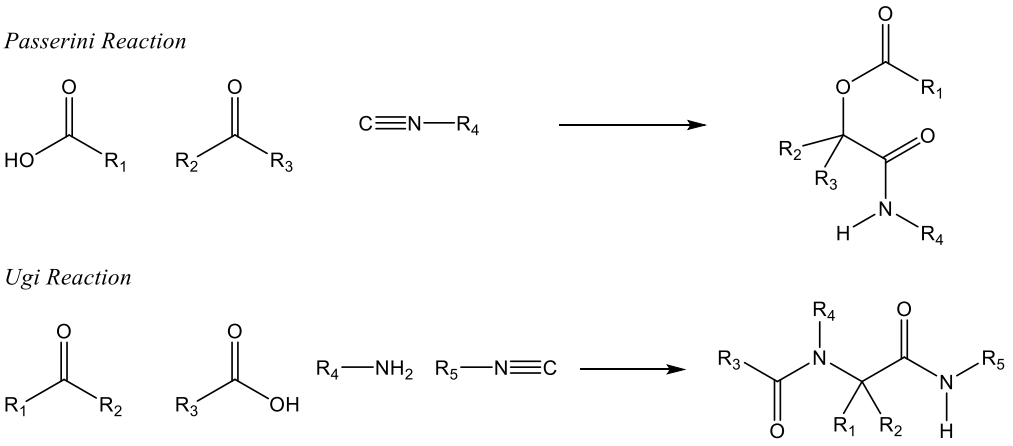

Figure 5-1. Passerini and Ugi reactions

In terms of heterofunctionalisation of isonitriles very little has been reported in the literature.[244] The one notable reaction is Figueroa's recent stoichiometric and uncatalysed 1,1-hydroboration of *m*-terphenylisocyanide to form a (boryl)iminomethane (Scheme 5-1). Using 0.5 equivalents of 9-BBN afforded the 1,1-hydroboration product whilst using a stoichiometric amount yielded the fully reduced 1,2-diborylated product. Attempts using HBpin required a 10 fold excess and prolonged heating at 100 °C to form the 1,1-diborylated product.[245] Whilst both of these reactions show the potential for the hydroboration of isonitriles, neither use a catalyst and the use of commercially available isonitriles is yet to be explored.

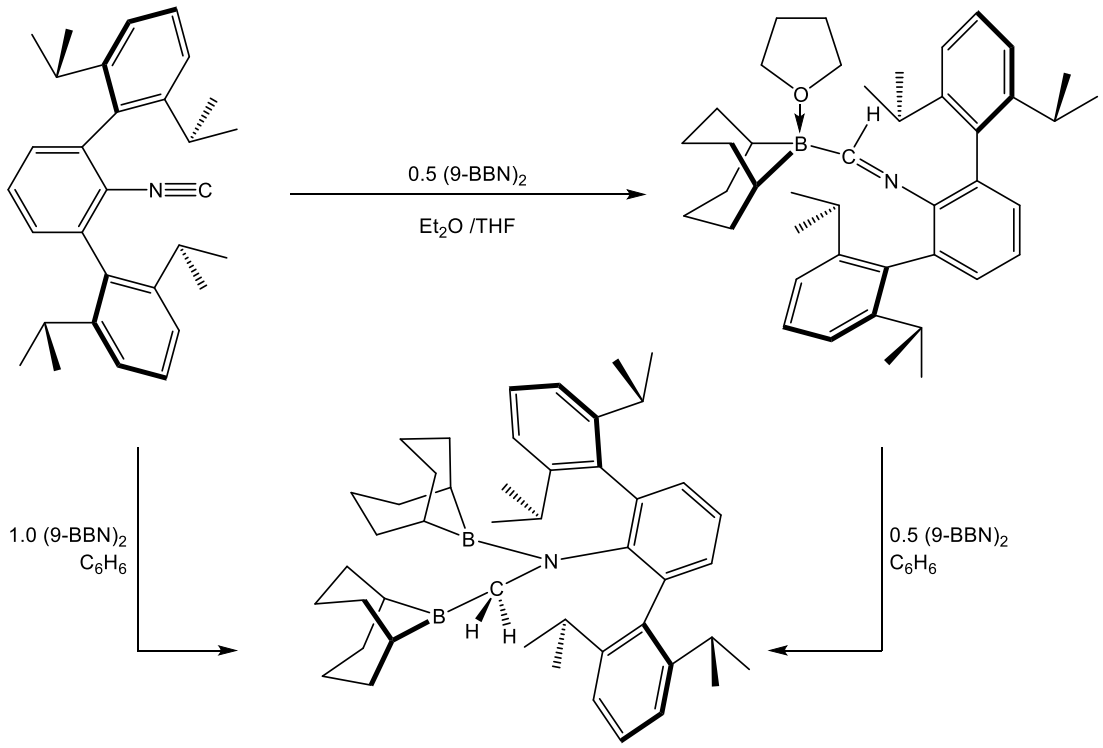

Scheme 5-1. Stoichiometric and uncatalysed hydroboration of *m*-terphenylisocyanide with 9-BBN

Other examples of heterofunctionalisation of isonitriles again involve stoichiometric reduction *via* aluminium hydrides; examples by Power,[246] Roesky[247] and Uhl[216] all show insertion into the aluminium hydride to form new C-H bonds. Harder *et al* have also reported the insertion of *tert*-butyl and cyclohexyl isonitrile into the *β*-diketiminate supported calcium hydride (**VIII**) to form calcium aldimide complexes (**XII**, Scheme 1-11) .[111]

5.2 Catalysis

An initial trial catalytic reaction using 10 mol% of **Ib** with cyclohexylisonitrile (CyNC) and 2 equivalents of HBpin at 60 °C was carried out (Table 5-1, entry 5-1). This reaction proceeded with full consumption of the starting reagents within 30 minutes. Inspection of the ^{11}B NMR spectrum showed no sign of the HBpin doublet; rather the spectrum was characterised by two new signals in a 1:1 ratio at δ 37.5 ppm and δ 27.8 ppm representative of new C-B and N-B bonds respectively. Analysis of the ^{1}H NMR spectrum also showed complete consumption of CyNC as identified by a downfield shift in the nitrogen-bound C*H* of the Cy group from δ 2.96 ppm to δ 3.32 ppm as well as a new 2H singlet at δ 2.81 ppm indicating reduction of the CyNC triple bond had occurred to form the desired C-B and N-B functionalised amine product, CyN(Bpin)CH_2Bpin (Scheme 5-2).

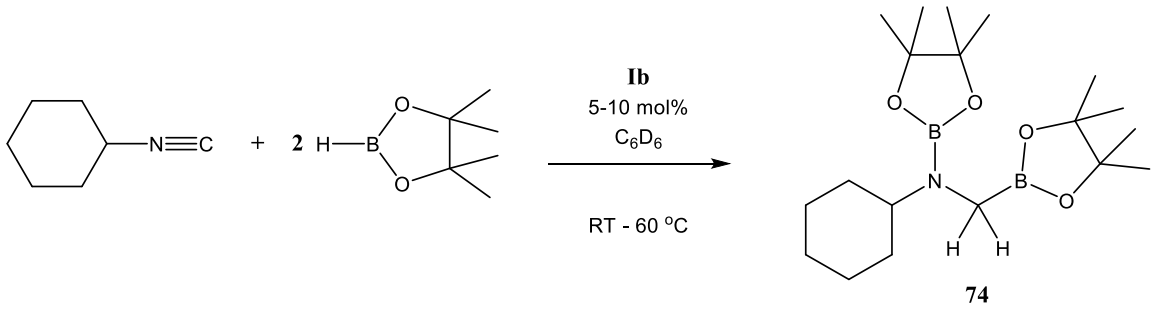

Scheme 5-2. Hydroboration of cyclohexyl isonitrile

As the trial reaction proceeded smoothly, the catalyst loading was reduced by half and catalysis was attempted at various temperatures in order to find the optimal conditions for reduction the of CyNC, which could then be applied to a variety of commercially available substrates (Table 5-1, entries 5-2 to 5-5). After 1 hr at room temperature (entry 5-2) only 7% of the CyNC starting material had reacted, however, full conversion was achieved after 48 hrs at room temperature. Increasing the temperature to 40 °C (entry 5-3) provided two-fold increase in conversion after 1 hr; whereas full conversion to the desired product could be achieved at 60 °C (entry 5-5) within the same time period. Notably, an identical reaction at 60 °C (entry 5-6) but undertaken without any magnesium pre-catalyst, provided negligible consumption of the HBpin or CyNC reagents after 24 hrs at 60 °C.

Table 5-1. Temperature optimisation study of magnesium-catalysed hydroboration of cyclohexylisonitrile

Entry	Catalyst (mol %)	Time (hrs)	Temp (°C)	NMR yield (%)
5-1	10	0.5	60	>99
5-2	5	1	RT	7
5-3	5	1	40	15
5-4	5	1	50	30
5-5	5	1	60	>99
5-6	0	24	60	5

After this successful hydroboration of CyNC, the scope of this reaction was expanded to various other commercially available isonitriles. Due to the foul smelling nature of this class of compound, only NMR studies in which they could be contained in a sealed Youngs tap NMR tube were undertaken. Table 5-2 shows several examples of hydroboration of isonitriles, using 5 mol% of **Ib** in C_6D_6. Reactions with alkyl isonitriles, 1-pentyl (entry 5-7) and *tert*-butyl isonitrile (entry 5-8), cleanly afforded the desired product in a relatively short time span. Surprisingly the rate of reaction was seemingly uninfluenced by the steric demands of the *tert*-butyl group compared to previous hydroboration reactions where a decrease in rate was

observed with increasing bulk. Benzylisonitrile (entry 5-9), however, provided more rapid conversion to the amine product compared to the alkyl isonitriles. Reactions with aryl isonitriles, containing 2-napthyl (entry 5-10) and 2,6-dimethylphenyl (entry 5-11) *N*-substitution, required increased temperatures of 100 °C and only reached 50% conversion after 48 hrs. Although undoubtedly a consequence of the change in the electronic nature of the aryl substitution, this reduced conversion is also attributed to redistribution of HBpin as seen previously at elevated temperatures/increased reaction times.

Table 5-2. Magnesium-catalysed hydroboration of isonitriles

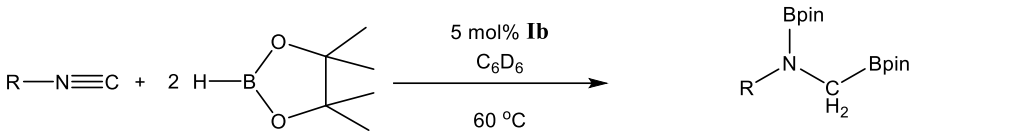

R = 1-C_5H_{11} (**75**), *t*-Bu (**76**),
Bn (**77**), 2-$C_{10}H_7$ (**78**), 2,6-(Me)Ph (**79**)

Entry	Isonitrile	Time (hrs)	Temp (°C)	NMR yield (%)
5-7	1-pentyl	1	60	>99
5-8	*tert*-butyl	1	60	>99
5-9	benzyl	0.5	60	>99
5-10	2-naphthyl	48	100	55
5-11	2,6-dimethylphenyl	48	100	53

Whilst the reactivity outlined in Table 5-2 is only of a narrow substrate scope, due to the limited number of reasonably priced commercial isonitriles, it reveals a clear difference between alkyl and aryl isonitrile reactivity. Reminiscent of the nitrile hydroboration catalysis described in Chapter 4, it is apparent that changing the nature of the substituent can have a subtle but notable effect on the mechanism of the reaction.

5.3 Stoichiometric Studies

A series of stoichiometric reactions were undertaken to probe the mechanism. Using the isolated *β*-diketiminato magnesium hydride (**XXII**) with 1 equivalent of CyNC (Scheme 5-3) yielded a new complex as identified in the ^{1}H NMR spectrum, which showed a new and characteristic downfield singlet at δ 9.99 ppm. This resonance was revealed by a subsequent HSCQ analysis to correlate with ^{13}C resonance at δ 217 ppm indicative of a new Mg-CH=NCy motif.

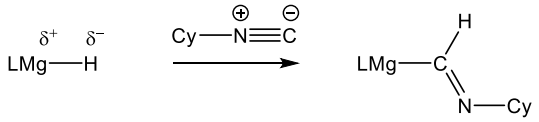

XXII **80**

Scheme 5-3. Insertion of CyNC into LMgH

Leaving the reaction to stand at room temperature overnight yielded colourless crystals of the insertion product, compound **80** (Figure 5-2), confirming the structure identified *via* NMR studies.

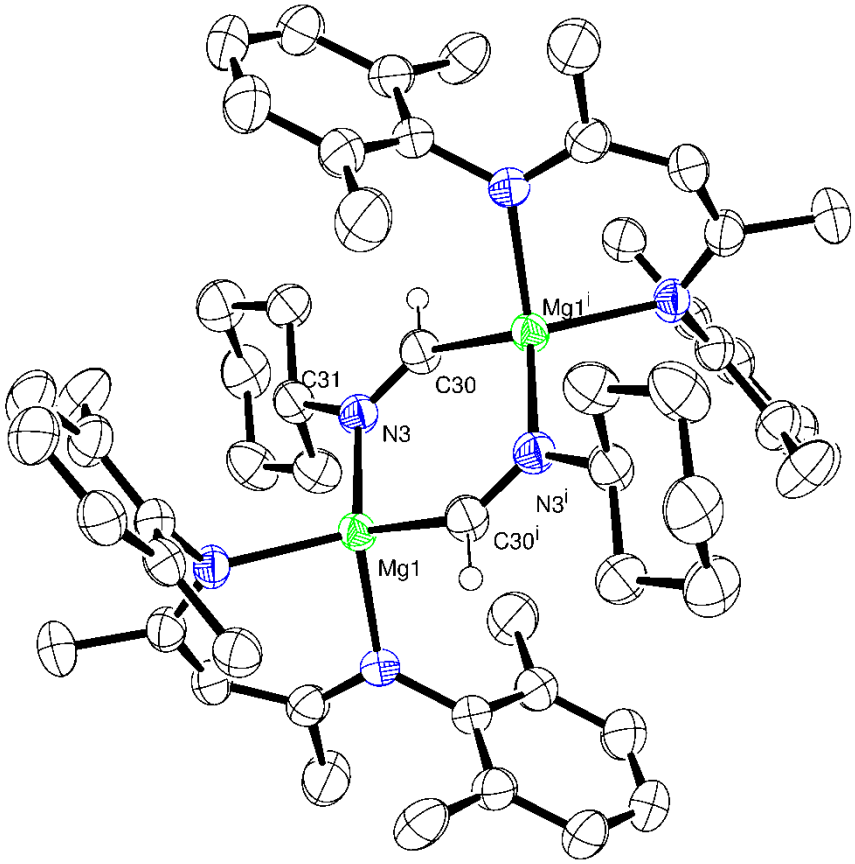

Figure 5-2. ORTEP representation of LMgCHNCy (**80**) ellipsoids set to 30%. Hydrogen atoms, except H30 and H30^{i}, and the methyl groups of the β-diketiminate 2,6-di-*iso*-propylphenyl substituents are removed for clarity. Selected bond lengths (Å) and angles (°): Mg(1)-N(1) 2.083(3), Mg(1)-N(2) 2.100(3), Mg(1)-N(3) 2.109(3), Mg(1)-C(30)^{i} 2.179(3), C(30)-N(3) 1.284(4), N(3)-C(31) 1.495(4), N(3)-Mg(1)-C(30)^{i} 112.90(12), C(30)-N(3)-Mg(1) 111.4(2), N(3)-C(30)-Mg(1)^{i} 135.7(2). Symmetry transformations used to generate equivalent atoms: -x,-y+1,-z+1.

The magnesium complex (**80**) crystallises as a centrosymmetric dimer as a result of the intermolecular interaction between the vacant coordination site on the Mg centre and the *β*-nitrogen atom. This leads to formation of a planar 6 membered heterocycle. This is also confirmed by the sum of the angles about both the N(3) and C(30) atoms, both of which are sp^2

hybridised (sum = 360°) and in plane with the *pseudo*-tetrahedral Mg centre [N(3)-Mg(1)-C(30)^{i} 112.90(12)°]. The Mg-N distances are typical of bonds of this type, whilst the C=N bond length of 1.284 Å is also consistent with a C=N double bond[248] and similar to the C=N bonds reported by Harder (**XII**)[111] and Uhl (**XLII**) (Figure 5-3).[216] The Mg-C distance of 2.179 Å resembles that of a single bond, and, as expected, is notably shorter than the reported Ca-C distance of 2.62 Å reported by Harder. This structure more closely resembles that reported by Uhl, in which the *t*-BuN=(H)C^{-} anion bridges through one Al-C and one Al-N bond.

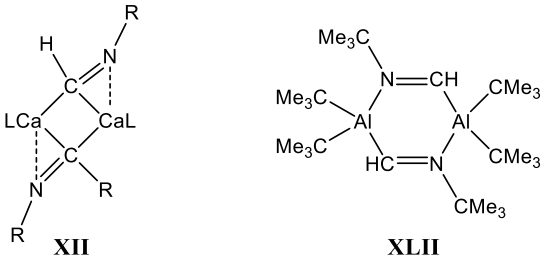

XII **XLII**

Figure 5-3. Structures reported by Harder and Uhl for the insertion of isonitriles into metal hydrides

Generation of the magnesium hydride by addition of HBpin to **Ib** and reaction with CyNC resulted in an instant colour change from the pale yellow hydride to an intense blue colour. On inspection of the NMR spectrum, the major product was identified as the insertion product, compound **80**. Other minor products were also observed but could not be identified through NMR studies and crystallisation attempts only yielded further isolation of the dimeric insertion product. It is thought that the blue colour arises from a series of unidentified side products and it is noticeable that a similar colour change was also previously reported by Harder from the insertion reaction of calcium hydride (**VIII**) with *t*-BuNC, which yielded a deep green solution.[111]

In order to avoid potential further side reactions, isolated crystals of compound **80** were used as the starting reagent in a stoichiometric reaction with HBpin. Addition of one equivalent of HBpin to the isolated crystals (Scheme 5-4), in C_6D_6, resulted in no obvious reaction when left at room temperature.

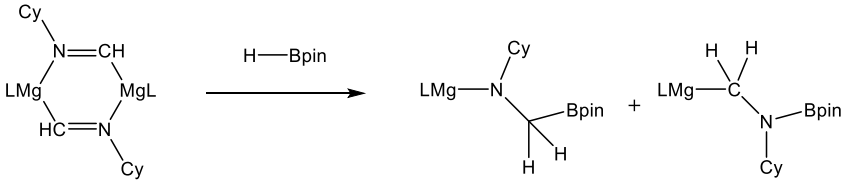

Scheme 5-4. Addition of HBpin to the dimeric insertion product

After heating at 60 °C for an hour the emergence of new C-B and N-B environments was apparent in the ^{11}B spectrum in a 1:1 ratio. Only a low conversion to these products was noted (<20%) as the dimer largely persisted throughout and crystallised from solution. Attempts to

redissolve compound **80** by heating to enable further reactivity were unsuccessful. Other attempts to study this stoichiometric reaction through variation of the stoichiometry of the reaction with the aim of saturating the magnesium centre with a coordinated HBpin or CyNC molecule to break up the dimer were also unsuccessful.

Attempts to isolate the *N*-boryl imine (CyNCHBpin) product through the catalytic reaction with 1 equivalent of HBpin failed to yield the desired (boryl)imine species and led to the isolation of the fully reduced product (CyN(Bpin)CH_2Bpin) with half the isonitrile reagent unreacted. This suggests a concerted mechanism reminiscent to that observed in the previously described nitrile hydroboration catalysis (Chapter 4).

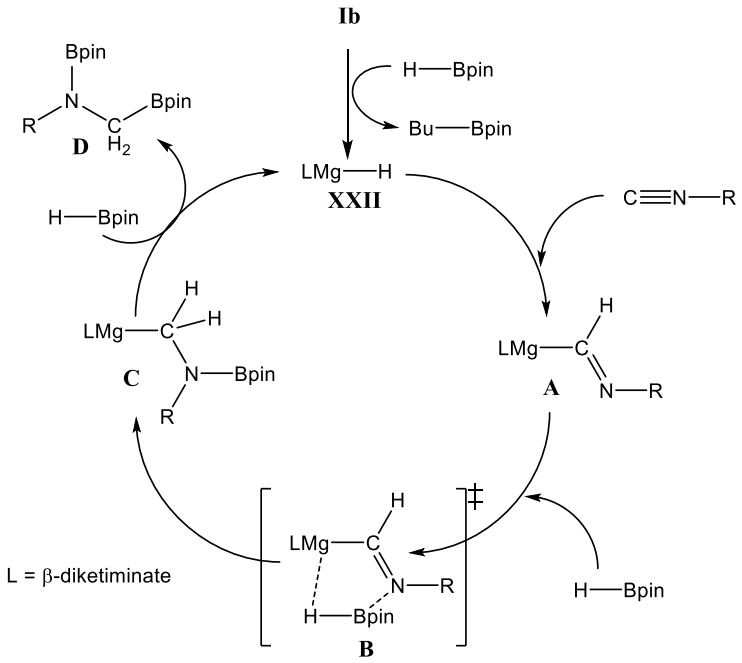

Scheme 5-5. Proposed catalytic cycle for the hydroboration of isonitriles

Scheme 5-5 outlines the proposed mechanism for the magnesium-catalysed hydroboration of isonitriles. Again a series of σ-bond metathesis and insertion reactions are required to fully reduce the C≡N triple bond. Initial insertion of isonitrile yields species **A**, analogous to the structurally characterised compound **80**, which then undergoes coordination with HBpin to yield a magnesium imino borane species (**B**) and subsequent intramolecular hydride transfer to yield a magnesium boryl amine complex (**C**). This species then undergoes σ-bond metathesis with the second equivalent of HBpin to produce the fully reduced isonitrile product (**D**) whilst allowing for subsequent catalytic turnover by reforming the active magnesium hydride catalyst (**XXII**).

5.4 Kinetic Study

To further investigate the mechanism of this magnesium-catalysed hydroboration of isonitriles a kinetic study was undertaken. Due to the diagnostic methine proton of the *N*-bound cyclohexyl group in both the starting material (δ 2.90 ppm) and product (δ 3.21 ppm), CyNC was selected for a series of kinetic reactions monitored by ^{1}H NMR spectroscopy. All reactions were carried out at 323 K unless stated otherwise. Figure 5-4 shows the stacked ^{1}H NMR spectra for the standard reaction utilising 5 mol% of **Ib** (0.02 M), with 0.82 M of HBpin and 0.4 M of CyNC from which it is possible to determine the overall order of the reaction.

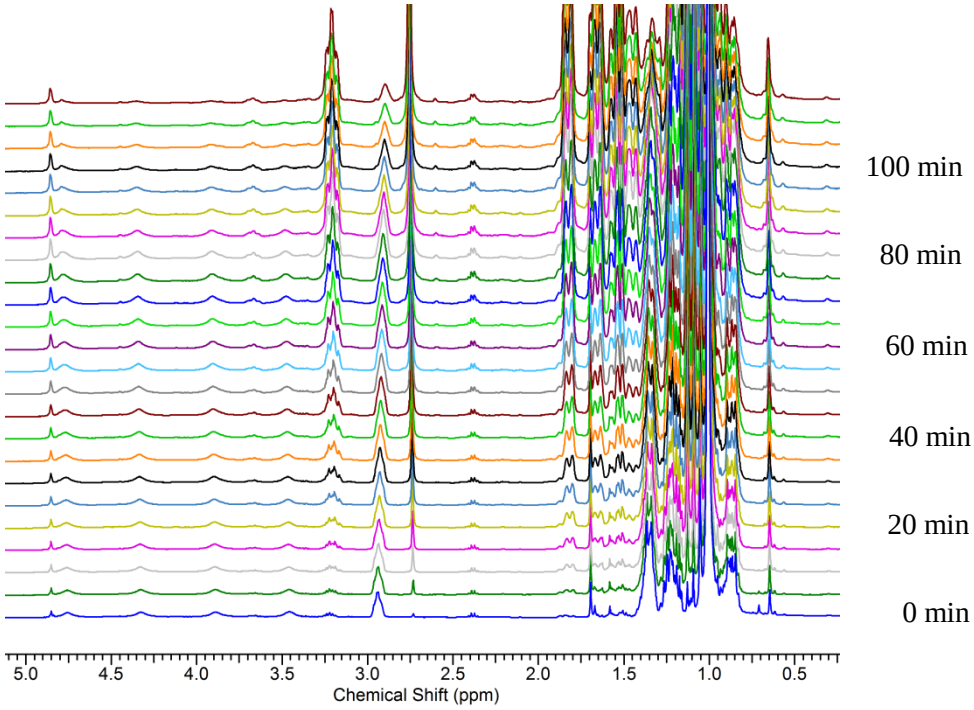

Figure 5-4. Series of ^{1}H NMR spectra, in C_6D_6, for the hydroboration of cyclohexylisonitrile, showing the consumption of the CyNC starting reagent (δ 2.90 ppm) and subsequent CyN(Bpin)CH_2Bpin formation (δ 3.21 ppm). Spectra were recorded every 5 minutes.

Figure 5-5 shows $f[CyNC]_0/[CyNC]_t$ vs time which allows for the comparison of a series of 0, 1st and 2nd order plots, indicating that the magnesium-catalysed hydroboration of isonitriles exhibits overall zero order kinetics as determined through R^2 values and least square error calculations (Figure S 5-1).

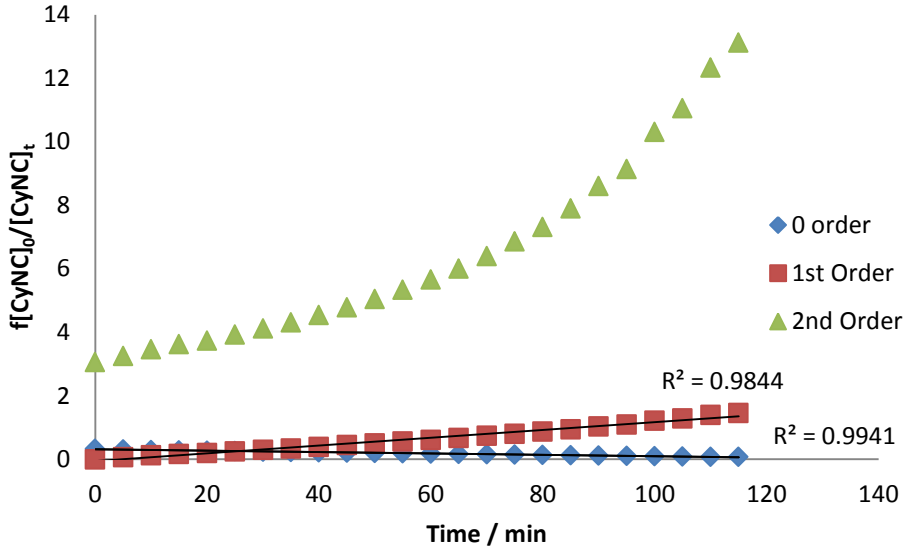

Figure 5-5. Series of different plots for $f[CyNC]_0/[CyNC]_t$ vs time

5.4.1 Determination of order in [Catalyst]

To determine the order with respect to the concentration of the magnesium pre-catalyst (**Ib**), a series of reactions were carried out using variable catalyst loadings whilst maintaining the standard ratio of 1:2 for CyNC (0.4 M) and HBpin (0.8 M) respectively.

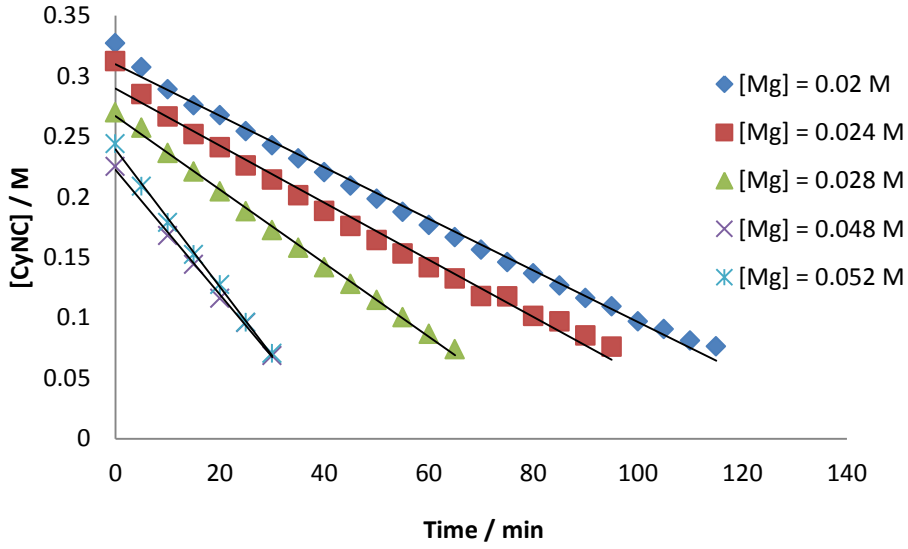

Figure 5-6. Plot of [CyNC] vs time for variable catalyst loadings

Least squares error calculations are provided in supplementary Figure S 5-1

Catalyst concentration was determined through comparison of ^{1}H NMR integrals against an added standard of tetramethylsilane. Figure 5-6 shows a series of zero order plots for 5 different concentrations of catalyst. Matching previous hydroboration kinetic studies, the rate increased

linearly with increasing catalyst concentration. This is confirmed by Figure 5-7 which shows a plot of the observed rate constants vs catalyst concentration.

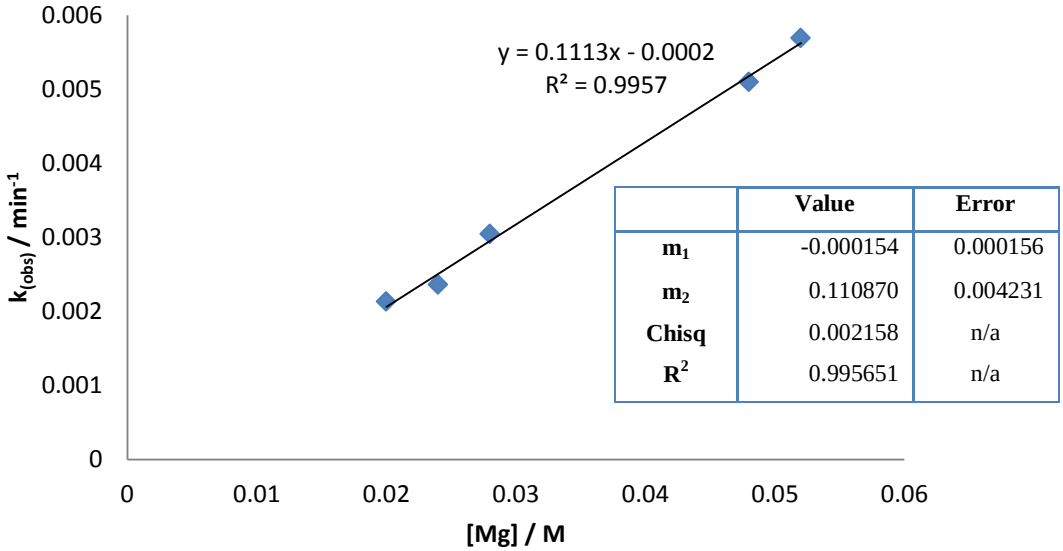

Figure 5-7. Plot of the observed rate ($k_{(obs)}$) vs [Mg] and least squares error calculations

Figure 5-7 indicates a first order dependence on [Mg], as seen previously with the hydroboration of pyridines and nitriles catalysed by a *β*-diketiminate magnesium species.

5.4.2 Determination of order in [CyNC]

Using *pseudo*-first order experiments it should, in theory, be possible to examine the order with respect to CyNC. Employing a large excess of HBpin (8.0 M) and varying the starting concentration of CyNC whilst keeping the catalyst concentration invariant (0.02 M) should provide the order of reaction with respect to [CyNC].

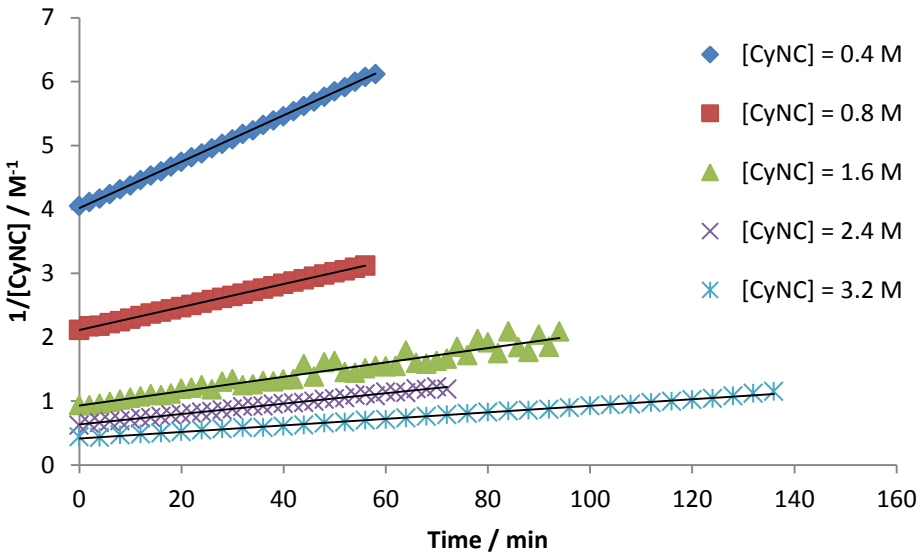

Figure 5-8. Second order plot of 1/[CyNC] vs time for variable [CyNC]
Least squares error calculations are provided in supplementary Figure S 5-7

Figure 5-8 shows a series of second order rate plots for the consumption of CyNC vs time for various starting concentrations of CyNC. Plotting the observed rate constants against [CyNC] indicated an inverse dependence upon starting concentration of [CyNC] (Figure 5-9). These results need to be interpreted with caution as seen previously with nitrile hydroboration kinetics (Chapter 4 of this thesis) utilising *pseudo*-first order conditions in HBpin can lead to a change in order with respect to catalyst concentration.

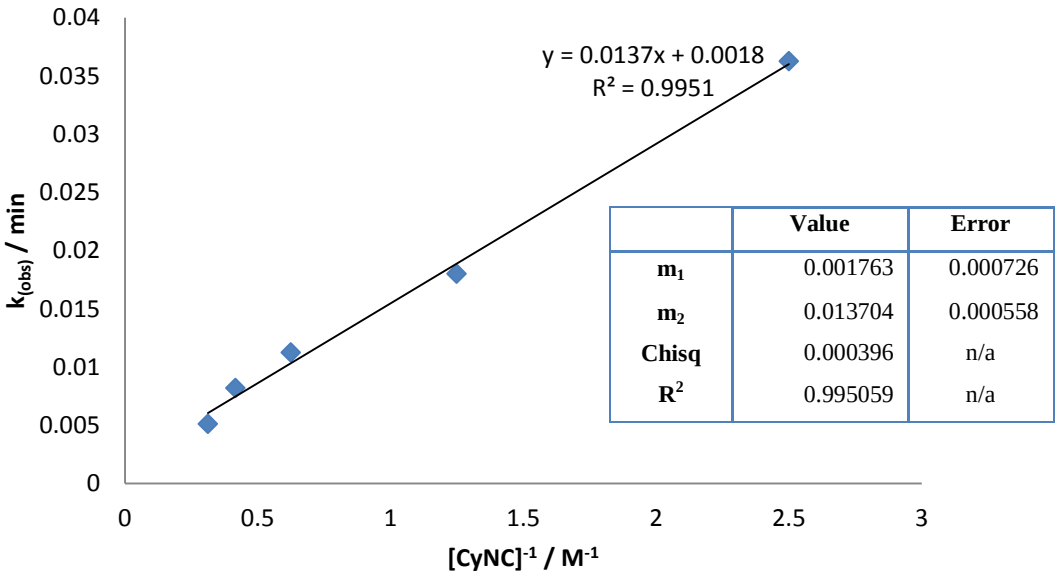

	Value	Error
m_1	0.001763	0.000726
m_2	0.013704	0.000558
Chisq	0.000396	n/a
R^2	0.995059	n/a

Figure 5-9. Plot of k(obs) vs $[CyNC]^{-1}$ and least squares error calculations

Whilst similar inhibition was earlier observed in the study of pyridine hydroboration described in chapter 3 of this thesis, the positive gradient of this graph compared to inhibition graphs which show a negative gradient, suggests that at low concentrations of CyNC the rate is

impeded more drastically than at high concentrations of CyNC. This effect must arise from the ability of the HBpin to coordinate to the metal centre and block the free coordination sites to the magnesium. This deduction is also in agreement with the inferred change in order with respect to magnesium under the high concentration of HBpin. Increasing the concentration of CyNC therefore, results in increased displacement of HBpin in order for the CyNC to coordinate to the magnesium centre for the onward hydroboration reaction to take place. Thus CyNC cannot be truly inhibiting the reaction, as increasing the concentration enhances the rate of reaction due to the increased breakup of the inferred catalyst resting state, $\{LMg(H_2Bpin)\}_3$.

5.4.3 Determination of order in [HBpin]

Examining the alternate *pseudo*-first order experiments, i.e. under a large excess of CyNC (8.0 M) should provide the order with respect to HBpin. Again keeping the catalyst concentration constant (0.02 M) and varying the concentrations of HBpin should provide information on the order of reaction with respect to HBpin.

Upon inspection of the first data set (HBpin = 0.8 M), a new peak observed at δ 5.95 ppm was identified in the ^{1}H NMR spectrum (Figure 5-10), which was shown to increase in intensity over time suggesting a new previously unseen product was being formed during the catalysis concurrent with the formation of the desired product, (CyN(Bpin)CH_2Bpin).

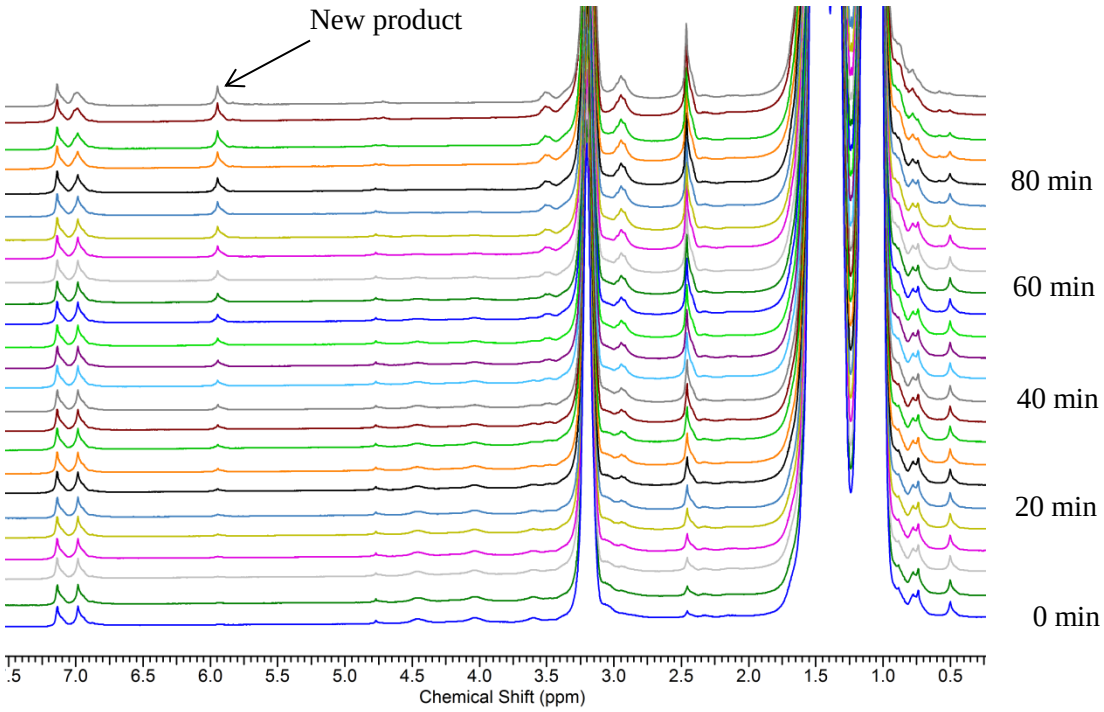

Figure 5-10. Series of ^{1}H NMR spectra, in C_6D_6, for hydroboration of CyNC under *pseudo*-first order conditions in CyNC. Spectra were collected every 4 minutes.

This new product was identified to be the result of C-C coupling reactions as a consequence of the large excess of CyNC present in solution. This product itself subsequently undergoes hydroboration (Scheme 5-6).

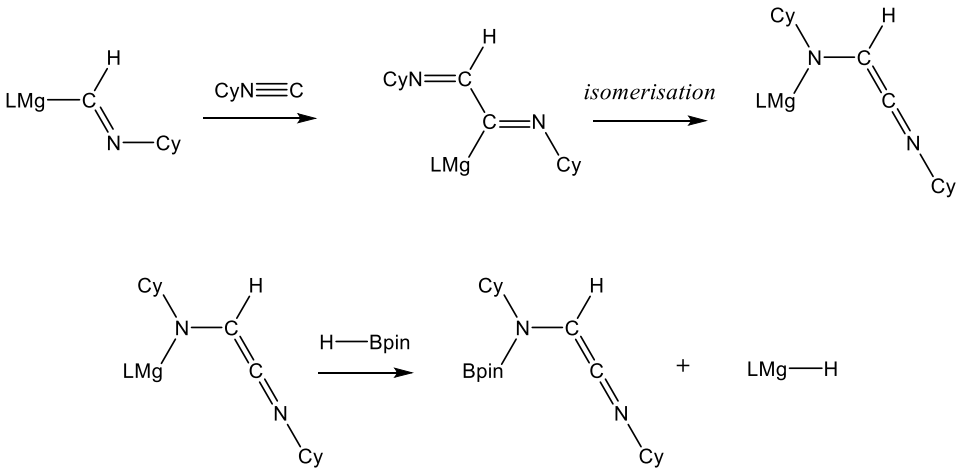

Scheme 5-6. Proposed mechanism for formation of C-C coupled product and subsequent hydroboration

This type of reactivity had also been previously reported by Harder,[111] in which an initial C-C coupled product was observed to undergo isomerisation to the more stable ketenimine species. A similar isomerisation process has also been observed in gallium chemistry.[249]

Whilst the di-hydroboration of the isonitrile is still observed under *pseudo*-first order conditions in CyNC, the competing C-C coupling reaction prevents any deduction of the order with respect to HBpin under these conditions. While it was observed that increasing the HBpin concentration under these *pseudo*-first order conditions did result in less C-C coupling, the product of this reaction was still present in all cases making it impossible to achieve the desired 3 half-lives required for this study. On a positive note, this shows direct competition between HBpin and CyNC for coordination to the metal centre, both may inhibit the reaction. Firstly excess HBpin results in formation of the catalyst trimer whilst reactions under excess CyNC results in C-C coupling products from subsequent insertion reactions of CyNC.

5.4.4 Eyring and Arrhenius analysis

The activation energy parameters for the hydroboration of isonitriles were obtained through variable temperature kinetic studies. This was carried out using the standard reaction of 5 mol% **Ib** (0.02 M), HBpin (0.82 M) and CyNC (0.4 M) over a range of 4 different temperatures (308 K to 325 K). Again overall zero order reaction rates were observed (Figure S 5-11) and use of the resultant rate constants enabled the construction of Eyring (Figure 5-11) and Arrhenius (Figure 5-12) plots.

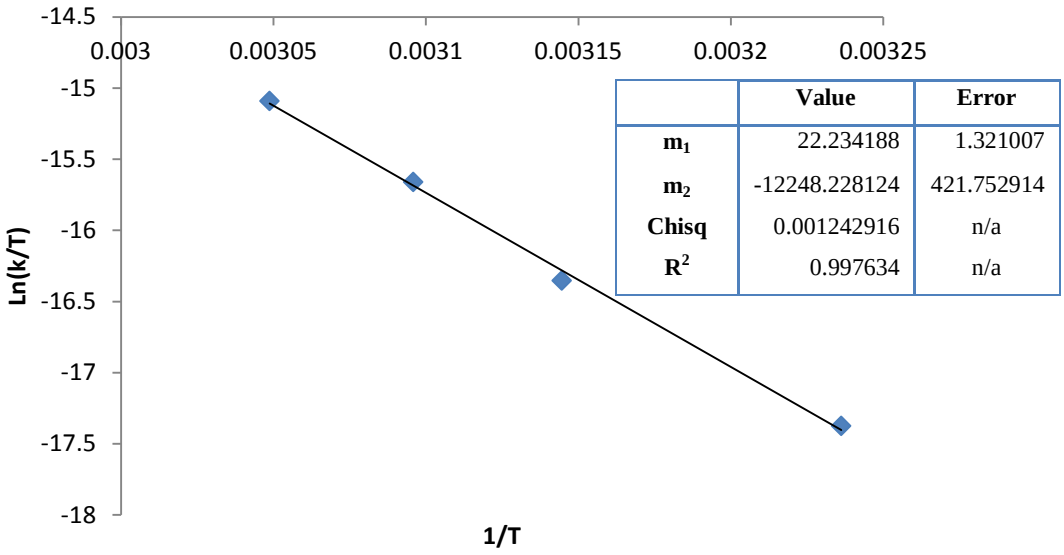

Figure 5-11. Eyring plot and least squares error calculations

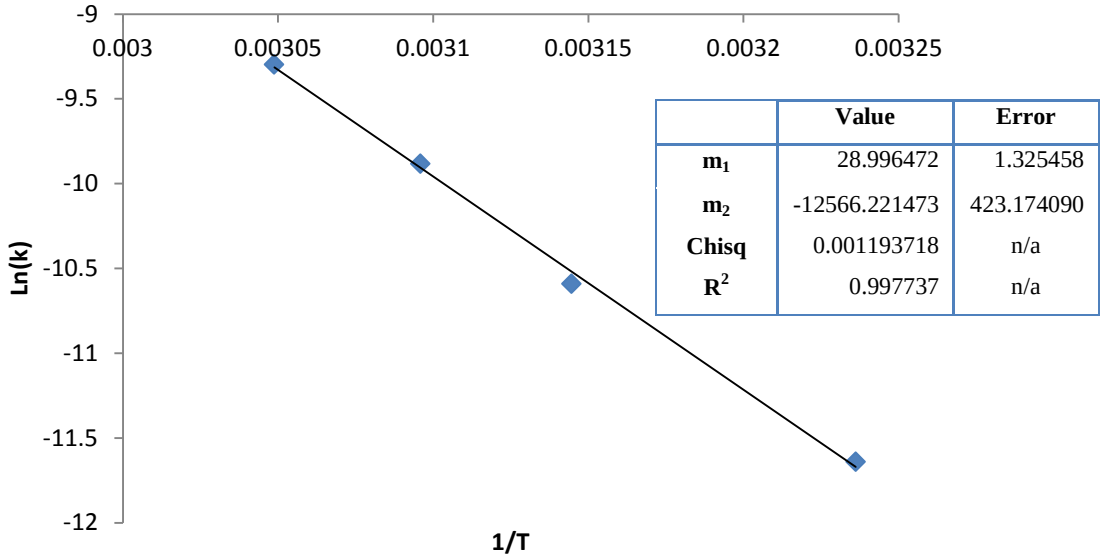

Figure 5-12. Arrhenius plot and least squares error calculations

Using these two graphs it is possible to calculate the following activation energy parameters (Table 5-3). Errors were calculated using the least squares method of linear regression.

Table 5-3. Kinetic activation parameters for the magnesium-catalysed hydroboration of CyNC

	Value	Error
Ea	104.5 kJ mol-1	± 3.5
$\Delta H^{\neq}$	101.8 kJ mol^{-1}	± 3.5
$\Delta S^{\neq}$	-12.7 J k^{-1} mol^{-1}	± 11.0
$\Delta G^{\neq}_{298}$	105.6 kJ mol^{-1}	n/a

Although little can be deduced from the values associated with the enthalpic activation of the reaction the effectively zero activation entropy, $\Delta S^{\neq}$, suggests that the components of the reaction are pre-assembled prior to rate determining C-H formation and B-H bond breaking process (Scheme 5-7).

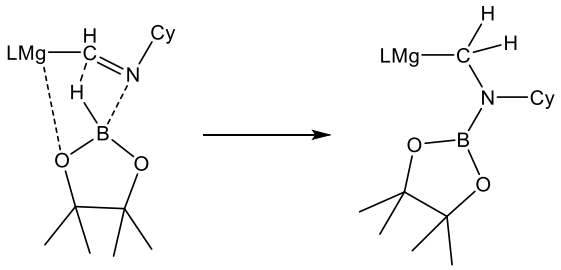

Scheme 5-7. Proposed pre-assembled transition state

5.5 Conclusion

In conclusion, **Ib** is a highly efficient catalyst for the hydroboration of alkyl isonitriles under mild temperatures with reasonable catalyst loadings. Whilst this did not achieve a similar level of reactivity with aryl isonitriles, it was still possible to achieve some turnover.

Attempts to further study the mechanistic aspects of this reaction were somewhat mixed. Whilst initial stoichiometric reactions confirmed the identity of the first insertion product, the stability and insolubility of this dimer hindered further study. Initial kinetic study showed the reaction to fit zero order overall kinetics, with a first order dependence on [catalyst]. However the order of reagents could not be deduced *via pseudo*-first order methods due to both reagents having different effects on the mechanism when employed in the large excess required for *pseudo*-first order conditions. Under a large excess of HBpin the nature of the active magnesium catalyst changes and does not reflect the true catalyst in the standard 2:1 (HBpin: CyNC) reaction. Similarly a large excess of CyNC results in an entirely different mechanism due to the formation of a further product through insertion of CyNC resulting in C-C coupling reactions. This shows a delicate competitive balance in the nature of the two reagents, showing that they both can inhibit and accelerate the reaction, whilst maintaining the overall zero order reaction rates.

This delicate balance between the starting concentrations of the two reagents was previously seen with the alkyl nitrile kinetics studied in the previous chapter. It is therefore unsurprising that the activation energy parameters are also virtually identical within experimental error. This suggests that the isonitrile hydroboration also has a loosely pre-assembled transition state possibly similar to that of the alkyl nitrile hydroboration in which it undergoes intramolecular hydride transfer to reduce the imino functionality.

Combination of the findings throughout this study provides the following proposed mechanism (Scheme 5-8). As noted for all group 2 catalytic reactions, this catalytic cycle again combines a series of σ-bond metathesis and insertion reactions in order to produce the desired product.

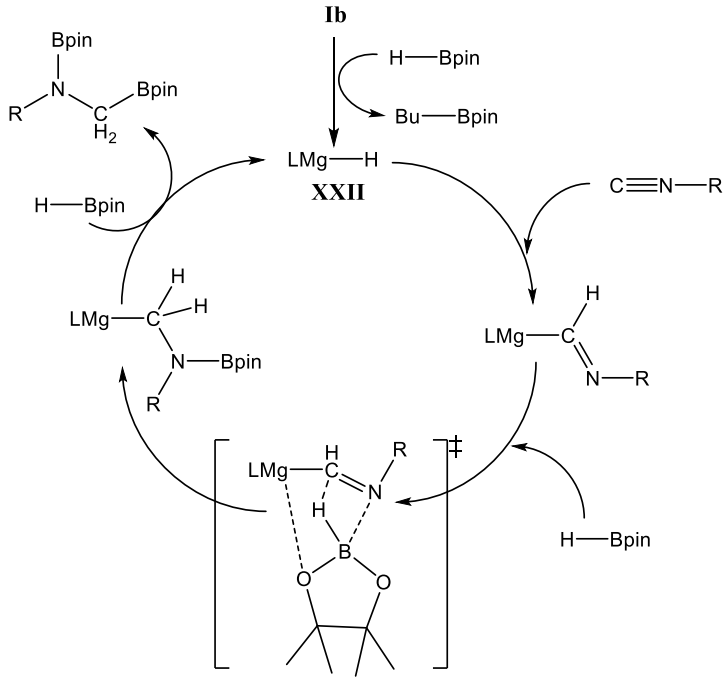

Scheme 5-8. Proposed catalytic cycle for the magnesium-catalysed hydroboration of isonitriles

The above Scheme 5-8 shows the proposed catalytic cycle for the magnesium catalysed hydroboration of isonitriles. As with all magnesium catalysed hydroborations, the initiation step requires conversion of the **Ib** precatalyst to the magnesium hydride. This subsequently inserts into the C≡N group of the isonitrile. Coordination of the first HBpin molecule and potential intramolecular hydride transfer is then suggested based on comparison with the alkyl nitrile activation energy parameters. The final step in the proposed mechanism is the σ-bond metathesis reaction to regenerate the magnesium hydride and formation of the doubly reduced product.

Chapter 6. Hydroboration of Heterocumulenes

6.1 Introduction

The intermolecular heterofunctionalisation of carbodiimides with protic amine, phosphine, or terminal alkyne reagents has provided access to the respective C-N, C-P and C-C coupled products and a plethora of guanidine,[83, 250] phosphaguanidine,[87, 251] and propargylamidine[65] molecules all using group 2 catalysis (Scheme 6-1).

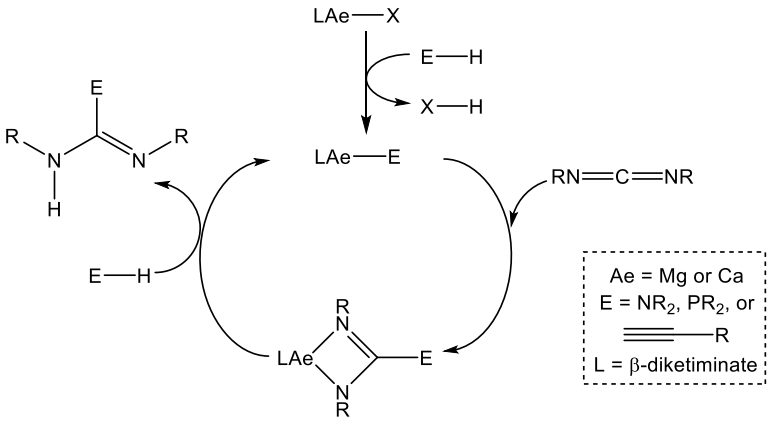

Scheme 6-1. Group 2 catalysed heterofunctionalisation of carbodiimides

Extension of these protic-derived catalytic cycles to hydridic based systems, however, has received little attention. The only report of group 2 mediated hydroboration of heterocumulenes is the reduction of carbon dioxide with HBpin to yield a methanol equivalent, MeOBpin.[158] This reactivity, however, requires the use of the Lewis acidic tris(pentafluorophenyl)borane (BCF) to afford the metal hydrido borate species as the catalyst and could therefore be considered frustrated Lewis pair (FLP) type reaction chemistry. This work was itself based upon a similar reaction utilising a decamethylscandocenium hydrido BCF species for the hydrosilylation of CO_2 to yield methane through a tandem process of metal-mediated silyl formate production and posited FLP reduction.[159] A further reported example of CO_2 hydroboration reaction has utilised a ruthenium hydride catalyst. In this case a number of products were observed, the majority product being the methanol equivalent with concomitant bis(boryl)oxide formation but a small amount of C-C coupled products were also observed by $^{13}CO_2$ labelling studies.[252]

Further use of FLP type chemistry for the reduction of carbodiimides was reported by Stephan and co-workers in which addition of BCF to a series of carbodiimides resulted in the formation of borane adducts which were prone to direct hydrogenation (Scheme 6-2).[253] In this case reactivity was limited to formal reduction of one of the double bonds to afford the amidinate

species. While further hydrogenation was observed to yield the hydridoborate anion, with R = *t*-Bu or Dipp, no further reduction of the carbodiimide moiety was observed.

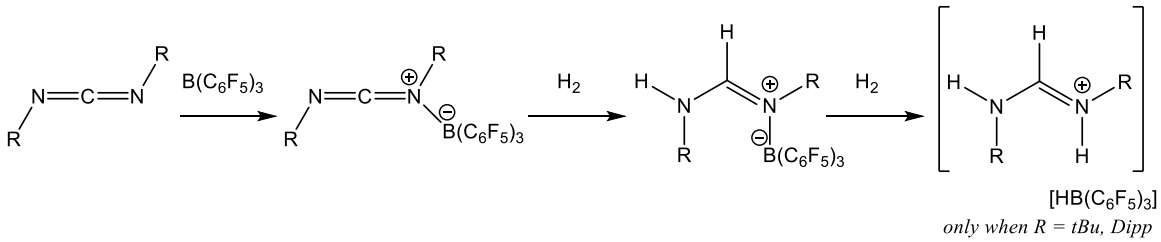

Scheme 6-2. BCF mediated hydrogenation of carbodiimides

The reaction of 9-BBN with carbodiimides does afford both the singly and doubly reduced amidinate and bis(boryl)aminal products without the need for a catalyst; the doubly reduced product, however, is only obtained under forcing conditions at 160 °C (Scheme 6-3).[254]

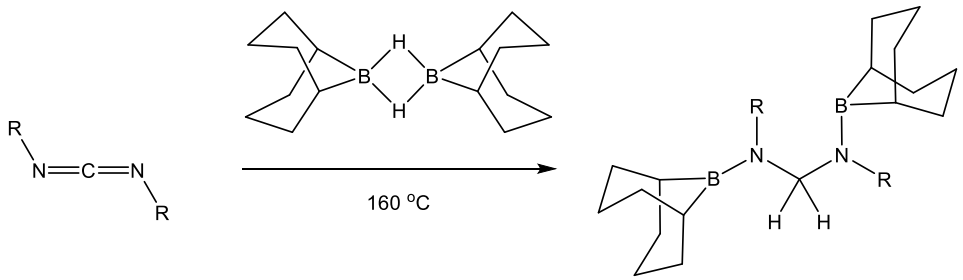

Scheme 6-3. Di-hydroboration of carbodiimide with 9-BBN

Reports of similar heterofunctionalisation reactions with isocyanates are even less common in the literature. The formation of substituted ureas by the group 2 mediated hydroamination of organic isocyanates proceeded with considerable efficiency.[84] Further examples of catalytic cycles employing organic isocyanates as a starting reagent have been limited due to the propensity of isocyanates to readily undergo C-N coupling in the presence of group 2 and other electrophilic metal centres to yield poly- or oligo- isocyanurates.[255, 256] This C-N coupling has been shown to arise from multiple isocyanate insertion reactions, as confirmed by Harder and co-workers through the isolation of a double insertion product from the reaction of cyclohexyl isocyanate with a calcium bis(iminophosphorano)diide.[97]

6.2 Hydroboration of Carbodiimides

Carbodiimides can be viewed as containing two imine functional groups, which have been shown previously to successfully undergo catalytic hydroboration using **Ib**. This, therefore, gives rise to the potential for the double reduction of carbodiimides to yield aminals, or stop after addition of a single equivalent of HBpin to yield formamidines. A possible mechanism for this process is outlined in Scheme 6-4.

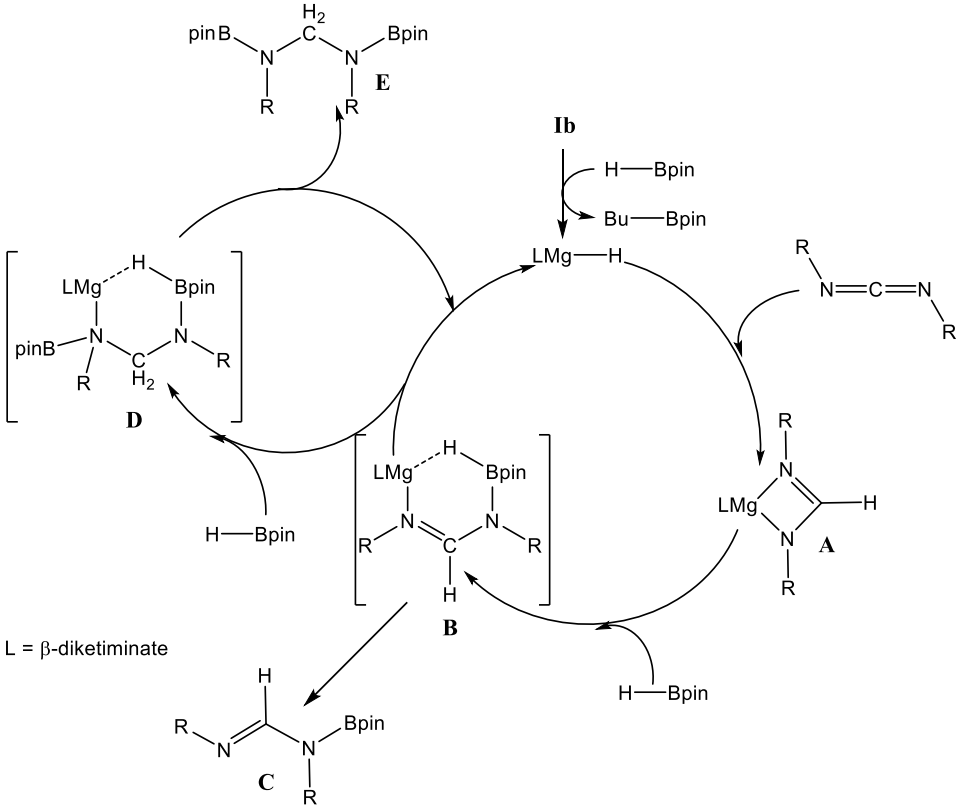

Scheme 6-4. Proposed mechanism for the magnesium-catalysed di-hydroboration of carbodiimides

The proposed mechanism again comprises a sequence of σ-bond metathesis steps, directed by the hydridic nature of HBpin, and insertion reactions. Similar to the mechanism displayed in Scheme 6-1 and the stoichiometric reactivity of a magnesium hydride complex with cyclohexylcarbodiimide to yield (**XXIII**, Scheme 1-17), initial insertion into the magnesium hydride catalyst is expected to yield the formamidinate species **A**. Subsequent reaction with HBpin yields the intermediate **B**, which either breaks down to the formamidine product (**C**) with the regeneration of **XXII** or undergoes further hydroboration to yield intermediate **D**, which then breaks down to give the fully reduced bis(boryl)aminal product, **E**.

6.2.1 Catalysis

An initial trial catalytic reaction using 10 mol% of **Ib** with *N*,*N*-di-*iso*-propyl carbodiimide (*i*PrNCN*i*Pr) and an equimolar equivalent of HBpin at 30 °C (Table 6-1, entry 6-1), provided

slow turnover to yield the desired singly reduced *N*-boryl formamidine product, which was identified by a singlet resonance, integrating to 1H in the NMR spectrum, at δ 8.23 ppm and a singlet resonance in the ^{11}B NMR spectrum at δ 28.5 ppm which appeared alongside the catalyst initiation by-product (BuBpin) at δ 37.5 ppm. Increasing the temperature led to reduced reaction time and increased conversion (Table 6-1, entries 6-2 to 6-4). An attempted reaction at 60 °C with 2 equivalents of HBpin, however, provided the same product and failed to yield the fully reduced bis(boryl)aminal, as observed by the retention of the HBpin doublet at δ 32.0 ppm in the ^{11}B NMR spectrum, along with the resonance of the same intensity at δ 28.5 ppm assigned to the formamidine. Increasing the temperature to 80-100 °C in an attempt to force the second reduction step only led to decomposition of HBpin, thus preventing any further reactivity. Entry 6-5 confirms the reaction does take place *via* the magnesium centre as no substantial reactivity was observed in the absence of **Ib**.

Table 6-1. Temperature optimisation study

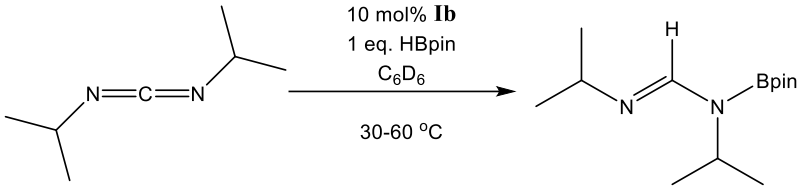

Entry	Catalyst (mol %)	Time (hrs)	Temp (°C)	NMR yield (%)
6-1	10	6 days	30	74
6-2	10	4 days	40	70
6-3	10	4 days	50	80
6-4	10	15	60	90
6-5	0	24	60	6

Extension of this study to a variety of *N*,*N*'-substituted carbodiimides was undertaken, and the results are shown in Table 6-2. Utilising smaller dialkyl carbodiimides (*iso*-propyl, entry 6-6 and cyclohexyl, 6-7) provided efficient turnover to the desired borylated formamidine product. Similar to the previously described nitrile hydroboration studies, increasing the steric bulk of the R group to *tert*-butyl (entry 6-8) induced prolonged reaction times and required heating at 80 °C. Although both carbodiimides bearing aryl substituents (Dipp, entry 6-9 and *p*-tolyl entry 6-10) also required this higher temperature, quantitative conversion was observed within 24 hours or less. In all cases, only a maximum of 90% conversion by NMR was observed even with prolonged heating.

Table 6-2. Magnesium-catalysed hydroboration of *N,N'*-substituted carbodiimides

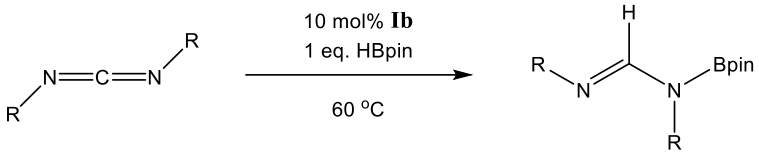

R = *i*-Pr (**81**), Cy (**82**), *t*-Bu (**83**), Dipp (**84**), *p*-Tolyl (**85**)

Entry	Carbodiimide	Time (hrs)	Temp (°C)	NMR yield (%)	Isolated yield (%)
6-6	di-*iso*-propylcarbodiimide	15	60	90	89
6-7	dicylcohexylcarbodiimide	15.5	60	90	69
6-8	di-*tert*-butylcarbodimide	2.5 days	80	88	87
6-9	bis(2,6-di-*iso*-propylphenyl)carbodiimide	24	80	80	77
6-10	1,3-di-*p*-tolylcarbodiimide	15	80	81	63

NMR experiments were carried out in C_6D_6, whereas large scale experiments were carried out in toluene. For full details see experimental section 7.6.1.

The constitution of the formamidine products was confirmed through isolation of single crystals suitable for X-ray crystallographic analysis from subsequent scale up of both *i*PrNCN*i*Pr and DippNCNDipp hydroboration reactions to yield compounds **81** and **84**. The results of these studies are shown in Figure 6-1 and Figure 6-2 respectively.

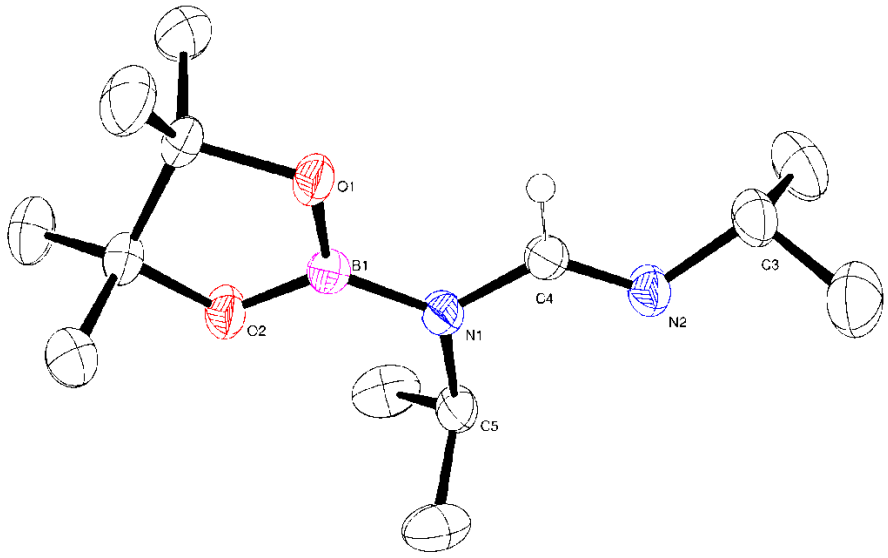

Figure 6-1. ORTEP representation of compound **81** with thermal ellipsoids set at 30% level of probability. Hydrogen atoms except those attached to C(4) are removed for clarity. Selected bond lengths (Å) and angles (°): B(1)-N(1) 1.42731(6), N(1)-C(4) 1.3883(15), N(1)-C(5) 1.4856(15), N(2)-C(4) 1.2645(15), N(2)-C(3) 1.4589(1); N(1)-C(4)-N(2) 123.81(11), B(1)-N(1)-C(4) 119.26 (10), B(1)-N(1)-C(5) 123.76(10), C(5)-N(1)-C(4) 116.98 (9), C(4)-N(2)-C(3) 117.24(10).

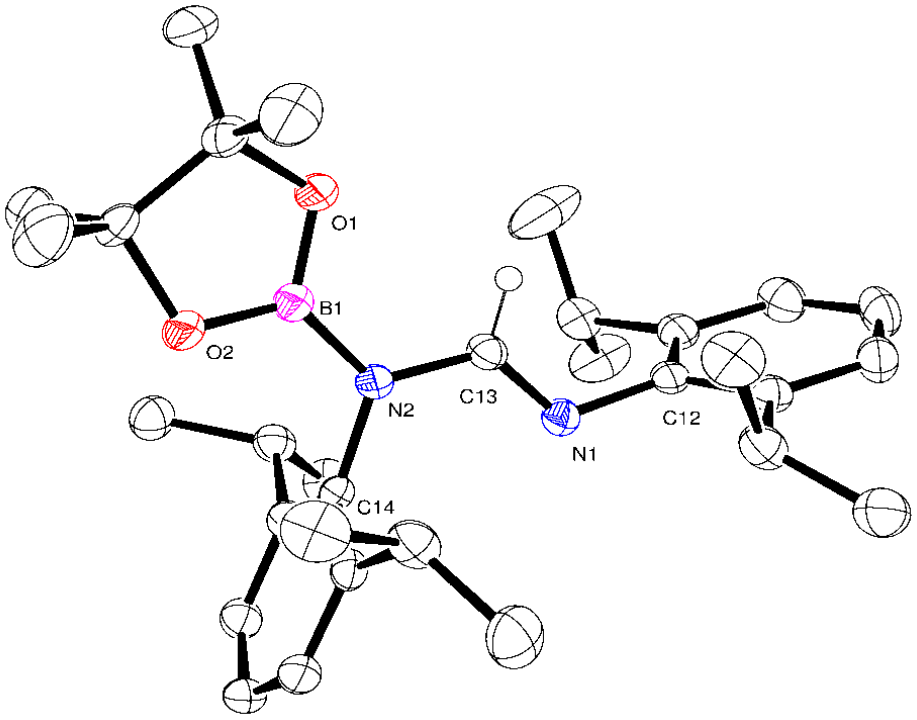

Figure 6-2. ORTEP representation of compound **84** with thermal ellipsoids set at 30% level of probability. Hydrogen atoms except those attached to C(13) are removed for clarity. Selected bond lengths (Å) and angles (°): B(1)-N(2) 1.431(2), N(2)-C(13) 1.3871(2), N(2)-C(14) 1.4557(2), N(1)-C(13) 1.2681(18), N(1)-C(12) 1.4292(18); N(2)-C(13)-N(1) 123.03(12), B(1)-N(2)-C(13) 120.22(11), B(1)-N(2)-C(14) 120.17(11), C(13)-N(1)-C(12) 117.66(11).

Both compounds, **81** and **84**, display the same overall structural features and in each case the (*E*)-stereoisomer is observed. The reduction to the formamidine product is also confirmed due to the sp^2 hybridisation of the central carbon of the now reduced carbodiimide fragment, and the non-linearity of the N-C-N bond angle [(**81**) 123.81(11)°, (**84**) 123.03(12)°]. The retention of one of the imine-like N=C bonds is also evident upon comparison of the N-C bond lengths [(**81**) N(2)-C(4) 1.2645(15), (**84**) N(1)-C(13) 1.2681(18) Å] compared to the now formally N-C single bonds [(**81**) N(1)-C(4) 1.3883(15), (**84**) N(2)-C(13) 1.3871(2) Å].

Further catalytic studies involved the use of unsymmetrically substituted carbodiimides, undertaken to assess any steric preference associated with addition of the Bpin group. Table 6-2 shows the results of this study. Whilst substrate scope was limited to two commercially available substrates, in both cases a 1:1 mix of the two possible regioisomers was observed in the ^{1}H NMR spectra as noted by two singlet resonances in the downfield region for the NC*H*N peak at [Entry 6-12 (**87a**) δ 8.14 ppm, (**87b**) δ 8.12 ppm].

Table 6-3. Magnesium-catalysed hydroboration of unsymmetrical carbodiimides

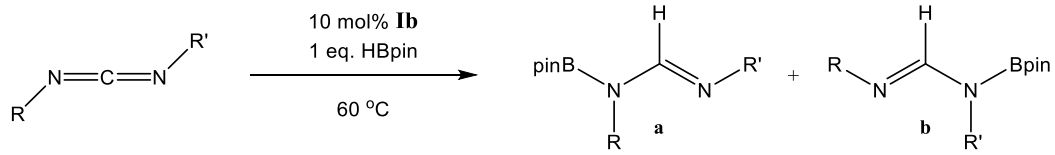

R, R' = *t*-Bu, Et (**86**); $PrNMe_2$, Et (**87**)

Entry	Carbodiimide	Time (hrs)	Temp (°C)	NMR yield (%)	Isolated yield (%)
6-11	1-*tert*-butyl-3-ethylcarbodiimide	20	60	75	87
6-12	*N*-(3-Dimethylaminopropyl)-*N*′-ethylcarbodiimide	5.5	60	90	87

NMR experiments were carried out in C_6D_6, whereas large scale experiments were carried out in toluene. For full details see experimental section 7.6.1.

6.2.2 Stoichiometric studies

It was noted during the catalytic hydroboration of *i*PrNCN*i*Pr that the ^{11}B NMR spectrum did not contain the characteristic peak at δ 37.5 ppm for the BuBpin by product from the *in situ* activation of the pre-catalyst, **Ib**. A stoichiometric reaction between **Ib** and *i*PrNCN*i*Pr, took place with an instant colour change from orange to yellow, and subsequent NMR analysis confirmed that the carbodiimide had inserted into the Mg-C bond to form the amidinate compound **88** (Scheme 6-5). Whilst the *in situ* hydride formation occurs within minutes, the competing insertion of the *i*PrNCN*i*Pr occurs much more readily. For each catalytic reaction **Ib**

was, thus, pre-mixed with HBpin for several minutes before the carbodiimide reagent was added to ensure full activation of **Ib** to the *in situ* generated hydride **XXII**.

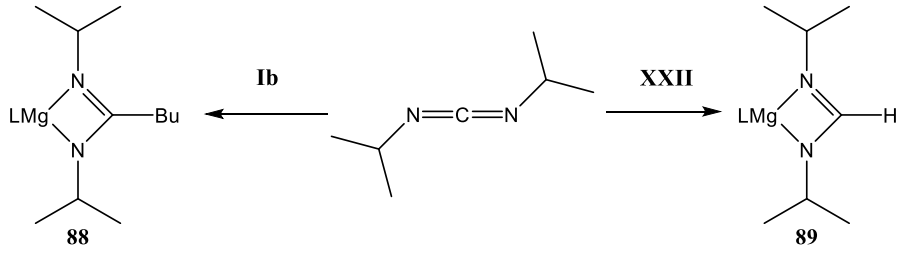

Scheme 6-5. Insertion of *i*PrNCN*i*Pr into **Ib** and **XXII** forming compounds **88** and **89**

The same precaution was taken during subsequent stoichiometric reactions. Addition of 1 equivalent of *i*PrNCN*i*Pr to the *in situ* generated hydride solution provided a colour change to very pale yellow and a resultant ^{1}H NMR spectrum displaying the desired 1H methine singlet at δ 7.77 ppm (Scheme 6-5). This latter resonance is a clear indication of formamidinate formation and is comparable to that reported by Jones and co-workers for the CyNCNCy insertion reaction to yield **XXIII** at δ 7.85 ppm.[117]

Based upon the proposed mechanistic cycle (Scheme 6-4) addition of 1 equivalent of HBpin to compound **89** was expected to proceed *via* intermediate **B** to form the hydroboration product with regeneration of the active hydride catalyst. Inspection of the resultant ^{1}H NMR spectrum (Figure 6-3) after addition at room temperature, however, revealed the presence of two new species. The minor product was found to be the expected borylated formamidine product, compound **81**; however the major product showed a small upfield shift in the formamidine, NC*H*N, 1H singlet from δ 7.77 to 7.62 ppm, suggesting the maintenance of its coordination to the magnesium centre. The upfield methyl signals associated with the Bpin fragment were observed as four 3H singlets, by integration, rather than the expected 12H singlet, suggesting formation of a well-defined product in which the Bpin fragment is locked in a conformation whereby rotation about the B-N bond is prevented.

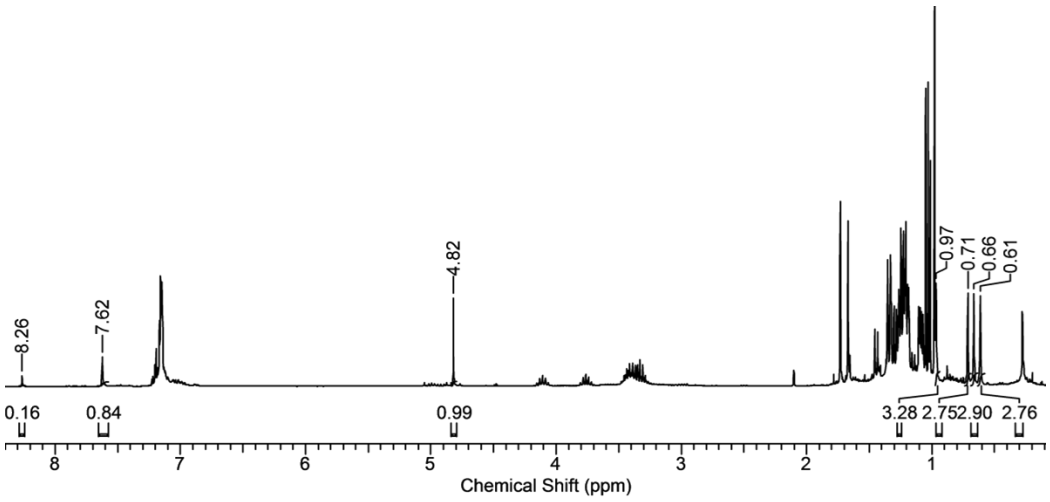

Figure 6-3. ^{1}H NMR spectrum, in C_6D_6, for compound **90**

The corresponding ^{11}B NMR spectrum showed a new doublet at δ 1.82 ppm (J_{HB} = 92 Hz), suggestive of a 4-coordinate borate species similar to that of the intermediate observed in the nitrile hydroboration studies (compound **71**). A subsequent scale-up reaction in toluene starting from isolated **XXII**, with a 1:1 ratio of *i*PrNCN*i*Pr and HBpin provided crystals suitable for X-ray crystallography, the results of which are shown in Figure 6-4 with relevant bond lengths and angles provided in the figure caption.

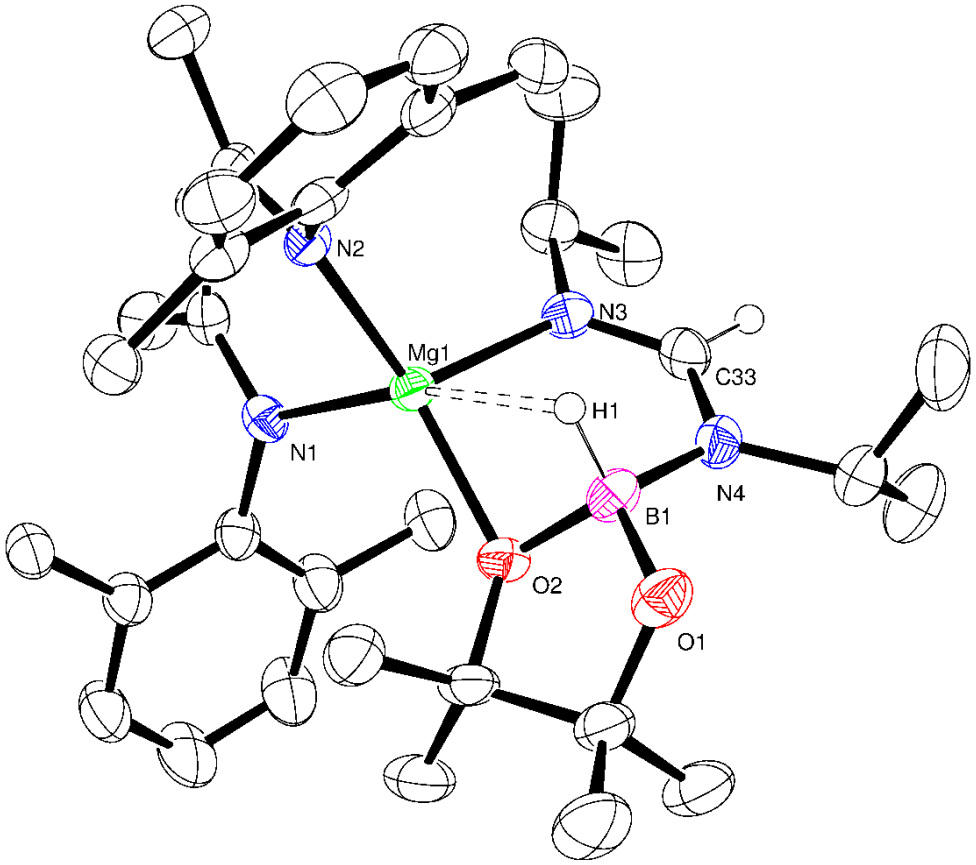

Figure 6-4. ORTEP representation of compound **90** with thermal ellipsoids set at 30% level of probability. Hydrogen atoms except those attached to C(33) and the methyl groups of the *β*-diketiminate 2,6-di-*iso*-propylphenyl substituents are removed for clarity. Selected bond lengths (Å) and angles (°): Mg(1)-N(3) 2.081(3), Mg(1)-O(2) 2.008(3), N(3)-C(33) 1.318(5), C(33)-N(4) 1.343(5), N(4)-B(1) 1.546(5), B(1)-O(1) 1.434(5), B(1)-O(2) 1.516 (5); O(2)-Mg(1)-N(3) 92.16(11), Mg(1)-O(2)-B(1) 91.11(19), Mg(1)-N(3)-C(33) 120.2(2), N(3)-C(33)-N(4) 124.0(3), C(33)-N(4)-B(1) 119.6(3).

Compound **90** was confirmed to be the proposed borate intermediate **B** in Scheme 6-4. Figure 6-4 shows a 5-coordinate magnesium species in which three of the coordination sites are occupied by the bidentate *β*-diketiminate ligand and the imino nitrogen of the reduced carbodiimide. The magnesium coordination number is further augmented by Mg-O coordination to the oxygen of the pinacol fragment and through an additional interaction with the hydride of the HBpin moiety. Comparison of the bond lengths in the formamidine component of the complex to the isolated product (Compound **81**) indicate delocalisation across the NCHN unit [N(3)-C(33) 1.318(5), C(33)-N(4) 1.343(5) Å] rather than formal double and single bonds as observed in compound **90**. The diastereotopic methyl groups of the Bpin unit, observed as a set of 4 discriminate resonances in the ^{1}H NMR spectrum (Figure 6-3), can thus be seen to arise from the maintenance of the 6-membered Mg-N-C-N-B-O heterocycle in solution.

Heating of compound **90** at 60 °C for 24 hours, unexpectedly provided no change in the observed NMR spectra. Further heating at 80 °C for another 24 hours similarly induced no breakdown of compound **90** to the desired borylated product (**81**) and magnesium hydride (**XXII**). Addition of a further equivalent of HBpin also failed to provide further reaction with compound **90**; the same was true of addition an extra equivalent of *i*PrNCN*i*Pr. Addition of both HBpin and *i*PrNCN*i*Pr to a solution of compound **90**, however, provided clean formation of the desired product (**81**) and regeneration of compound **90** (Scheme 6-6). The stability of compound **90** and this apparent requirement for both additional HBpin and *i*PrNCN*i*Pr also explains the maximum conversion of 90% observed during the catalysis studies performed with 10 mol% of the precatalyst (Table 6-2 and Table 6-3). Complex **90** can thus been seen as the resting state of the catalytic cycle.

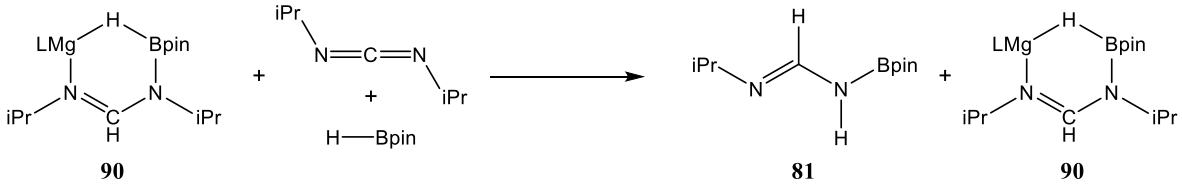

Scheme 6-6. Stoichiometric reaction of compound **90** with equimolar amounts of both HBpin and *i*PrNCN*i*Pr

6.2.3 Kinetic Studies

In an attempt to further probe this mechanism and the influence of the observed intermediate (compound **90**), a kinetic study was undertaken. A 0.4 M solution of dicyclohexyl carbodiimide (CyNCNCy) as the reagent of choice due to the clearly defined product and starting material peaks in the ^{1}H NMR spectra, was, thus, reacted with 10 mol% **Ib** and an equimolar quantity of a 0.42 M solution of HBpin in C_6D_6 at 330 K. Figure 6-5 displays a series of ^{1}H NMR spectra recorded at 20 minute intervals under these reaction conditions.

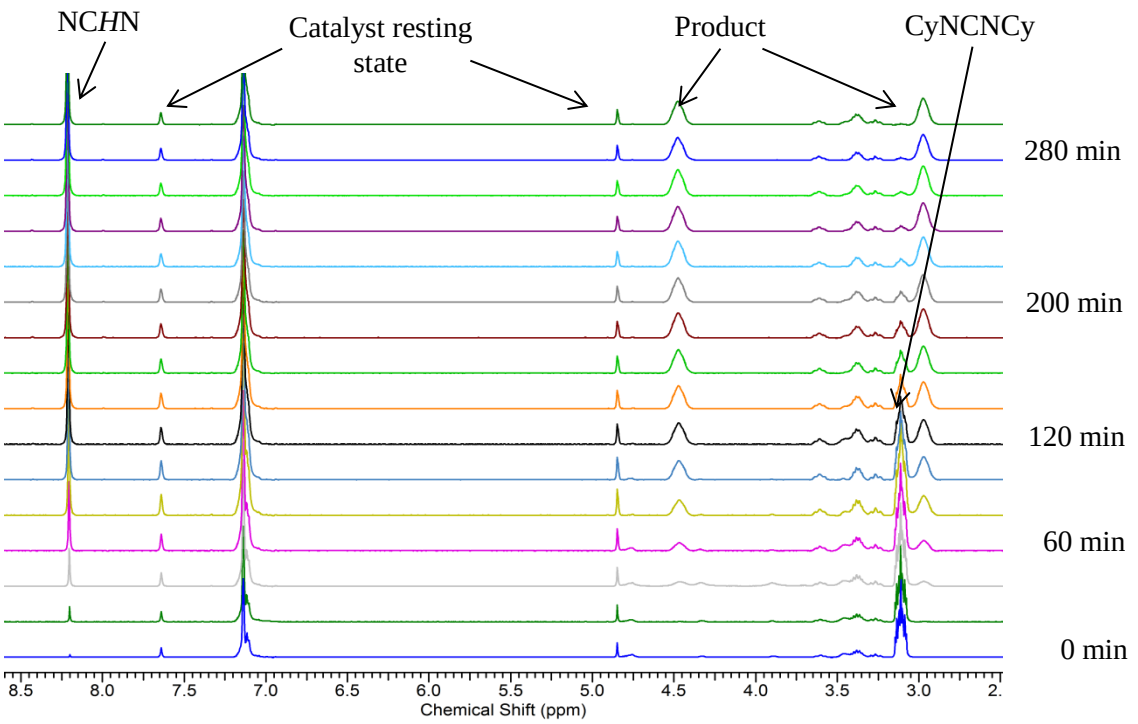

Figure 6-5. Series of stacked ^{1}H NMR spectra, in C_6D_6, for the hydroboration of CyNCNCy with 10 mol% **Ib**

The persistence of a compound analogous to compound **90** was clearly observed throughout the catalysis. Notably this species provided the only observable *β*-diketiminate backbone methine singlet, again suggesting its identity as the active catalyst rather than **XXII**. A plot of concentration of [CyNCNCy] vs time (Figure 6-6) provided a sigmoid curve, and all attempts to fit this data to a straight line failed to match any reasonable reaction order. Variation of the catalyst loading provided similar sigmoidal kinetic profiles with 5 and 10 mol% (Figure S 6-1). Due to this increased complexity, no further kinetic studies of this reaction were carried out.

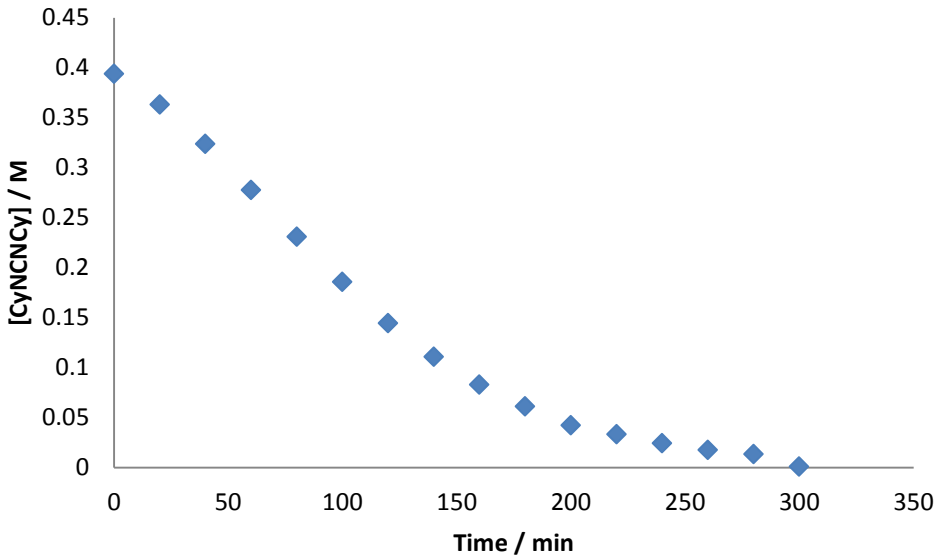

Figure 6-6. [CyNCNCy] vs time

Similar sigmoidal kinetic profiles are usually found in enzyme kinetics, and are generally suggestive of positive cooperative binding (allosteric effect). This can be defined as a process involving multiple identical incremental steps in which intermediate states are statistically underrepresented relative to the hypothetical system.[257] A classic example of positive cooperativity is provided by haemoglobin; the affinity of haemoglobin's four binding sites for oxygen coordination is increased once a single oxygen molecule binds. From this definition, the intermediate state in this case, could be defined as compound **90** as this is only 10 mol% of the solution compared to the larger quantities of HBpin and carbodiimide present. As discerned from the stoichiometric reactions, both an additional equivalent of HBpin and carbodiimide are required in order for turnover to occur. This could arise from further coordination of one substrate binding to the magnesium centre which in turn increases the affinity for the other substrate and results in the Mg-O and B-H cleavage necessary for product formation. Further inspection of the crystal structure of compound **90** (Figure 6-7), depicts a large O(2)-Mg(1)-N(2) bond angle of 140.1°, which could be sufficiently obtuse to allow occupation of a sixth coordination site by either a second equivalent of HBpin or carbodiimide, thus, increasing its affinity for the remaining substrate.

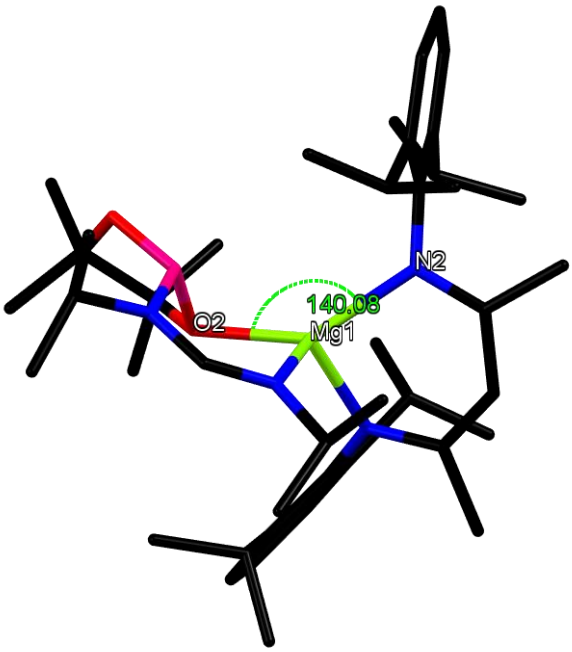

Figure 6-7. Crystal structure of compound **90**, identifying space for coordination to further molecules. For a space filling model see supplementary Figure S 6-3

As noted, the persistence of a compound analogous to compound **90** throughout the course of the catalysis suggests this species may be the active catalyst rather than **XXII**. Performance of a reaction using 10 mol% of compound **90** with *i*PrNCN*i*Pr and 1 eq. of HBpin at 60 °C, provided comparable reaction rates to **Ib** under identical conditions. Repetition of this latter reaction with monitoring of the reaction at set time intervals also provided a sigmoidal kinetic profile for a plot of decreasing [*i*PrNCN*i*Pr] vs time. Similar monitoring of a stoichiometric reaction between compound **90**, *i*PrNCN*i*Pr and HBpin also provided sigmoidal kinetics (Figure S 6-2). Use of compound **90** as a catalyst for other carbodiimide hydroboration reactions was also attempted. A stoichiometric reaction with compound **90**, CyNCNCy and 1 eq. of HBpin provided a roughly even split between the 2 formamidine products and the two possible borate intermediates in a 1:1 ratio by integration of the ^{1}H NMR spectrum (Figure 6-8).

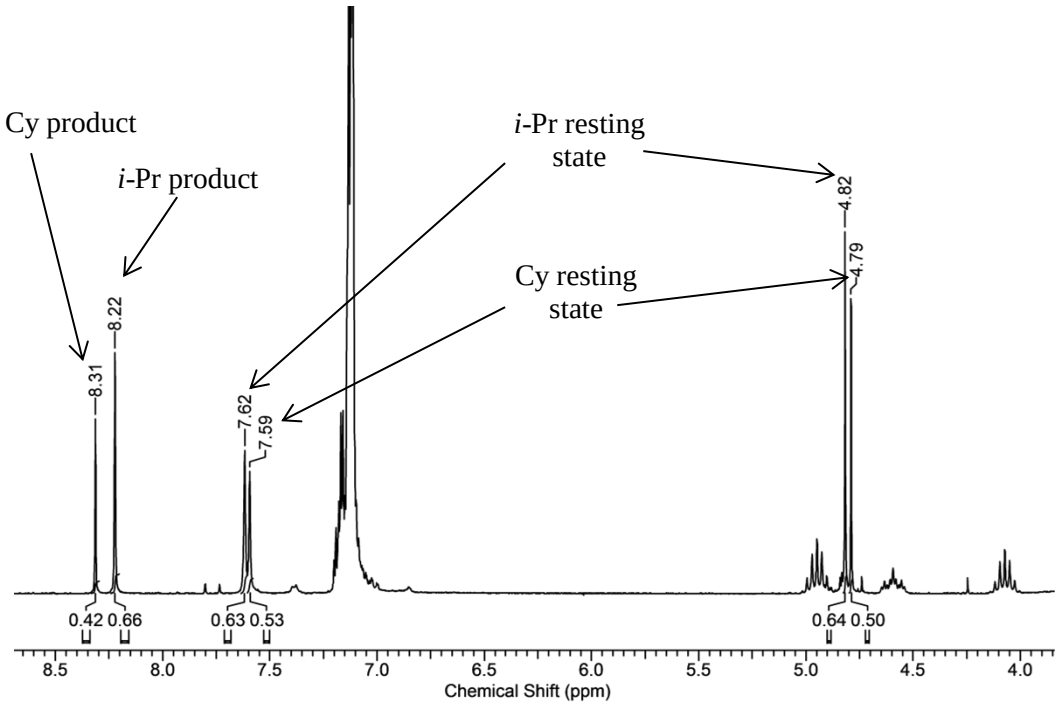

Figure 6-8. ^{1}H NMR spectrum, in C_6D_6, showing both the *i*-Pr and Cy catalytic resting states and formamidine products

This latter observation suggests that the product may also coordinate to the magnesium hydride in a reversible fashion and is also consistent with the earlier observation that all catalytic reactions did not reach 100% conversion to the desired product, in which case binding of the product in preference to the insertion of a carbodiimide will result in the cessation of reaction.

The combination of these proposed steps required a revision of the proposed mechanistic cycle (Scheme 6-7). Subsequent to the *in situ* formation of the magnesium hydride, insertion of the carbodiimide occurs to form complex **A**, whereupon HBpin complexes to the catalytic centre to form the resting state **B**. In the presence of excess carbodiimide and HBpin turnover can then occur to form the product **C**, through path **D**. At low concentrations of both starting reagents, i.e. towards the end of the reaction, however, product **C** can bind to the magnesium hydride and reform the resting state **B** *via* path **E** thus suppressing further catalysis.

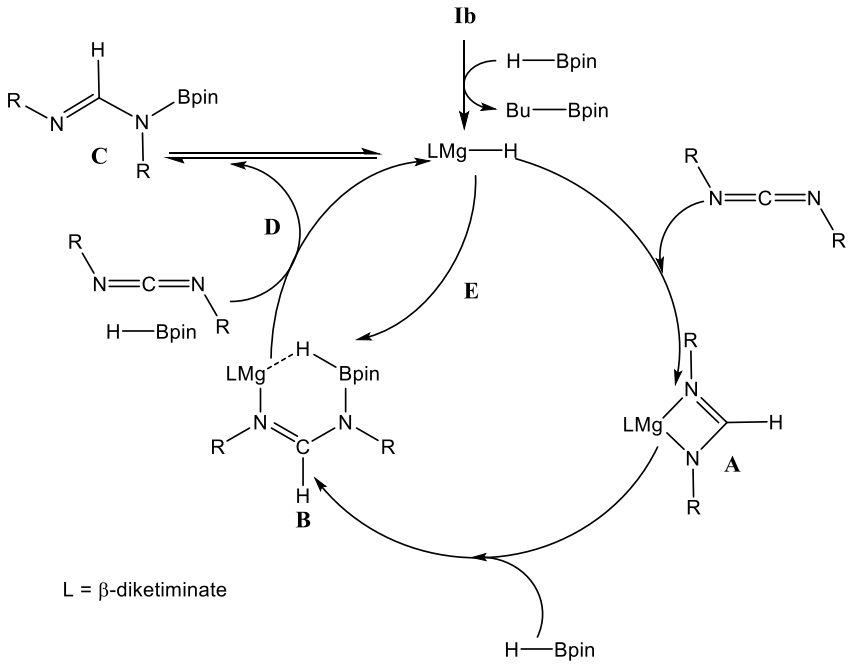

Scheme 6-7. Proposed mechanism for the magnesium-catalysed hydroboration of carbodiimides

6.3 Hydroboration of Isocyanates

Extension of this catalytic hydroboration reactivity to the isoelectronic isocyanate functional group was subsequently undertaken. The isocyanate functional group can be viewed as a cumulated ketone and an imine functional group, both of which have been shown to readily undergo hydroboration using **Ib**, under mild conditions. Scheme 6-8 shows the proposed mechanism for the di-hydroboration of isocyanates. This cycle again comprises of a series of σ-bond metathesis and insertion reactions and is expected to yield either the formamidate (**C**) or hemi-aminal (**E**) products *via* intermediates similar to those observed during the carbodiimide hydroboration study (Compound **90**).

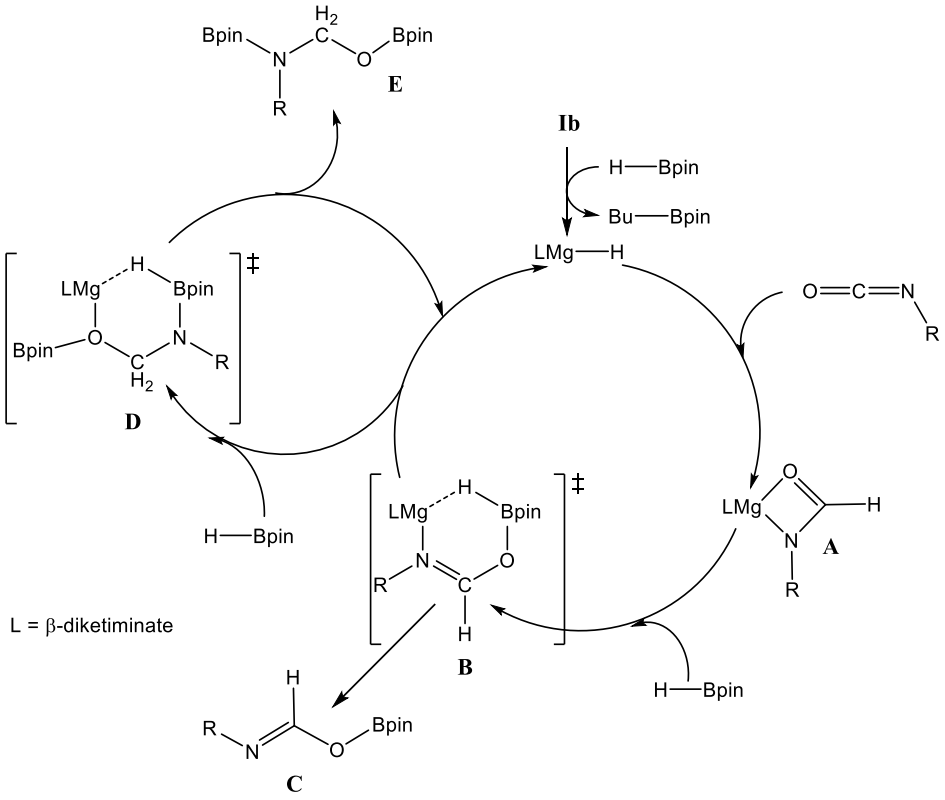

Scheme 6-8. Proposed mechanism for the dihydroboration of isocyanates with **Ib**

As shown in Scheme 6-8, it is predicted that addition at the carbonyl moiety will occur first due to the oxophilicity of boron, whilst the viability of the second reductive step at the imino moiety is thought to be more likely than for a carbodiimide, due to the reduction in the substrate steric demands.

6.3.1 Catalysis

A trial catalytic reaction with 10 mol% of **Ib**, 2,4,6-trimethylphenyl isocyanate (MesNCO) and 2 equivalents of HBpin at room temperature provided full conversion to the desired bis-borylated hemi-aminal product in less than 5 minutes (Table 6-4, entry 6-1). Inspection of the resulting ^{11}B NMR spectrum indicated complete consumption of HBpin due to the disappearance of the diagnostic doublet at δ 32 ppm. Also observed were 2 new single resonances at δ 27.4 and δ 25.3 ppm indicative of new N-*B* and O-*B* environments respectively. Reduction of both double bonds was also indicated by the appearance of a new 2H signal, by integration, at δ 5.32 ppm in the ^{1}H NMR spectrum. Repetition of the reaction with half the catalyst loading (5 mol %) again provided efficient catalytic turnover at room temperature with similar full conversion being observed after 10 minutes (entry 6-2). Use of the bulkier DippNCO isocyanate substrate (entry 6-3) also yielded clean and efficient formation of the desired bis-borylated hemi-aminal product. Subsequent scale up reactions in toluene provided suitable single crystals of compound **91** for X-ray diffraction analysis (Figure 6-9).

Table 6-4. Magnesium-catalysed di-hydroboration of aryl isocyanates

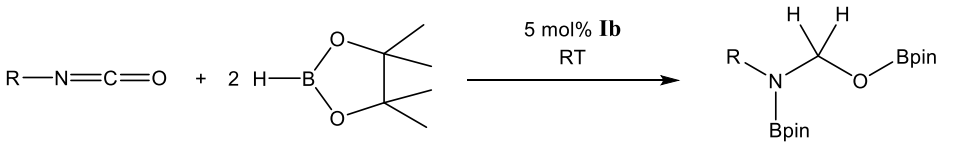

R = Mes (**91**), Dipp (**92**)

Entry	Isocyanate	Catalyst / mol%	Time/ min	Temp / °C	NMR Yield / %
6-1	2,4,6-trimethylphenyl isocyanate	10	<5	25	>99
6-2	2,4,6-trimethylphenyl isocyanate	5	10	25	>99
6-3	2,6-di-*iso*-propylphenyl isocyanate	5	15	25	>99

NMR experiments were carried out in C_6D_6, whereas large scale experiments were carried out in toluene. For full details see experimental section 7.6.2.

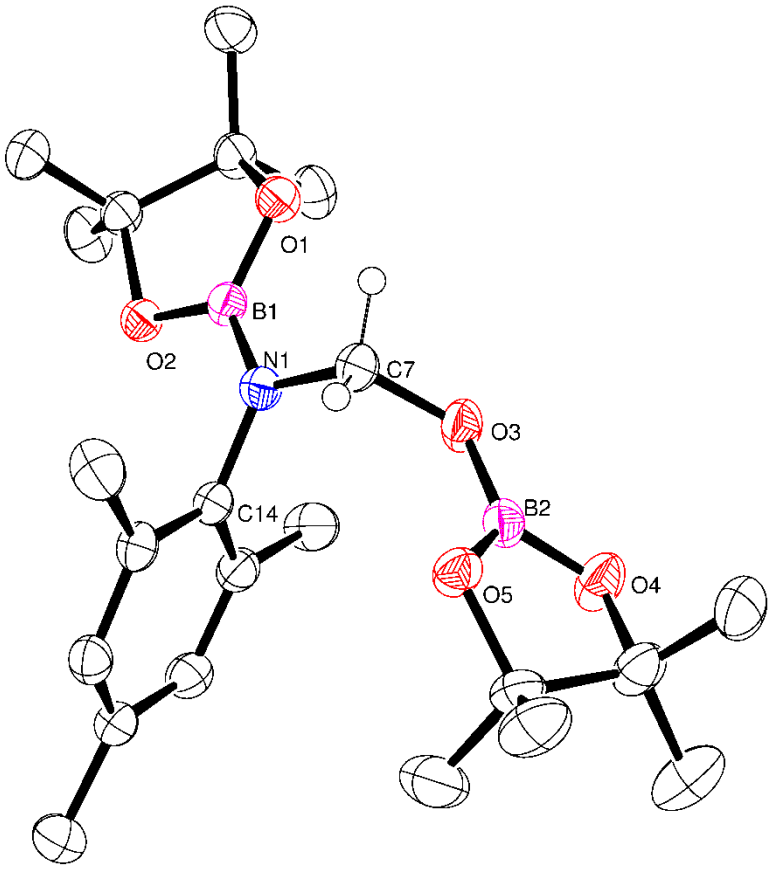

Figure 6-9. ORTEP representation of compound **91** with thermal ellipsoids set at 30% level of probability. Hydrogen atoms except those attached to C(7) are removed for clarity. Selected bond lengths (Å) and angles (°): B(1)-N(1) 1.414(2), N(1)-C(7) 1.4390(19), C(7)-O(3) 1.4397(19), O(3)-B(2) 1.357(2); B(1)-N(1)-C(7) 120.81(13), N(1)-C(7)-O(3) 111.75(13), C(7)-O(3)-B(2) 119.13(12).

Figure 6-9 shows the results of the X-ray diffraction analysis performed on compound **91**, which crystallises with 2 molecules in the asymmetric unit cell, and confirms the identity of the hemi-aminal species. The central carbon of the isocyanate can be seen to have been reduced from *sp* to sp^3 hybridisation [N(1)-C(7)-O(3) 111.75(13)°]. This is further confirmed by the elongation of both the N-C and O-C bonds indicative of single bond character [N(1)-C(7) 1.4390(19), C(7)-O(3) 1.4397(19) Å].

Extension of this reactivity to phenyl isocyanate (PhNCO) (Table 6-5, entry 6-4) using 10 mol% of **Ib** with 2 equivalents of HBpin, provided a slow reaction at room temperature. The ^{1}H NMR spectrum comprised of a new 3H singlet, by integration, at δ 3.01 ppm consistent with the formation of a CH_3 group and suggestive of either N-C or C-O cleavage. Repetition of this reaction with 3 equivalents of HBpin, to provide the additional hydride equivalent, at 60 °C (entry 6-5) showed full consumption of PhNCO by ^{1}H NMR spectroscopy in 21 hrs. Analysis of the corresponding ^{11}B NMR spectrum (Figure 6-10) revealed the presence of unreacted HBpin and two further singlet resonances in a 1:2 ratio at δ 27.7 and 24.8 ppm respectively.

This 1:2 ratio was further confirmed by integration of the corresponding resonances in the ^{1}H NMR spectrum.

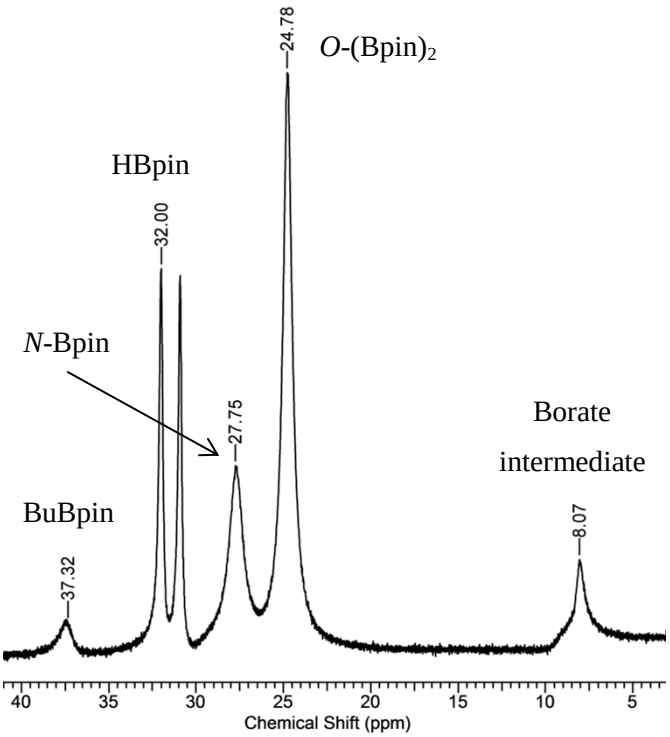

Figure 6-10. ^{11}B NMR spectrum, in C_6D_6, of the catalytic reaction of PhNCO with 3 eq. of HBpin, forming compound **93** and bis(boryl)oxide

The ^{11}B resonance at δ 24.8 ppm was identified as the bis(boryl)oxide, $O(Bpin)_2$, through comparison with literature data[158] indicating that HBpin reduction of PhNCO had resulted in complete cleavage of the C=O bond within the substrate with consequent formation of the *N*-borylated *N*-methyl aniline (Scheme 6-9). A further singlet in the ^{11}B NMR spectrum at δ 8.07 ppm was comparable to the 4-coordinate borate species identified as compound **90** in the carbodiimide hydroboration study. This latter observation supports the likelihood of species similar to **B** or **D** shown in Scheme 6-8, as likely intermediates for this reaction.

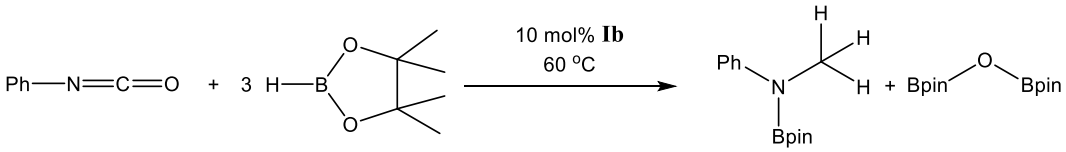

Scheme 6-9. Magnesium-catalysed hydroboration of phenyl isocyanate

Further heating of the solution, in an attempt to force the remaining HBpin to react, only provided the formation of the B_2pin_3 decomposition product. Extension of this reactivity to other commercially available alkyl isocyanates provided similar reactivity to PhNCO. Table 6-5, entries 6-6 to 6-11, presents the outcome of this reaction performed with a range of alkyl

isocyanates of increasing steric bulk. Contrary to previous trends, increased RNCO substituent steric bulk provided faster reaction times; R=*i*-Pr (entry 6-8) and *t*-Bu (entry 6-9) evidenced complete consumption of the isocyanate in less than 4 hours compared to Et (entry 6-6) and Pr (entry 6-7) which required 21 hours. The increased reactivity associated with increasing alkyl substituent steric demands also coincided with the onset of secondary side reactions and a consequent decrease in formation of the *N*-methyl amine products. Although attempts to identify the products of these side reactions were unsuccessful it is likely that oligomerisation of the isocyanates is competitive with the reductive C=O cleavage. During the monitoring of these catalytic reactions, both the RNCHOBpin and RN(Bpin)CH_2OBpin products (Scheme 6-8, species **C** and **E**, respectively) could be identified as intermediates from their characteristic singlet resonances associated with the formamidine methine (ca. δ 8-9 ppm) and hemi-aminal methylene (ca. δ 5.0 ppm) resonances in the ^{1}H NMR spectrum.

Table 6-5. Magnesium-catalysed hydroboration and reductive C=O cleavage of alkyl isocyanates

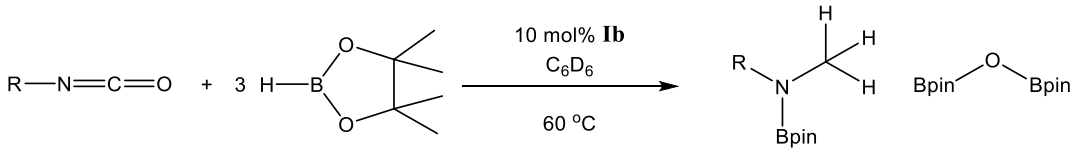

R = Ph (**93**), Et (**94**), Pr (**95**), *i*-Pr (**96**), *t*-Bu (**97**), Cy (**98**), Ad (**99**)

Entry	Isocyanate	Time / hr	Temp / °C	NMR Yield / %
6-4	phenyl isocyanate	24	25	33
6-5	phenyl isocyanate	21	60	73
6-6	ethyl isocyanate	21	60	70
6-7	propyl isocyanate	21	60	75
6-8	*iso*-propyl isocyanate	1.5	60	64
6-9	*tert*-butyl isocyanate	3.5	60	52
6-10	cyclohexyl isocyanate	4.5	60	78
6-11	1-adamantyl isocyanate	4.5	60	65

6.3.2 Mechanistic studies

Attempts to probe the mechanism of this methylation reaction *via* stoichiometric reactions were not instructive. Reaction of either the *in situ* generated hydride or isolated **XXII** with 1 equivalent of *i*-PrNCO indicated the formation of a variety of unidentified products by NMR analysis (Figure 6-11). Several singlet peaks were observed in the downfield region in the vicinity of the expected formamidine NC*H*O resonance. Unfortunately attempts to isolate

products *via* various different crystallisation and separation techniques failed. Similar observations have been previously described by Jones and co-workers during the stoichiometric reaction of **XXII** with *t*-BuNCO.[117]

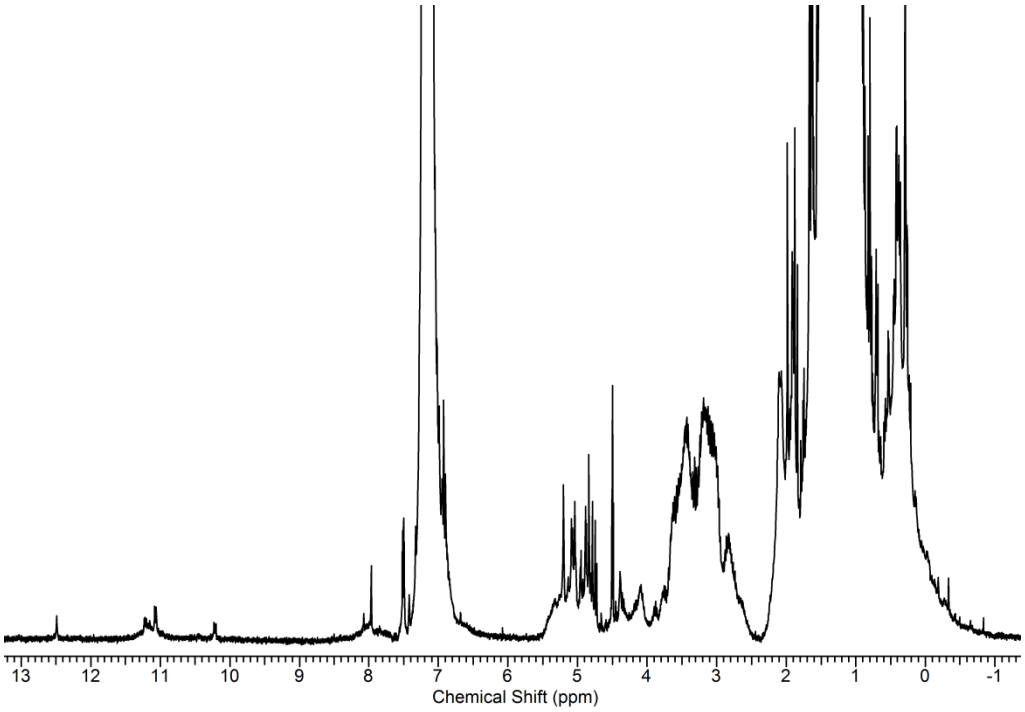

Figure 6-11. ^{1}H NMR spectrum, in C_6D_6, of the stoichiometric reaction of **XXII** with *i*-PrNCO

ESI mass spectrometry performed on the products of the catalytic reactions also demonstrated the formation of several additional products. Most notable was the absence of the *β*-diketiminate ligand at 419 *m/z*. A peak at 504 *m/z* was, however, observed indicating the reaction of the isocyanate with the supporting ligand (Scheme 6-10). A similar reaction has been reported recently by Hill and co-workers during the insertion of CO_2 into the *β*-diketiminate ligand with a magnesium hydride BCF complex (**XXXVIIa**).[158] Reactions with tin and lead complexes supported by the same *β*-diketiminate ligand have also provided similar reactivity which may be rationalised as the net result of a nucleophilic attack by the *γ*-carbon atom of the *β*-diketiminato ligand at the electrophilic carbon centre of phenylisocyanate.[258]

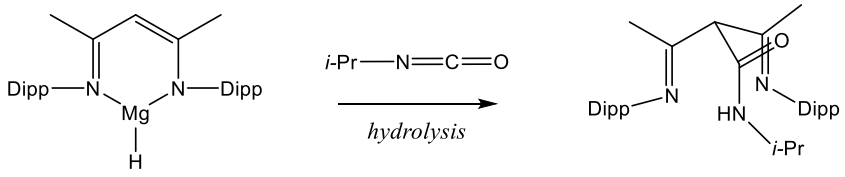

Scheme 6-10. Insertion of *i*-PrNCO into the *β*-diketiminate ligand

Whilst both of these recent publications support a hypothesis of insertion into the *β*-diketiminate ligand, this reaction seemingly only occurs towards the end of catalysis. Although re-inspection

of the NMR spectra recorded during catalysis revealed singlet resonances at δ 13.2 and 13.4 ppm which may be assigned to the N*H* resonance of the protonated isocyanate insertion ligand (cf. *β*-diketiminate N*H* δ 12.5 ppm), this only appeared after ca. 70% conversion of the isocyanate reagent. A similar ligand insertion reaction was subsequently confirmed for all of the alkyl and phenyl isocyanate reactions by ESI mass spectrometry. In each case a new mass ion equal to [*β*-diketiminate+H]$^+$ (419 *m/z*) plus the corresponding isocyanate could be observed.

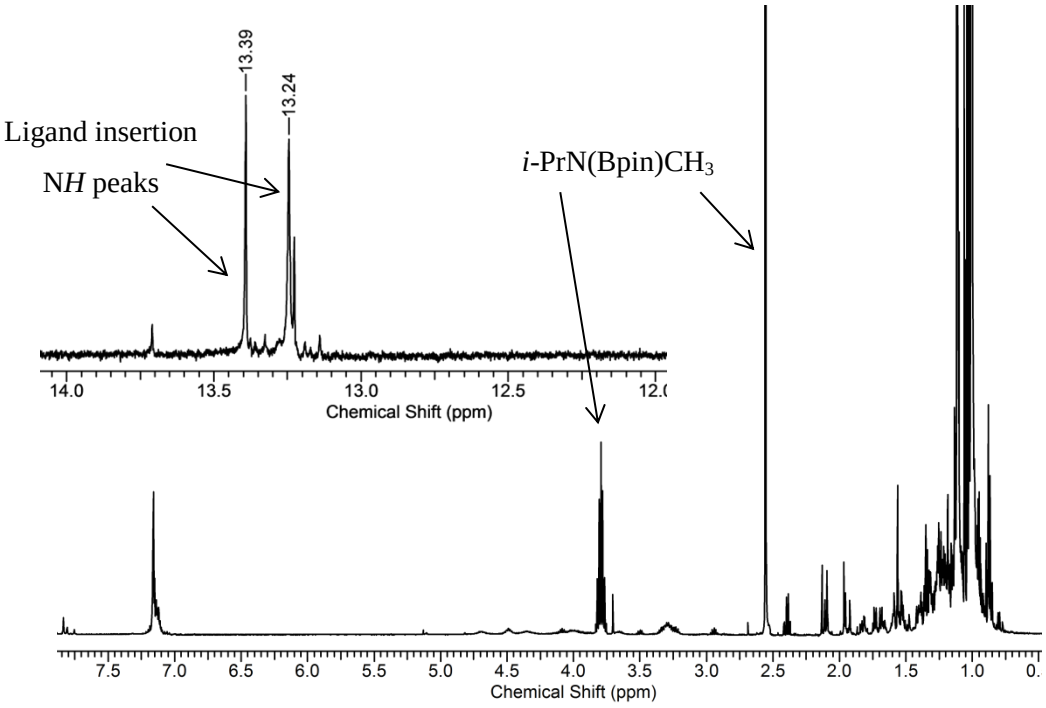

Figure 6-12. ^{1}H NMR spectrum, in C_6D_6, for the catalytic hydroboration of *i*-PrNCO with **Ib**

The overall progress of the catalysis (Figure 6-13) was assessed by monitoring the reaction of *i*-PrNCO with 3 eq. of HBpin and 10 mol% **Ib** at set time intervals. Consistent with the proposed mechanism the initial formation of *i*-PrNCHOBpin was observed followed by subsequent reduction to *i*-PrN(Bpin)CH_2OBpin. This latter species was then observed to be consumed with concomitant production of the final product of C-O cleavage, the *N*-methyl amine product, *i*-PrN(Bpin)CH_3, with simultaneous formation of the bis(boryl)oxide by-product.

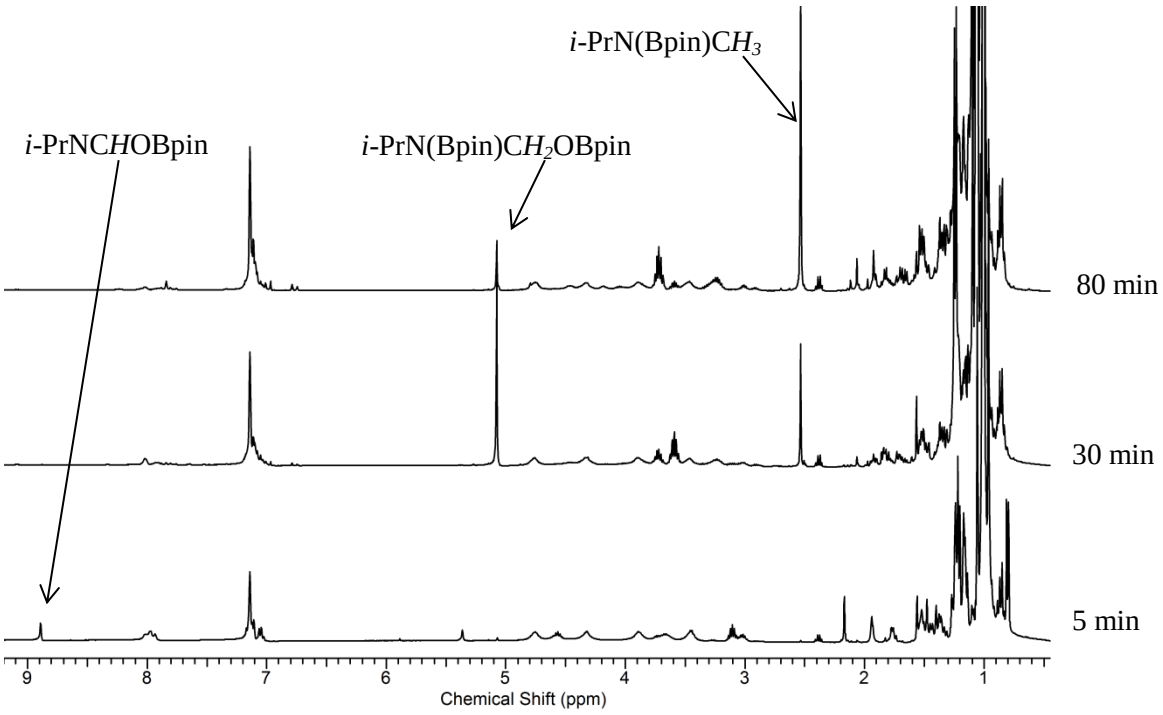

Figure 6-13. Stacked ^{1}H NMR spectra, in C_6D_6, for the hydroboration of *i*-PrNCO with **Ib**

A plot of [product] vs time provided a further indication of the sequential nature of the hydroboration of *i*-PrNCO (Figure 6-14). Unlike the previous di-hydroboration reactions of nitriles and *iso*-nitriles in which the second reduction was deduced to occur *via* an intramolecular hydride transfer and retention of the imine-derived products within the coordination sphere of the magnesium centre, the observed intermediate products display a build-up in concentration greater than that of the catalyst loading suggesting that each of the formamidine and hemi-aminal species are released and can re-insert into the catalytic cycle to undergo further reduction.

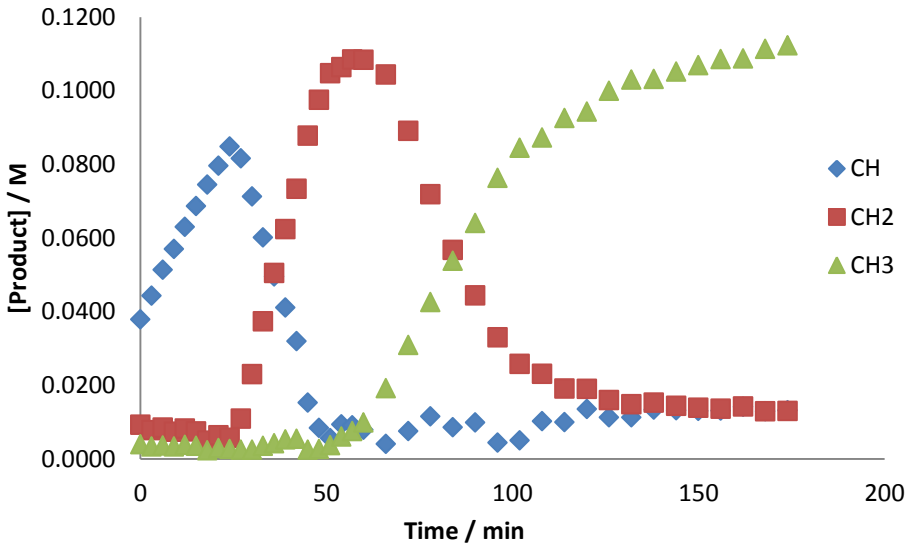

Figure 6-14. Plot of [Product] vs time

Attempts to isolate each of the individual reaction intermediates for *i*-PrNCO, to enable further mechanistic studies, were unsuccessful. In each case further reduction to the *N*-methyl amine was observed indicating the instability of the formamidine and hemi-aminal products of the alkyl isocyanates. Use of the aryl isocyanates MesNCO and DippNCO, however, allowed the isolation of a more stable hemi-aminal product suitable for further study. Although addition of compound **91** to a solution of HBpin and 10 mol% of **Ib** provided no reaction at room temperature, heating overnight at 60 °C induced the formation of the bis(boryl)oxide. Rather than the expected formation of the *N*-methyl amine, however, two 1H doublet resonances, by integration, were observed in the ^{1}H NMR spectrum (Figure 6-15). These were shown to couple to each other by a ^{1}H-^{1}H COSY NMR experiments, and could be identified as the *N*-mesityl methylene imine, MesN=CH_2 (compound **100**).

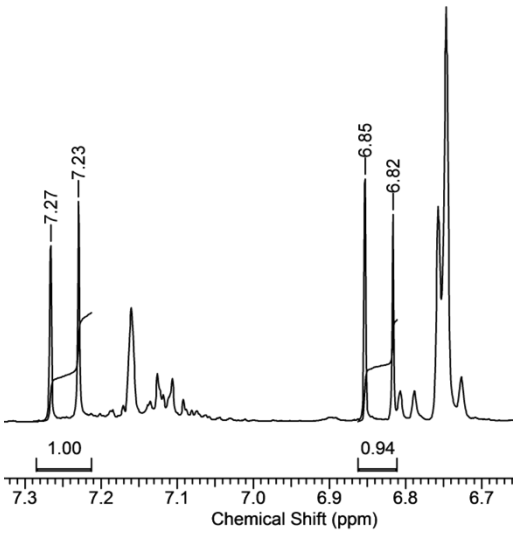

Figure 6-15. ^{1}H NMR spectrum, in C_6D_6, showing formation of the mesityl imine, compound **100**

Repetition of this reaction using compound **92** (Scheme 6-11) also led to formation of the methylene imine (compound **101**) and, upon further heating, the precipitation of an insoluble crystalline product which was identified as a magnesium boryloxide through the use of single crystal X-ray crystallography (Figure 6-16).

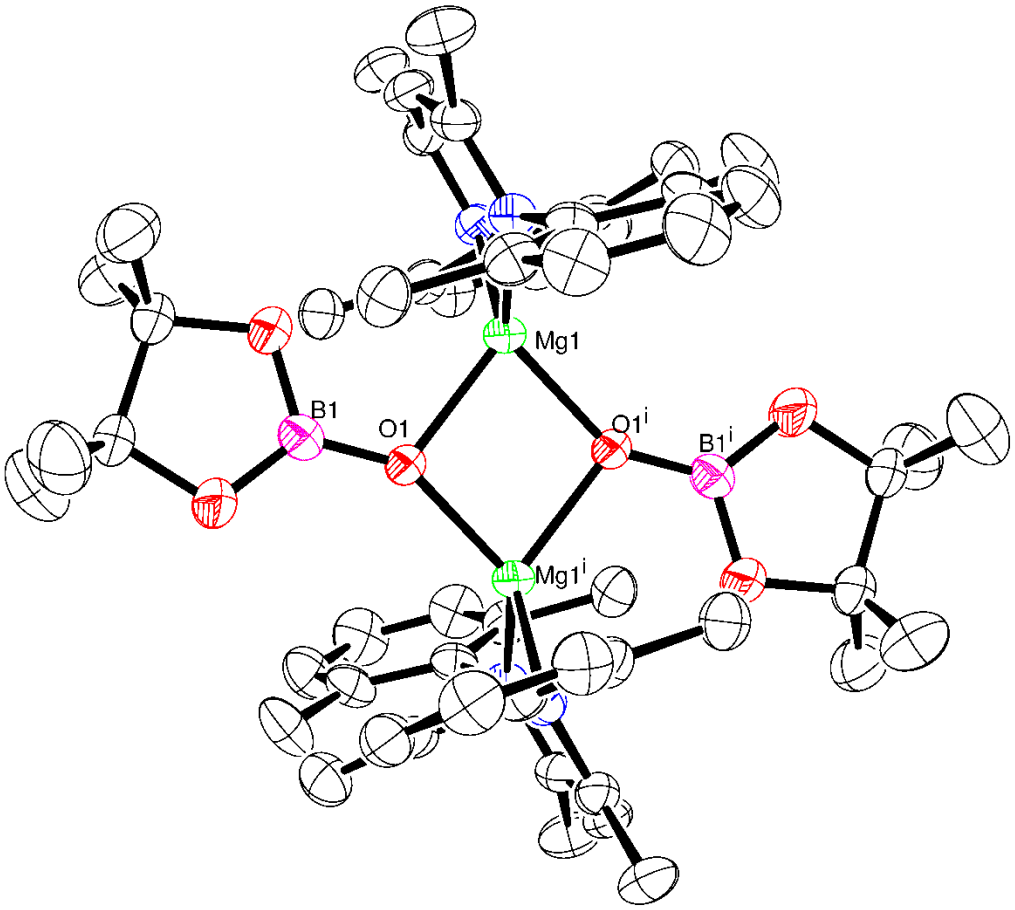

Figure 6-16. ORTEP representation of compound **102** with thermal ellipsoids set at 30% level of probability. The methyl groups of the *β*-diketiminate 2,6-di-*iso*-propylphenyl substituents are removed for clarity. Selected bond lengths (Å) and angles (°): Mg(1)-O(1) 2.0400(16), $Mg(1)^{i}$-O(1) 1.9872(16), O(1)-B(1) 1.343(3), B(1)-O(1)-Mg(1) 112.82(14), O(1)-Mg(1)-$O(1)^{i}$ 81.83(7). Symmetry transformations used to generate equivalent atoms: -x,-y+1,-z.

Figure 6-16 shows the structure of compound **102**, which comprises a dimeric magnesium complex in which the monomeric unit consists of a magnesium-oxy(boryl) complex. The 4-coordinate magnesium centre comprises of bidentate coordination to the *β*-diketiminate ligand and to two bridging oxygen atoms which are bound the pinacolato boryl moiety. The Mg-O bond lengths within compound **102** are comparable to the previously reported two peroxo-centred mixed metal magnesium/alkali metal 'inverse crown' structures,[259] [{[$(Me_3Si)_2N]_4K_2Mg_2(O_2)$}•] 2.010(2), 2.015(1) Å; (**102**) Mg(1)-O(1) 2.0400(16), $Mg(1)^{i}$-O(1) 1.9872(16) Å] however the O(1)-$O(1)^{i}$ distance of 2.64 Å is much longer than the peroxo bond length for similarly *β*-diketiminato magnesium peroxo complexes (ca. 1.65 Å).[124]

Although the formation of compound **102** suggests that the C-O cleavage reaction is magnesium mediated, the insolubility of this complex in C_6D_6 mitigates against onward further reactivity through this mechanism. To assess the possibility that these products may arise from the decomposition of the hemi-aminal upon heating, the isolated hemi-aminal (compound **91**) was

heated in C_6D_6 solution at 60 °C overnight. Whilst imine formation was observed, a lower conversion was noted indicating that the magnesium centre is likely to act as a catalyst for the decomposition of the hemi-aminal compounds (Scheme 6-11). The final reduction of the imine species arises from insertion into the magnesium hydride to yield the magnesium amide species and subsequent σ-bond metathesis with HBpin.

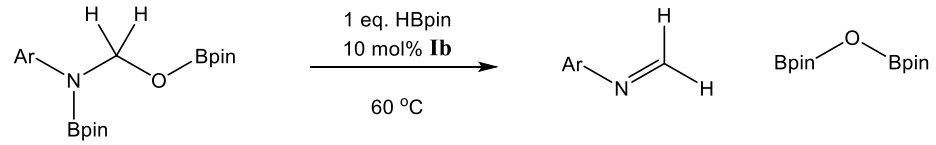

Ar = Mes (**91**), Dipp (**92**)

Ar = Mes (**100**), Dipp (**101**)

Scheme 6-11. Further reactivity of the isolated aryl hemi-aminal compounds to form imine species and the bis(boryl)oxide compounds

These mechanistic studies allow the construction of a new proposed mechanism for the effective tri-hydroboration of isocyanates to yield *N*-methyl amine products (Scheme 6-12). The proposed mechanism contains 4 different cycles (1-4), which after the first turnover are each proposed to act independently and in competition for the active catalyst as well as with other unknown competing reactions of isocyanates.

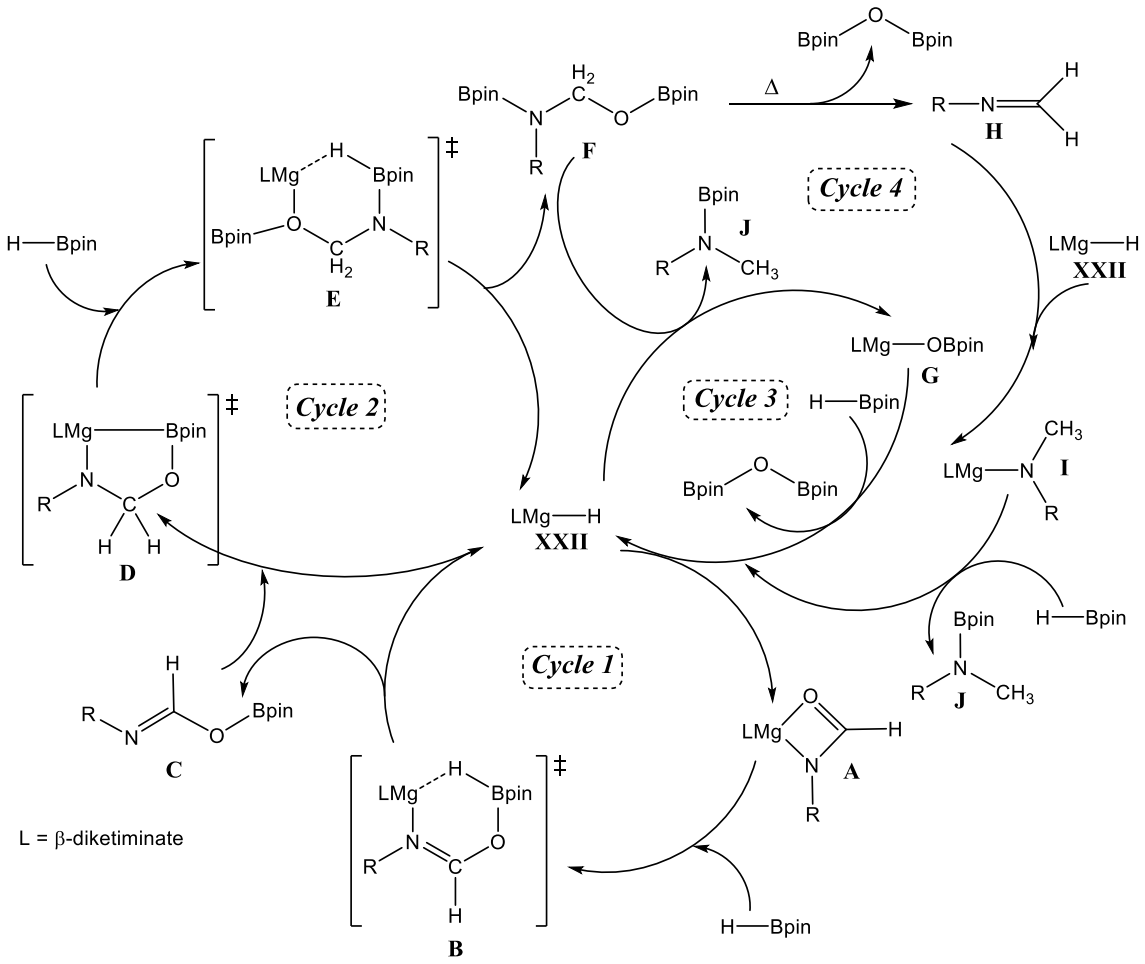

Scheme 6-12. Proposed mechanism for the tri-hydroboration of isocyanates mediated by **Ib**

Cycle 1 describes the initial formation of the formamidate product (**C**) through Mg-H insertion of the isocyanate to form the formamidinate complex **A**, which then undergoes σ-bond metathesis *via* intermediate borate **B** to yield the formamidine **C** with regeneration of the active catalyst. Here the magnesium hydride can react further with product **C** and proceed around cycle 2 or can engage with further isocyanate and continue cycle 1.

Cycle 2 provides the second reduction of the isocyanate to the hemi-aminal product **F**. Reaction of product C with **XXII** yields the intermediate amido complex **D**, which undergoes subsequent σ-bond metathesis *via* the borate intermediate **E** with the second equivalent of HBpin to result in the re-formation of the active catalyst and product **F**. Having been regenerated, **XXII** can now react with either a further molecule of isocyanate (cycle 1) or the formamidine product **C** (cycle 2) or alternatively undergo further reactivity *via* cycles 3 or 4.

Both cycles 3 and 4 compete for the hemi-aminal product **F**, as evidence for both cycle products, the imine **H** and the *N*-methyl amine, was observed during the reactions of the isolated aryl hemi-aminal products. Cycle 3 proceeds through insertion of the hemi-aminal product **F** into the magnesium hydride to form the *N*-methyl amine product with production of the

magnesium oxy-boryl by-product **G**. While this latter product can undergo σ-bond metathesis with the final equivalent of HBpin to form the bis(boryl)oxide and regenerate the active catalyst, cycle 4 entails the spontaneous breakdown of the hemi-aminal product with heating to form the imine product **H** and the bis(boryl)oxide. This imine species can also insert into the Mg-H bond to yield the magnesium-*N*-methyl amide product **I**, which, on σ-bond metathesis with the third equivalent of HBpin, forms the borylated *N*-methyl amine product (**J**) with reformation of **XXII**.

6.4 Hydroboration of Carbon Dioxide

Previously described reactivity of CO_2 with group 2 supported *β*-diketiminate complexes and HBpin has required the use of the Lewis acidic BCF to yield a methanol equivalent (Scheme 1-38). As the hydroboration of isocyanates also resulted in C-O cleavage, a study into the hydroboration of CO_2 without the addition of a catalytic amount of BCF was undertaken. An initial trial reaction using 10 mol% of **Ib** and HBpin in C_6D_6 was freeze-thawed de-gassed before condensing CO_2 into the Youngs tap NMR tube. Monitoring of this reaction at 60 °C *via* NMR spectroscopy (Figure 6-17), revealed the initial formation of a borate intermediate. This is predicted to be a 4-coordinate borate species similar to those identified during the hydroboration of carbodiimides and isocyanates. Although the desired products were seen to appear after 48 hrs, extended heating of this solution over the course of a week showed no further increase in product formation, alongside an increase in decomposition products as evidenced by BH_3 formation in the ^{11}B NMR spectrum.

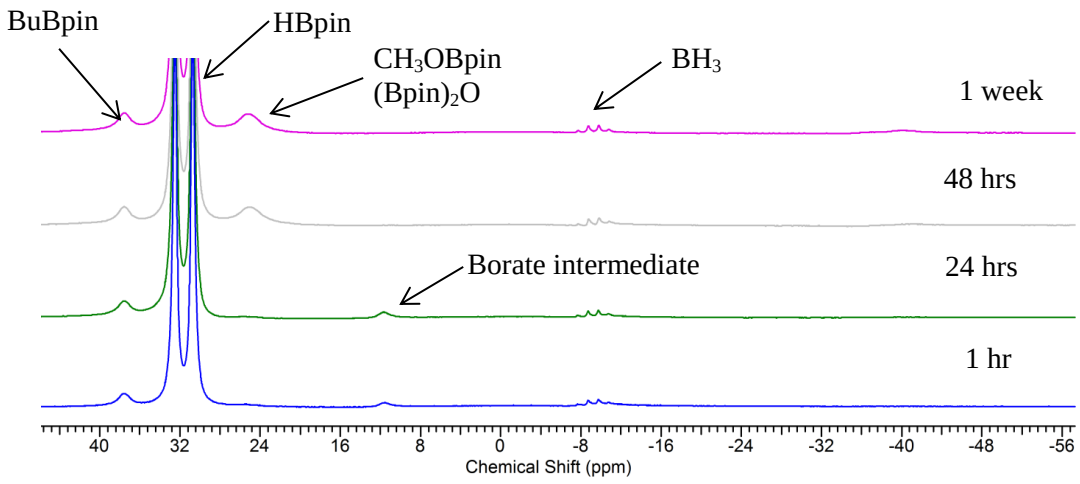

Figure 6-17. Series of ^{11}B NMR spectrum for the hydroboration of CO_2 in C_6D_6

Whilst some evidence of catalytic turnover was observed, this system was only poorly active. This was thought to be due to poor solubility of CO_2 in C_6D_6. The reaction was, therefore repeated in d_8-toluene, whereupon NMR monitoring of the reaction at 60 °C, revealed the same

sequence of reactivity. Increased conversion to the methanol equivalent was observed (25 % in 6 days compared to 13 % in 7 days for C_6D_6). This was, however, still poor in comparison to the reactivity observed with a co-catalytic amount of BCF. An analogous reaction performed in d_8-THF showed enhanced conversion to the desired methanol equivalent, with 55% conversion observed after 6 days (Figure 6-18).

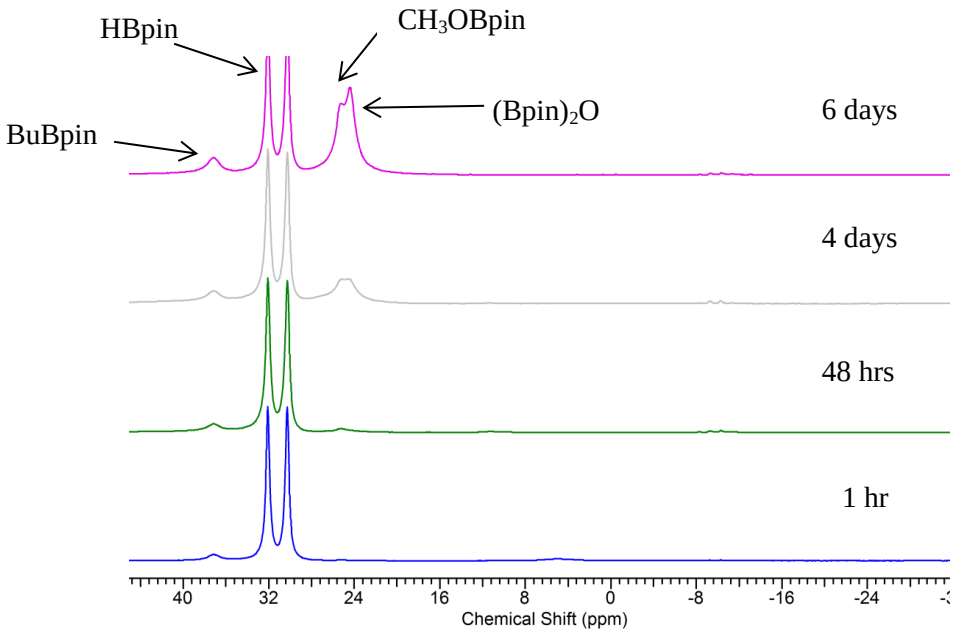

Figure 6-18. Series of stacked ^{11}B NMR spectra for the hydroboration of CO_2 in d_8-THF

Whilst still not reaching the conversions as seen with the reactions including BCF, using d_8-THF provided less decomposition of HBpin. Although the reasons for this are unclear, the mechanism of the reaction may be broadly analogous to that proposed for the hydroboration of isocyanates. A simplified version is outlined in Scheme 6-13.

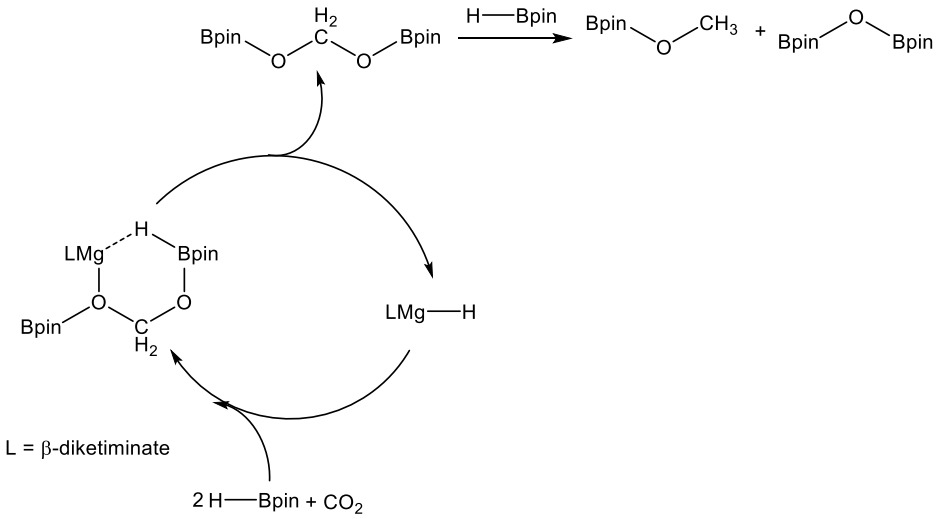

Scheme 6-13. Proposed mechanism for the hydroboration of CO_2 by **Ib**

The reductive hydroboration of CO_2 is again proposed to occur *via* σ-bond metathesis and insertion reactions, which initially form the acetal-derived product which is proposed to be more unstable than the alkyl hemi-aminal species observed in the isocyanate hydroboration studies. This species as a result, breaks down even more readily into the methoxyborane and bis(boryl)oxide species. This could also occur *via* the metal centre leading to the formation of the magnesium oxy-boryl (compound **102**) which then undergoes σ-bond metathesis with the final equivalent of HBpin to yield the observed products.

6.5 Conclusions

In conclusion, the hydroboration of heterocumulenes with **Ib** proceeds efficiently to reduce the heterocumulene. In the case of carbodiimides, reduction is observed to occur only once to yield the borylated formamidine. The identification of the borate intermediate (compound **90**) is crucial to this reaction, and this has also been shown to act as a similarly active catalyst for the hydroboration of carbodiimides.

Extension of this study to isoelectronic isocyanates showed extremely efficient turnover for the aryl isocyanates to the desired hemi-aminal products, however extension to alkyl isocyanates and phenyl isocyanate provided an unexpected C-O cleavage reaction to yield *N*-methyl-*N*-boryl-amines and bis(boryl)oxide. This final cleavage step in the reaction is proposed to occur either through direct σ-bond metathesis with HBpin or *via* insertion into the magnesium hydride to form a magnesium-oxy-boryl complex (compound **102**) which then undergoes σ-bond metathesis with HBpin to yield the bis(boryl)oxide.

Finally magnesium catalysed hydroboration of CO_2 in the absence of a BCF co-catalyst provided limited turnover to MeOBpin in C_6D_6 but enhanced reactivity in THF. Even in this latter case, however, after 6 days only 55% conversion to the methoxyborane was observed. Whilst this study demonstrated the viability of **Ib** as the pre-catalyst, the use of a co-catalytic amount of the Lewis acidic BCF provides amplified reactivity for the reductive hydroboration of CO_2.

Significantly, in a preliminary assessment of the effect of a co-catalytic quantity of BCF the hydroboration of carbodiimides was repeated. Using 10 mol% of **Ib** and BCF, 2 equivalents of HBpin and *i*PrNCN*i*Pr (Scheme 6-14) yielded complete reduction of the carbodiimide to the bis(borylated)aminal at room temperature in less than 24 hours, as indicated by the appearance of a distinctive CH_2 singlet at δ 4.6 ppm (Figure 6-19). Further work is on-going into the role played by BCF in the catalytic hydroboration reactions of both carbodiimides and CO_2.

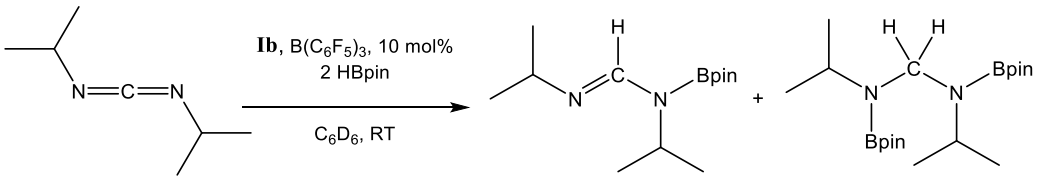

Scheme 6-14. Dihydroboration of carbodiimides using **Ib** and a co-catalytic amount of BCF

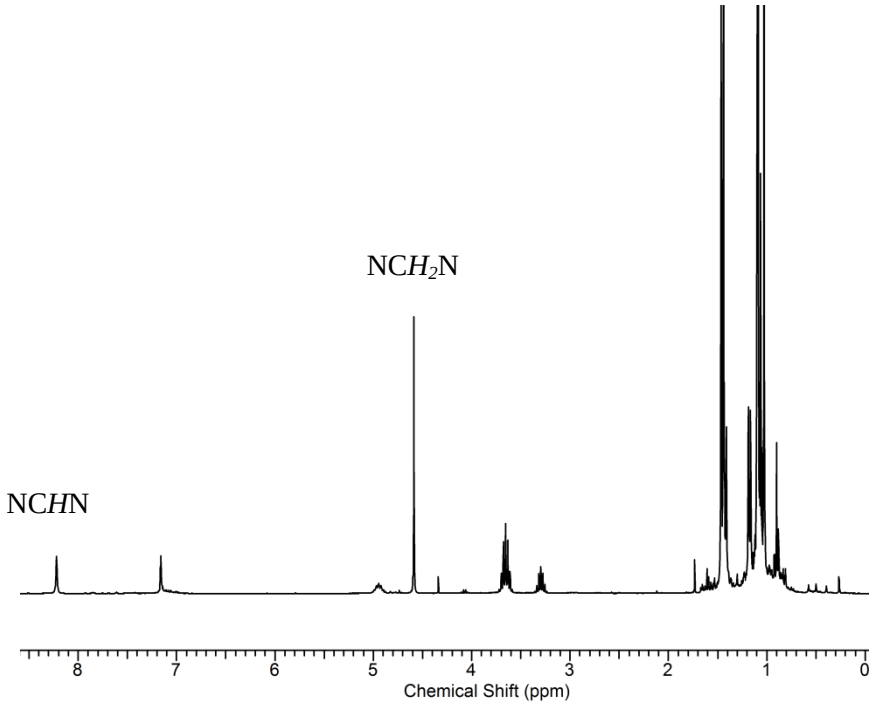

Figure 6-19. ^{1}H NMR spectrum, in C_6D_6, for the dihydroboration of carbodiimides with **Ib** and a co-catalytic amount of BCF

Chapter 7. Experimental Data

7.1 General Proceedures

7.1.1 Analytical Methods

Nuclear Magnetic Resonance (NMR) Spectroscopy

NMR experiments were conducted in Youngs tap NMR tubes made up and sealed in a Glovebox. All spectra were collected at 298 K unless stated otherwise. NMR spectra were collected on a Bruker AV300 spectrometer operating at 300.2 MHz (^{1}H), 75.5 MHz (^{13}C), and 96.25 MHz (^{11}B), or on a Bruker 400 UltrashieldTM for variable temperature, kinetics and 2D experiments (400 MHz (^{1}H) and 100 MHz (^{13}C)). ^{1}H/^{13}C NMR spectra were referenced using residual solvent resonances.

X-ray Crystallography

X-ray diffraction data for compounds **2**, **12**, **13**, **14**, **16**, **32**, **46**, **53**, **69**, **70**, **71**, **73**, **81**, **84**, **90**, and **102** were collected on a Nonius Kappa CCD with a low temperature device at 150 K, utilizing Mo-Kα radiation monochromated with graphite (λ = 0.71070 Å). Data processing was carried out with the Nonius software,[260] and structure solution and refinement was undertaken using X-Seed, SHELXS and SHELXL and visualised with ORTEP.

X-ray diffraction data for compound **80** was collected on an Agilent Supernova (Dual source) CCD with a low temperature device at 150 K, utilising a Cu-Kα radiation (λ = 1.5418 Å). Data processing was carried out with the CrysAlis^{Pro} software, and structure solution and refinement was undertaken using X-seed, SHELXS and SHELXL and visualised with ORTEP.

Mass Spectrometry

Mass spectrometry was performed on a Bruker Daltonik microTOF electrospray time-of-flight (ESI-TOF) mass spectrometer coupled to an Agilent 1200 LC system as an auto sampler. 10 μL of sample was injected into a 30:70 flow of water: methanol at 0.4 mL/min followed by injection of 10 μL of 5 mM sodium formate to act as a calibrant over the mass range 50-1500 *m/z*.

Elemental Analysis

Elemental analyses were determined by the department of Health and Human Sciences at London Metropolitan University and conducted by Stephan Boyer. Results are quoted in weight percent of a particular element.

7.1.2 Solvents and Reagents

Solvents for air- and moisture-sensitive reactions were provided by an Innovative Technology Solvent Purification System. Hexane, toluene and benzene were used as collected whereas THF and diethyl ether were first dried by distillation over sodium-benzophenone ketyl. All solvents were stored under argon over molecular sieves activated at 150 °C in vacuo. C_6D_6, d_8-THF and d_8-toluene were purchased from Fluorochem and dried over molten potassium prior to vacuum transfer into a sealed ampoule and storage in the glovebox under argon.

All reagents were either bought from Sigma-Aldrich, Alfa Aesar, Acros or TCI chemicals, except for 3-Picoline-d_7 and *iso*-Quinoline-d_7 which were acquired from CDN isotopes. In general chemicals were used as bought; further purification by drying over CaH_2 and distillation under an inert atmosphere was used for pyridines and nitriles, whilst freeze-pump-thaw degassing was used for HBpin and isocyanates.

7.1.3 General Experimental Techniques

The following compounds were prepared according to literature proceedures:

- β-diketiminate ligand [(Dipp)NC(Me)CHC(CMe)NH(Dipp)][261]
- **Ib -** [HC{(Me)CN(Dipp)}$_2$Mg*n*Bu][262]
- **XXVIIa,c,d** and **XXVIII** – Magnesium dihydropyridide complexes[124]

Experimental work described in this report involved the use and isolation of air-sensitive and hygroscopic magnesium complexes. As a result all synthetic work involving these complexes was carried out under a dry inert gas atmosphere (Ar) using a vacuum line and/or glovebox. Generally, standard inert-atmosphere Schlenk techniques were employed. Glassware, Youngs NMR tubes, Celite and molecular sieves were dried for 24 hours in an oven at 150 °C prior to use.

Catalytic NMR experiments

The relevant amounts of dry substrates, catalyst and deuterated solevent were directly added to a Youngs tap NMR tube under inert atmosphere. All liquids were measured with Eppendorf pipettes. A homogenous solution was obtained by repeatedly turning the tube upside down.

Kinetic Studies

In a glovebox a stock solution of the precatalyst was made to the relevant concentration, 0.5 mL of the catalyst solution was transferred to a Youngs tap NMR tube followed by addition of the relevant quantity of HBpin, followed by the chosen substrate. The tube was sealed, removed from the glovebox, immediately frozen with liquid nitrogen and thawed just prior to loading

into the NMR spectrometer which had been preheated to a chosen temperature (if required). ^{1}H NMR spectra were recorded at regular intervals. Reaction kinetics were monitored using the intensity changes in the substrate resonances over three or more half-lives on the basis of substrate consumption. Data was normalised against the initial substrate concentration $[Substrate]_{t=0}$ so that:

$$Ct = \frac{[Substrate]_{t=0}}{[Substrate]_{t=0} + [Substrate]_{t}}$$

Reaction rates were derived from the plot of Ct vs time (or Ln(Ct), 1/Ct) by using linear trendlines generated by Microsoft Excel software. To obtain Arrhenius and Eyring plots, kinetic analyses were conducted at 4-5 different temperatures, each separated by approximately 5 K.

7.2 Reactions of Dihydropyridides

7.2.1 Reactions of Dihydropyridides with Isocyanates

General Experimental procedure: *Reactions of Dihydropyridides with Isocyanates*

Stoichiometric reactions between 30 mg of the dihydropyridide complex **XXVIIa,c,d** and **XXVIII** and isocyanate were carried out in 0.5 mL of either C_6D_6 or d_8-toluene in a sealed Youngs tap NMR tube. In most cases an instant colour change was observed, although if no reaction had occurred at room temperature the NMR tube was heated to either 60 °C or 80 °C and regularly monitored by ^{1}H NMR spectroscopy until completion. For scale-up experiments 100 – 500 mg of the dihydropyridide complex was again reacted with a stoichiometric amount of isocyanate in 5 mL of toluene and left to stir overnight or heated to the appropriate temperature to effect reaction. The desired product was crystallised from a toluene solution at -30 °C.

1,4-Dihydropyridide reactions, XXVIIa

Synthesis of Compound 1

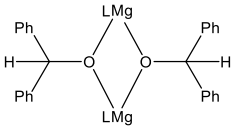

NMR Scale: 30 mg (0.05 mmol) **XXVIIa** with 9 mg (0.05 mmol) of benzophenone. **Large Scale:** 300 mg (0.5 mmol) of **XXVIIa** with 91 mg (0.5 mmol) benzophenone. This was stirred for 1 hr at room temperature in 5 mL of hexanes. The solution quickly lost its orange colour before precipitating the product (**1**) as a colourless microcrystalline solid (290mg, 92%). **LMgOCHPh$_2$** ^{1}H NMR (300 MHz, C_6D_6, 300 K) δ_H (ppm): 7.36 – 7.00 (16H, m, Ar-*H*), 6.15 (1H, s, OC*H*), 5.0 (1H, s, NC(CH$_3$)C*H*), 3.25 (4H, m, C*H*(CH$_3$)$_2$), 1.81 (6H, s, NC(C*H*$_3$)CH), 1.15 (12H, d, J_{HH} = 6 Hz, CH(C*H*$_3$)$_2$), 0.79 (12H, br.s, CH(C*H*$_3$)$_2$). ^{13}C{^{1}H} NMR (75 MHz, C_6D_6, 300 K) δ_C (ppm): 169.4 (N*C*(CH$_3$)CH), 152.7, 145.8, 142.9, 136.5, 128.2, 126.7, 125.7, 124.3, 94.2 (NC(CH$_3$)*C*H), 78.6 (O*C*H), 28.9 (*C*H(CH$_3$)$_2$), 24.7 (CH(*C*H$_3$)$_2$), 24.5 (NC(*C*H$_3$)CH). Elemental Analysis for $C_{42}H_{52}MgN_2O$ (found): C 80.69 (80.86); H 8.38 (8.40); N 4.48 (4.53).

Synthesis of Compound 2

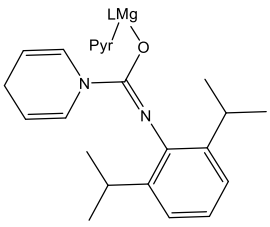

NMR Scale: 30 mg (0.05 mmol) **XXVIIa** complex with 10.7 μL (0.05 mmol) of DippNCO. **Large Scale:** 300 mg (0.5 mmol) of **XXVIIa** with 106.8 μL (0.5 mmol) of DippNCO. This was stirred for 1 hour at room temperature, solvent removed then redissolved in hexanes and crystals of **2** were obtained at -30 °C (130 mg, 33 %). **LMg(Pyr)OC(Pyr(H))NDipp** ^{1}H NMR (300 MHz, C_6D_6, 300 K) δ_H (ppm): 8.43 (2H, m, *o*-Pyr), 7.21 – 6.98 (9H, m, Ar-*H*), 6.89 (2H, m, *p*-Pyr), 6.71 (2H, m, NC*H*CH), 6.56 (2H, m, *m*-

Pyr), 5.02 (1H, s, NC(CH_3)C*H*), 4.42 (2H, m, NCHC*H*), 3.33 (4H, m, C*H*(CH_3)$_2$), 2.76 (2H, m, NC(C*H*(CH_3)$_2$), 2.66 (2H, m, NCHCHCH_2), 1.74 (6H, s, NC(CH_3)$_2$), 1.25-1.16 (30H, m, CH(CH_3)$_2$), 0.93 (6H, d, J_{HH} = 9 Hz, CH(CH_3)$_2$). $^{13}C\{^1H\}$ NMR (75 MHz, C_6D_6, 300 K) δ_C (ppm): 170.2 (N*C*(CH_3)CH), 150.4 (*o*-Pyr), 145.5, 143.0 (*p*-DippL), 142.0, 136.8 (*p*-Pyr), 127.0 (N*C*HCH), 126.1, 124.6 (*m*-DippL), 124.2 (*m*-Pyr), 123.7, 115.2 (O*C*N), 103.0 (NCH*C*H), 95.3 (NC(CH_3)*C*H), 28.8 (NC(*C*H(CH_3)$_2$), 28.6 (*C*H(CH_3)$_2$), 25.0 (CH(*C*H_3)$_2$), 24.7 (CH(*C*H_3)$_2$), 24.5 (NC(*C*H_3)CH), 24.1 (CH(*C*H_3)$_2$), 23.5 (CH(*C*H_3)$_2$), 23.1 (NCHCH*C*H_2). Elemental Analysis for $C_{52}H_{69}MgN_5O$ (found): C 77.54 (77.67); H 8.76 (8.72); N 8.69 (8.80). HRMS (ESI) calcd. for hydrolysed product $[M^+Na^+]^+$ $C_{18}H_{24}N_2NaO$ *m/z* 307.18, found 307.1786.

Synthesis of Compound 3

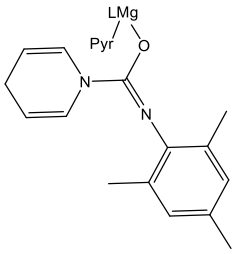

NMR Scale: 30 mg (0.05 mmol) of **XXVIIa**, 8.0 mg (0.05 mmol) of MesNCO. **Large Scale:** 50 mg (0.083 mmol) of **XXVIIa** with 13.4 mg (0.083 mmol) of MesNCO. This was left at room temperature for a few hours before solvent was removed *in vacuo* to yield yellow crystals of compound **3** (41 mg, 67 % yield). **LMg(Pyr)OC(Pyr(H))NMes** ^1H NMR (300 MHz, C_6D_6, 300 K) δ_H (ppm): 8.58 (2H, m, *o*-Pyr), 7.14-6.99 (6H, m, Ar-*H*), 6.92 (1H, m, *p*-Pyr), 6.61 (4H, m, *m*-Mes-*H*, m-Pyr), 6.44 (2H, m, NC*H*CH), 4.96 (1H, s, NC(CH_3)C*H*), 4.26 (2H, m, NCHC*H*), 3.22 (4H, m, C*H*(CH_3)$_2$), 2.54 (2H, m, NCHCHCH_2), 2.11 (6H, s, *o*-CH_3(Mes)), 1.73 (6H, s, NC(CH_3CH), 1.62 (3H, s, *p*-CH_3(Mes)), 1.28 – 0.85 (24H, m, CH(CH_3)$_2$). $^{13}C\{^1H\}$ NMR (75 MHz, C_6D_6, 300 K) δ_C (ppm): 169.2 (N*C*(CH_3)CH), 150.2 (*o*- Pyr),148.3, 146.3, 142.4, 125.2 (N*C*H), 123.9 (*m*-Pyr), 116.2 (O*C*N), 106.4 (NCH*C*H), 94.7 (NC(CH_3)*C*H), 28.8 (*p*-*C*H_3(Mes)), 28.5 (*o*-*C*H_3(Mes)), 24.4 (CH(*C*H_3)$_2$), 24.3 (NC(*C*H_3)CH), 24.2 (CH(*C*H_3)$_2$), 24.0 (CH(*C*H_3)$_2$), 22.6 (NCHCH*C*H_2), 20.8(CH(*C*H_3)$_2$). Elemental Analysis for $C_{49}H_{63}MgN_5O$ (found): C 77.20 (77.05); H 8.33 (8.41); N 9.19 (9.12).

Synthesis of Compound 4

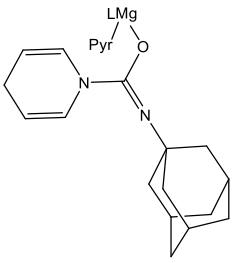

NMR Scale: 30 mg (0.05 mmol) of **XXVIIa** with 8.8 mg (0.05 mmol) of AdNCO. **Large Scale:** 50 mg (0.083 mmol) of **XXVIIa** with 14.7 mg (0.083 mmol) of 1-AdNCO. This was left at room temperature for a few hours before solvent was removed *in vacuo* to yield colourless crystals of **4** (32 mg, 52 % yield). **LMg(Pyr)OC(Pyr(H))NAd** ^1H NMR (300 MHz, C_6D_6, 300 K) δ_H (ppm): 8.53 (2H, s, *o*-Pyr), 7.23 – 7.00 (6H, m, Ar-*H*), 6.66 (1H, m, *p*-Pyr), 6.63 (2H, m, *m*-Pyr), 6.51 (2H, m, NC*H*CH), 4.99 (1H, s, NC(CH_3)C*H*), 4.51 (2H, m, NCHC*H*), 3.72 (1H, m, NC*H*(Ad)), 3.32 (4H, m, C*H*(CH_3)$_2$), 2.63 (2H, m, NCHCHCH_2), 1.71 (6H, s, NC(CH_3)CH), 1.51 – 1.37 (15, m, Ad-*H*), 1.22 (12H, d, J_{HH} = 7.2 Hz, CH(CH_3)$_2$), 1.16 (12H, d, J_{HH} = 6.8 Hz, CH(CH_3)$_2$). $^{13}C\{^1H\}$ NMR (75 MHz, C_6D_6, 300 K)

δC (ppm): 170.0(NC(CH3)CH), 148.9 (o-Pyr),143.2, 129.7, 126.0, 125.4 (NCH), 124.0 (m-Pyr), 104.2 (NCHCH), 94.6 (NC(CH3)CH), 29.0 (NCH(Ad)), 28.7 (CH(CH3)2), 26.2 (Ad-C), 25.0 (NC(CH3)CH), 24.9, 24.7, 24.0, 23.8 (NCHCHCH2), 21.8. Despite repeated attempts, an acceptable elemental analysis could not be obtained for this highly air and moisture sensitive compound. HRMS (ESI) calcd. for hydrolysed product $[M^+]^+$ $C_{16}H_{23}N_2O$ *m/z* 259.37, found 259.1810. $[M^+Na^+]^+$ $C_{16}H_{22}N_2NaO$ *m/z* 281.35, found 281.1629.

Synthesis of Compound 5

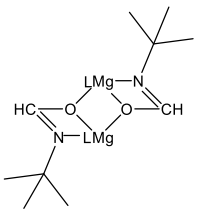

NMR Scale: 30 mg (0.05 mmol) of **XXVIIa** with 5.7 μL (0.05 mmol) of *t*-BuNCO. **Large Scale:** 50 mg (0.083 mmol) of **XXVIIa** with 9.5 μL (0.083 mmol) of *t*-BuNCO, heated at 80 °C overnight. Solvent was removed *in vacuo* to yield yellow crystals of **5** (20 mg, 22 % yield). **LMgOCHN^{t}Bu** ^{1}H NMR (300 MHz, C_6D_6, 300 K) δ_H (ppm): 7.14 – 7.07 (6H, m, Ar-*H*), 7.03 (1H, s, NC*H*O), 4.89 (1H, s, NC(CH$_3$)C*H*), 3.32 (4H, m, C*H*(CH$_3$)$_2$), 1.67 (6H, s, NC(C*H*$_3$)CH), 1.29 (9H, s, C(C*H*$_3$)$_3$), 1.22 (12H, d, J_{HH} = 7.2 Hz, CH(C*H*$_3$)$_2$), 1.16 (12H, d, J_{HH} = 6.8 Hz, CH(C*H*$_3$)$_2$). ^{13}C{^{1}H} NMR (75 MHz, C_6D_6, 300 K) δ_C (ppm): 171.3 (N*C*(CH$_3$)CH), 143.1, 136.8 (*p*-Ar), 129.7 (N*C*HO), 128.9, 126.2 (*m*-Ar), 93.8 (NC(CH$_3$)*C*H),29.0 (*C*H(CH$_3$)$_2$), 24.8 (NC(*C*H$_3$)CH), 23.8 (CH(*C*H$_3$)$_2$), 21.8 (C(*C*H$_3$)$_3$). Elemental Analysis for $C_{44}H_{61}MgN_5O$ (found): C 75.46 (75.34); H 8.78 (8.78); N 10.00 (9.86).

1,4-Dihydro-3-picolide reactions, XXVIIc

Synthesis of Compound 6

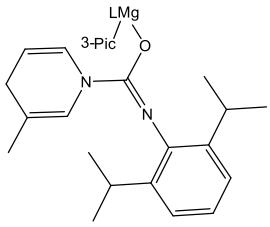

NMR Scale: 30 mg (0.047 mmol) of **XXVIIc** with 10.3 μL (0.047 mmol) of DippNCO. **Large Scale:** 50 mg (0.08 mmol) of **XXVIIc** with 17 μL (0.08 mmol) of DippNCO. This was dissolved in toluene at room temperature. Solvent was removed *in vacuo* to yield a yellow oil of **6** (42 mg, 61 % yield). **LMg(3-Pic)OC(3-Pic(H))NDipp** ^{1}H NMR (300 MHz, C_6D_6, 300 K) δ_H (ppm): 8.03 (1H, *o*-3-Pic), 7.90 (1H, *o*-3-Pic), 7.21 – 7.02 (9H, m, Ar-*H*), 6.98 (1H, s, NC*H*), 6.81 (3H, m, NC*H*, *m*-Dipp*H*(NCO)), 6.72 (1H, d, J_{HH} = 9 Hz, *p*-3-Pic), 6.47 (1H, m, *m*-3-Pic), 4.95 (1H, s, NC(CH$_3$)C*H*), 4.45 (1H, m, NCHC*H*), 3.27 (4H, m, C*H*(CH$_3$)$_2$), 2.67 (2H, m, C*H*(CH$_3$)$_2$), 2.59 (2H, m, NCHCHC*H*$_2$), 1.71 (6H, s, NC(C*H*$_3$)CH), 1.66 (3H, s, 3-(C*H*$_3$)Pyr), 1.42 (3H, s, NCHC(C*H*$_3$)),1.16 (12H, d, J_{HH} = 9 Hz, CH(C*H*$_3$)$_2$), 1.07 (12H, d, J_{HH} = 9 Hz, CH(C*H*$_3$)$_2$), 0.81 (6H, d, J_{HH} = 6 Hz, CH(C*H*$_3$)$_2$(NCO)). ^{13}C{^{1}H} NMR (75 MHz, C_6D_6, 300 K) δ_C (ppm): 169.3 (N*C*(CH$_3$)CH), 150.1 (*o*-3-Pic), 146.8 (*o*-3-Pic), 145.7, 142.6, 141.0, 138.3, 133.8, 126.4, 125.5, 124.0, 123.7, 122.8, 121.8, 115.8 (O*C*N), 100.9 (NCH*C*H), 94.6 (NC(CH$_3$)*C*H), 28.5, 28.4, 28.1, 24.5, 24.4, 24.3, 24.2, 23.8 (NCHCH*C*H$_2$). Elemental Analysis for $C_{54}H_{73}MgN_5O$ (found): C 77.91 (77.71); H 8.84 (8.94);

N 8.41 (8.32). HRMS (ESI) calcd. for hydrolysed product $[M]^+$ $C_{19}H_{26}N_2O$ *m/z* 298.43, found 299.2124.

Synthesis of Compound 7

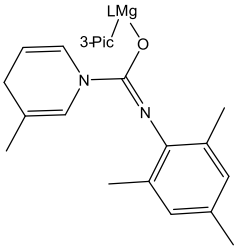

NMR Scale: 30 mg (0.047 mmol) of **XXVIIc** with 7.7 mg (0.047 mmol) of MesNCO. **Large Scale:** 300 mg (0.47 mmol) of **XXVIIc** with 77.0 mg (0.47 mmol) of MesNCO. This was dissolved in toluene at room temperature. Solvent was removed *in vacuo* to yield yellow crystals of **7** (221 mg, 59 % yield). **LMg(3-Pic)OC(3-Pic(H))NMes** ^{1}H NMR (300 MHz, d_8-Tol, 300 K) δ_H (ppm): 8.51 (1H, m, *o*-3-Pic), 8.41 (1H, m, *o*-3-Pic), 7.02 (1H, m, *p*-3-pic), 6.98 (1H, m, NC*H*), 6.92 (1H, s, NC*H*), 6.78 (2H, m, p-Ar*H*), 6.68 (*m*-3-pic), 6.59 (4H, m, *m*-Ar*H*), 6.42 (2H, s, *m*-Mes-*H*), 4.97 (1H, s, NC(CH_3)C*H*), 4.30 (1H, m, NCHC*H*), 3.25 (2H, m, C*H*(CH_3)$_2$), 2.94 (2H, m, C*H*(CH_3)$_2$), 2.42 (2H, m, NCHCHCH_2), 2.08 (6H, s, *o*-CH_3Mes), 1.75 (3H, s, *p*-CH_3Mes), 1.73 (6H, s, NC(CH_3)CH), 1.58 (6H, s, CH_3-3-Pic), 1.17 (12H, d, J_{HH} = 7.23 Hz, CH(CH_3)$_2$), 1.03 (12H, d, J_{HH} = 6.63 Hz, CH(CH_3)$_2$). ^{13}C{^{1}H} NMR (75 MHz, d_8-Tol, 300 K) δ_C (ppm): 169.1 (N*C*(CH_3)CH), 146.2 (*o*-3-Pic), 142.6 (*o*-3-Pic), 136.3, 133.5, 131.6, 125.2, 123.8, 123.3, 115.0 (O*C*N), 102.0 (NCH*C*H), 94.7 (NC(CH_3)*C*H), 28.4 (*C*H(CH_3)$_2$), 24.5 (NC(*C*H_3)CH), 24.3 (CH(*C*H_3)$_2$), 23.1 (CH(*C*H_3)$_2$), 20.8 (*C*H_3-Mes), 20.8 (*C*H_3-Mes), 18.4 (*C*H_3-3-Pic), 17.8 (*C*H_3-3-Pic(H)). Despite repeated attempts, an acceptable elemental analysis could not be obtained for this highly air and moisture sensitive compound. HRMS (ESI) calcd. for hydrolysed product $[M]^+$ $C_{16}H_{20}N_2O$ *m/z* 256.34, found 257.1654; $[M^+Na^+]^+$ $C_{16}H_{20}N_2NaO$ *m/z* 279.34, found 279.1473.

Synthesis of Compound 8

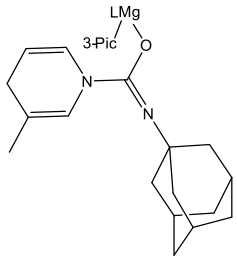

NMR Scale: 30 mg (0.047 mmol) of **XXVIIc** with 8.5 mg (0.047 mmol) of 1-AdNCO. **Large Scale:** 50 mg (0.08 mmol) of **XXVIIc** with 14.1 mg (0.08 mmol) of 1-AdNCO. This was dissolved in toluene at room temperature. Solvent was removed *in vacuo* to yield yellow crystals of **8** (38 mg, 59 % yield). **LMg(3-Pic)OC(3-Pic(H))NAd** ^{1}H NMR (300 MHz, d_8-Tol, 300 K) δ_H (ppm): 8.37 (2H, m, *o*-3-Pic), 7.48 (1H, s, NC*H*), 7.39 (1H, m, NC*H*), 7.23 – 6.98 (6H, m, Ar-*H*), 6.59 (1H, m, *p*-3-Pic), 6.23 (1H, m, *m*-3-Pic), 5.01 (1H, s, NC(CH_3)C*H*), 4.71 (1H, m, NCHC*H*), 3.90 (1H, m, C*H*-Ad), 3.67 (2H, m, C*H*(CH_3)$_2$), 3.08 (2H, m, NCHCHCH_2), 3.04 (2H, m, C*H*(CH_3)$_2$), 1.77 (6H, s, CH_3-3-Pic, CH_3-3-Pic(H)), 1.74 (6H, s, NC(CH_3)CH), 1.44 (6H, d, J_{HH} = 6.65 Hz, CH(CH_3)$_2$), 1.34 (6H, d, J_{HH} = 6.65 Hz, CH(CH_3)$_2$), 1.10 (6H, d, J_{HH} = 7.02 Hz, CH(CH_3)$_2$), 0.68 (6H, d, J_{HH} = 7.02 Hz, CH(CH_3)$_2$). ^{13}C{^{1}H} NMR (75 MHz, d_8-Tol, 300 K) δ_C (ppm): 169.4 (N*C*(CH_3)CH), 146.0 (*o*-3-Pic), 144.9 (*o*-3-Pic), 141.9 (*o*-3-Pic(H)), 135.3, 125.7, 125.0, 123.4, 117.7 (O*C*N), 105.7

(NCH*C*H), 97.1 (NC(CH_3)*C*H), 44.6 (*C*H-Ad), 37.5, 35.7, 30.6 (NCHCH*C*H_2), 28.6 (*C*H(CH_3)$_2$), 28.4 (*C*H(CH_3)$_2$), 25.6 (CH(*C*H_3)$_2$), 24.7 (NC(*C*H_3)CH), 24.5 (CH(*C*H_3)$_2$), 24.2 (CH(*C*H_3)$_2$), 23.4 (CH(*C*H_3)$_2$), 17.8 (*C*H_3-3-Pic), 17.7 (*C*H_3-3-Pic(H)). Elemental Analysis for $C_{52}H_{71}MgN_5O$ (found): C 77.44 (77.32); H 8.87 (8.73); N 8.68 (8.57).

Synthesis of Compound 9

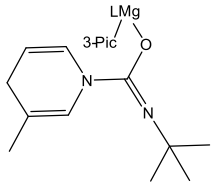

NMR Scale: 30 mg (0.047 mmol) of **XXVIIc** with 5.4 μL (0.047 mmol) of *t*-BuNCO. **Large** S**cale:** 50 mg (0.08 mmol) of **XXVIIc** with 9.0 μL (0.08 mmol) of *t*-BuNCO. This was dissolved in toluene at room temperature. Solvent was removed *in vacuo* to yield yellow crystals of **9** (40 mg, 69 % yield). **LMg(3-Pic)OC(3-Pic(H))N^{t}Bu** ^{1}H NMR (300 MHz, d_8-Tol, 300 K) δ_H (ppm): 8.19 (1H, br.s, NC*H*C(CH_3)CH), 7.55 (1H, br.s, NC*H*CHCH_2), 7.32 (1H, br.s, NC*H*CHCH), 7.20 – 6.98 (7H, m, Ar-*H*), 6.56 (1H, br.s, *p*-*H* (3-Pic)), 6.20 (1H, br.s, *m*-*H* (3-Pic)), 5.01 (1H, s, NC(CH_3)C*H*), 4.71 (1H, m, NCHC*H*CH_2), 3.62 (2H, m, C*H*(CH_3)$_2$), 3.12 (2H, m, C*H*(CH_3)$_2$), 3.07 (2H, br.s, NCHCHC*H*$_2$), 1.76 (6H, s, NC(C*H*$_3$)CH), 1.40 (12H, d, J_{HH} = 9 Hz, CH(C*H*$_3$)$_2$), 1.09 (12H, d, J_{HH} = 9 Hz, CH(C*H*$_3$)$_2$), 0.94 (9H, s, C(C*H*$_3$)$_3$). ^{13}C{^{1}H} NMR (75 MHz, d_8-Tol, 300 K) δ_C (ppm): 169.3 (N*C*(CH_3)CH), 149.5 (*o*-*C* (3-Pic)), 148.6 (*o*-*C* (3-Pic)), 145.8, 144.8, 143.6, 142.7, 141.9 (*o*-*C* (3-Pic(H)), 140.0, 124.3, 123.4, 105.7 (NCH*C*HCH_2), 97.2 (NC(CH_3)*C*H), 50.0 (*C*(CH_3)$_3$), 31.5 (NCHCH*C*H_2), 28.6 (*C*H(CH_3)$_2$), 28.4 (*C*H(CH_3)$_2$), 25.2, 24.6, 24.2, 23.4, 21.4 (C(*C*H_3)$_3$), 17.6 (*C*H_3 (3-Pic(H)). Despite repeated attempts, an acceptable elemental analysis could not be obtained for this highly air and moisture sensitive compound.

1,4-dihydro-3,5-lutidide reactions, XXVIId

Synthesis of Compound 10

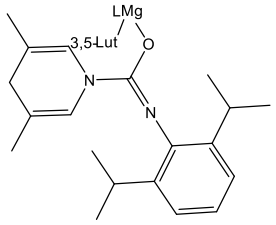

NMR Scale: 20 mg (0.03 mmol) of **XXVIId** with 6.4 μL (0.03 mmol) of DippNCO. **Large Scale:** 50 mg (0.076 mmol) of **XXVIId** with 16.4 μL (0.076 mmol) of DippNCO. This was dissolved in toluene at room temperature. Solvent was removed *in vacuo* to yield yellow crystals of **10** (40 mg, 63 % yield). **LMg(3,5Lut)OC(3,5Lut(H))NDipp** ^{1}H NMR (300 MHz, d_8-Tol, 300 K) δ_H (ppm): 7.87 (2H, s, *o*-*H* (3,5-Lut)), 7.17 – 7.07 (12H, m, Ar-*H*), 6.98 (1H, s, *p*-*H* (3,5-Lut)), 6.61 (2H, s, *o*-*H* (3,5-Lut(H)), 4.96 (1H, s, NC(CH_3)C*H*), 3.52 (2H, s, C*H*$_2$), 3.30 (4H, m, C*H*(CH_3)$_2$), 3.13 (2H, m, C*H*(CH_3)$_2$), 1.73 (12H, s, *m*-C*H*$_3$ (3,5-Lut and 3,5-Lut(H)), 1.71 (6H, s, NC(C*H*$_3$)CH), 1.24 (12H, d, J_{HH} = 6 Hz, CH(C*H*$_3$)$_2$), 1.03 (12H, d, J_{HH} = 6 Hz, CH(C*H*$_3$)$_2$), 0.78 (12H, d, J_{HH} = 6 Hz, CH(C*H*$_3$)$_2$). ^{13}C{^{1}H} NMR (75 MHz, d_8-Tol, 300 K) δ_C (ppm): 169.3 (N*C*(CH_3)CH), 158.4 (*o*-*C* (3,5-Lut), 147.1 (*o*-*C* (3,5-Lut(H)), 145.7, 141.7, 140.7, 133.4, 125.5, 123.5, 121.3, 120.8. 94.5 (NC(CH_3)*C*H), 61.2 (*C*H$_2$), 32.0 (N*C*H(CH_3)$_2$),

28.5 (*C*H(CH_3)$_2$), 28.1 (*C*H(CH_3)$_2$), 24.5 (CH(*C*H_3)$_2$), 24.3, (CH(*C*H_3)$_2$), 24.2 (NC(*C*H_3)CH), 23.5 (CH(*C*H_3)$_2$), 23.1 (*m*-*C*H_3 (3,5-Lut)), 17.9 (*m*-*C*H_3 (3,5-Lut(H))). Despite repeated attempts, an acceptable elemental analysis could not be obtained for this highly air and moisture sensitive compound. HRMS (ESI) calcd. for hydrolysed product $[M^+Na^+]^+$ $C_{20}H_{28}N_2NaO$ *m/z* 335.45, found 335.2099.

Synthesis of Compound 11

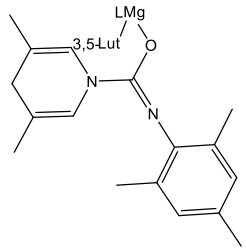

NMR Scale: 30 mg (0.046 mmol) of **XXVIId** with 7.4 mg (0.046 mmol) of MesNCO. **Large Scale:** 50 mg (0.076 mmol) of **XXVIId** with 12.3 mg (0.076 mmol) of MesNCO. This was dissolved in toluene at room temperature. Solvent was removed *in vacuo* to yield yellow crystals of **11** (43 mg, 66 % yield). **LMg(3,5Lut)OC(3,5Lut(H))NMes** ^{1}H NMR (300 MHz, d_8-Tol, 300 K) δ_H (ppm): 8.31 (2H, s, *o*-*H* (3,5-Lut)), 7.18 – 7.06 (6H, m, Ar-*H*), 7.02 (1H, s, *p*-*H* (3,5Lut)), 6.98 (2H, s, *m*-*H* (Mes)), 6.57 (2H, s, *o*-*H* (3,5-Lut(H))), 4.97 (1H, s, NC(CH_3)C*H*), 3.30 (2H, m, C*H*(CH_3)$_2$), 3.28 (2H, s, CH_2), 2.94 (2H, m, C*H*(CH_3)$_2$), 1.79 (12H, s, CH_3 (3,5-Lut), (3,5-Lut(H))), 1.74 (6H, s, NC(CH_3)CH), 1.55 (3H, s, *p*-CH_3 (Mes)), 1.53 (6H, s, *o*-CH_3 (Mes)), 1.17 (12H, d, J_{HH} = 9 Hz, CH(CH_3)$_2$), 1.05 (12H, d, J_{HH}= 9 Hz,CH(CH_3)$_2$). ^{13}C{^{1}H} NMR (75 MHz, d_8-Tol, 300 K) δ_C (ppm): 169.0 (N*C*(CH_3)CH), 147.7, 146.1, 142.8, 134.9, 133.1, 131.8, 125.2, 123.9, 123.3, 94.6 (NC(CH_3)*C*H), 33.7 (*C*H_2), 28.4 (*C*H(CH_3)$_2$), 27.2, 26.7, 24.7, 24.5, 24.2, 23.7, 23.1, 19.6, 18.4 (*C*H_3 3,5-Lut), 17.8 (*C*H_3 3,5-Lut(H)). Elemental Analysis for $C_{53}H_{71}MgN_5O$ (found): C 77.78 (77.63); H 8.74 (8.85); N 8.56 (8.43). HRMS (ESI) calcd. for hydrolysed product $[M]^+$ $C_{17}H_{22}N_2O$ *m/z* 270.38, found 271.1810; $[M^+Na^+]^+$ $C_{17}H_{22}N_2NaO$ *m/z* 293.37, found 293.1630.

Synthesis of Compound 12

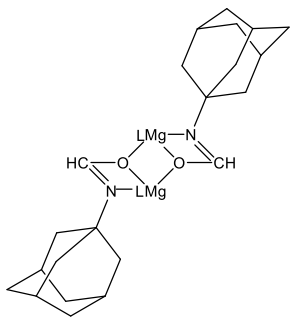

2 products identified in the NMR spectra, **12a** and **12b**, these were observed in a 70:30 ratio, respectively. **NMR Scale:** 20 mg (0.03 mmol) of **XXVIId** with 5.3 mg (0.03 mmol) of 1-AdNCO. **Large Scale:** 330 mg (0.5 mmol) of **XXVIId** with 88.6 mg (0.5 mmol) of 1-AdNCO was dissolved in toluene at room temperature. Solvent was removed *in vacuo* to yield yellow crystals of **12a** (216 mg, 70 % yield). **12a.LMgOCHNAd** ^{1}H NMR (300 MHz, d_8-Tol, 300 K) δ_H (ppm): 7.04 - 6.74 (12H, m, Ar-*H*), 6.19 (2H, s, NC*H*O), 4.84 (2H, s, NC(CH_3)C*H*), 3.29 (2H, m, C*H*(CH_3)$_2$), 3.10 (3H, m, CH(CH_3)$_2$), 2.92 (3H, m, CH(CH_3)$_2$), 2.41 (12H, d, J_{HH} = 6 Hz, CCH_2CHCH_2), 2.21 (6H, m, CCH_2C*H*CH_2), 1.96 (6H, s, NC(CH_3), 1.65 (6H, s, NC(CH_3)), 1.43 (12H, d, J_{HH} = 6 Hz, CCH_2CHCH_2), 1.25 (18H, d, J_{HH} = 9Hz, CH(CH_3)$_2$), 1.19 (18H, d, J_{HH} = 6 Hz, CH(CH_3)$_2$), 0.89 (12H, d, J_{HH} = 9 Hz, CH(CH_3)$_2$). ^{13}C{^{1}H} NMR (75 MHz, d_8-Tol, 300 K)

δ_C (ppm): 169.70 (N*C*HO) 148.61, 146.69, 146.49, 146.23, 145.26, 144.90, 142.57, 142.36, 140.93, 135.13, 125.92, 125.73, 125.42, 123.99, 123.73, 122.97, 105.42 (NC(CH_3)*C*H), 96.45, 51.32 (N*C*CH_2), 46.40 (NC*C*H_2), 38.46 (NCCH_2*C*H), 30.98 (NCH_2CH*C*H_2), 29.11, 28.77, 28.54, 28.32, 25.77, 25.63, 25.33, 25.21, 25.10, 24.96, 24.69, 24.58, 24.40, 23.74, 21.70 (CH(*C*H_3)$_2$), 21.05 (CH(*C*H_3)$_2$), 18.05 (CH(*C*H_3)$_2$). Elemental Analysis for $C_{40}H_{57}MgN_3O$ (found): C 77.46 (77.52); H 9.26 (9.18); N 6.78 (6.85).

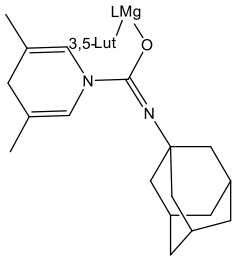

12b. LMg(3,5Lut)OC(3,5Lut(H))NAd. Due to overlapping resonances, only key peaks associated with insertion product are listed, no other characterisation was carried out as always crystallised with the major product **12a**. ^{1}H NMR (300 MHz, d_8-Tol, 300 K) δ_H (ppm): 6.39 (2H, s, NC*H*C(CH_3)CH_2), 5.02 (1H, NC(CH_3)C*H*), 3.98 (2H, m, NCHC(CH_3)CH_2).

Synthesis of Compound 13

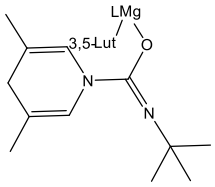

NMR Scale: 20 mg (0.03 mmol) of **XXVIId** with 3.4 μL (0.03 mmol) of *t*-BuNCO. **Large** S**cale:** 330 mg (0.5 mmol) of **XXVIId** with 52.4 μL (0.5 mmol) of *t*-BuNCO. This was dissolved in toluene at room temperature. Solvent was removed *in vacuo* to yield yellow crystals of **13** (210 mg, 55 % yield). **LMg(3,5Lut)OC(3,5Lut(H))N^{t}Bu** ^{1}H NMR (300 MHz, d_8-Tol, 300 K) δ_H (ppm): 7.40 (2H, s, *o-H* (3,5-Lut)), 7.23 - 6.98 (6H, m, Ar-*H*), 6.85 (2H, s, *o-H* (3,5-Lut(H))), 6.49 (1H, s, *p-H* (3,5-Lut)), 5.05 (1H, s, NC(CH_3)C*H*), 3.63 (2H, m, C*H*(CH_3)$_2$), 3.13 (2H, m, C*H*(CH_3)$_2$), 2.92 (2H, s, NCHC(CH_3)CH_2), 1.83 (6H, s, NCHC(CH_3)CH), 1.81 (6H, s, NCHC(CH_3)CH_2), 1.57 (6H, s, NC(CH_3)), 1.38 (6H, d, J_{HH} = 6 Hz, CH(CH_3)$_2$), 1.28 (6H, d, J_{HH} = 6 Hz, CH(CH_3)$_2$), 1.11 (6H, d, J_{HH} = 6 Hz, CH(CH_3)$_2$), 0.93 (9H, s, C(CH_3)$_3$), 0.72 (6H, d, J_{HH} = 9 Hz, CH(CH_3)$_2$). ^{13}C{^{1}H} NMR (75 MHz, d_8-Tol, 300 K) δ_C (ppm): 169.15 (*o*-Pyr), 146.55, 145.88, 141.95, 140.46, 137.44, 134.36, 123.29, 104.86 (NC(CH_3)*C*H), 95.62 (NCH*C*(CH_3)CH_2), 31.08 (NCHC(CH_3)*C*H_2), 28.69 (*C*H(CH_3)$_2$), 28.44 (*C*H(CH_3)$_2$), 24.99 (CH(*C*H_3)$_2$), 24.74 (CH(*C*H_3)$_2$), 24.14 (NCHC(*C*H_3)CH_2), 17.52 (C(*C*H_3)$_3$). Elemental Analysis for $C_{48}H_{69}MgN_5O$ (found): C 76.22 (76.05); H 9.19 (9.11); N 9.26 (9.16). HRMS (ESI) calcd. for hydrolysed product $[M^+Na^+]^+$ $C_{12}H_{20}N_2NaO$ *m/z* 231.15, found 231.1473.

1,2-dihydro-*iso*-quinolide reactions, XXVIII

Synthesis of Compound 14

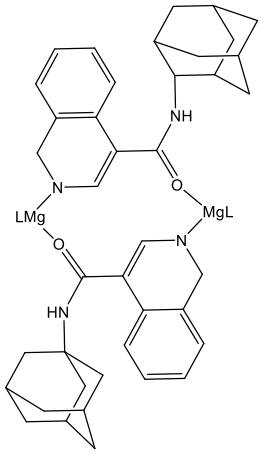

NMR Scale: 30 mg (0.043 mmol) of **XXVIII** with 7.5 mg (0.043 mmol) of 1-AdNCO**. Large Scale:** 100 mg (0.14 mmol) of **XXVIII** with 24.8 mg (0.14 mmol) of 1-AdNCO. This was dissolved in toluene at room temperature. Solvent was removed *in vacuo* to yield yellow crystals of **14** (35 mg, 33 % yield). **LMgOC(NHAd)iQuin(H)** ^{1}H NMR (300 MHz, C_6D_6, 300 K) δ_H (ppm): 7.43-6.78 (20H, m, Ar), 6.63 (2H, s, NC*H*), 4.60 (2H, s, NC(CH$_3$)C*H*), 4.14 (2H, s, N*H*), 3.54 (4H, s, NCH_2), 3.29 (4H, m, C*H*(CH$_3$)$_2$), 2.94 (4H, m, C*H*(CH$_3$)$_2$), 1.94 (12H, d, J_{HH} = 9 Hz, CH_2CH), 1.56 (12H, s, NC(CH_3)), 1.35-1.24 (18H, m, CH$_2$C*H*CH_2), 1.21 (12H, d, J_{HH} = 6 Hz, CH(CH_3)$_2$), 1.14 (12H, d, J_{HH} = 6 Hz, CH(CH_3)$_2$), 0.90 (12H, d, J_{HH} = 6 Hz, CH(CH_3)$_2$), 0.86 (12H, d, J_{HH} = 6 Hz, CH(CH_3)$_2$). ^{13}C NMR (75.5 MHz, C_6D_6, 300 K) δ_c (ppm): 159.94, 142.70, 125.81, 123.50, 120.21, 97.83 (N(CH$_3$)C*H*), 43.17 (N*C*O), 32.03, 30.07 (*C*H(CH$_3$)$_2$), 28.63 (*C*H(CH$_3$)$_2$), 24.48 (CH(CH_3)$_2$), 23.70 (CH(CH_3)$_2$), 23.36 (CH(CH_3)$_2$), 23.10 (CH(CH_3)$_2$). Elemental Analysis for $C_{98}H_{128}MgN_8O_2$ (found): C 78.54 (78.32); H 8.61 (8.50); N 7.48 (7.25). HRMS (ESI) calcd. for hydrolysed product $[M^+H^+]^+$ $C_{20}H_{25}N_2O$ *m/z* 308.42, found 309.1967.

Synthesis of Compound 15

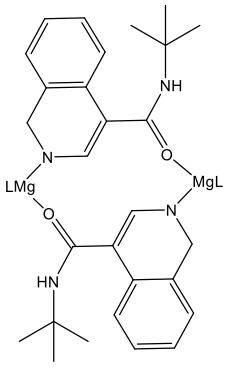

NMR Scale: 30 mg (0.043 mmol) of **XXVIII** with 4.9 μL (0.043 mmol) of *t*-BuNCO. **Large Scale:** 100 mg (0.14 mmol) of **XXVIII** with 16.0 μL (0.14 mmol) of *t*-BuNCO. This was dissolved in toluene at room temperature. Solvent was removed *in vacuo* to yield yellow crystals of **15** (40 mg, 43 % yield). **LMgOC(NH^{t}Bu)iQuin(H)** ^{1}H NMR (300 MHz, d_8-Tol, 300 K) δ_H (ppm): 7.30-6.98 (20H, m, Ar), 5.86 (2H, s, NC*H*), 4.94 (2H, s, NC(CH$_3$)C*H*), 4.12 (4H, s, NCH_2), 3.56 (2H, m, C*H*(CH$_3$)$_2$), 3.35 (2H, m, C*H*(CH$_3$)$_2$), 3.26 (2H, m, C*H*(CH$_3$)$_2$), 3.11 (2H, m, C*H*(CH$_3$)$_2$), 1.82 (6H, d, J_{HH} = 9 Hz, CH(CH_3)$_2$), 1.68 (12H, s, NC(CH_3)), 1.32 (6H, d, J_{HH} = 6 Hz, CH(CH_3)$_2$), 1.30 (18H, s, C(CH_3)$_3$), 1.26 (6H, d, J_{HH} = 6 Hz, CH(CH_3)$_2$), 1.21 (6H, d, J_{HH} = 6 Hz, CH(CH_3)$_2$), 0.90 (6H, d, J_{HH} = 6 Hz, CH(CH_3)$_2$), 0.88 (6H, d, J_{HH} = 6 Hz, CH(CH_3)$_2$), 0.86 (6H, d, J_{HH} = 6 Hz, CH(CH_3)$_2$), 0.53 (6H, d, J_{HH} = 6 Hz, CH(CH_3)$_2$). ^{13}C{^{1}H} NMR (75 MHz, d_8-Tol, 300 K) δ_C (ppm): 152.98, 146.37, 143.67, 143.39, 142.35, 135.98, 129.98, 126.96, 126.50, 123.65, 120.27, 95.75 (NC(CH$_3$)*C*H), 50.54, 32.03 (*C*H(CH$_3$)$_2$), 29.70 (*C*H(CH$_3$)$_2$), 28.18 (*C*H(CH$_3$)$_2$), 27.72 (CH(*C*H$_3$)$_2$), 25.12 (CH(*C*H$_3$)$_2$), 24.73 (CH(*C*H$_3$)$_2$), 24.47 (CH(*C*H$_3$)$_2$), 24.00 (CH(*C*H$_3$)$_2$), 23.77 (CH(*C*H$_3$)$_2$), 23.35 (CH(*C*H$_3$)$_2$), 23.09 (C(*C*H$_3$)$_3$), 14.32 (CH(*C*H$_3$)$_2$).

Elemental Analysis for $C_{86}H_{116}Mg_2N_8O_2$ (found): C 76.94 (76.80); H 8.71 (8.63); N 8.35 (8.20). HRMS (ESI) calcd. for hydrolysed product $[M^+Na^+]^+$ $C_{14}H_{18}N_2NaO$ *m/z* 252.15, found 253.1317.

Synthesis of Compound 16

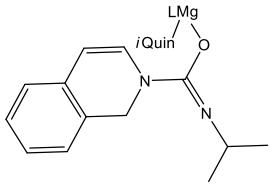

NMR Scale: 30 mg (0.043 mmol) of **XXVIII** with 4.2 μL (0.043 mmol) of *i*-PrNCO. **Large** S**cale:** 100 mg (0.14 mmol) of **XXVIII** with 13.7 μL (0.14 mmol) of *i*-PrNCO. This was dissolved in toluene at room temperature. Solvent was removed *in vacuo* to yield yellow crystals of **16** (34 mg, 31 % yield). **LMg(iQuin)OC(iQuin(H))N^{i}Pr** ^{1}H NMR (300 MHz, d_8-Tol, 300 K) δ_H (ppm): 9.15 (1H, s, *o*-H iQuin), 8.43 (1H, s, *o-H* iQuin), 7.22 – 6.82 (15H, m, Ar-*H*), 6.33 (1H, d, J_{HH} = 6 Hz, NC*H*), 5.58 (1H, d, J_{HH} = 6 Hz, NCHC*H*), 5.37 (2H, s, NCH_2), 5.03 (1H, s, NC(CH_3)C*H*), 3.59 (2H, m, C*H*(CH_3)$_2$), 3.21 (1H, m, C*H*(CH_3)$_2$), 2.84 (2H, m, C*H*(CH_3)$_2$), 1.78 (6H, s, NC(CH_3)$_2$), 1.51 (6H, d, J_{HH} = 9 Hz, CH(CH_3)$_2$), 1.27 (6H, d, J_{HH} = 6 Hz, CH(CH_3)$_2$), 1.09 (6H, d, J_{HH} = 6 Hz, NCH(CH_3)$_2$), 1.00 (6H, d, J_{HH} = 6 Hz, CH(CH_3)$_2$), 0.14 (6H, d, J_{HH} = 6 Hz, CH(CH_3)$_2$). ^{13}C{^{1}H} NMR (75 MHz, d_8-Tol, 300 K) δ_C (ppm): 170.3 (N*C*(CH_3)CH), 152.3 (*o*-*C*H iQuin), 150.3 (N*C*H), 145.3, 143.3, 139.7 (o-*C*H iQuin), 136.8, 135.2, 131.5, 130.7, 127.4, 126.7, 126.2, 125.1, 124.3, 123.2, 95.7 (NCH*C*H), 94.7 (NC(CH_3)*C*H), 48.20 (N*C*H_2), 46.4 (N*C*H(CH_3)$_2$), 29.4 (*C*H(CH_3)$_2$), 28.5 (*C*H(CH_3)$_2$), 26.9 (NCH(*C*H_3)$_2$)), 25.2 (CH(*C*H_3)$_2$), 24.9 (CH(*C*H_3)$_2$), 24.6 (NC(CH_3)CH), 24.5 (CH(*C*H_3)$_2$), 24.4 (CH(*C*H_3)$_2$). Despite repeated attempts, an acceptable elemental analysis could not be obtained for this highly air and moisture sensitive compound.

Synthesis of Compound 17

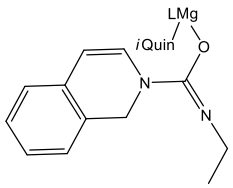

NMR Scale: 30 mg (0.043 mmol) of **XXVIII** with 3.4 μL (0.043 mmol) of EtNCO. **Large** S**cale:** 100 mg (0.14 mmol) of **XXVIII** with 11.1 μL (0.14 mmol) of EtNCO. This was dissolved in toluene at room temperature. Solvent was removed *in vacuo* to yield yellow crystals of **17** (40 mg, 37 % yield). **LMg(iQuin)OC(iQuin(H))NEt** ^{1}H NMR (300 MHz, d_8-Tol, 300 K) δ_H (ppm): 9.53 (1H, s, *o-H* iQuin), 8.78 (1H, s, *o-H* iQuin), 7.39 – 6.82 (15H, m, Ar-*H*), 6.63 (1H, d, J_{HH} = 6 Hz, NC*H*), 5.65 (1H, d, J_{HH} = 9 Hz, 5.18 (1H, s, NC(CH_3)C*H*), 4.94 (2H, s, NCH_2), 3.36 (3H, m, C*H*(CH_3)$_2$), 2.86 (1H, m, C*H*(CH_3)$_2$), 2.26 (2H, q, J_{HH} = 9 Hz, NCH_2CH$_3$), 1.90 (6H, s, NC(CH_3)CH), 1.24 (12H, d, J_{HH} = 6 Hz, CH(CH_3)$_2$), 1.04 (12H, d, J_{HH} = 6 Hz, CH(CH_3)$_2$), 0.76 (3H, t, J_{HH} = 6 Hz, NCH$_2$CH_3). ^{13}C{^{1}H} NMR (75 MHz, d_8-Tol, 300 K) δ_C (ppm): 168.7 (N*C*(CH_3)CH), 154.1 (*o*-*C*H iQuin), 148.6 (*o*-*C*H iQuin), 143.1, 142.9, 136.8, 133.4, 132.7 (N*C*H), 131.7, 129.0, 126.5, 126.2, 125.2, 124.3, 124.0, 121.7, 106.3 (NCH*C*H), 94.8 (NC(CH_3)*C*H), 53.0 (N*C*H_2), 42.0 (N*C*H_2CH$_3$), 29.1 (*C*H(CH_3)$_2$), 28.6 (*C*H(CH_3)$_2$), 25.5

(NC(CH_3)CH), 25.0 (CH(CH_3)$_2$), 24.9 (CH(CH_3)$_2$), 24.8 (CH(CH_3)$_2$), 24.4 (CH(CH_3)$_2$), 15.4 (NCH_2CH_3). Despite repeated attempts, an acceptable elemental analysis could not be obtained for this highly air and moisture sensitive compound.

Synthesis of Compound 18

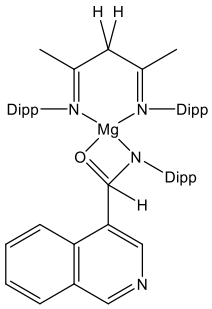

NMR Scale: 30 mg (0.043 mmol) of **XXVIII** with 9.2 μL (0.043 mmol) of DippNCO. **Large Scale:** 100 mg (0.14 mmol) of **XXVIII** with 30.5 μL (0.14 mmol) of DippNCO. This was dissolved in toluene at room temperature. Solvent was removed *in vacuo* to yield yellow crystals of **18** (48 mg, 43 % yield). **(H)LMgOCH(iQuin)NDipp** . ^{1}H NMR (300 MHz, d_8-Tol, 300 K) δ_H (ppm): 8.75 (1H, s, *o*-C*H*), 7.39 (1H, s, *o*-C*H*), 7.26 – 6.86 (13H, m, Ar-*H*), 3.92 (1H, s, NC*H*O), 3.58 (2H, m, C*H*(CH$_3$)$_2$), 3.49 (2H, m, C*H*(CH$_3$)$_2$), 3.28 (2H, s, NC(CH$_3$)C*H*$_2$), 2.94 (2H, m, C*H*(CH$_3$)$_2$), 1.55 (6H, s, NC(C*H*$_3$)CH$_2$), 1.43 (6H, d, J_{HH} = 6 Hz, CH(C*H*$_3$)$_2$), 1.25 (12H, d, J_{HH} = 6 Hz, CH(C*H*$_3$)$_2$), 1.16 (12H, d, J_{HH} = 6 Hz, CH(C*H*$_3$)$_2$), 0.80 (6H, d, J_{HH} = 6 Hz, CH(C*H*$_3$)$_2$). ^{13}C{^{1}H} NMR (75 MHz, d_8-Tol, 300 K) δ_C (ppm): 169.1 (N*C*(CH$_3$)CH$_2$), 145.1, 143.8 (*o*-*C*H), 143.3, 141.7, 136.3, 133.6, 131.9, 129.7, 126.4, 124.3, 124.2, 124.0, 123.6, 123.3, 122.2, 63.5 (NC(CH$_3$)*C*H$_2$), 59.0 (N*C*HO), 28.8 (N*C*H(CH$_3$)$_2$), 28.3 (*C*H(CH$_3$)$_2$), 28.2 (*C*H(CH$_3$)$_2$), 27.1 (CH(*C*H$_3$)$_2$), 25.4 (CH(*C*H$_3$)$_2$), 24.7 (NC(*C*H$_3$)CH$_2$), 23.1 (CH(*C*H$_3$)$_2$), 22.1 (CH(*C*H$_3$)$_2$). Despite repeated attempts, an acceptable elemental analysis could not be obtained for this highly air and moisture sensitive compound. HRMS (ESI) calcd. for hydrolysed product [M$^+$H$^+$]$^+$ $C_{22}H_{26}N_2O$ *m/z* 334.45, found 335.2123.

Synthesis of Compound 19

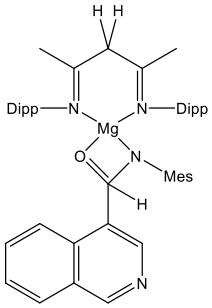

NMR Scale: 30 mg (0.043 mmol) of **XXVIII** with 6.9 mg (0.043 mmol) of MesNCO. **Large Scale:** 100 mg (0.14 mmol) of **XXVIII** with 22.6 mg (0.14 mmol) of MesNCO. This was dissolved in toluene at room temperature. Solvent was removed *in vacuo* to yield yellow crystals of **19** (53 mg, 52 % yield). **(H)LMgOCH(iQuin)NMes** ^{1}H NMR (300 MHz, d_8-Tol, 300 K) δ_H (ppm): 8.08 (1H, s, *o*-*H*), 7.39 (1H, s, *o*-*H*), 7.25 – 6.98 (10H, m, Ar-*H*), 6.78 (2H, s, *m*-*H* Mes), 3.70 (1H, s, NC*H*O), 3.28 (2H, s, NC(CH$_3$)C*H*$_2$), 3.27 (2H, m, C*H*(CH$_3$)$_2$), 2.94 (2H, m, C*H*(CH$_3$)$_2$), 2.05 (6H, s, *o*-C*H*$_3$ Mes), 1.85 (3H, s, *p*-C*H*$_3$ Mes), 1.55 (6H, s, NC(C*H*$_3$)CH$_2$), 1.19 (12H, d, J_{HH} = 6 Hz, CH(C*H*$_3$)$_2$), 1.17 (12H, d, J_{HH} = 6 Hz, CH(C*H*$_3$)$_2$). ^{13}C{^{1}H} NMR (75 MHz, d_8-Tol, 300 K) δ_C (ppm): 167.5 (N*C*(CH$_3$)CH$_2$), 153.5 (*o*- *C*H), 151.1 (*o*-*C*H), 143.1, 136.3, 134.8, 132.5, 126.4, 124.0, 123.5,123.2, 53.0 (N*C*HO), 46.9 (N(CH$_3$)*C*H$_2$), 29.1 (*C*H(CH$_3$)$_2$), 28.3 (*C*H(CH$_3$)$_2$), 24.5 (NC(*C*H$_3$)CH$_2$), 23.7 (CH(*C*H$_3$)$_2$), 23.1 (CH(*C*H$_3$)$_2$), 20.7 (*o*-*C*H$_3$ Mes), 20.5 (*p*-*C*H$_3$ Mes).

Elemental Analysis for $C_{48}H_{60}MgN_4O$ (found): C 78.62 (78.88); H 8.25 (8.13); N 7.64 (7.52). HRMS (ESI) calcd. for hydrolysed product $[M^+H^+]^+$ $C_{19}H_{20}N_2O$ *m/z* 292.40, found 293.1654, $[M^+Na^+]^+$ $C_{19}H_{20}N_2ONa$ *m/z* 315.36, found 315.1473.

7.2.2 Reactions of Dihydropyridides with Carbodiimides

General Experimental procedure: *Reactions of Dihydropyridides with Carbodiimides*

Stoichiometric reactions between 30 mg of the dihydropyridide complex (**XXVIIa,c,d** and **XXVIII**) and carbodiimide were reacted together in 0.5 mL of either C_6D_6 or d_8-toluene in a sealed Youngs tap NMR tube. In most cases an instant colour change was observed, although if no reaction had occurred at room temperature the NMR tube was heated to either 60 °C or 80 °C and regularly monitored by ^{1}H NMR spectroscopy until completion. For scale-up experiments 50 – 100 mg of the di-hydropyridine complex was again reacted with a stoichiometric amount of carbodiimide in 5 mL of Toluene and left to stir overnight or heated to the appropriate temperature to effect the reaction. The desired product was crystallised from a toluene solution at -30 °C.

1,4-Dihydropyridide reactions, XXVIIa

Synthesis of Compound 20

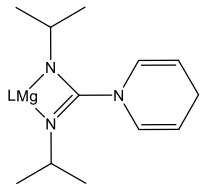

NMR Scale: 30 mg (0.05 mmol) **XXVIIa** with 5.5 µL (0.05 mmol) of *i*PrNCN*i*Pr. **Large Scale:** 50 mg (0.083 mmol) of **XXVIIa** with 12.8 µL (0.083 mmol) of *i*PrNCN*i*Pr, this was dissolved in toluene and left to stir at room temperature overnight. Solvent was removed *in vacuo* to yield yellow crystals of **20** (35 mg, 67% yield). **LMgN(iPr)C(Pyr(H))N(iPr)** ^{1}H NMR (300 MHz, d_8-Tol, 300 K) δ_H (ppm): 7.11 – 6.94 (6H, m, Ar-*H*), 5.94 (2H, dt, J_{HH} = 9 Hz, NC*H*), 4.83 (1H, s, NC(CH$_3$)C*H*), 4.38 (2H, dt, ^3J = 9 Hz, ^4J = 3Hz, NCHC*H*), 3.48 (2H, sept, J_{HH} = 6Hz, NC*H*(CH$_3$)$_2$), 3.41 (4H, sept, J_{HH} = 6 Hz, C*H*(CH$_3$)$_2$), 2.89 (2H, m, NCHCHC*H$_2$*), 1.64 (6H, s, NC(C*H*$_3$)), 1.27 (12H, d, J_{HH} = 6 Hz, CH(C*H*$_3$)$_2$), 1.24 (12H, d, J_{HH} = 6 Hz, CH(C*H*$_3$)$_2$), 0.88 (6H, d, J_{HH} = 6Hz, NCH(C*H*$_3$)$_2$). ^{13}C{^{1}H} NMR (75.5 MHz, d_8-Tol, 300 K) δ_C (ppm): 169.6 (N*C*(CH$_3$), 164.3 (*C*N$_3$), 145.6 (*ipso*-Ar), 142.6 (*o*-Ar), 129.3 (*p*-Ar), 128.1 (N*C*H), 123.8 (*m*-Ar), 99.0 (NCH*C*H), 94.9 (NC(CH$_3$)*C*H), 45.0 (N*C*H(CH$_3$)$_2$), 28.26 (*C*H(CH$_3$)$_2$), 26.0 (NCH(*C*H$_3$)$_2$), 25.4 (CH(*C*H$_3$)$_2$), 24.5 (CH(*C*H$_3$)$_2$), 24.3 (NC(*C*H$_3$)), 22.9 (NCHCH*C*H$_2$). HRMS (ESI) calcd. for hydrolysed product $[M^+]$ $C_{12}H_{21}N_3$ *m/z* 207.32, found 208.1862.

Synthesis of Compound 21

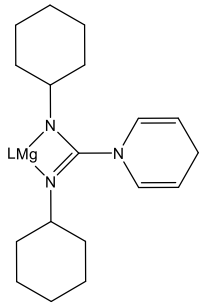

NMR Scale: 30 mg (0.05 mmol) **XXVIIa** with 6.8 mg (0.05 mmol) of CyNCNCy. **Large Scale:** 50 mg (0.083 mmol) of **XXVIIa** with 17.2 mg (0.083 mmol) of CyNCNCy, this was dissolved in toluene and left to stir at room temperature overnight. Solvent was removed *in vacuo* to yield yellow crystals of **21** (30 mg, 52% yield). **LMgN(Cy)C(Pyr(H))N(Cy)** ^{1}H NMR (300 MHz, d_8-Tol, 300 K) δ_H (ppm): 7.14 – 6.96 (6H, m, Ar-*H*), 6.00 (2H, dt, J_{HH} = 9 Hz, NC*H*), 4.85 (1H, s, NC(CH$_3$)C*H*), 4.40 (2H, dt, ^{3}J = 9 Hz, ^{4}J = 3 Hz, NCHC*H*), 3.44 (4H, sept, J_{HH} = 6 Hz, C*H*(CH$_3$)$_2$), 3.10 (2H, m, NC*H*(CH$_2$)$_2$), 2.87 (2H, m, NCHCHC*H*$_2$), 1.86 – 0.78 (20H, m, Cy-*H*), 1.65 (6H, s, NC(C*H*$_3$)), 1.33 (12H, d, J_{HH} = 9 Hz, CH(C*H*$_3$)$_2$), 1.26 (12H, d, J_{HH} = 9 Hz, CH(C*H*$_3$)$_2$). ^{13}C{^{1}H} NMR (75.5 MHz, d_8-Tol, 300 K) δ_C (ppm): 169.7 (N*C*(CH$_3$), 163.8 (*C*N$_3$), 145.6 (*ipso*-Ar), 142.6 (*o*-Ar), 128.1 (N*C*H), 125.3 (*o*-Ar),123.9 (*m*-Ar), 99.1 (NCH*C*H), 94.8 (NC(CH$_3$)*C*H), 53.5 (N*C*H(CH$_2$)$_2$), 37.0 (CH(*C*H$_2$)$_2$), 28.7 (*C*H(CH$_3$)$_2$), 26.5 (CH(*C*H$_2$)$_2$), 26.0 (CH(*C*H$_3$)$_2$), 25.8 (CH(CH$_2$)$_2$(*C*H$_2$)$_2$), 25.6 (CH(*C*H$_3$)$_2$), 24.5 (NC(*C*H$_3$)), 24.3 (CH(CH$_2$)$_4$*C*H$_2$), 22.8 (NCHCH*C*H$_2$). HRMS (ESI) calcd. for hydrolysed product [M$^+$] $C_{18}H_{29}N_3$ *m/z* 287.45, found 288.2549.

Synthesis of Compound 22

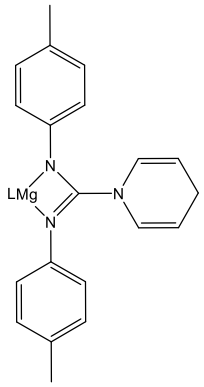

NMR Scale: 30 mg (0.05 mmol) **XXVIIa** with 11.1 mg (0.05 mmol) of *p*-TolNCN*p*-Tol. **LMgN(*p*-Tol)C(Pyr(H))N(*p*-Tol)** ^{1}H NMR (300 MHz, d_8-Tol, 300 K) δ_H (ppm): 7.11 – 6.99 (6H, m, Dipp-*H*), 6.81 (4H, m, *o*-*H* (*p*-Tol)), 6.67 (4H, m, *m*-*H* (*p*-Tol)), 6.00 (2H, d, J_{HH} = 9 Hz, NC*H*CH), 4.88 (1H, s, NC(CH$_3$)C*H*), 4.20 (2H, m, NCHC*H*), 3.64 (4H, m, C*H*(CH$_3$)$_2$), 2.68 (2H, s, NCHCHC*H*$_2$), 2.11 (6H, s, *p*-C*H*$_3$), 1.69 (6H, s, NC(C*H*$_3$)CH), 1.26 (12H, d, J_{HH} = 6 Hz, CH(C*H*$_3$)$_2$), 1.14 – 1.10 (12H, m, CH(C*H*$_3$)$_2$. ^{13}C{^{1}H} NMR (75.5 MHz, d_8-Tol, 300 K) δ_C (ppm): 168.3 (N*C*(CH$_3$)), 159.9 (*ipso*-*C* Dipp), 147.9 (*o*-*C* Dipp), 146.4 (*ipso*-*C* *p*-Tol), 143.0 (*o*-*C* *p*-Tol), 136.8(*p*-*C* *p*-Tol), 128.9 (*m*-*C* Dipp), 128.7 (*m*-*C* *p*-Tol), 124.9 (*p*-*C* Dipp),124.0 (N*C*HCH), 100.7 (NCH*C*H), 97.6 (NC(CH$_3$)*C*H), 32.0 (*C*H(CH$_3$)$_2$), 27.9 (NCHCH*C*H$_2$), 25.0 (*p*-*C*H$_3$), 24.7 (NC(*C*H$_3$), 21.2 (CH(*C*H$_3$)$_2$), 20.8 (CH(*C*H$_3$)$_2$). HRMS (ESI) calcd. for hydrolysed product [M$^+$H$^+$]$^+$ $C_{20}H_{21}N_3$ *m/z* 303.41, found 304.1814.

1,4-Dihydro-3-picolide reactions, XXVIIc

Synthesis of Compound 23

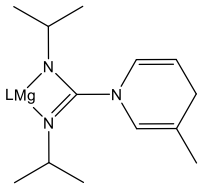

NMR Scale: 30 mg (0.048 mmol) **XXVIIc** with 4.9 µL (0.048 mmol) of *i*PrNCN*i*Pr. **Large Scale:** 200 mg (0.32 mmol) of **XXVIIc** with 49.3 µL (0.32 mmol) of *i*PrNCN*i*Pr, this was dissolved in toluene and left to stir at room temperature overnight. Solvent was removed *in vacuo* to yield yellow crystals of **23** (140 mg, 66% yield). **LMgN(iPr)C(3-Pic(H))N(iPr)** ^{1}H NMR (300 MHz, d_8-Tol, 300 K) δ_H (ppm): 7.12 – 6.98 (6H, m, Ar), 6.02 (1H, dm, ^{3}J = 6 Hz, ^{4}J = 3Hz, NC*H*CH), 5.87 (1H, m, NC*H*C(CH_3)), 4.85 (1H, s, NC(CH_3)C*H*), 4.46 (1H, dt, ^{3}J = 9 Hz, ^{4}J = 3 Hz, NCHC*H*), 3.43 (2H, sept, J_{HH} = 6 Hz, NC*H*(CH_3)$_2$), 3.33 (4H, sept, J_{HH} = 6 Hz, C*H*(CH_3)$_2$), 2.81 (2H, m, NC- HCHC*H*$_2$), 1.87 (3H, s, NCHC(C*H*$_3$)), 1.65 (6H, s, NC(C*H*$_3$), 1.28 (12H, d, J_{HH} = 6 Hz, CH(C*H*$_3$)$_2$), 1.24 (12H, d, J_{HH} = 6 Hz, CH(C*H*$_3$)$_2$), 1.05 (12H, d, J_{HH} = 6 Hz, NCH(C*H*$_3$)$_2$). ^{13}C{^{1}H} NMR (75.5 MHz, d_8-Tol, 300 K) δ_C (ppm): 169.5 (N*C*(CH_3)), 164.5 (*C*N$_3$), 145.8 (*ipso*-Ar), 142.7 (*o*-Ar), 127.5 (N*C*H), 125.3 (*p*-Ar), 123.9 (*m*-Ar), 123.5 (N*C*HC(CH_3)), 107.1 (NCH*C*(CH_3)), 98.0 (NC(CH_3)*C*H), 95.0 (NCH*C*H), 45.0 (N*C*H(CH_3)$_2$), 28.3 (*C*H(CH_3)$_2$), 26.0(NCH(*C*H$_3$)$_2$), 25.4 (CH(*C*H$_3$)$_2$), 24.8 (NC(*C*H$_3$)), 24.3 (CH(*C*H$_3$)$_2$), 20.9 (NCHCH*C*H$_2$), 18.0 (NCHC(*C*H$_3$)).

Synthesis of Compound 24

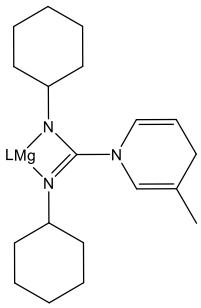

NMR Scale: 30 mg (0.048 mmol) **XXVIIc** with 11.5 mg (0.048 mmol) of CyNCNCy. **Large Scale:** 200 mg (0.31 mmol) of **XXVIIc** with 65.7 mg (0.31 mmol) of CyNCNCy, this was dissolved in toluene and left to stir at room temperature overnight. Solvent was removed *in vacuo* to yield yellow crystals of **24** (175 mg, 72% yield). **LMgN(Cy)C(3-Pic(H))N(Cy)** ^{1}H NMR (300 MHz, d_8-Tol, 300 K) δ_H (ppm): 7.15 – 7.07 (6H, m, Ar), 6.07 (1H, dm, J_{HH} = 6 Hz, NC*H*CH), 5.92 (1H, m, NC*H*C(CH_3)), 4.86 (1H, s, NC(CH_3)C*H*), 4.47 (1H, dt, ^{3}J = 6 Hz, ^{4}J = 3 Hz, NCHC*H*), 3.46 (4H, sept, J_{HH} = 6 Hz, C*H*(CH_3)$_2$), 3.12 (2H, m, NC*H*(CH_2)$_2$), 2.78 (2H, m, NCHCHC*H*$_2$), 1.83 (3H, s, NCHC(C*H*$_3$)), 1.73 (4H, m, Cy-*H*), 1.55 (4H, m, Cy-*H*), 1.66 (6H, s, NC(C*H*$_3$)), 1.34 (12H, d, J_{HH} = 6Hz, CH(C*H*$_3$)$_2$), 1.26 (12H, d, J_{HH} = 6Hz, CH(C*H*$_3$)$_2$), 1.29 – 0.99 (8H, m, Cy-*H*), 0.85 (4H, m, CH(CH_2)$_2$ (CH_2)$_2$C*H*$_2$). ^{13}C{^{1}H} NMR (75.5 MHz, d_8-Tol, 300 K) δ_C (ppm): 169.7 (N*C*(CH_3)), 164.0 (*C*N$_3$), 145.7 (*ipso*-Ar), 142.7 (*o*-Ar), 127.5 (N*C*H), 125.3 (*p*-Ar), 123.9 (*m*-Ar), 122.8 (N*C*HC(CH_3)), 107.3 (NCH*C*(CH_3)), 98.1 (NC(CH_3)*C*H), 94.9 (NCH*C*H), 53.6 (N*C*H(CH_2)$_2$), 37.0 (NCH(*C*H$_2$)$_2$), 28.4 (*C*H(CH_3)$_2$), 26.5 (CH(CH_2)$_2$(*C*H$_2$)$_2$), 26.1 (CH(*C*H$_3$)$_2$), 25.5 (CH(*C*H$_3$)$_2$), 24.6 (NC(*C*H$_3$)), 24.4 (CH(CH_2)$_4$*C*H$_2$), 20.9 (NCHCH*C*H$_2$) 18.0 (NCHC(*C*H$_3$)).

Synthesis of Compound 25

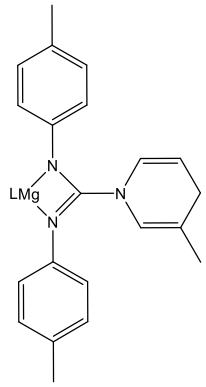

NMR Scale: 30 mg (0.048 mmol) **XXVIIc** with 10.6 mg (0.048 mmol) of *p*-TolNCN*p*-Tol. **LMgN(*p*-Tol)C(3-Pic(H))N(*p*-Tol)** ^{1}H NMR (300 MHz, d_8-Tol, 300 K) δ_H (ppm): 7.10 – 6.98 (6H, m, Dipp-*H*), 6.76 (4H, m, *o*-*H* (*p*-Tol)), 6.52 (4H, m, *m*-*H* (*p*-Tol)), 6.08 (1H, m, NC*H*CH), 5.89 (1H, s, NC*H*C(CH_3)), 4.88 (1H, s, NC(CH_3)C*H*), 4.30 (1H, m, NCHC*H*), 3.63 (4H, m, C*H*(CH_3)$_2$), 2.59 (2H, s, NCHCHC*H*$_2$), 2.07 (6H, s, *p*-C*H*$_3$), 1.70 (6H, s, NC(C*H*$_3$)CH), 1.26 (12H, d, J_{HH} = 6 Hz, CH(C*H*$_3$)$_2$), 1.20 (3H, s, NCHC(C*H*$_3$), 1.11 – 1.08 (12H, m, CH(C*H*$_3$)$_2$. ^{13}C{^{1}H} NMR (75.5 MHz, d_8-Tol, 300 K) δ_C (ppm): 168.2 (N*C*(CH_3)), 159.7 (*ipso*-*C* Dipp), 148.0 (*o*- *C* Dipp), 146.6 (*ipso*-*C* *p*-Tol), 143.1 (*o*-*C* *p*-Tol), 137.2 (*p*-*C* *p*-Tol), 128.8 (*m*-*C* Dipp), 128.6 (*m*-*C* *p*-Tol), 124.8 (*p*-*C* Dipp), 124.0 (N*C*HCH), 123.8 (N*C*H(CH_3)), 108.9 (NCH*C*H), 100.1 (NCH*C*(CH_3), 97.5 (NC(CH_3)*C*H), 28.5 (NCHCH*C*H$_2$), 28.0 (CH(*C*H$_3$)$_2$)), 25.1 (*p*-*C*H$_3$), 24.7 (NC(*C*H$_3$), 20.8 (*C*H(CH_3)$_2$), 17.7 (NCHC(*C*H$_3$)). HRMS (ESI) calcd. for hydrolysed product [M$^+$H$^+$]$^+$ $C_{21}H_{23}N_3$ *m/z* 317.44, found 318.2011.

1,4-Dihydro-3,5-lutidide reactions, XXVIId

Synthesis of Compound 26

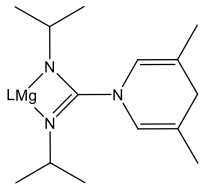

NMR Scale: 30 mg (0.046 mmol) **XXVIId** with 4.7 µL (0.046 mmol) of *i*PrNCN*i*Pr. **Large Scale:** 50 mg (0.076 mmol) of **XXVIId** with 11.7 µL (0.076 mmol) of *i*PrNCN*i*Pr, this was dissolved in toluene and left to stir at room temperature overnight. Solvent was removed *in vacuo* to yield yellow crystals of **26** (40 mg, 78% yield). **LMgN(iPr)C(3,5Lut(H))N(iPr)** ^{1}H NMR (300 MHz, d_8-Tol, 300 K) δ_H (ppm): 7.15 – 7.08 (6H, m, Ar), 5.94 (2H, s, NC*H*), 4.86 (1H, s, NC(CH_3)C*H*), 3.53 (2H, sept, J_{HH} = 6 Hz, NC*H*(CH_3)$_2$), 3.45 (4H, sept, J_{HH} = 6 Hz, C*H*(CH_3)$_2$), 2.65 (2H, s, NCHC(CH_3)C*H*$_2$), 1.53 (6H, s, NCHC(C*H*$_3$)), 1.30 (12H, d, J_{HH} = 9 Hz, CH(C*H*$_3$)$_2$), 1.25 (12H, d, J_{HH} = 6 Hz, CH(C*H*$_3$)$_2$), 0.86 (6H, d, J_{HH} = 6 Hz, NCH(C*H*$_3$)$_2$). ^{13}C{^{1}H} NMR (75.5 MHz, d_8-Tol, 300 K) δ_C (ppm): 169.4 (N*C*(CH_3)), 164.7 (*C*N$_3$), 146.0 (*ipso*-Ar), 142.1 (*o*-Ar), 125.2 (*p*-Ar), 123.9 (*m*-Ar), 122.4 (N*C*H), 106.0 (NCH*C*(CH_3)), 95.1 (NC(CH_3)*C*H), 45.1 (N*C*H(CH_3)$_2$), 34.3 (NCHC(CH_3)*C*H$_2$), 28.2 (*C*H(CH_3)$_2$), 26.0 (CH(*C*H$_3$)$_2$), 25.3 (CH(*C*H$_3$)$_2$), 24.7 (CH(*C*H$_3$)$_2$), 24.4 (NC(*C*H$_3$)), 20.7 (NCHC(*C*H$_3$)). HRMS (ESI) calcd. for hydrolysed product [M$^+$] $C_{14}H_{25}N_3$ *m/z* 235.38, found 236.2214.

Synthesis of Compound 27

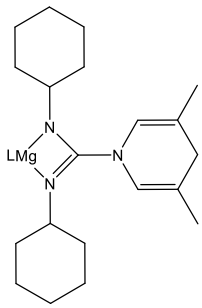

NMR Scale: 30 mg (0.046 mmol) **XXVIId** with 6.3 mg (0.046 mmol) of CyNCNCy. **Large Scale:** 50 mg (0.076 mmol) of **XXVIId** with 15.7 mg (0.076 mmol) of CyNCNCy, this was dissolved in toluene and left to stir at room temperature overnight. Solvent was removed *in vacuo* to yield yellow crystals of **27** (30 mg, 52% yield). **LMgN(Cy)C(3,5Lut(H))N(Cy)** ^{1}H NMR (300 MHz, d_8-Tol, 300 K) δ_H (ppm): 7.15 – 7.08 (6H, m, Ar), 6.01 (2H, s, NC*H*), 4.90 (1H, s, NC(CH$_3$)C*H*), 3.51 (2H, sept, J_{HH} = 6 Hz, NC*H*(CH$_3$)$_2$), 3.16 (2H, m, NC*H*(CH$_2$)$_2$), 2.62 (2H, s, NCHC(CH$_3$)C*H*$_2$), 1.89 (6H, s, NCHC(C*H*$_3$), 1.75 – 1.55 (8H, m, Cy-*H*), 1.70 (6H, s, NC(C*H*$_3$)), 1.38 (12H, d, J_{HH} = 6 Hz, CH(C*H*$_3$)$_2$), 1.30 (12H, d, J_{HH} = 6 Hz, CH(C*H*$_3$)$_2$), 1.29 – 1.05 (8H, m, Cy-*H*), 0.90 (4H, m, CH(CH$_2$)$_2$(CH$_2$)$_2$C*H*$_2$). ^{13}C{^{1}H} NMR (75.5 MHz, d_8-Tol, 300 K) δ_C (ppm): 169.6 (N*C*(CH$_3$)), 164.1 (*C*N$_3$), 145.8 (*ipso*-Ar), 142.7 (*o*-Ar), 125.2 (*p*-Ar),123.9 (*m*-Ar), 122.4 (N*C*H), 106.3 (NCH*C*(CH$_3$)), 94.9 (NC(CH$_3$)*C*H), 53.7 (N*C*H(CH$_2$)$_2$), 37.0 (NCH(*C*H$_2$)$_2$), 35.4 (NCHC(CH$_3$)*C*H$_2$), 28.4 (*C*H(CH$_3$)$_2$), 26.5 (CH(CH$_2$)$_2$(*C*H$_2$)$_2$), 26.1 (CH(*C*H$_3$)$_2$), 25.5 (CH(*C*H$_3$)$_2$), 24.6 (NC(*C*H$_3$)), 24.4 (CH(CH$_2$)$_4$*C*H$_2$), 17.9 (NCHC(*C*H$_3$)).

Synthesis of Compound 28

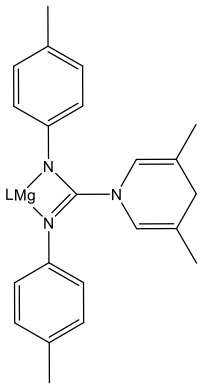

NMR Scale: 30 mg (0.046 mmol) **XXVIId** with 10.1 mg (0.046 mmol) of *p*-TolNCN*p*-Tol. **LMgN(*p*-Tol)C(3,5Lut(H))N(*p*-Tol)** ^{1}H NMR (300 MHz, d_8-Tol, 300 K) δ_H (ppm): 7.11 – 6.98 (6H, m, Dipp-*H*), 6.81 (4H, m, *o*-*H* (*p*-Tol)), 6.61 (4H, m, *m*-*H* (*p*-Tol)), 5.98 (2H, s, NC*H*C(CH$_3$)), 4.89 (1H, s, NC(CH$_3$)C*H*), 3.69 (4H, m, C*H*(CH$_3$)$_2$), 2.46 (2H, s, NCHC(CH$_3$)C*H*$_2$), 2.06 (6H, s, *p*-C*H*$_3$), 1.73 (6H, s, NC(C*H*$_3$)CH), 1.29 (6H, s, NCHC(C*H*$_3$)) 1.15 – 1.12 (12H, m, CH(C*H*$_3$)$_2$), 0.93 – 0.89 (12H, m, CH(C*H*$_3$)$_2$. ^{13}C{^{1}H} NMR (75.5 MHz, d_8-Tol, 300 K) δ_C (ppm): 168.0 (N*C*(CH$_3$)), 159.7 (*ipso*-*C* Dipp), 148.1 (*o*- *C* Dipp), 146.9 (*ipso*-*C p*-Tol), 143.2 (*o*-*C p*-Tol), 132.8 (*p*-*C p*-Tol), 128.6 (*m*-*C* Dipp), 128.4 (*m*-*C p*-Tol), 124.7 (*p*-*C* Dipp), 124.0 (N*C*HCH), 108.1 (NCH*C*(CH$_3$), 97.5 (NC(CH$_3$)*C*H), 34.2 (*C*H(CH$_3$)$_2$), 28.0 (NCHC(CH$_3$)*C*H$_2$), 25.2 (*p*-*C*H$_3$), 24.7 (NC(*C*H$_3$), 20.7 (CH(*C*H$_3$)$_2$), 20.6 (CH(*C*H$_3$)$_2$), 17.7 (NCHC(*C*H$_3$)). HRMS (ESI) calcd. for hydrolysed product [M$^+$H$^+$]$^+$ $C_{22}H_{25}N_3$ *m/z* 331.46, found 332.2207, [M$^+$Na$^+$]$^+$ $C_{22}H_{25}N_3Na$ *m/z* 354.45, found 354.2028.

1,2-dihydro-*iso*-quinolide reactions, XXVIII

Synthesis of Compound 29

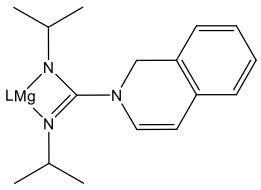

NMR Scale: 30 mg (0.043 mmol) **XXVIII** with 4.4 μL (0.043 mmol) of *i*PrNCN*i*Pr. **Large Scale:** 50 mg (0.071 mmol) of **XXVIII** with 11.0 μL (0.071 mmol) of *i*PrNCN*i*Pr, this was dissolved in toluene and left to stir at room temperature overnight. Solvent was removed *in vacuo* to yield red crystals of **29** (30 mg, 61% yield). **LMgN(iPr)C(iQuin(H))N(iPr)** ^{1}H NMR (300 MHz, d_8-Tol, 300 K) δ_H (ppm): 7.24 – 6.74 (10H, m, Ar-*H*, iQuin-*H*), 6.31 (1H, d, J_{HH} = 6 Hz, NC*H*), 5.50 (1H, d, J_{HH} = 6 Hz, NCHC*H*), 4.84 (1H, s, NC(CH_3)C*H*), 4.46 (2H, s, NCH_2), 3.44 (6H, m, C*H*(CH_3)$_2$, NC*H*(CH_3)$_2$), 1.65 (6H, s, NC(CH_3)), 1.30 (12H, d, J_{HH} = 6 Hz, CH(CH_3)$_2$), 1.25 (12H, d, J_{HH} = 6 Hz, CH(CH_3)$_2$), 0.79 (12H, d, J_{HH} = 6 Hz, CH(CH_3)$_2$). ^{13}C{^{1}H} NMR (75.5 MHz, d_8-Tol, 300 K) δ_C (ppm): 169.6 (N*C*(CH_3), 165.4 (*C*N_3), 145.6 (*ipso*-Ar), 142.7 (*o*-Ar), 135.5 (iQuin(H)-*C*), 133.6 (iQuin(H)-*C*), 132.9 (N*C*H), 126.4 (iQuin(H)-*C*), 125.8 (iQuin(H)-*C*), 125.3 (*p*-Ar), 123.8 (*m*-Ar), 102.4 (NCHC*H*), 94.8 (NC(CH_3)*C*H), 52.4 (N*C*H_2), 45.1 (N*C*H(CH_3)$_2$), 28.3 (*C*H(CH_3)$_2$), 26.1 (CH(*C*H_3)$_2$), 25.4 (CH(*C*H_3)$_2$), 24.5 (NC(*C*H_3)), 24.3 (CH(*C*H_3)$_2$), 23.9 (CH(*C*H_3)$_2$). Despite repeated attempts, an acceptable elemental analysis could not be obtained for this highly air and moisture sensitive compound. HRMS (ESI) calcd. for hydrolysed product [M^+] $C_{16}H_{23}N_3$ *m/z* 257.38, found 258.2035.

Synthesis of Compound 30

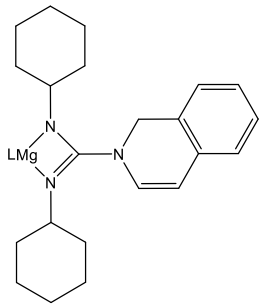

NMR Scale: 30 mg (0.043 mmol) **XXVIII** with 5.9 mg (0.043 mmol) of CyNCNCy. **Large Scale:** 50 mg (0.071 mmol) of **XXVIII** with 14.6 mg (0.071 mmol) of CyNCNCy, this was dissolved in toluene and left to stir at room temperature overnight. Solvent was removed *in vacuo* to yield red crystals of **30** (37 mg, 67% yield). **LMgN(Cy)C(iQuin(H))N(Cy)** ^{1}H NMR (300 MHz, d_8-Tol, 300 K) δ_H (ppm): 7.10 – 6.74 (10H, m, Ar-*H*, iQuin(H)-*H*), 6.37 (1H, d,^{3}J = 9 Hz, NC*H*), 5.52 (1H, d, J_{HH} = 9 Hz, NCHC*H*), 4.87 (1H, s, NC(CH_3)C*H*), 4.52 (2H, s, NCH_2), 3.47 (4H, sept, J_{HH} = 6 Hz, C*H*(CH_3)$_2$), 3.05 (2H, m, NC*H*(CH_2)$_2$), 1.66 (6H, s, NC(CH_3), 1.58 – 1.38 (8H, m, Cy-*H*), 1.33 (12H, d, J_{HH} = 6 Hz, CH(CH_3)$_2$), 1.26 (12H, d, J_{HH} = 6 Hz, CH(CH_3)$_2$), 1.14 – 0.76 (12H, m, Cy-*H*). ^{13}C{^{1}H} NMR (75.5 MHz, d_8-Tol, 300 K) δ_C (ppm): 169.6 (N*C*(CH_3)), 165.2 (*C*N_3), 145.8 (*ipso*-Ar), 142.7 (*o*-Ar), 136.0 (iQuin(H)-*C*), 133.7 (iQuin(H)-*C*), 132.9 (N*C*H), 127.7 (iQuin(H)-*C*), 126.4 (iQuin(H)-*C*), 125.3 (*p*-Ar), 123.8 (*m*-Ar), 102.4 (NCH*C*H), 94.9 (NC(CH_3)*C*H), 53.9 (N*C*H(CH_2)$_2$), 50.8 (N*C*H_2), 37.1 (Cy-*C*), 35.4 (Cy-*C*), 28.3 (*C*H(CH_3)$_2$), 26.4 (Cy-*C*), 26.0 (CH(*C*H_3)$_2$), 25.8 (Cy-*C*), 25.5 (CH(*C*H_3)$_2$), 24.6 (NC(*C*H_3)), 24.4 (CH(*C*H_3)$_2$), 23.9 (CH(*C*H_3)$_2$). Despite repeated attempts, an acceptable

elemental analysis could not be obtained for this highly air and moisture sensitive compound. HRMS (ESI) calcd. for hydrolysed product $[M^+]$ $C_{22}H_{31}N_3$ *m/z* 337.51, found 338.2714.

Synthesis of Compound 31

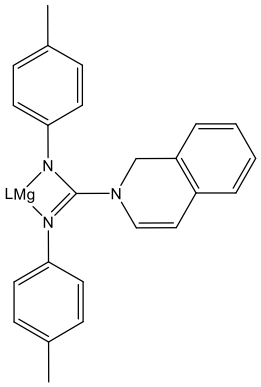

NMR Scale: 30 mg (0.043 mmol) **XXVIII** with 9.5 mg (0.043 mmol) of *p*-TolNCN*p*-Tol. **LMgN(p-Tol)C(iQuin(H))N(p-Tol)** ^{1}H NMR (500 MHz, C_6D_6, 300 K) δ_H (ppm): 7.24 – 6.41 (18H, m, Ar-*H*), 6.07 (1H, d, J_{HH} = 5 Hz, NC*H*CH), 5.32 (1H, d, J_{HH} = 5 Hz, NCHC*H*), 4.94 (1H, s, NC(CH$_3$)C*H*), 4.40 (2H, s, NC*H*$_2$), 3.32 (4H, m, C*H*(CH$_3$)$_2$), 1.76 (6H, s, NC(C*H*$_3$)CH), 1.67 (6H, s, *p*-C*H*$_3$), 1.63 (12H, d, J_{HH} = 5 Hz, CH(C*H*$_3$)$_2$), 1.22 (12H, d, J_{HH} = 5 Hz, CH(C*H*$_3$)$_2$). ^{13}C{^{1}H} NMR (125.75 MHz, d$_8$-Tol, 300 K) δ_C (ppm): 168.7 (N*C*(CH$_3$)CH), 161.9 (N$_3$*C*), 148.5 (*ipso*-*C* Ar), 147.0 (*ipso*-*C* *p*-Tol), 143.7 (*o*-*C* *p*-Tol), 143.1 (*o*-*C* Ar), 136.4 (iQuin(H)-*C*), 133.6 (iQuin(H)-*C*), 133.5 (*p*-*C* *p*-Tol), 130.4 (N*C*H), 129.8 (iQuin(H)-*C*), 129.0 (*p*-Ar-*C*), 128.7 (iQuin(H)-*C*), 127.8 (iQuin(H)-*C*), 126.9 (iQuin(H)-*C*), 126.6 (*m*-*C* *p*-Tol), 126.1 (*m*-*C* Ar), 105.4 (NCH*C*H), 94.6 (NC(CH$_3$)*C*H), 51.5 (N*C*H$_2$), 37.3 (*C*H(CH$_3$)$_2$), 29.0 (NC(*C*H$_3$)CH), 28.4 (*p*-*C*H$_3$ *p*-Tol), 25.5 (CH(*C*H$_3$)$_2$), 25.2 (CH(*C*H$_3$)$_2$), 24.4 (CH(*C*H$_3$)$_2$), 23.8 (CH(*C*H$_3$)$_2$). HRMS (ESI) calcd. for hydrolysed product $[M^+H^+]^+$ $C_{24}H_{23}N_3$ *m/z* 353.47, found 354.1970.

Synthesis of Compound 32

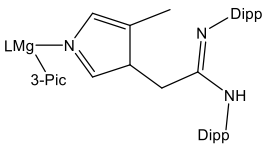

NMR Scale: 30 mg (0.048 mmol) **XXVIIc** with 17.3 mg (0.048 mmol) of DippNCNDipp. **Large Scale:** 200 mg (0.32 mmol) of **XXVIIc** with 115.4 mg (0.32 mmol) of DippNCNDipp, this was dissolved in toluene and left to stir at room temperature overnight. Solvent was removed *in vacuo* to yield yellow crystals of **32** (220 mg, 69% yield). ^{1}H NMR (300 MHz, d$_8$-Tol, 300 K) δ_H (ppm): 7.76 (1H, m, *o*-C*H* 3Pic), 7.13- 6.98 (12H, m, Ar-*H*), 6.67 (1H, s, *o*-C*H*C(CH$_3$) 3Pic), 6.64 (1H, m, *p*-*H*, 3Pic), 6.35 (1H, m, *m*-*H* 3Pic), 6.09 (1H, s, NC*H*), 5.89 (1H, s, NC*H*), 5.83 (1H, s, C*H*$_2$), 4.92 (1H, s, NC(CH$_3$)C*H*), 4.17 (1H, s, C*H*$_2$), 4.01 (1H, s, N*H*), 3.90 (2H, m, C*H*(CH$_3$)$_2$), 3.61 (2H, m, C*H*(CH$_3$)$_2$), 3.41 (4H, m, C*H*(CH$_3$)$_2$), 1.75 (6H, s, NC(C*H*$_3$)CH), 1.73 (3H, s, NCHC(C*H*$_3$), 1.61 (3H, s, *m*-C*H*$_3$ 3Pic), 1.38 – 1.09 (39H, m, CH(C*H*$_3$)$_2$, 3-C*H*$_3$ 3Pic), 1.23 (12H, d, J_{HH} = 6 Hz, CH(C*H*$_3$)$_2$). ^{13}C{^{1}H} NMR (125.75 MHz, d$_8$-Tol, 300 K) δ_C (ppm): 169.7 (N*C*(CH$_3$)CH), 150.5 (N*C*NH), 149.2 (*ipso*-*C*), 146.8 (*ipso*-*C* NCN), 146.7 (*ipso*-*C* NCNH), 145.2 (*o*-*C*), 143.4 (*o*-*C* NCN), 141.9 (*o*-C NCNH), 138.1 (*o*-*C* Pyr), 136.9 (*o*-C Pyr), 135.9 (*p*-*C*), 130.2 (*p*-*C* NCN), 128.7 (*p*-*C* NCNH), 127.6 (*p*-*C* Pyr), 126.6 (*m*-*C*(CH$_3$) Pyr), 126.2 (NCH*C*CH$_2$), 125.9 (NCH*C*(CH$_3$)C), 124.1 (*m*-*C*), 123.9 (*m*-*C* NCN), 123.6 (*m*-*C* NCNH), 120.0 (N*C*HC(CH$_3$)), 117.3 (N*C*H), 94.6 (NC(CH$_3$)*C*H), 70.0 (*C*H$_2$), 29.9 (*C*H(CH$_3$)$_2$), 28.7 (*C*H(CH$_3$)$_2$ NCN), 28.5

(*C*H(CH_3)$_2$ NCNH), 28.0 (NC(*C*H_3)CH), 26.6 (CH(*C*H_3)$_2$), 25.8 (CH(*C*H_3)$_2$), 24.6 (CH(*C*H_3)$_2$), 24.4 (*C*H_3), 23.8 (CH(*C*H_3)$_2$), 14.3 (3-*C*H_3 3Pic). Elemental Analysis for $C_{66}H_{91}MgN_6$ (found): C 79.85 (79.98); H 9.24 (9.38); N 8.47 (8.19). HRMS (ESI) calcd. for hydrolysed product $[M^+H^+]^+$ $C_{31}H_{43}N_3$ *m/z* 457.71, found 458.3667.

Synthesis of Compound 33

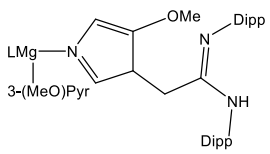

NMR Scale: 50 mg of **Ib** (0.1 mmol), with 2 equivalents of 3-(MeO)pyridine (20.2 µL, 0.2 mmol) and 1 equivalent of $PhSiH_3$ (12.3 µL, 0.1 mmol) was heated for 2 days at 60 °C to form the dihydropyridide complex, 0.1 mmol of DippNCNDipp (36 mg) was then added. ^{1}H NMR (500 MHz, C_6D_6, 300 K) δ_H (ppm): 7.48 (1H, m, *o*-C*H* 3Pic), 7.13 – 6.95 (14H, m, Ar-*H*, *o*,*m*-C*H* 3Pic), 6.86 (1H, s, NC*H*), 6.68 (1H, d, J_{HH} = 5 Hz, *p*-C*H* 3Pic), 5.77 (1H, s, NC*H*), 5.47 (1H, s, CH_2), 4.89 (1H, s, N(CH$_3$)C*H*), 4.18 (1H, s, CH_2), 4.00 (1H, s, N*H*), 3.88 (2H, m, C*H*(CH$_3$)$_2$), 3.60 (2H, m, C*H*(CH$_3$)$_2$), 3.51 (2H, m, C*H*(CH$_3$)$_2$), 3.34 (3H, s, OCH_3), 3.28 (C*H*(CH$_3$)$_2$), 2.81 (3H, s, OCH_3 Pyr), 1.73 (6H, s, NC(CH_3)CH), 1.33 (12H, m, CH(CH_3)$_2$), 1.21 (12H, d, J_{HH} = 5 Hz, CH(CH_3)$_2$), 1.12 (24H, m, CH(CH_3)$_2$). ^{13}C{^{1}H} NMR (125.75 MHz, d_8-Tol, 300 K) δ_C (ppm): 169.7 (N*C*(CH$_3$)CH), 157.1 (N*C*NH), 149.4 (*ipso*-*C*), 147.5 (*ipso*-*C* NCN), 146.5 (*ipso*-*C* NCNH), 145.0 (*o*-*C*), 143.7 (*o*-*C* NCN), 142.3 (*o*-C NCNH), 137.3 (*o*-*C* Pyr), 136.7 (*o*-C Pyr), 135.9 (*p*-*C*), 130.2 (*p*-*C* NCN), 128.7 (*p*-*C* NCNH), 127.5 (*p*-*C* Pyr), 126.5 (*m*-*C*(CH$_3$) Pyr), 125.9 (NCH*C*CH$_2$), 125.8 (NCH*C*(CH$_3$)C) 124.1 (*m*-*C*), 123.9 (*m*-*C*), 123.6 (*m*-*C* NCN), 123.1 (*m*-*C* NCNH), 111.0 (N*C*HC(CH$_3$), 108.3 (N*C*H), 94.5 (NC(CH$_3$)*C*H), 74.4 (*C*H$_2$), 58.0 (O*C*H$_3$), 56.1 (O*C*H$_3$ Pyr), 29.9 (*C*H(CH$_3$)$_2$), 28.7 (*C*H(CH$_3$)$_2$ NCN), 28.6 (*C*H(CH$_3$)$_2$ NCNH), 28.0 (NC(*C*H$_3$)CH), 26.5 (CH(*C*H$_3$)$_2$), 24.6 (CH(*C*H$_3$)$_2$), 24.3 (CH(*C*H$_3$)$_2$), 23.7 (CH(*C*H$_3$)$_2$), 23.1 (CH(*C*H$_3$)$_2$).

Synthesis of Compound 34

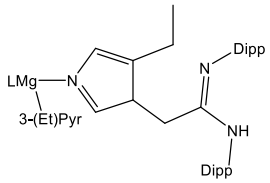

NMR Scale: 50 mg of **Ib** (0.1 mmol), with 2 equivalents of 3-(Et)pyridine (22.4 µL, 0.2 mmol) and 1 equivalent of $PhSiH_3$ (12.3 µL, 0.1 mmol) was heated for 2 days at 60 °C to form the dihydropyridide complex, 0.1 mmol of DippNCNDipp (36 mg) was then added. ^{1}H NMR (500 MHz, C_6D_6, 300 K) δ_H (ppm): 7.48 (1H, m, *o*-C*H* Pyr), 7.14 – 7.02 (13H, m, Ar-*H*, *o*-C*H* Pyr), 6.81 (1H, m, *p*-C*H* Pyr), 6.49 (1H, m, *m*-C*H* Pyr), 6.19 (1H, s, NC*H*), 5.86 (1H, s, NC*H*), 5.83 (1H, s, CH_2), 4.21 (1H, s, CH_2), 4.03 (1H, s, N*H*), 3.87 (2H, m, C*H*(CH$_3$)$_2$), 3.60 (2H, m, C*H*(CH$_3$)$_2$), 3.40 (2H, m, C*H*(CH$_3$)$_2$), 2.80 (2H, m, C*H*(CH$_3$)$_2$), 2.44 (2H, m, CH_2CH$_3$), 2.05 (2H, m, 3-CH_2CH$_3$ Pyr), 1.74 (6H, s, NC(CH_3)CH), 1.35 (12H, m, CH(CH_3)$_2$), 1.20 (12H, d, J_{HH} = 5 Hz, CH(CH_3)$_2$), 1.13 (12H, m, CH(CH_3)$_2$), 1.08 (3H, t, J_{HH} = 10 Hz, 3-CH$_2$CH_3), 0.93 (3H, t, J_{HH} = 10 Hz, 3-CH$_2$CH_3 Pyr), 0.77 (12H, m, CH(CH_3)$_2$). ^{13}C{^{1}H} NMR (125.75 MHz,

d_8-Tol, 300 K) δ_C (ppm): 169.7 (NC(CH$_3$)CH), 150.2 (NCNH), 149.2 (*ipso-C*), 146.9 (*ipso-C* NCN), 145.2 (*ipso-C* NCNH), 143.7 (*o-C*), 143.4 (*o-C* NCN), 142.8 (*o*-C NCNH), 137.4 (*o-C* Pyr), 136.8 (*o*-C Pyr), 135.9 (*p-C*), 130.2 (*p-C* NCN), 128.7 (*p-C* NCNH), 127.6 (*p-C* Pyr), 126.7 (*m-C*(CH$_3$) Pyr), 126.0 (NCH*C*CH$_2$), 125.2 (N*C*HC(CH$_3$)) 125.9 (NCH*C*(CH$_3$)C), 124.4 (*m-C*), 124.1 (*m-C*), 123.9 (*m-C* NCN), 123.6 (*m-C* NCNH), 119.5 (N*C*H), 108.3 (N*C*H), 94.5 (NC(CH$_3$)*C*H), 76.0 (*C*H$_2$), 29.9 (*C*H(CH$_3$)$_2$), 29.3 (*C*H$_2$CH$_3$), 28.9 (3-*C*H$_2$CH$_3$ Pyr), 28.6 (*C*H(CH$_3$)$_2$ NCN), 28.5 (*C*H(CH$_3$)$_2$ NCNH), 28.0 (NC(*C*H$_3$)CH), 26.5 (CH(*C*H$_3$)$_2$), 26.4 (CH(*C*H$_3$)$_2$), 24.6 (CH(*C*H$_3$)$_2$), 24.7 (CH$_2$*C*H$_3$), 24.5 (3-CH$_2$*C*H$_3$ Pyr), 23.7 (CH(*C*H$_3$)$_2$), 23.2 (CH(*C*H$_3$)$_2$).

7.3 Hydroboration of Pyridines

General Procedure: *Methyl- and phenyl-substituted pyridines*

To 0.5 mL of an 0.08 M solution of the magnesium precatalyst in C_6D_6 or d_8-toluene (10 mol%) were added 400 μmol of the pyridine derivative and 64.0 μL (440 μmol) of pinacolborane. The solution was transferred to a sealed Youngs tap NMR tube, heated at 70 ^oC, and the reaction was regularly monitored by ^1H and ^{11}B NMR spectroscopy until complete conversion of the reactants or until the reaction ceased. For scale-up experiments, 100 mg of the magnesium precatalyst (0.2 mmol) was dissolved in 4 mL of hexanes. Pinacolborane (306 μL, 2.1 mmol) was added, followed by the pyridine derivative (2 mmol). The reaction mixture was left to stir overnight at 70 ^oC under argon. After removal of the solvent *in vacuo*, the product was either distilled *in vacuo* or recrystallised from hexanes at -30 ^oC.

Hydroboration of pyridine

NMR scale: 32.3 μL of pyridine. **Large scale:** 161 μL of pyridine. The product mixture was isolated by recrystallisation of the crude reaction mixture in hexanes at -30 ^oC to yield pale yellow low-melting crystals (253 mg, 59% yield).

35. ***N-{B(OCMe$_2$)$_2$}-1,2-dihydropyridine***

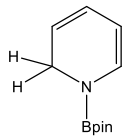

^1H NMR (300 MHz, C_6D_6, 300 K) δ_H (ppm): 6.70 (1H, m, NCHCHC*H*), 5.78 (1H, m, NCHC*H*), 5.10 (1H, m, NCH$_2$C*H*), 5.05 (1H, d, J_{HH} = 5.4 Hz, NC*H*), 4.14 (2H, d, J_{HH} = 4.3 Hz, NC*H*$_2$), 1.00 (12H, s, C(C*H*$_3$)$_2$). $^{13}C\{^1H\}$ NMR (75 MHz, C_6D_6, 300 K) δ_C (ppm): 132.6 (N*C*H), 124.2 (NCHCH*C*H), 114.9 (NCH$_2$*C*H), 103.8 (NCH*C*H), 83.1 (*C*(CH$_3$)$_2$), 42.5 (N*C*H$_2$), 22.8 (C(*C*H$_3$)$_2$). ^{11}B NMR (96 MHz, C_6D_6, 300 K) δ_B (ppm): 27.1 (s, *B*-N).

36. ***N-{B(OCMe$_2$)$_2$}-1,4-dihydropyridine***

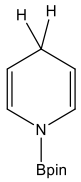

^{1}H NMR (300 MHz, C_6D_6, 300 K) δ_H (ppm): 6.51 (2H, d, J_{HH} = 8.4 Hz, NC*H*), 4.56 (2H, m, NCHC*H*), 2.81 (2H, m, NCHCHCH_2), 0.96 (s, 12H, C(CH_3)$_2$). ^{13}C{^{1}H} NMR (75 MHz, C_6D_6, 300 K) δ_C (ppm): 127.5 (N*C*H), 102.8 (NCH*C*H), 83.3 (*C*(CH$_3$)$_2$), 25.0 (NCHCH- *C*H$_2$), 24.7 (C(*C*H$_3$)$_2$). ^{11}B NMR (96 MHz, C_6D_6, 300 K) δ_B (ppm): 27.1 (s, *B*N).

Hydroboration of 2-picoline

NMR scale: 39.5 μL of 2-picoline

37. ***N-{B(OCMe$_2$)$_2$}-1,2-dihydro-2-methylpyridine***

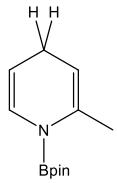

^{1}H NMR (300 MHz, C_6D_6, 300 K) δ_H (ppm): 6.73 (1H, m, NC*H*), 4.67 (1H, m, NCHC*H*), 4.45 (1H, m, NC(CH$_3$)C*H*), 2.82 (2H, m, NCHCHCH_2), 2.03 (3H, m, NC(CH_3)) 1.09 (s, 12H, C(CH_3)$_2$). ^{13}C{^{1}H} NMR (75 MHz, C_6D_6, 300 K) δ_C (ppm): 135.7 (N*C*(CH$_3$)), 129.8 (N*C*H), 102.8 (NCH*C*H), 102.5 (N(CH$_3$)*C*H), 82.7 (*C*(CH$_3$)$_2$), 24.5 (C(*C*H$_3$)$_2$), 23.9 (NCHCH*C*H$_2$), 22.4 (NC(*C*H$_3$)). ^{11}B NMR (96 MHz, C_6D_6, 300 K) δ_B (ppm): 27.4 (s, *B*-N).

Hydroboration of 3-picoline

NMR scale: 39.0 μL of 3-picoline. **Large scale:** 195 μL of 3-picoline. The product mixture was isolated as a thick pale yellow oil by vacuum distillation at 67 ^{o}C, 0.1 mbar (258 mg, 58% yield), which crystallized overnight as a low-melting solid (Mp ~ 20 ^{o}C).

38. ***N-{B(OCMe$_2$)$_2$}-1,2-dihydro-3-methylpyridine***

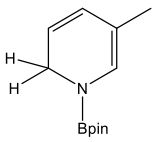

^{1}H NMR (300 MHz, C_6D_6, 300 K) δ_H (ppm): 6.57 (1H, m NC*H*), 5.51 (1H, m, NCH$_2$CHC*H*), 5.03 (1H, m, NCH$_2$C*H*), 4.08 (2H, m, NCH_2), 1.48 (3H, s, NCHC(CH_3)), 1.09 (12H, s, C(CH_3)$_2$). ^{13}C{^{1}H} NMR (75 MHz, C_6D_6, 300 K) δ_C (ppm): 129.3 (N*C*H), 124.7(NCH$_2$CH*C*H), 110.4 (NCH*C*(CH$_3$)), 103.1 (NCH$_2$*C*H), 83.1 (*C*(CH$_3$)$_2$), 47.3 (N*C*H$_2$), 24.8 (C(*C*H$_3$)$_2$), 20.7 (NCHC(*C*H$_3$)). ^{11}B NMR (96 MHz, C_6D_6, 300 K) δ_B (ppm): 27.2 (s, *B*-N).

39. ***N-{B(OCMe$_2$)$_2$}-1,4-dihydro-3-methylpyridine***

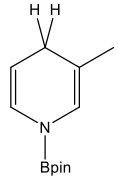

^{1}H NMR (300 MHz, C_6D_6, 300 K) δ_H (ppm): 6.60 (1H, m, NC*H*), 6.37 (1H, m, NC*H*C(CH$_3$)), 4.63 (1H, m, NCHC*H*), 2.71 (2H, m, NCHCHCH_2), 1.46 (3H, s, NCHC(CH_3)), 1.06 (12H, s, C(CH_3)$_2$). ^{13}C{^{1}H} NMR (75 MHz, C_6D_6, 300 K) δ_C (ppm): 127.0 (N*C*H), 122.1 (N*C*HC(CH$_3$)), 118.6 (NCH*C*(CH$_3$)), 102.0

(NCH*C*H), 83.2 (*C*(CH_3)$_2$), 28.4 (NCHCH*C*H_2), 24.6 (C(*C*H_3)$_2$), 20.8 (NCHC(*C*H_3)). ^{11}B NMR (96 MHz, C_6D_6, 300 K) δ_B (ppm): 27.2 (s, *B*-N).

Hydroboration of 3,5-lutidine

NMR scale: 45.4 μL of 3,5-lutidine. **Large scale:** 227 μL of 3,5-lutidine. The product mixture was isolated by vacuum distillation at 90 ^{o}C, 0.1 mbar, as a colourless oil which crystallised overnight (370 mg, 77% yield, Mp ~ 20 ^{o}C). Elemental analysis: Calculated(found) for $C_{13}H_{23}NBO_2$: C 66.41(66.36); H 9.43(9.35); N 5.96(5.81) .

40. *N-{B(OCMe$_2$)$_2$}-1,2-dihydro-3,5-dimethylpyridine*

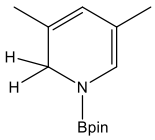

^{1}H NMR (300 MHz, C_6D_6, 300 K) δ_H (ppm): 6.42 (1H, s, NC*H*), 5.43 (1H, s, NCHC(CH$_3$)C*H*), 4.03 (2H, s, NC*H*$_2$), 1.62 (3H, s, NCH$_2$C(C*H*$_3$)), 1.47 (3H, s, NCHC(C*H*$_3$)), 1.05 (12H, s, C(C*H*$_3$)$_2$). ^{13}C{^{1}H} NMR (75 MHz, C_6D_6, 300 K) δ_C (ppm): 125.5 (NC- H$_2$*C*(CH$_3$)), 124.6 (N*C*H), 122.6 (NCHC(CH$_3$)*C*H), 111.1 (NCH*C*(CH$_3$)), 82.8 (*C*(CH$_3$)$_2$), 47.1 (N*C*H$_2$), 25.0 (NCH$_2$C(*C*H$_3$)), 24.8 (C(*C*H$_3$)$_2$), 18.1 (NCHC(*C*H$_3$)). ^{11}B NMR (96 MHz, C_6D_6, 300 K) δ_B (ppm): 27.3 (s, *B*-N).

41. *N-{B(OCMe$_2$)$_2$}-1,4-dihydro-3,5-dimethylpyridine*

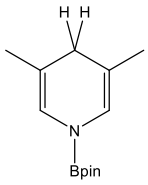

^{1}H NMR (300 MHz, C_6D_6, 300 K) δ_H (ppm): 6.44 (2H, s, NC*H*), 2.56 (2H, s, NCHC(CH$_3$)C*H*$_2$), 1.47 (6H, s, NCHC(C*H*$_3$)), 1.02 (12H, s, C(C*H*$_3$)$_2$). ^{13}C{^{1}H} NMR (75 MHz, C_6D_6, 300 K) δ_C (ppm): 121.7 (N*C*H), 109.6 (NCH*C*(CH$_3$)), 83.1 (*C*(CH$_3$)$_2$), 34.1 (NCHC(CH$_3$)*C*H$_2$), 24.7 (C(*C*H$_3$)$_2$), 20.6 (NCHC(*C*H$_3$)). ^{11}B NMR (96 MHz, C_6D_6, 300 K) δ_B (ppm): 27.3 (s, *B*N).

Hydroboration of 4-picoline

NMR scale: 39.5 μL of 4-picoline. **Large scale:** 195 μL of 4-picoline. The product mixture was isolated by recrystallisation of the crude reaction mixture in hexanes at -30 ^{o}C to yield a colourless crystalline solid (302 mg, 68% yield).

42. *N-{B(OCMe$_2$)$_2$}-1,2-dihydro-4-methylpyridine*

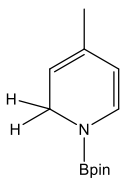

^{1}H NMR (300 MHz, C_6D_6, 300 K) δ_H (ppm): 6.69 (1H, d, J_{HH} = 7.5 Hz, NC*H*), 4.95 (1H, m, NCHC*H*), 4.82-4.90 (1H, m, NCH$_2$C*H*), 4.15 (2H, m, NC*H*$_2$), 1.57 (3H, m, NCHCHCH(C*H*$_3$)), 1.01 (12H, s, C(C*H*$_3$)$_2$). ^{13}C{^{1}H} NMR (75 MHz, C_6D_6, 300 K) δ_C (ppm): 132.3 (N*C*H), 131.8 (NCHCH*C*H(CH$_3$)), 110.4 (NCH*C*H), 106.8 (NCH$_2$*C*H), 83.1 (*C*(CH$_3$)$_2$), 43.0 (N*C*H$_2$), 24.7 (C(*C*H$_3$)$_2$), 20.7 (NCHCHCH(*C*H$_3$)). ^{11}B NMR (96 MHz, C_6D_6, 300 K) δ_B (ppm): 27.1 (s, *B*-N).

43. ***N-{B(OCMe$_2$)$_2$}-1,4-dihydro-4-methylpyridine***

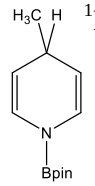

^{1}H NMR (300 MHz, C_6D_6, 300 K) δ_H (ppm): 6.51 (2H, m, NC*H*), 4.57 (2H, m, NCHC*H*), 3.02 (1H, m, NCHCHC*H*(CH_3)), 1.04-1.06 (3H, m, NCHCHCH(CH_3)), 1.0 (12H, s, C(CH_3)$_2$). ^{13}C{^{1}H} NMR (75 MHz, C_6D_6, 300 K) δ_C (ppm): 126.0 (N*C*H), 108.8 (NCH*C*H), 83.4 (*C*(CH_3)$_2$), 27.7 (NCHCH*C*H), 25.0 (NCHCHCH(*C*H_3)), 24.6 (C(*C*H_3)$_2$). ^{11}B NMR (96MHz, C_6D_6, 300 K) δ_B (ppm): 27.1 (s, *B*-N).

Hydroboration of 4-phenylpyridine

NMR scale: 62 mg of 4-phenylpyridine. **Large scale:** 310 mg of 4-phenylpyridine. The product mixture was isolated by recrystallisation of the crude reaction mixture in hexanes at -30 ^{o}C to yield a colourless crystalline solid (453 mg, 80% yield).

44. ***N-{B(OCMe$_2$)$_2$}-1,2-dihydro-4-phenylpyridine***

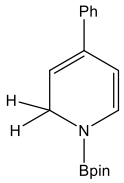

^{1}H NMR (300 MHz, C_6D_6, 300 K) δ_H (ppm): 7.14-7.35 (2H, m, *p*-Ph-*H*), 7.08-7.18 (3H, m, *o*/*m*-Ph-*H*), 6.86 (1H, m, NC*H*), 5.52 (1. H, m, NCHC*H*), 5.36 (1H, m, NCH_2CH), 4.28 (2H, d, J_{HH} = 4.5 Hz, NCH_2), 1.05 (12H, s, C(CH_3)$_2$). ^{13}C{^{1}H} NMR (75 MHz, C_6D_6, 300 K) δ_C (ppm): 140.2 (N*C*H), 136.1 (*i*-Ph-*C*), 133.6 (NCHCH*C*(Ph)), 128.6 (*o*-Ph-*C*), 127.3 (*p*-Ph-*C*), 125.8 (*m*-Ph-*C*), 111.3 (NCH*CH*), 104.5 (NCH_2CH), 83.3 (*C*(CH_3)$_2$), 43.2 (NCH_2), 24.7 (C(*C*H_3)$_2$). ^{11}B NMR (96 MHz, C_6D_6, 300 K) δ_B (ppm): 27.2 (s, *B*-N).

General Procedure: *Hydroboration of quinoline and iso-quinoline*

To 0.5 mL of an 0.04 M solution of the magnesium precatalyst in C_6D_6 (5 mol%) were added 400 μmol of the pyridine derivative and 61.0 μL (420 μmol) of pinacolborane. The solution was transferred to a sealed Youngs tap NMR tube, and the reaction was regularly monitored by ^{1}H and ^{11}B NMR spectroscopy at room temperature until complete conversion of the reactants. For scale-up experiments, 50 mg of the magnesium precatalyst (0.1 mmol) was dissolved in 4 mL of hexanes. Pinacolborane (306 μL, 2.1 mmol) was added, followed by the quinoline derivative (2 mmol). The reaction mixture was left to stir overnight at room temperature under argon. After removal of the solvent *in vacuo*, the product was either distilled *in vacuo* or recrystallised from hexanes at –30 ^{o}C.

Hydroboration of quinoline

NMR scale: 47.0 μL of quinoline. **Large scale:** 236 μL of quinoline. The product was recrystallised from the crude reaction mixture in hexanes at -30 ^{o}C. Three crops of colourless crystals were isolated (380 mg, 72%).

45. ***N*-{B(OCMe$_2$)$_2$}-1,4-dihydroquinoline**

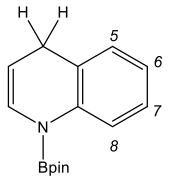

^{1}H NMR (300 MHz, C_6D_6, 300 K) δ_H (ppm): 7.78 (1H, d, J_{HH} = 8.1 Hz, *H*-5), 7.07 (1H, m, *H*-6), 6.83 (1H, m, *H*-7), 6.80 (1H, m, *H*-8), 6.24 (1H, d, J_{HH} = 9.6 Hz, NCH$_2$CHC*H*), 5.57 (1H, m, NCH$_2$C*H*), 4.14 (2H, d, J_{HH} = 4.0 Hz, NC*H*$_2$), 1.03 (12H, s, C(CH$_3$)$_2$). ^{13}C{^{1}H} NMR (75 MHz, C_6D_6, 300 K) δ_C (ppm): 142.3 (N*C*), 128.1 (*C*-6), 126.9 (NCH$_2$CH*C*H), 126.8 (*C*-7), 124.6 (NCH$_2$*C*H), 124.1 (NCH$_2$CHCH*C*), 121.9 (*C*-8), 121.2 (*C*-5), 82.8 (*C*(CH$_3$)$_2$), 43.6 (N*C*H$_2$), 24.7 (C(*C*H$_3$)$_2$). ^{11}B NMR (96 MHz, C_6D_6, 300 K) δ_B (ppm): 27.3 (s, *B*-N).

Hydroboration of iso-quinoline

NMR scale: 47.3 μL of *iso*-quinoline. **Large scale:** 235 μL of *iso*-quinoline. The product was isolated as a viscous colourless oil by vacuum distillation at 110 ^{o}C, 0.1 mbar (238 mg, 50% yield, Mp ~ 10 ^{o}C).

46. ***N*-{B(OCMe$_2$)$_2$}-1,2-dihydro-iso-quinoline**

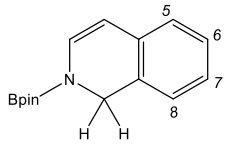

^{1}H NMR (300 MHz, C_6D_6, 300 K) δ_H (ppm): 6.99 (1H, m, *H*-6), 6.89 (1H, m, *H*-7), 6.82 (1H, d, J_{HH} = 7.4 Hz, NC*H*), 6.80 (1H, m, *H*-5), 6.72 (1H, m, *H*-8), 5.62 (1H, d, J_{HH} = 7.4 Hz, NCHC*H*), 4.62 (2H, s, NC*H*$_2$), 1.02 (12H, s, C(C*H*$_3$)$_2$). ^{13}C{^{1}H} NMR (75 MHz, C_6D_6, 300 K) δ_C (ppm): 133.6 (NCH$_2$*C*), 132.8 (N*C*H), 129.0 (NCHCH*C*), 127.6 (*C*-8), 126.1 (*C*-7), 125.4 (*C*-6), 123.7 (*C*-5), 106.2 (NCH*C*H), 83.3 (*C*(CH$_3$)$_2$), 46.2 (N*C*H$_2$), 24.7 (C(*C*H$_3$)$_2$). ^{11}B NMR (96 MHz, C_6D_6, 300 K) δ_B (ppm): 27.0 (s, *B*-N).

General Procedure: *Functional group tolerance*

To 0.5 mL of an 0.08 M solution of the magnesium precatalyst in C_6D_6 or d_8-toluene (10 mol%) were added 400 μmol of the pyridine derivative and 64.0 μL (440 μmol) of pinacolborane. The solution was transferred to a sealed Youngs tap NMR tube, heated at 70 ^{o}C, and the reaction was regularly monitored by ^{1}H and ^{11}B NMR spectroscopy until complete conversion of the reactants or until conversion stopped.

Hydroboration of 3-pyridinecarboxaldehyde

NMR scale: 37.5 μL of 3-pyridinecarboxaldehyde

47. ***O*-{B(OCMe$_2$)$_2$}-3-oxymethylpyridine**

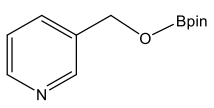

^{1}H NMR (300 MHz, C_6D_6, 300 K) δ_H (ppm): 8.78 (1H, d, J_{HH} = 1.8 Hz, NC*H*C(R)), 8.57 (1H, m, NC*H*), 7.45 (1H, m, NCHCHC*H*), 6.85 (1H, m,

NCHC*H*), 4.85 (2H, s, NCHC(CH_2)), 1.14(12H, s, C(CH_3)$_2$). ^{13}C{^{1}H} NMR (75 MHz, C_6D_6, 300 K) δ_C (ppm): 149.3 (N*C*HC(R)), 149.2 (N*C*H), 134.9 (NCH*C*(R)), 134.3 (NCHCH*C*H), 123.2 (NCH*C*H), 82.9 (*C*(CH$_3$)$_2$), 24.6 (C(*C*H$_3$)$_2$). ^{11}B NMR (96 MHz, C_6D_6, 300 K) δ_B (ppm): 25.9 (s, *B*-O).

Hydroboration of 3-cyanopyridine

NMR scale: 42 mg of 3-cyanopyridine, 3 eq. of pinacolborane

48. *N,N',N'-{B(OCMe2)2}3-3-aminomethyl-1,2-dihydropyridine*

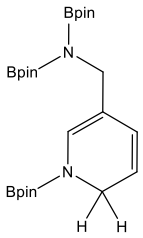

^{1}H NMR (300 MHz, C_6D_6, 300 K) δ_H (ppm): 6.52 (1H, d, J_{HH} = 7.3 Hz, NC*H*), 5.86 (1H, d, J_{HH} = 5.7 Hz, NCHCHC*H*), 5.04 (1H, m, NCHC*H*), 4.29 (2H, s, NCH_2), 3.82 (2H, s, NCH$_2$C(CH_2)). Signals for the pinacol methyl groups were overlapping with those of B. The species was not present in sufficient concentration to determine ^{13}C{^{1}H} and ^{11}B NMR data.

49. *N,N',N'-{B(OCMe2)2}3-3-aminomethyl-1,4-dihydropyridine*

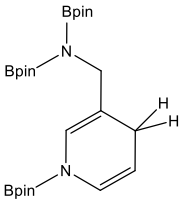

^{1}H NMR (300 MHz, C_6D_6, 300 K) δ_H (ppm): 6.62 (1H, m, NC*H*), 6.37 (1H, br. s, NC*H*C(CR)), 4.53 (1H, m, NCHC*H*), 4.11 (2H, s, NCHC(CH_2)), 2.66 (2H, m, NCHCHCH_2), 1.03 (24H, s, C(CH_3)$_2$)), 1.02 (12H, s, C(CH_3)$_2$). ^{13}C{^{1}H} NMR (75 MHz, C_6D_6, 300 K) δ_C (ppm): 129.6, 124.0, 123.1, 100.4, 82.7, 82.6, 42.5 (NCHC(*C*H$_2$)), 28.4 (NCH*C*(CH$_2$)), 24.8 (C(*C*H$_3$)$_2$), 24.7 (C(*C*H$_3$)$_2$).

Hydroboration of 4-cyanopyridine

NMR scale: 42 mg of 4-cyanopyridine, 3 eq. of pinacolborane

50. *N,N-{B(OCMe$_2$)$_2$}$_2$-4-aminomethylpyridine*

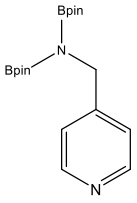

(Formed at room temperature) ^{1}H NMR (300 MHz, C_6D_6, 300 K) δ_H (ppm): 8.54 (2H, d, J_{HH} = 5.2 Hz, NC*H*), 7.13 (2H, d, J_{HH} = 5.2Hz, NCHC*H*), 4.33 (2H, s, NCHCHC(CH_2)), 1.01 (24H, s, C(CH_3)$_2$). ^{13}C{^{1}H} NMR (75 MHz, C_6D_6, 300 K) δ_C (ppm): 152.1 (NCHCH*C*), 149.7 (N*C*H), 122.4 (NCH*C*H), 83.0(*C*(CH$_3$)$_2$), 46.9 (NCHCHC(*C*H$_2$)), 25.0 (C(*C*H$_3$)$_2$). ^{11}B NMR (96 MHz, C_6D_6, 300 K) δ_B (ppm): 25.8 (br. *B*-N).

51. ***N,N',N'-{B(OCMe$_2$)$_2$}$_3$-4-aminomethyl-1,2-dihydropyridine***

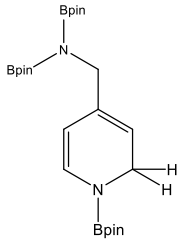

(Obtained at 80 °C) ^{1}H NMR (300 MHz, C_6D_6, 300 K) δ_H (ppm): 6.66 (1H, m, NC*H*), 5.29 (1H, m, NCHC*H*), 5.24 (1H, m, NCH$_2$C*H*), 4.22 (2H, m, NC*H$_2$*), 3.90 (2H, s, NCHCHC(C*H$_2$*)), 0.89 (24H, s, C(C*H$_3$*)$_2$), 0.86 (12H, s, C(C*H$_3$*)$_2$). ^{11}B NMR (96 MHz, C_6D_6, 300 K) δ_B (ppm): 27.6 + 25.8 (br. *B*-N).

52. ***N,N',N'-{B(OCMe$_2$)$_2$}$_3$-4-aminomethyl-1,4-dihydropyridine***

The formation of compound **52** was easily recognisable by its characteristic multiplet at 2.78 ppm, but could not be fully assigned due to its low concentration in solution.

7.4 Hydroboration of Nitriles

Catalytic reactions

General Procedure NMR scale: 10 mg (0.02 mmol, i.e. 10 mol%) of **Ib** was dissolved in 0.5 ml of C_6D_6 60.9 μL (0.42 mmol) of pinacolborane was then added followed by 0.2 mmol of nitrile. This mixture was then transferred to a sealed Youngs tap NMR tube and the reaction was kept in an oil bath at 60 °C. The reactions were regulary monitored by ^{1}H and ^{11}B NMR spectroscopy until complete conversion was observed.

General Procedure Large Scale: In a Schlenk flask 50mg (0.1 mmol, i.e. 10 mol%) of **Ib** was dissolved in 5 ml of toluene, 304.7 μL (2.1 mmol) of pinacolborane was then added followed by 1 mmol of nitrile. This mixture was then transferred to an oil bath at 60 °C for the observed NMR reaction time. Toluene was then removed *in vacuo* and the remaining solid was redissolved in the minimum volume of hexane and left to crystallise in the freezer overnight.

Hydroboration of propionitrile

53. ***N-{B(OCMe$_2$)$_2$}-propan-1-amine***

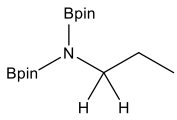

NMR Scale: 14.3 μL of propionitrile. ***Large scale:*** 71.3 μL of propionitrile, 60 °C for 1 hr. Isolated yellow crystals (228 mg, 70% yield). ^{1}H NMR (300 MHz, C_6D_6, 300 K) δ_H (ppm): 3.42 (2H, t, J_{HH} = 6 Hz, NC*H$_2$*), 1.75 (2H, m, J_{HH} = 6 Hz, C*H$_2$*CH$_3$), 1.07 (24H, s, OCC*H$_3$*), 0.96 (3H, J_{HH} = 9 Hz, CH$_2$C*H$_3$*). ^{13}C{^{1}H} NMR (75.5 MHz, C_6D_6, 300 K) δ_C (ppm): 82.6 (O*C*(CH$_3$)$_2$), 46.5 (N*C*H$_2$), 27.2 (CH$_2$*C*H$_2$CH$_3$), 25.1 (OC(*C*H$_3$)$_2$), 11.9 (CH$_2$*C*H$_3$). ^{11}B NMR (96.3 MHz, C_6D_6, 300 K) δ_B (ppm): 29.5 N*B*.

Hydroboration of isobutyronitrile

54. ***N-{B(OCMe$_2$)$_2$}-2-methylpropan-1-amine***

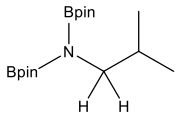

NMR scale: 18.0 μL of isobutyronitrile. ***Large scale:*** 89.8 μL of isobutyronitrile. Isolated yellow oil (313 mg, 96% yield). ^{1}H NMR (300 MHz, C_6D_6, 300 K) δ_H (ppm): 3.28 (2H, d, J_{HH} = 6 Hz, NCH_2), 2.05 (1H, m, J_{HH} = 6 Hz, CH(CH$_3$)$_2$), 1.07 (24H, s, OC(CH_3)$_2$), 1.01 (6H, d, J_{HH} = 6 Hz, CH(CH_3)$_2$). ^{13}C{^{1}H} NMR (75.5 MHz, C_6D_6, 300 K) δ_C (ppm): 82.6 (OC(CH$_3$)$_2$), 52.1 (NCH$_2$), 31.6 (CH(CH$_3$)$_2$), 25.1 (OC(CH$_3$)$_2$), 20.7 (CH(CH$_3$)$_2$). ^{11}B NMR (96.3 MHz, C_6D_6, 300 K) δ_B (ppm): 29.6 N*B*.

Hydroboration of Trimethylacetonitrile

55. ***N-{B(OCMe$_2$)$_2$}-2,2-dimethylpropan-1-amine***

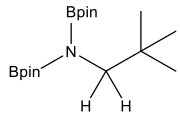

NMR scale: 22.1 μL trimethylacetonitrile. ***Large scale:*** 110.5 μL of trimethylacetonitrile. Isolated colourless crystals (181 mg, 54% yield). ^{1}H NMR (300 MHz, C_6D_6, 300 K) δ_H (ppm): 3.30 (2H, s, NCH_2), 1.08 (24H, s, OC(CH_3)$_2$), 1.03 (9H, s, C(CH_3)$_3$). ^{13}C{^{1}H} NMR (75.5 MHz, C_6D_6, 300 K) δ_C (ppm): 82.6 (OC(CH$_3$)$_2$), 55.3 (NCH$_2$), 34.0 (C(CH$_3$)$_3$), 28.4 (C(CH$_3$)$_3$), 25.1 (OC(CH$_3$)$_2$)). ^{11}B NMR (96.3MHz, C_6D_6, 300 K) δ_B (ppm): 29.5 N*B*.

Hydroboration of Cyclohexanitrile

56. ***N-{B(OCMe$_2$)$_2$}–cyclohexylmethanamine***

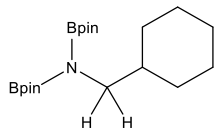

NMR scale*:** 23.8 μL cyclohexanitrile. ***Large scale: 118.8 μL of cyclohexanitrile, 60 ^{o}C for 1 hr. Isolated colourless crystals (265 mg, 75% yield). ^{1}H NMR (300 MHz, C_6D_6, 300 K) δ_H (ppm): 3.31 (2H, d, J_{HH} = 6 Hz, NCH_2), 1.92 (2H, m, NCH$_2$CH) 1.70 – 1.20 (10H, m, Cy-*H*), 1.07 (24H, s, OCCH_3). ^{13}C{^{1}H} NMR (75.5 MHz, C_6D_6, 300 K) δ_C (ppm): 82.6 (OC(CH$_3$)$_2$), 50.8 (NCH$_2$), 41.3 (NCH$_2$$C$H), 31.5 (Cy-*C*), 27.6 (Cy-*C*), 27.0 (Cy-*C*), 25.1 (OC(CH$_3$)$_2$). ^{11}B NMR (96.3 MHz, C_6D_6, 300 K) δ_B (ppm): 29.7 N*B*.

Hydroboration of benzonitrile

57. ***N-{B(OCMe$_2$)$_2$}–phenylmethanamine***

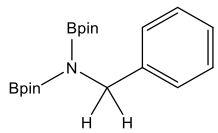

NMR scale: 19.5 μL benzonitrile. ***Large scale:*** 103.12 μL of benzonitrile, 60 ^{o}C for 15 hrs. Isolated colourless crystals (202 mg, 56% yield). ^{1}H NMR (300 MHz, C_6D_6, 300 K) δ_H (ppm): 7.57 (2H, m, *o*-H), 7.25 (2H, m, *m*-*H*), 7.11 (1H, m, *p*-*H*), 4.60 (2H, s, NCH_2), 1.02 (24H, s, OC(CH_3)$_2$). ^{13}C{^{1}H} NMR (75.5 MHz,

C_6D_6, 300 K) δ_C (ppm): 144.1 (*o*-*C*), 128.4 (*p*-C), 127.0 (*m*-*C*), 82.9 O*C*$(CH_3)_2$, 48.2 (N*C*H_2), 25.1 (OC(*C*$H_3)_2$). ^{11}B NMR (96.3 MHz, C_6D_6, 300 K) δ_B (ppm): 29.5 N*B*.

Hydroboration of o-tolunitrile

58. ***N-{B(OCMe$_2$)$_2$}-o-tolylmethanamine***

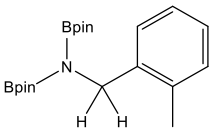

NMR scale: 23.7 µL *o*-tolunitrile. ***Large scale:*** 118.5 µL of *o*-tolunitrile, 60 ^oC for 15 hrs. Isolated colourless crystals (275 mg, 73% yield). ^{1}H NMR (300 MHz, C_6D_6, 300 K) δ_H (ppm): 7.64 (1H, d, J_{HH} = 6 Hz, *o*-*H*), 7.24 (1H, m, *p*-H), 7.08 (1H, m, *m*-*H*), 7.00 (1H, m, *m*-*H*), 4.60 (2H, s, NCH_2), 2.12 (3H, s, *o*-CH_3), 1.03 (24H, s, OC(C$H_3)_2$). ^{13}C{^{1}H} NMR (75.5 MHz, C_6D_6, 300 K) δ_C (ppm): 141.5 (*o*-*C*), 135.7 (*o*-*C*CH_3), 130.5 (*p*-*C*), 126.3 (*m*-*C*), 125.9 (*m*-*C*HC(CH_3), 82.9 (O*C*$(CH_3)_2$), 45.8 (N*C*H_2), 25.0 (OC(*C*$H_3)_2$), 19.4 (*o*-*C*H_3). ^{11}B NMR (96.3 MHz, C_6D_6, 300 K) δ_B (ppm): 29.8 N*B*. Elemental Analysis for $C_{20}H_{33}B_2NO_4$ (M_w = 373.11), Calculated (found): C 64.40 (64.45); H 8.92 (8.85); N 3.75 (3.63).

Hydroboration of m-tolunitrile

59. ***N-{B(OCMe$_2$)$_2$}-m-tolylmethanamine***

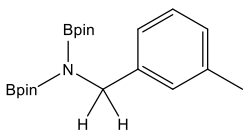

NMR scale: 22.0 µL *m*-tolunitrile. ***Large scale:*** 120.0 µL of *m*-tolunitrile, 60 ^oC for 15 hrs. Isolated colourless crystals (305 mg, 81% yield). ^{1}H NMR (300 MHz, C_6D_6, 300 K) δ_H (ppm): 7.43 (1H, d, J_{HH} = 6 Hz, *o*-*H*), 7.38 (1H, s, *o*-*H*), 7.20 (1H, m, *p*-*H*), 6.95 (1H, m, *m*-*H*), 4.60 (2H, s, NCH_2), 2.19 (3H, s, *m*-CH_3), 1.04 (24H, s, OC(C$H_3)_2$). ^{13}C{^{1}H} NMR (75.5 MHz, C_6D_6, 300 K) δ_C (ppm): 144.0 (*o*-*C*), 137.8 (*o*-*C*HC(CH_3)), 129.3 (*p*-*C*), 128.7 (*i*-C) 127.7 (*m*-*C*CH_3), 125.4 (*m*-*C*), 82.9 (O*C*$(CH_3)_2$), 48.2 (N*C*H_2), 25.1 (OC(*C*$H_3)_2$), 21.9 (Ar*C*H_3). ^{11}B NMR (96.3 MHz, C_6D_6, 300 K) δ_B (ppm): 29.9 N*B*.

Hydroboration of 3-(fluoro)benzonitrile

60. ***N-{B(OCMe$_2$)$_2$}-3-(fluoro)phenylmethanamine***

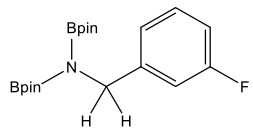

NMR scale: 21.4 µL 3-(fluoro)benzonitrile. ***Large scale:*** 106.9 µL of 3-(fluoro)benzonitrile, 60 ^oC for 14 hrs. Isolated pale yellow crystals (215 mg, 59% yield). ^{1}H NMR (300 MHz, C_6D_6, 300 K) δ_H (ppm): 7.40 (1H, m, *o*-C*H*), 7.25 (1H, d, J_{HH} = 7.3 Hz, *o*-C*H*), 7.00 (2H, m, *m*-C*H*, *p*-C*H*), 4.51 (2H, s, NCH_2), 1.02 (24H, s, OC(C$H_3)_2$). ^{13}C{^{1}H} NMR (75.5 MHz, C_6D_6, 300 K) δ_C (ppm): 130.2 (*o*-*C*), 128.7 (*o*-*C*), 128.5 (*p*-*C*), 128.5 (*m*-*C*), 128.3 (*m*-*C*), 83.1 (O*C*$(CH_3)_2$), 47.8 (N*C*H_2), 25.0 (OC(*C*$H_3)_2$). ^{11}B NMR (96.3 MHz, C_6D_6, 300 K) δ_B (ppm): 29.5 N*B*.

Hydroboration of 3-(methoxy)benzonitrile

61. ***N-{B(OCMe$_2$)$_2$}-3-(methoxy)phenylmethanamine***

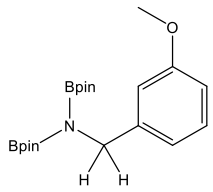

NMR scale: 24.5 μL 3-(methoxy)benzonitrile. ***Large scale:*** 122.3 μL of 3-(methoxy)benzonitrile, 60 ^{o}C for 15 hrs. Isolated pale yellow crystals (308 mg, 81% yield). ^{1}H NMR (300 MHz, C_6D_6, 300 K) δ_H (ppm): 7.26 (1H, m, *o*-C*H*), 7.25 (1H, m, *o*-C*H*), 6.78 (1H, m, *p*-C*H*), 6.64 (1H, m, *m*-C*H*), 4.64 (2H, s, NCH_2), 3.41 (3H, s, OCH_3), 1.05 (24H, s, OC(CH_3)$_2$). ^{13}C{^{1}H} NMR (75.5 MHz, C_6D_6, 300 K) δ_C (ppm): 129.7 (*o*-*C*), 128.7 (*o*-*C*), 128.5 (*p*-*C*), 128.3 (*m*-*C*, 82.9 (O*C*(CH$_3$)$_2$), 55.0 (O*C*H$_3$), 48.3 (N*C*H$_2$), 25.1 (OC(*C*H$_3$)$_2$). ^{11}B NMR (96.3 MHz, C_6D_6, 300 K) δ_B (ppm): 30.0 N*B*

Hydroboration of p-tolunitrile

62. ***N-{B(OCMe$_2$)$_2$}-p-tolylmethanamine***

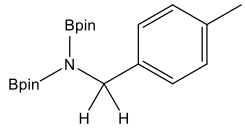

NMR scale: 23.9 μL *p*-tolunitrile. ***Large scale:*** 119.4 μL of *p*-tolunitrile, 60 ^{o}C for 15 hrs. Isolated colourless crystals (270 mg, 72% yield). ^{1}H NMR (300 MHz, C_6D_6, 300 K) δ_H (ppm): 7.50 (2H, d, J_{HH} = 9 Hz, *o*-*H*), 7.06 (2H, d, J_{HH} = 9 Hz, *m*-*H*), 4.58 (2H, s, NCH_2), 2.15 (3H, s, *p*-CH_3), 1.04 (24H, s, OC(CH_3)$_2$). ^{13}C{^{1}H} NMR (75.5 MHz, C_6D_6, 300 K) δ_C (ppm): 141.2 (*o*-*C*), 136.1 (*p*-*C*), 129.4 (*i*-*C*), 128.5 (*m*-*C*), 82.9 (O*C*(CH$_3$)$_2$), 47.9 (N*C*H$_2$), 25.1 (OC(*C*H$_3$)$_2$), 21.5 (*p*-*C*H$_3$). ^{11}B NMR (96.3 MHz, C_6D_6, 300 K) δ_B (ppm): 29.7 N*B*.

Hydroboration of 4-(fluoro)benzonitrile

63. ***N-{B(OCMe$_2$)$_2$}-4-(fluoro)phenylmethanamine***

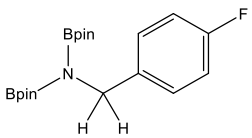

NMR scale: 21.9 μL 4-(fluoro)benzonitrile. ***Large scale:*** 109.4 μL of 4-(fluoro)benzonitrile, 60 ^{o}C for 15 hrs. Isolated colourless crystals (230 mg, 61% yield). ^{1}H NMR (300 MHz, C_6D_6, 300 K) δ_H (ppm): 7.40 (2H, m, *o*-*H*), 6.88 (2H, t, J_{HH} = 9 Hz, *m*-H), 4.45 (2H, s, NCH_2), 1.02 (24H, s, OC(CH_3)$_2$). ^{13}C{^{1}H} NMR (75.5 MHz, C_6D_6, 300 K) δ_C (ppm): 164.2 (*p*-*C*), 139.9 (*o*-*C*), 130.1 (*i*-*C*), 115.5 (*m*-*C*), 82.9 (O*C*(CH$_3$)$_2$), 47.5 (N*C*H$_2$), 25.1 (OC(*C*H$_3$)$_2$). ^{11}B NMR (96.3 MHz, C_6D_6, 300 K) δ_B (ppm): 29.7 N*B*. ^{19}F NMR (376.5 MHz, C_6D_6, 300 K) δ_F (ppm): -116.89 4-*F*

Hydroboration of 4-(chloro)benzonitrile

64. ***N-{B(OCMe$_2$)$_2$}-4-(chloro)phenylmethanamine***

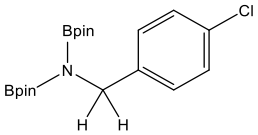

NMR scale: 27.5 mg 4-(chloro)benzonitrile. ***Large scale:*** 137.6 mg of 4-(chloro)benzonitrile, 60 ^{o}C for 12 hrs. Isolated pale yellow crystals (231 mg, 59% yield). ^{1}H NMR (300 MHz, C_6D_6, 300 K) δ_H (ppm): 7.36 (2H, d, J_{HH} = 7.3 Hz, *o*-C*H*), 7.20 (2H, d, J_{HH} = 7.3 Hz, *m*-C*H*), 4.46 (2H, s, NCH_2), 1.02 (24H, s, OC(CH_3)$_2$). ^{13}C{^{1}H} NMR (75.5 MHz, C_6D_6, 300 K) δ_C (ppm): 129.9 (*o*-*C*), 128.9 (*p*-*C*), 128.7 (*m*-*C*), 83.0 (O*C*(CH$_3$)$_2$), 47.5 (N*C*H$_2$), 25.1 (OC(*C*H$_3$)$_2$). ^{11}B NMR (96.3 MHz, C_6D_6, 300 K) δ_B (ppm): 29.0 (N*B*).

Hydroboration of 4-(trifluoromethyl)benzonitrile

65. ***N-{B(OCMe$_2$)$_2$}–4-(trifluoromethyl)phenylmethanamine***

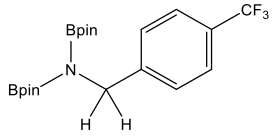

NMR scale: 26.8 µL 4-(trifluoromethyl)benzonitrile. ***Large scale:*** 133.9 µL of 4-(trifluoromethyl)benzonitrile, 60 ^{o}C for 15 hrs. Isolated colourless crystals (325 mg, 76% yield). ^{1}H NMR (300 MHz, C_6D_6, 300 K) δ_H (ppm): 7.41 (4H, s, Ar-*H*), 4.46 (2H, s, NCH_2), 1.01 (24H, s, OC(CH_3)$_2$). ^{13}C{^{1}H} NMR (75.5 MHz, C_6D_6, 300 K) δ_C (ppm): 148.1 (*o*-*C*), 128.5 (*p*-C), 125.6 (*m*-*C*), 83.1 (O*C*(CH$_3$)$_2$), 47.8 (N*C*H$_2$), 25.0 (OC(*C*H$_3$)$_2$). ^{11}B NMR (96.3 MHz, C_6D_6, 300 K) δ_B (ppm): 29.6 N*B*. ^{19}F NMR (376.5 MHz, C_6D_6, 300 K) δ_F (ppm): -61.94 CF_3.

Hydroboration of 4-(methoxy)benzonitrile

66. ***N-{B(OCMe$_2$)$_2$}–4-(methoxy)phenylmethanamine***

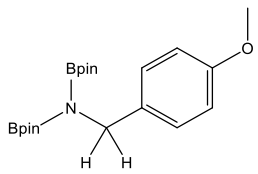

NMR scale: 26.6 mg 4-(methoxy)benzonitrile. ***Large scale:*** 133.2 mg of 4-(methoxy)benzonitrile, 60 ^{o}C for 15 hrs. Isolated colourless crystals (225 mg, 58% yield). ^{1}H NMR (300 MHz, C_6D_6, 300 K) δ_H (ppm): 7.53 (2H, d, J_{HH} = 6 Hz, *o*-*H*), 6.85 (2H, d, J_{HH} = 9 Hz, *m*-*H*), 4.54 (2H, s, NCH_2), 3.36 (3H, s, OCH_3), 1.04 (24H, s, OC(CH_3)$_2$). ^{13}C{^{1}H} NMR (75.5 MHz, C_6D_6, 300 K) δ_C (ppm): 159.3 (*p*-*C*), 136.4 (*o*-*C*), 129.8 (*i*-*C*), 114.2 (*m*-*C*), 82.9 (O*C*(CH$_3$)$_2$), 55.1 (O*C*H$_3$), 47.6 (N*C*H$_2$), 25.1 (OC(*C*H$_3$)$_2$). ^{11}B NMR (96.3 MHz, C_6D_6, 300 K) δ_B (ppm): 29.7 N*B*.

Hydroboration of diphenylacetonitrile

67. *N-{B(OCMe$_2$)$_2$}–diphenylacetoamine*

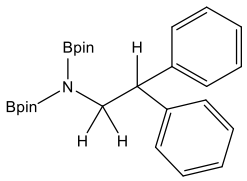

NMR scale*:** 38.6 mg diphenylacetonitrile. ***Large scale: 133.2 mg of diphenylacetonitrile, 60 ^{o}C for 30 hrs. Isolated colourless crystals (199 mg, 43% yield). ^{1}H NMR (300 MHz, C_6D_6, 300 K) δ_H (ppm): 7.43 (4H, d, J_{HH} = 6 Hz, *o-H*), 7.05 (4H, m, *m-H*), 6.94 (2H, m, *p-H*), 4.65 (1H, t, J_{HH} = 6 Hz, NCH$_2$C*H*), 4.10 (2H, d, J_{HH} = 9 Hz, NC*H*$_2$CH), 1.02 (24H, s, C(C*H*$_3$)$_2$). ^{13}C{^{1}H} NMR (75.5 MHz, C_6D_6, 300 K) δ_C (ppm): 144.28 (*ipso-C*), 129.62 (*o-C*), 128.87 (*p-C*), 126.71 (*m-C*), 82.70 (*C*(CH$_3$)$_2$), 54.44 (NCH$_2$*C*H), 49.55 (N*C*H$_2$CH), 25.07 (C(*C*H$_3$)$_2$). ^{11}B NMR (96.3 MHz, C_6D_6, 300 K) δ_B (ppm): 29.6 N*B*.

Stoichiometric Reactions

68. *LMgNCH^{t}Bu*

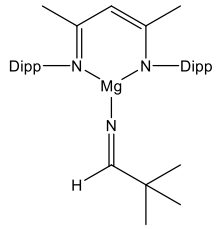

NMR Scale: **Ib** (0.04 mmol, 20 mg) was dissolved in 0.5 ml of C_6D_6 along with HBpin (0.04 mmol, 5.8 µL). This was left at room temperature for 5 minutes to form LMgH *in situ* before adding ^{t}BuCN (0.04 mmol, 4.4 µL). This was heated at 60 ^{o}C overnight to yield the insertion product, LMgNCH^{t}Bu. ^{1}H NMR (300 MHz, C_6D_6, 300 K) δ_H (ppm): 7.83 (1H, s, N=C*H*), 7.21 – 7.11 (6H, m, Ar-*H*), 4.85 (1H, s, NC(CH$_3$)C*H*), 3.32 (2H, sept, J_{HH} = 6 Hz, C*H*(CH$_3$)$_2$), 3.13 (2H, sept, J_{HH} = 6 Hz, C*H*(CH$_3$)$_2$), 1.66 (6H, s, NC(C*H*$_3$)CH), 1.43 (6H, d, J_{HH} = 9 Hz, CH(C*H*$_3$)$_2$), 1.23 (6H, d, J_{HH} = 9 Hz, CH(C*H*$_3$)$_2$), 1.20 (6H, d, J_{HH} = 9 Hz, CH(C*H*$_3$)$_2$), 1.12 (6H, d, J_{HH} = 9 Hz, CH(C*H*$_3$)$_2$), 1.03 (9H, s, C(C*H*$_3$)$_3$. ^{13}C{^{1}H} NMR (75 MHz, C_6D_6, 300 K) δ_C (ppm): 174.5 (N=*C*H), 170.5 (N*C*(CH$_3$)), 147.0 (*ipso-C*-Ar), 142.8 (*ortho-C*-Ar), 142.5 (*ortho-C*-Ar), 126.2 (*para-C*-Ar), 124.6 (*meta-C*-Ar), 96.1 (NC(CH$_3$)*C*H), 37.5 (N=CH*C*(CH$_3$)$_3$), 29.2 (*C*H(CH$_3$)$_2$), 27.2, 27.1, 26.1, 25.7, 25.0, 24.8.

69. *LMgNCHPh(3-MeO)*

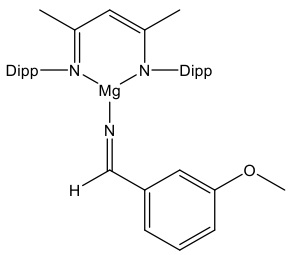

NMR Scale: **Ib** (0.06 mmol, 30 mg) was dissolved in 0.5 ml of C_6D_6 along with HBpin (0.06 mmol, 8.4 µL). This was left at room temperature for 5 minutes to form LMgH *in situ* before adding 3-(MeO)BnCN (0.06 mmol, 7.3 µL). This was heated at 60 ^{o}C overnight to yield the insertion product, LMgNCHPh(3-MeO). ^{1}H NMR (300 MHz, C_6D_6, 300 K) δ_H (ppm): 8.63 (1H, s, NC*H*), 7.56 – 6.80 (10H, m, Ar-*H*), 4.89 (1H, s, NC(CH$_3$)C*H*), 3.42 (3H, s, OC*H*$_3$), 3.29 (4H, m, C*H*(CH$_3$)$_2$), 1.68 (6H, s, NC(C*H*$_3$)CH), 1.42 (6H, d, J_{HH} = 6Hz, CH(C*H*$_3$)$_2$), 1.24 (6H, d, J_{HH} = 6Hz,

$CH(CH_3)_2$), 0.97 (6H, d, J_{HH} = 6Hz, $CH(CH_3)_2$), 0.90 (6H, d, J_{HH} = 6Hz, $CH(CH_3)_2$). $^{13}C\{^1H\}$ NMR (75 MHz, C_6D_6, 300 K) δ_C (ppm): 172.5 (N=*C*H), 170.4 (N*C*(CH_3)CH), 165.0, 160.9, 147.7, 145.2, 144.1, 142.9, 139.4, 130.3, 126.2, 124.8, 95.2 (NC(CH_3)*C*H), 55.6 (O*C*H_3), 32.3 (*C*H$(CH_3)_2$), 29.6, 28.7, 28.2, 27.2, 24.7, 23.4.

70. *LMgNCHPh(4-MeO)*

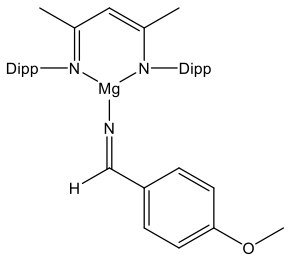

NMR Scale: **Ib** (0.06 mmol, 30 mg) was dissolved in 0.5 ml of C_6D_6 along with HBpin (0.06 mmol, 8.4 μL). This was left at room temperature for 5 minutes to form LMgH *in situ* before adding 4-(MeO)BnCN (0.06 mmol, 8.0 mg). This was heated at 60 ^oC overnight to yield the insertion product, LMgNCHPh(4-MeO). ^1H NMR (300 MHz, C_6D_6, 300 K) δ_H (ppm): 8.58 (1H, s, NC*H*), 7.80 – 6.81 (10H, m, Ar-*H*), 4.87 (1H, s, NC(CH_3)C*H*), , 3.66 (4H, m, C*H*$(CH_3)_2$), 2.99 (3H, s, OCH_3) 1.73 (6H, s, NC(CH_3)CH), 1.47 (6H, d, J_{HH} = 6Hz, $CH(CH_3)_2$), 1.32 (6H, d, J_{HH} = 6Hz, $CH(CH_3)_2$), 0.91 (6H, d, J_{HH} = 6Hz, $CH(CH_3)_2$), 0.89 (6H, d, J_{HH} = 6Hz, $CH(CH_3)_2$). $^{13}C\{^1H\}$ NMR (75 MHz, C_6D_6, 300 K) δ_C (ppm): 171.7 (N=*C*H), 169.6 (N*C*(CH_3)CH), 162.3, 147.7, 146.7, 144.1, 142.9, 135.0, 126.2, 124.2, 94.7 (NC(CH_3)*C*H), 55.3 (O*C*H_3), 32.3 (*C*H$(CH_3)_2$), 29.8, 28.8, 27.2, 26.1, 25.8, 24.9, 24.6, 23.4.

71. *LMgN(BpinH)CH^{t}Bu*

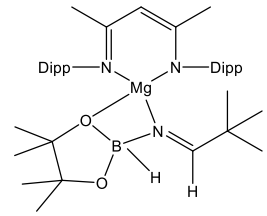

NMR Scale: To a solution of compound **68** in C_6D_6 additional HBpin (0.04 mmol, 5.8 μL) was added and left overnight at room temperature to yield the borate intermediate. ^1H NMR (300 MHz, C_6D_6, 300 K) δ_H (ppm): 7.97 (1H, s, N=C*H*), 7.21 – 7.10 (6H, m, Ar-*H*), 4.84 (1H, s, NC(CH_3)C*H*), 3.36 (1H, s, Mg*H*), 3.34 (2H, sept, J_{HH} = 6 Hz, C*H*$(CH_3)_2$, 3.21 (2H, sept, J_{HH} = 6 Hz, C*H*$(CH_3)_2$), 1.63 (6H, s, NC(CH_3)CH), 1.40 (6H, d, J_{HH} = 9 Hz, $CH(CH_3)_2$), 1.37 (6H, d, J_{HH} = 9 Hz, $CH(CH_3)_2$), 1.23 (6H, d, J_{HH} = 9 Hz, $CH(CH_3)_2$), 1.21 (6H, d, J_{HH} = 9 Hz, $CH(CH_3)_2$), 1.07 (12H, s, OC(CH_3)$_2$), 1.00 (9H, s, C(CH_3)$_3$). $^{13}C\{^1H\}$ NMR (75 MHz, C_6D_6, 300 K) δ_C (ppm): 178.4 (N=*C*H), 170.5 (N*C*(CH_3)), 145.7 (*ipso*-*C*-Ar), 143.3 (*ortho*-*C*-Ar), 142.6 (*ortho*-*C*-Ar), 126.1 (*para*-*C*-Ar), 124.7 (*meta*-*C*-Ar), 124.4 (*meta*-*C*-Ar), 96.0 (NC(CH_3)*C*H), 83.0 (O*C*$(CH_3)_2$), 82.6 (O*C*$(CH_3)_2$), 37.8 (N=CH*C*$(CH_3)_3$), 29.17 (*C*H$(CH_3)_2$), 28.4 (*C*H$(CH_3)_2$), 27.5, 27.2, 26.1, 25.9, 25.3 (OC(*C*H_3)$_2$), 25.1. ^{11}B NMR (96 MHz, C_6D_6, 300 K) δ_B (ppm): 8.5 (d, J_{HB} = 105.6 Hz, N*B*H).

72. *LMgN(Bpin)CH$_2$^{t}Bu*

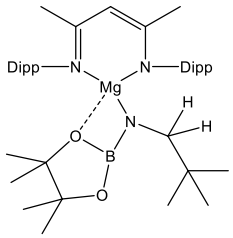

NMR Scale: A NMR sample of compound **71** in C_6D_6 was left at room temperature for 48 hrs. ^{1}H NMR (300 MHz, C_6D_6, 300 K) δ_H (ppm): 7.21 – 7.10 (6H, m, Ar-*H*), 4.83 (1H, s, NC(CH$_3$)C*H*), 3.46 (2H, sept, J_{HH} = 6 Hz, C*H*(CH$_3$)$_2$), 3.35 (2H, s, NC*H*$_2$), 3.31 (2H, sept, J_{HH} = 6 Hz, C*H*(CH$_3$)$_2$), 1.64 (6H, s, NC(C*H*$_3$)CH), 1.39 (12H, d, J_{HH} = 6 Hz, CH(C*H*$_3$)$_2$), 1.26 (12H, d, J_{HH} = 6 Hz, CH(C*H*$_3$)$_2$), 1.06 (24H, s, OC(C*H*$_3$)$_2$). ^{13}C{^{1}H} NMR (75 MHz, C_6D_6, 300 K) δ_C (ppm): 170.6 (N*C*(CH$_3$)CH), 145.8 (*ipso*-*C*-Ar), 143.1 (*ortho*-*C*-Ar), 125.8 (*para*- *C*-Ar), 124.4 (*meta*-*C*-Ar), 95.8 (NC(CH$_3$)*C*H), 83.1 (O*C*(CH$_3$)$_2$), 82.6 (O*C*(CH$_3$)$_2$), 58.5 (N*C*H$_2$), 34.3 (NCH$_2$*C*(CH$_3$)$_3$), 28.6, 28.4, 27.2, 26.2, 25.9, 25.3, 25.1, 14.7 (C(*C*H$_3$)$_3$). ^{11}B NMR (96 MHz, C_6D_6, 300 K) δ_B (ppm): 7.05 (d, J_{HB} = 105.6 Hz, N*B*H).

73. *LMg(NCCPh$_2$){BpinH$_2$}MgL(NCCHPh$_2$)*

Compound crystallised upon addition, and was insoluble therefore no NMR data could be obtained.

7.5 Hydroboration of Isonitriles

Catalytic reactions

General Procedure NMR scale: 5 mg (0.01 mmol, i.e. 5 mol%) of **Ib** was dissolved in 0.5 ml of C_6D_6, 60.9 µL (0.42 mmol) of pinacolborane was then added followed by 0.2 mmol of isonitrile. This mixture was then transferred to a sealed Youngs tap NMR tube and the reaction was kept in an oil bath at 60 ^{o}C. The reactions were regularly monitored by ^{1}H and ^{11}B NMR spectroscopy until complete conversion was observed.

Hydroboration of cyclohexylisonitrile

NMR scale: 24.8 µL of cyclohexylisonitrile

74. *N,C-{B(OCMe$_2$)$_2$}$_2$-N-methylcyclohexylamine*

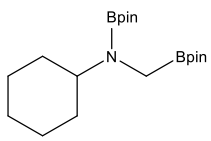

^{1}H NMR (300 MHz, C_6D_6, 300 K) δ_H (ppm): 3.32 (1H, m, C*H*(Cy)), 2.81 (2H, s, NC*H*$_2$B), 1.89 – 1.33 (10H, m, Cy-*H*), 1.15 (12H, s, NB(OC(C*H*$_3$)$_2$)$_2$), 1.10 (12H, s, CB(OC(C*H*$_3$)$_2$)$_2$). ^{13}C{^{1}H} NMR (75 MHz, C_6D_6, 300 K) δ_C (ppm): 83.4 NB(O*C*(CH$_3$)$_2$)$_2$), 83.2 (CB(O*C*(CH$_3$)$_2$)$_2$), 57.0 (N*C*H$_2$B), 33.0 (*C*H-Cy), 27.1 (Cy-*C*), 26.9 (Cy-*C*), 26.4 (Cy-*C*), 25.3 (NB(OC(*C*H$_3$)$_2$)$_2$), 25.2 CB(OC(*C*H$_3$)$_2$)$_2$). ^{11}B NMR (96 MHz, C_6D_6, 300 K) δ_B (ppm): 37.5 C*B*, 27.8 N*B*.

Hydroboration of 1-pentylisonitrile

NMR scale: 25.1 µL of 1-pentylisonitrile

75. *N,C-{B(OCMe$_2$)$_2$}$_2$-N-methyl-1-pentylamine*

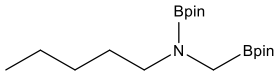

^{1}H NMR (300 MHz, C_6D_6, 300 K) δ_H (ppm): 3.22 (2H, t, J_{HH} = 9 Hz, NC*H*$_2$CH$_2$), 2.90 (2H, s, NC*H*$_2$B), 1.50 (2H, m, NCH$_2$C*H*$_2$), 1.27 (4H, m, NCH$_2$CH$_2$(C*H*$_2$)$_2$), 1.13 (12H, s, NB(OC(C*H*$_3$)$_2$)$_2$), 1.06 (12H, CB(OC(C*H*$_3$)$_2$)$_2$), 0.86 (3H, t, J_{HH} = 6 Hz, N(CH$_2$)$_4$C*H*$_3$). ^{13}C{^{1}H} NMR (75 MHz, C_6D_6, 300 K) δ_C (ppm): 83.5 (NB(O*C*(CH$_3$)$_2$)$_2$), 82.3 (CB(O*C*(CH$_3$)$_2$)$_2$), 49.2 (N*C*H$_2$B), 29.5 (N*C*H$_2$CH$_2$), 29.2 (NCH$_2$*C*H$_2$), 25.3 (NB(OC(C*H*$_3$)$_2$)$_2$), 25.2 (CB(OC(C*H*$_3$)$_2$)$_2$), 23.3 (NCH$_2$CH$_2$(*C*H$_2$)$_2$), 14.8 (N(CH$_2$)$_4$*C*H$_3$). ^{11}B NMR (96 MHz, C_6D_6, 300 K) δ_B (ppm): 37.2 C*B*, 27.9 N*B*.

Hydroboration of tert-butylisonitrile

NMR scale: 22.6 µL of *tert*-butylisonitrile

76. *N,C-{B(OCMe$_2$)$_2$}$_2$-N-methyl-tert-butylamine*

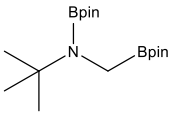

^{1}H NMR (300 MHz, C_6D_6, 300 K) δ_H (ppm): 2.90 (2H, s, NC*H*$_2$B), 1.39 (9H, s, NC(C*H*$_3$)$_3$), 1.14 (12H, s, NB(OC(C*H*$_3$)$_2$)$_2$), 1.09 (12H, s, CB(OC(C*H*$_3$)$_2$)$_2$). ^{13}C{^{1}H} NMR (75 MHz, C_6D_6, 300 K) δ_C (ppm): 83.5 (NB(O*C*(CH$_3$)$_2$)$_2$), 83.3 (CB(O*C*(CH$_3$)$_2$)$_2$), 81.6 (NC(CH$_3$)$_3$), 53.1 (N*C*H$_2$B), 30.8 (NC(*C*H$_3$)$_3$), 25.3 (NB(OC(*C*H$_3$)$_2$)$_2$), 25.2 (CB(OC(*C*H$_3$)$_2$)$_2$). ^{11}B NMR (96 MHz, C_6D_6, 300 K) δ_B (ppm): 36.9 C*B*, 26.9 N*B*.

Hydroboration of benzylisonitrile

NMR scale: 24.3 µL of benzylisonitrile

77. *N,C-{B(OCMe$_2$)$_2$}$_2$-N-methylbenzylamine*

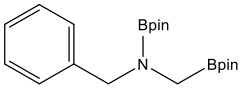

^{1}H NMR (300 MHz, C_6D_6, 300 K) δ_H (ppm): 7.45 (2H, d, J_{HH} = 6 Hz, *o*-C*H*), 7.27 (2H, m, *m*-C*H*), 7.17 (1H, m, *p*-C*H*), 4.53 (2H, s, BnC*H*$_2$N), 2.93 (NC*H*$_2$B), 1.24 (12H, s, NB(OC(C*H*$_3$)$_2$)$_2$), 1.11 (12H, s, CB(OC(C*H*$_3$)$_2$)$_2$). ^{13}C{^{1}H} NMR (75 MHz, C_6D_6, 300 K) δ_C (ppm): 141.4 (*ipso-C*), 129.3 (*o-C*), 128.9 (*p-C*), 128.7 (*m-C*), 127.2 (Bn*C*H$_2$N), 83.5 (NB(O*C*(CH$_3$)$_2$)$_2$), 82.7 (CB(O*C*(CH$_3$)$_2$)$_2$), 53.3 (N*C*H$_2$B), 25.3 (NB(OC(*C*H$_3$)$_2$)$_2$), 25.2 (CB(OC(*C*H$_3$)$_2$)$_2$). ^{11}B NMR (96 MHz, C_6D_6, 300 K) δ_B (ppm): 37.4 C*B*, 28.3 N*B*.

Hydroboration of 2-napthylisonitrile

NMR scale: 30.6 mg of 2-napthylisonitrile

78. *N,C-{B(OCMe$_2$)$_2$}$_2$-N-methyl-2-napthylamine*

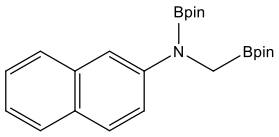

^{1}H NMR (300 MHz, C_6D_6, 300 K) δ_H (ppm): 8.26 (1H, m, *o-H*), 7.66 (2H, m, *o-H*, *m*-H), 7.27 (2H, m, Ar-*H*), 7.16 (2H, m, Ar-*H*), 3.61 (2H, s, NC*H*$_2$B), 1.12 (12H, s, NB(OC(C*H*$_3$)$_2$)$_2$), 0.93 (12H, s, CB(OC(C*H*$_3$)$_2$)$_2$). ^{13}C{^{1}H} NMR (75 MHz, C_6D_6, 300 K) δ_C (ppm): 161.9 (*ipso-C*), 147.1 (*o-C*), 143.1 (*o-C*), 135.4, 129.9, 127.5, 126.5, 123.9, 123.2, 113.6, 83.3 (NB(O*C*(CH$_3$)$_2$)$_2$), 82.2 (CB(O*C*(CH$_3$)$_2$)$_2$), 47.2 (N*C*H$_2$B), 25.1 (NB(OC(*C*H$_3$)$_2$)$_2$), 25.0 (CB(OC(*C*H$_3$)$_2$)$_2$). ^{11}B NMR (96 MHz, C_6D_6, 300 K) δ_B (ppm): 37.6 C*B*, 28.0 N*B*.

Hydroboration of 2,6-(Methyl)phenylisonitrile

NMR scale: 26.2 mg of 2,6-(methyl)phenylisonitrile

79. *N,C-{B(OCMe$_2$)$_2$}$_2$-N-methyl-2,6-(methyl)phenylamine*

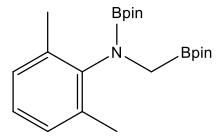

^{1}H NMR (300 MHz, C_6D_6, 300 K) δ_H (ppm): 6.76 (1H, m, *p*-C*H*), 6.62 (2H, m, *m*-C*H*), 3.03 (2H, s, NC*H*$_2$B), 2.46 (6H, s, *o*-C*H*$_3$), 1.03 (12H, s, NB(OC(C*H*$_3$)$_2$)$_2$), 1.00 (12H, s, CB(OC(C*H*$_3$)$_2$)$_2$). ^{13}C{^{1}H} NMR (75 MHz, C_6D_6, 300 K) δ_C (ppm): 146.8 (*ipso- C*), 136.9 (*o-C*), 128.9 (*p-C*), 128.2 (*m-C*), 83.6 (NB(O*C*(CH$_3$)$_2$)$_2$), 83.5 (CB(O*C*(CH$_3$)$_2$)$_2$), 47.2 (N*C*H$_2$B), 25.3 (NB(OC(*C*H$_3$)$_2$)$_2$), 25.2 (CB(OC(*C*H$_3$)$_2$)$_2$), 19.3 (*o-C*H$_3$). ^{11}B NMR (96 MHz, C_6D_6, 300 K) δ_B (ppm): 36.9 C*B*, 27.3 N*B*.

Stoichiometric reactions

***NMR scale:* XXII** (0.2 mmol, 100 mg) was dissolved in 0.5 ml of C_6D_6 along with CyNC (0.2 mmol, 29.8 μL). The insertion product formed cleanly at room temperature and colourless crystals precipitated from solution on standing.

***NMR scale:* Ib** (0.1 mmol, 50 mg) was dissolved in 0.5 ml of C_6D_6 along with HBpin (0.1 mmol, 14.5 μL). This reaction was left for 5 minutes to form the hydride before addition of CyNC (0.1 mmol, 12.4 μL). An intense blue solution was formed upon addition and upon leaving solution for half an hour colourless crystals precipitated from solution.

80. LMgCHNCy

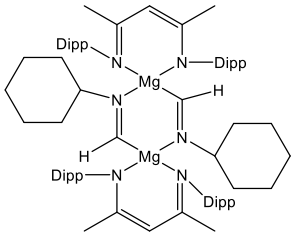

^{1}H NMR (300 MHz, C_6D_6, 300 K) δ_H (ppm): 9.99 (2H, s, MgC*H*), 7.14 – 7.00 (12H, m, Ar-*H*), 4.80 (2H, s, NC(CH$_3$)C*H*), 3.67 (4H, m, C*H*(CH$_3$)$_2$), 2.86 (4H, m, C*H*(CH$_3$)$_2$), 2.30 (2H, m, C*H*(Cy), 1.70 (12H, s, NC(C*H*$_3$)CH), 1.49 (12H, d, J_{HH} = 3 Hz, CH(C*H*$_3$)$_2$), 1.41 – 0.96 (20H, m, Cy-*H*), 1.24 (12H, d, J_{HH} = 3 Hz, CH(C*H*$_3$)$_2$), 0.87 (12H, d, J_{HH} = 3 Hz, CH(C*H*$_3$)$_2$), 0.22 (12H, d, J_{HH} = 3 Hz, CH(C*H*$_3$)$_2$). ^{13}C{^{1}H} NMR (75 MHz, C_6D_6, 300 K) δ_C (ppm): 217.0 (Mg*C*H), 169.6 (N*C*(CH$_3$)CH), 147.4 (*ipso-C*), 146.5 (*o-C*), 142.7 (*p-C*), 125.5 (*m-C*), 94.5 (NC(CH$_3$)*C*H), 35.8 (*C*HCy), 34.3 (*C*H(CH$_3$)$_2$), 32.3 (*C*H(CH$_3$)$_2$), 28.9 (NC(*C*H$_3$)$_2$), 27.2 (CH(*C*H$_3$)$_2$), 26.9 (*C*-Cy), 26.8 (*C*-Cy), 26.1 (CH(*C*H$_3$)$_2$), 25.0 (*C*-Cy), 24.7 (CH(*C*H$_3$)$_2$), 14.7 (CH(*C*H$_3$)$_2$). Despite repeated attempts, an acceptable elemental analysis could not be obtained for this highly air- and moisture-sensitive compound.

7.6 Hydroboration of Heterocumulenes

7.6.1 Hydroboration of Carbodiimides

Catalytic reactions

General Procedure NMR scale: 10 mg (0.02 mmol, i.e. 10 mol%) of **Ib** was dissolved in 0.5 ml of C_6D_6, 60.9 µL (0.42 mmol) of pinacolborane was then added followed by 0.2 mmol of carbodiimide. This mixture was then transferred to a sealed Youngs tap NMR tube and the reaction was kept in an oil bath at 60 ^{o}C. The reactions were regulary monitored by ^{1}H and ^{11}B NMR spectroscopy until maximum conversion was observed.

Hydroboration of N,N'-diisopropylcarbodiimide

81. *N-{B(OCMe$_2$)$_2$}-isopropylformamidinate*

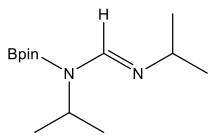

NMR scale: 30.7 µL of *N,N'*-diisopropylcarbodiimide. ***Large Scale:*** 154.8 µL of *N,N'*-diisopropylcarbodiimide, 60 ^{o}C for 15 hrs. Isolated yellow crystals (226 mg, 89% yield). ^{1}H NMR (300 MHz, C_6D_6, 300 K) δ_H (ppm): 8.23 (1H, s, NC*H*), 4.96 (1H, sept, ^{3}J = 6 Hz, BNC*H*(CH$_3$)$_2$), 3.30 (1H, sept, ^{3}J = 6 Hz, NC*H*(CH$_3$)$_2$), 1.43 (6H, d, ^{3}J = 6 Hz, BNCH(C*H*$_3$)$_2$), 1.18 (6H, d, ^{3}J = 6 Hz, NCH(C*H*$_3$)$_2$), 1.02(12H, s, C(C*H*$_3$)$_2$). ^{13}C{^{1}H} NMR (75.5 MHz, C_6D_6, 300 K) δ_C (ppm): 150.3 (N*C*HN), 83.1 (O*C*(CH$_3$)$_2$), 57.6 (BN*C*H(CH$_3$)$_2$), 44.0 (N*C*H(CH$_3$)$_2$), 26.1 (BNCH(*C*H$_3$)$_2$), 24.5 (C(*C*H$_3$)$_2$), 22.2 (CH(*C*H$_3$)$_2$). ^{11}B NMR (96.3 MHz, C_6D_6, 300 K) δ_B (ppm): 28.5 (br. s, N*B*).

Hydroboration of N,N'-dicyclohexylcarbodiimide

82. *N-{B(OCMe$_2$)$_2$}-cyclohexylformamidinate*

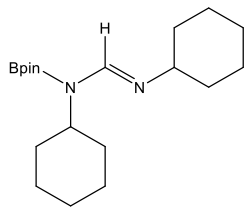

NMR scale: 41.3 mg of *N,N'*-dicyclohexylcarbodiimide. ***Large scale:*** 206.3 mg of *N,N'*-dicyclohexylcarbodiimide, 60 ^{o}C for 15 hrs. Isolated yellow crystals (232 mg, 69% yield). ^{1}H NMR (300 MHz, C_6D_6, 300 K) δ_H (ppm): 8.31 (1H, s, NC*H*), 4.59 (1H, m, BNC*H*$(CH_2)_2$), 2.97 (1H, m, NC*H*$(CH_2)_2$), 2.12 (2H, m, CH$(C)_2$), 1.94 – 1.11 (18H, m, Cy-*H*), 1.05 (12H, s, C(C*H*$_3)_2$). ^{13}C{^{1}H} NMR (75.5 MHz, C_6D_6, 300 K) δ_C (ppm): 150.9 (N*C*HN), 83.1 (*C*$(CH_3)_2$), 65.8 (BN*C*H$(CH_2)_2$), 52.0 (N*C*H$(CH_2)_2$), 36.5 (BNCH(*C*H$_2)_2$(CH$_2)_2$CH$_2$), 32.4 (NCH(*C*H$_2)_2$(CH$_2)_2$CH$_2$), 27.2 (BNCH(CH$_2)_2$(*C*H$_2)_2$CH$_2$), 26.6 (BNCH(CH$_2)_2$(CH$_2)_2$*C*H$_2$), 26.5 (NCH(CH$_2)_2$(CH$_2)_2$*C*H$_2$), 25.7 (NCH(CH$_2)_2$(*C*H$_2)_2$CH$_2$), 24.9 (C(*C*H$_3)_2$). ^{11}B NMR (96.3 MHz, C_6D_6, 300 K) δ_B (ppm): 28.4 (br. s, N*B*). HRMS (ESI) calcd. for hydrolysed product $[M^+H^+]^+$ $C_{13}H_{25}N_2$ *m/z* 209.35, found 209.2114.

Hydroboration of N,N'-di-tert-butylcarbodiimide

83. *N-{B(OCMe$_2$)$_2$}-tert-butylformamidinate*

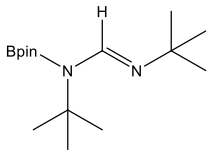

NMR scale: 38.7 µL of *N,N'*-di-*tert*-butylcarbodiimide. ***Large scale:*** 385.6 µL of *N,N'*-di-*tert*-butylcarbodiimide, 80 ^{o}C for 2.5 days. Isolated yellow crystals (220 mg, 87% yield). ^{1}H NMR (300 MHz, C_6D_6, 300 K) δ_H (ppm): 8.30 (1H, s, NC*H*), 1.51 (18H, s, C(C*H*$_3)_3$), 1.01 (12H, s, C$(CH_3)_2$). ^{13}C{^{1}H} NMR (75.5 MHz, C_6D_6, 300 K) δ_C (ppm): 149.5 (NC*H*N), 82.5 (*C*$(CH_3)_2$), 55.4 (*C*$(CH_3)_3$), 30.9 (C(*C*H$_3)_3$), 24.8(C(*C*H$_3)_2$). ^{11}B NMR (96.3 MHz, C_6D_6, 300 K) δ_B (ppm): 28.7 (br. s, N*B*). HRMS (ESI) calcd. for hydrolysed product $[M^+H^+]^+$ $C_9H_{21}N_2$ *m/z* 157.27, found 147.1720.

Hydroboration of N,N'-2,6-diisopropylphenylcarbodiimide

84. *N-{B(OCMe$_2$)$_2$}-2,6-diisopropylphenylformamidinate*

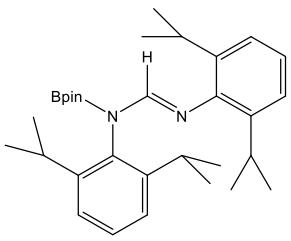

NMR scale: 72.5 mg of *N,N'*-2,6-diisopropylphenylcarbodiimide. ***Large scale:*** 362.55 mg of *N,N'*-2,6-diisopropylphenylcarbodiimide, 80 ^{o}C for 24 hrs. Isolated yellow crystals (378 mg, 77% yield). ^{1}H NMR (300 MHz, C_6D_6, 300 K) δ_H (ppm): 8.43 (1H, s, NC*H*N), 7.32 (2H, m, *m-H*), 7.24 (2H, m, *m-H*), 7.17 (2H, s, *p-H*), 3.47 (2H, m, C*H*$(CH_3)_2$), 3.39 (2H, m, C*H*$(CH_3)_2$), 1.51 (6H, d, J_{HH} = 6 Hz, CH(C*H*$_3)_2$), 1.49 (6H, d, J_{HH} = 6 Hz, CH(C*H*$_3)_2$), 1.24 (12H, d, J_{HH} = 9 Hz, CH(C*H*$_3)_2$), 1.09 (12H, s, C(C*H*$_3)_2$). ^{13}C{^{1}H} NMR (75.5 MHz, C_6D_6, 300 K) δ_C (ppm): 152.8 (*ipso-C*), 148.6 (*ipso-C*), 146.6 (*o-C*), 143.3 (*o-C*),

140.0 (*o-C*), 125.8 (*p-C*), 124.1 (*m-C*), 123.5 (*p-C*), 84.3 (*C*(CH_3)$_2$), 29.9 (*C*H(CH_3)$_2$), 29.4 ((*C*H(CH_3)$_2$), 28.1 (*C*H(CH_3)$_2$), 25.7 (CH(*C*H_3)$_2$), 24.8 (CH(*C*H_3)$_2$), 24.6 (CH(*C*H_3)$_2$), 23.8 (CH(*C*H_3)$_2$). ^{11}B NMR (96.3 MHz, C_6D_6, 300 K) δ_B (ppm): 28.4 (br. s, N*B*). Elemental Analysis for $C_{31}H_{47}BN_2O_2$ (found): C 75.90 (75.67); H 9.66 (9.70); N 5.71 (5.78). HRMS (ESI) calcd. for hydrolysed product $[M^+Na^+]^+$ $C_{25}H_{36}N_2Na_1$ *m/z* 387.57, found 387.2776.

Hydroboration of N,N'-1,3-di-p-tolylcarbodiimide

85. ***N-{B(OCMe$_2$)$_2$}-1,3-di-p-tolylformamidinate***

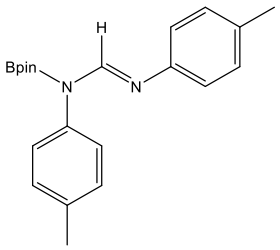

NMR scale: 72.5 mg of *N,N'*-1,3-di-*p*-tolylcarbodiimide. ***Large scale:*** 444.6 mg of *N,N'*-1,3-di-*p*-tolylcarbodiimide, 80 ^{o}C for 2.5 days. Isolated yellow crystals (222 mg, 63% yield). ^{1}H NMR (300 MHz, C_6D_6, 300 K) δ_H (ppm): 8.65 (1H, s, NC*H*N), 7.19 – 7.16 (4H, m, *o-H*), 6.80 (4H, m, *m-H*), 2.08 (6H, s, *p*-CH_3), 1.01 (12H, s, OC(CH_3)$_2$). ^{13}C{^{1}H} NMR (75.5 MHz, C_6D_6, 300 K) δ_C (ppm): 151.7 (N*C*HN), 148.3 (*ipso-C*), 147.4 (*ipso-C*), 135.2 (*ortho-C*), 133.6 (*ortho-C*), 130.6 (*para-C*), 130.1 (*para-C*), 122.8 (*meta-C*), 120.3 (*meta-C*), 84.3 (O*C*(CH_3)$_2$), 24.8 (OC(*C*H_3)$_2$), 21.3 (*para-C*H_3). ^{11}B NMR (96.3 MHz, C_6D_6, 300 K) δ_B (ppm): 28.9 N*B*. HRMS (ESI) calcd. for hydrolysed product $[M^+H^+]^+$ $C_{15}H_{16}N_2$ *m/z* 224.31, found 225.1392.

Hydroboration of N-tert-butyl-N'-ethylcarbodiimide

86. ***N,N-{B(OCMe$_2$)$_2$}-ethyl-N'-tert-butylformamidinate***

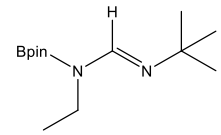

NMR scale: 31.0 µL of *N-tert*-butyl-*N'*-ethylcarbodiimide. ***Large Scale:*** 307.6 µL of *N*-tert-butyl-*N'*-ethylcarbodiimide, 60 ^{o}C for 20 hrs. Isolated yellow crystals (220 mg, 87% yield). ^{1}H NMR (300 MHz, C_6D_6, 300 K) δ_H (ppm): 8.18 (1H, s, NC*H*N), 3.79 (2H, q, J_{HH} = 6 Hz, NCH_2), 1.34 (3H, t, J_{HH} = 6 Hz, NCH_2CH_3), 1.22 (9H, s, NC(CH_3)$_3$), 1.04 (12H, s, OC(CH_3)$_2$). ^{13}C{^{1}H} NMR (75.5 MHz, C_6D_6, 300 K) δ_C (ppm): 146.6 (N*C*HN), 83.4 (O*C*(CH_3)$_2$), 54.3 (*C*(CH_3)$_3$), 32.6 (NCH_2), 24.9 (NCH_2CH_3), 23.4 (OC(*C*H_3)$_2$), 14.7 (C(*C*H_3)$_3$). ^{11}B NMR (96.3 MHz, C_6D_6, 300 K) δ_B (ppm): 28.5 N*B*.

Hydroboration of N-(3-dimethylaminopropyl)-N'-ethylcarbodiimide

NMR scale: 35.4 µL of *N*-(3-dimethylaminopropyl)-*N'*-ethylcarbodiimide. ***Large Scale:*** 354.0 µL of *N*-(3-dimethylaminopropyl)-*N'*-ethylcarbodiimide, 60 ^{o}C for 5.5 hrs. Isolated yellow crystals (253 mg, 89% yield).

87 a. ***N,N-{B(OCMe$_2$)$_2$}-(3-Dimethylaminopropyl)-N'-ethylformamidinate*** ^{1}H NMR (300 MHz, C_6D_6, 300 K) δ_H (ppm): 8.14 (1H, s, NC*H*N), 3.79 (2H, t, J_{HH} = 6 Hz, N(Bpin)CH_2CH$_2$), 3.33 (2H, q, J_{HH} = 6 Hz, NCH_2CH$_3$), 2.28 (4H, m, N(Bpin)CH$_2$CH_2CH_2), 2.12 (6H, s, N(Bpin)PrN(CH_3)$_2$), 1.16 (3H, t, J_{HH} = 6 Hz, NCH$_2$CH_3), 1.05 (12H, s, OC(CH_3)$_2$). ^{13}C{^{1}H} NMR (75.5 MHz, C_6D_6, 300 K) δ_C (ppm): 151.5(N*C*HN), 83.5 (O*C*(CH$_3$)$_2$), 58.3 (N(Bpin)*C*H$_2$CH$_2$), 51.6 (N*C*H$_2$CH$_3$), 46.0 (N(Bpin)PrN(*C*H$_3$)$_2$), 41.2 (N(Bpin)CH$_2$*C*H$_2$), 30.9 (N(Bpin)CH$_2$CH$_2$*C*H$_2$), 25.1 (OC(*C*H$_3$)$_2$), 15.7 (NCH$_2$*C*H$_3$). ^{11}B NMR (96.3 MHz, C_6D_6, 300 K) δ_B (ppm): 28.12 N*B*.

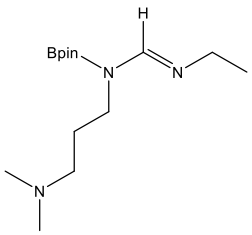

87 b. ***N,N-{B(OCMe$_2$)$_2$}-ethyl-N'-(3-Dimethylaminopropyl)-formamidinate***

^{1}H NMR (300 MHz, C_6D_6, 300 K) δ_H (ppm): 8.12 (1H, s, NC*H*N), 3.75 (2H, q, J_{HH} = N(Bpin)CH_2CH$_3$), 3.41 (2H, t, J_{HH}= 6 Hz, NCH_2CH$_2$), 2.08 (6H, s, NPrN(CH_3)$_2$), 1.76 (4H, m, NCH$_2$CH_2CH_2), 1.30 (3H, t, J_{HH} = 6 Hz, N(Bpin)CH$_2$CH_3), 1.03 (12H, s, OC(CH_3)$_2$). ^{13}C{^{1}H} NMR (75.5 MHz, C_6D_6, 300 K) δ_C (ppm): 151.3 (N*C*HN), 83.4 (O*C*(CH$_3$)$_2$), 58.2 (N(Bpin)*C*H$_2$CH$_3$), 55.1 (N*C*H$_2$CH$_2$), 45.9 (NPrN(*C*H$_3$)$_2$), 37.5 (NCH$_2$*C*H$_2$), 28.1 (NCH$_2$CH$_2$*C*H$_2$), 25.0 (OC(*C*H$_3$)$_2$), 18.3 (N(Bpin)CH$_2$*C*H$_3$). ^{11}B NMR (96.3 MHz, C_6D_6, 300 K) δ_B (ppm): 28.12 N*B*.

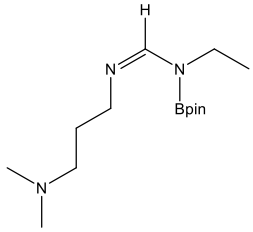

Stoichiometric reactions

88. ***LMgN(iPr)C(Butyl)N(iPr)***

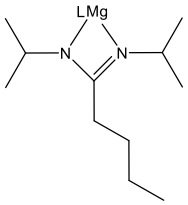

NMR scale: **Ib** (0.04 mmol, 20 mg) was dissolved in 0.5 ml of C_6D_6 along with *i*PrNCN*i*Pr (0.04 mmol, 3.5 µL). The insertion product formed cleanly at room temperature, 71% yield by NMR. ^{1}H NMR (300 MHz, C_6D_6, 300 K) δ_H (ppm): 7.21 (6H, m, Ar-*H*), 4.93 (1H, s, NC(CH$_3$)C*H*), 3.55 (4H, m, Ligand C*H*(CH$_3$)$_2$), 3.22 (2H, m, C*H*(CH$_3$)$_2$), 2.17 (2H, m, CCH_2), 1.73 (6H, s, NC(CH_3)CH), 1.37 – 1.32 (24H, m, Ligand CH(CH_3)$_2$), 1.28 (4H, m, CH_2CH_2CH$_3$), 0.95 (12H, d, J_{HH} = 6 Hz, CH(CH_3)$_2$), 0.87 (3H, t, ^3J = 9 Hz, CH$_2$CH_3). ^{13}C{^{1}H} NMR (75.5 MHz, C_6D_6, 300 K) δ_C (ppm): 176.8 (N*C*(CH$_3$)), 169.7 (*ipso*-*C*), 143.1 (*o*-*C*), 125.5 (*p*-*C*), 124.4 (N*C*(CH$_2$)N), 124.2 (*m*-*C*), 94.8 (NC(CH$_3$)*C*H), 28.9 (*C*H(CH$_3$)$_2$), 28.6 (Ligand *C*H(CH$_3$)$_2$), 27.3 (Ligand CH(*C*H$_3$)$_2$), 27.1 (C*C*H$_2$), 25.6 (CH(*C*H$_3$)$_2$), 24.9 (NC(*C*H$_3$)), 24.6 (CCH$_2$*C*H$_2$), 24.2 (*C*H$_2$CH$_3$), 14.7 (CH$_2$*C*H$_3$).

89. ***LMgN(iPr)CHN(iPr)***

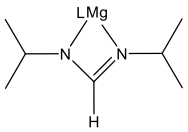

NMR Scale: **XXII** (0.023 mmol, 20 mg) was dissolved in 0.5 ml of C_6D_6 along with *i*PrNCN*i*Pr (0.046 mmol, 7.0 μL). The insertion product formed cleanly at room temperature, 71% yield by NMR. ^{1}H NMR (300 MHz, C_6D_6, 300 K) δ_H (ppm): 7.77 (1H, s, NC*H*N), 7.23 – 6.99 (6H, m, Ar-*H*), 3.43 (2H, m, NC*H*$(CH_3)_2$), 3.12 (4H, m, C*H*$(CH_3)_2$), 1.68 (6H, s, NC(CH_3)CH), 1.32 (6H, d, J_{HH} = 9 Hz, NCH(C*H*$_3)_2$), 1.27 (6H, d, J_{HH} = 6 Hz, NCH(C*H*$_3)_2$), 1.05 (12H, d, J_{HH} = 6 Hz, CH(C*H*$_3)_2$), 0.85 (12H, d, J_{HH}= 9 Hz, CH(C*H*$_3)_2$). ^{13}C{^{1}H} NMR (75.5 MHz, C_6D_6, 300 K) δ_C (ppm): 169.9 (N*C*(CH_3)CH), 168.6 (N*C*HN), 145.8 (*ipso-C*), 143.0 (*ortho-C*), 142.4 (*para-C*), 124.2 (*meta-C*), 95.1 (NC(CH_3)*C*H), 49.3 (N*C*H$(CH_3)_2$), 48.7 (N*C*H$(CH_3)_2$), 28.5 (*C*H$(CH_3)_2$), 26.2 (NC(*C*H_3)CH), 25.8 (NCH(*C*$H_3)_2$), 25.2 (NCH(*C*$H_3)_2$), 24.8 (CH(*C*$H_3)_2$) 24.6 (CH(*C*$H_3)_2$).

90. ***LMgN(iPr)C(H)N(iPr)BpinH***

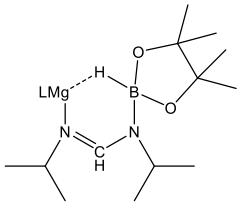

NMR Scale: To an NMR sample of compound **89** 1 equivalent of HBpin was added (0.046 mmol, 6.8 μL). Product formed upon addition.^{1}H NMR (500 MHz, C_6D_6, 300 K) δ_H (ppm): 7.63 (1H, s, NC*H*N), 7.18 – 7.02 (6H, m, Ar-*H*), 4.82 (1H, s, NC(CH_3)C*H*), 4.06 (1H, m, NC*H*$(CH_3)_2$), 3.74 (1H, m, NC*H*$(CH_3)_2$), 3.40 (4H, m, C*H*$(CH_3)_2$), 1.73 (3H, s, NC(C*H*$_3$)CH), 1.67 (3H, s, NC(C*H*$_3$)CH), 1.34 (6H, d, J_{HH} = 6 Hz, CH(C*H*$_3)_2$), 1.28 (3H, d, J_{HH} = 6 Hz, NCH(C*H*$_3)_2$), 1.24 (6H, d, J_{HH} = 6 Hz, CH(C*H*$_3)_2$), 1.21 (6H, d, J_{HH} = 6 Hz, CH(C*H*$_3)_2$), 1.19 (3H, d, J_{HH} = 6 Hz, CH(C*H*$_3)_2$), 1.09 (6H, d, J_{HH} = 6 Hz, CH(C*H*$_3)_2$), 0.94 (3H, s, OC(C*H*$_3)_2$), 0.66 (3H, s, OC(C*H*$_3)_2$), 0.64 (3H, s, OC(C*H*$_3)_2$), 0.57 (3H, s, OC(C*H*$_3)_2$). ^{13}C{^{1}H} NMR (125.7 MHz, C_6D_6, 300 K) δ_C (ppm): 169.7 (N*C*(CH_3)CH), 169.0 (N*C*(CH_3)CH), 158.1 (N*C*HN) 146.6 (*ispo-C*), 146.1 (*ipso-C*), 143.4 (*ortho-C*), 143.2 (*ortho-C*), 142.6 (*para-C*), 141.5 (*para-C*), 124.2 (*meta-C*), 123.4 (*meta-C*), 94.7 (NC(CH_3)*C*H), 80.7 (O*C*$(CH_3)_2$), 78.7 (O*C*$(CH_3)_2$), 50.7 (N*C*H$(CH_3)_2$), 45.6 (N*C*H$(CH_3)_2$), 29.0 (*C*H$(CH_3)_2$), 28.4 (*C*H$(CH_3)_2$), 28.1 (NC(*C*H_3)CH), 27.9 (NC(*C*H_3)CH), 26.2 (CH(*C*$H_3)_2$), 25.7 (CH(*C*$H_3)_2$), 25.4 (NCH(*C*$H_3)_2$), 25.2 (CH(*C*$H_3)_2$), 25.1 (CH(*C*$H_3)_2$), 25.0 (NCH(*C*$H_3)_2$), 24.9 (CH(*C*$H_3)_2$), 24.8 (CH(*C*$H_3)_2$), 24.7 (NCH(*C*$H_3)_2$), 24.6 (NCH(*C*$H_3)_2$), 24.5 (CH(*C*$H_3)_2$), 24.2 (OC(*C*$H_3)_2$), 24.1 (OC(*C*$H_3)_2$), 23.8 (OC(*C*$H_3)_2$), 23.4 (OC(*C*$H_3)_2$). ^{11}B NMR (160.5 MHz, C_6D_6, 300 K) δ_B (ppm): 1.82, d, J_{HB} = 92.9 Hz, *B*H.

7.6.2 Hydroboration of Isocyanates

General Procedure NMR scale: 10 mg (0.02 mmol, i.e. 10 mol%) of **Ib** was dissolved in 0.5 ml of C_6D_6, 90.0 µL (0.62 mmol) of pinacolborane was then added followed by 0.2 mmol of isocyanate. This mixture was then transferred to a sealed Youngs tap NMR tube and the reaction was heated in an oil bath at 60 ^oC. These reactions were regularly monitored by ^1H and ^{11}B NMR spectroscopy until maximum conversion was observed.

Hydroboration of 2,4,6-trimethylphenyl isocyanate

91. ***N,O-{B(OCMe$_2$)$_2$}$_2$-(methoxy)-2,4,6-trimethylphenylamine***

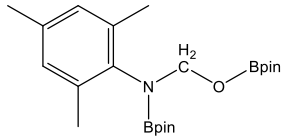

NMR scale: 32.2 mg of 2,4,6-trimethylphenyl isocyanate. ^1H NMR (400 MHz, C_6D_6, 300 K) δ_H (ppm): 6.76 (2H, s, *m-H*), 5.32 (2H, s, NCH_2O), 2.36 (6H, s, *o*-CH_3), 2.08 (3H, s, *p*-CH_3), 1.01 (12H, s, O-B(OC(CH_3)$_2$)$_2$), 0.92 (12H, s, N-B(OC(CH_3)$_2$)$_2$). $^{13}C\{^1H\}$ NMR (100.6 MHz, C_6D_6, 300 K) δ_C (ppm): 139.7 (*ipso-C*), 137.0 (*o-C*), 135.6 (*p-C*), 129.7 (*m-C*), 83.5 (O-BO*C*(CH$_3$)$_2$), 82.6 (N-BO*C*(CH$_3$)$_2$), 77.0 (N*C*H$_2$O), 25.3 (O-BOC(*C*H$_3$)$_2$), 24.9 (N-BOC(*C*H$_3$)$_2$), 21.3 (*o-C*H$_3$), 19.2 (*p-C*H$_3$). ^{11}B NMR (128.4 MHz, C_6D_6, 300 K) δ_B (ppm): 27.4 (br. s, N*B*), 25.3 (br. s. O*B*).

Hydroboration of 2,6-diisopropylphenyl isocyanate

92. ***N,O-{B(OCMe$_2$)$_2$}$_2$-(methoxy)-2,6-diisopropylphenylamine***

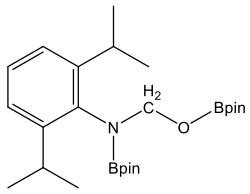

NMR scale: 42.8 µL of 2,6-di-*iso*-propylphenyl isocyanate. ^1H NMR (400 MHz, C_6D_6, 300 K) δ_H (ppm): 7.14 (1H, t, J_{HH} = 4 Hz, *p-H*), 7.10 (2H, d, J_{HH} = 4 Hz, *m-H*), 5.35 (2H, s, NCH_2O), 3.55 (2H, sept, J_{HH} = 8 Hz, C*H*(CH$_3$)$_2$), 1.41 (6H, d, J_{HH} = 8 Hz, CH(CH_3)$_2$), 1.31 (6H, d, J_{HH} = 8 Hz, CH(CH_3)$_2$), 1.00 (12H, s, O-B(OC(CH_3)$_2$)$_2$), 0.92 (12H, s, N-B(OC(CH_3)$_2$)$_2$). $^{13}C\{^1H\}$ NMR (125.8 MHz, C_6D_6, 300 K) δ_C (ppm): 155.3 (*ipso-C*), 148.2 (*o-C*), 137.2 (*p-C*), 123.6 (*m-C*), 83.3 (O-B(O*C*(CH$_3$)$_2$)$_2$), 82.6 (N-B(O*C*(CH$_3$)$_2$)$_2$), 77.9 (N*C*H$_2$O), 28.9 (*C*H(CH$_3$)$_2$), 25.3 (*C*H(CH$_3$)$_2$), 25.0 (O-B(OC(*C*H$_3$)$_2$)$_2$), 24.9 (N-B(OC(*C*H$_3$)$_2$)$_2$). ^{11}B NMR (96.3 MHz, C_6D_6, 300 K) δ_B (ppm): 28.3 (br. s, N*B*), 24.8 (br. s. O*B*).

Hydroboration of phenyl isocyanate

93. ***N,N-methyl-{B(OCMe$_2$)$_2$}-phenylamine***

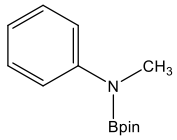

NMR scale: 21.7 µL of phenyl isocyanate. ^1H NMR (500 MHz, C_6D_6, 300 K) δ_H (ppm): 7.45 (2H, m, *o-H*), 7.21 (1H, m, *p-H*), 6.87 (2H, m, *m-H*), 3.01 (3H, s, NCH_3), 1.08 (12H, s, OC(CH_3)$_2$). $^{13}C\{^1H\}$ NMR (125.8 MHz, C_6D_6, 300 K)

δ_C (ppm): 164.2 (*ipso*-*C*), 148.3 (*o*-*C*), 129.2 (*p*-*C*), 121.4 (*m*-*C*), 83.5 (O*C*$(CH_3)_2$), 34.7 (N*C*H_3), 25.3 (OC(*C*$H_3)_2$). ^{11}B NMR (160.4 MHz, C_6D_6, 300 K) δ_B (ppm): 27.7 (br. s, N*B*).

Hydroboration of ethyl isocyanate

94. *N,N-methyl-{B(OCMe$_2$)$_2$}-ethylamine*

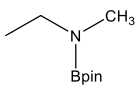

NMR scale: 15.8 µL of ethyl isocyanate. ^{1}H NMR (500 MHz, C_6D_6, 300 K) δ_H (ppm): 3.00 (2H, q, J_{HH} = 5 Hz, NC*H*$_2$), 2.62 (3H, s, NC*H*$_3$), 1.11 (12H, s, OC(C*H*$_3)_2$), 0.98 (3H, t, J_{HH} = 5 Hz, NCH$_2$C*H*$_3$). ^{13}C{^{1}H} NMR (125.8 MHz, C_6D_6, 300 K) δ_C (ppm): 82.3 (O*C*$(CH_3)_2$), 43.7 (N*C*H$_2$), 33.4 (N*C*H$_3$), 25.0 (OC(*C*$H_3)_2$), 15.0 (NCH$_2$*C*H$_3$). ^{11}B NMR (160.4 MHz, C_6D_6, 300 K) δ_B (ppm): 27.2 (br. s, N*B*).

Hydroboration of propyl isocyanate

95. *N,N-methyl-{B(OCMe$_2$)$_2$}-propylamine*

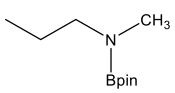

NMR scale: 18.7 µL of propyl isocyanate. ^{1}H NMR (500 MHz, C_6D_6, 300 K) δ_H (ppm): 2.93 (2H, t, J_{HH} = 5 Hz, NC*H*$_2$), 2.60 (3H, s, NC*H*$_3$), 1.40 (2H, q, J_{HH} = 5 Hz, NC*H*$_2$CH$_2$), 1.11 (12H, s, OC(C*H*$_3)_2$), 0.81 (3H, t, J_{HH} = 5 Hz, CH$_2$C*H*$_3$). ^{13}C{^{1}H} NMR (125.8 MHz, C_6D_6, 300 K) δ_C (ppm): 83.5 (O*C*$(CH_3)_2$), 50.9 (N*C*H$_2$), 33.7 (N*C*H$_3$), 25.3 (OC(*C*$H_3)_2$), 22.0 (NCH$_2$*C*H$_2$), 11.5 (CH$_2$*C*H$_3$). ^{11}B NMR (160.4 MHz, C_6D_6, 300 K) δ_B (ppm): 27.4 (br. s, N*B*).

Hydroboration of iso-propyl isocyanate

96. *N,N-methyl-{B(OCMe$_2$)$_2$}-iso-propylamine*

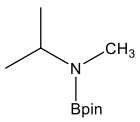

NMR scale: 19.7 µL of *iso*-propyl isocyanate. ^{1}H NMR (500 MHz, C_6D_6, 300 K) δ_H (ppm): 3.79 (1H, sept, J_{HH} = 5 Hz, C*H*$(CH_3)_2$), 2.56 (3H, s, NC*H*$_3$), 1.11 (12H, s, OC(C*H*$_3)_2$), 1.03 (6H, d, J_{HH} = 10 Hz, CH(C*H*$_3)_2$). ^{13}C{^{1}H} NMR (125.8 MHz, C_6D_6, 300 K) δ_C (ppm): 83.2 (O*C*$(CH_3)_2$), 46.8 (N*C*H$_3$), 27.5 (N*C*H$(CH_3)_2$), 25.2 (OC(*C*$H_3)_2$), 21.4 (CH(*C*$H_3)_2$). ^{11}B NMR (160.4 MHz, C_6D_6, 300 K) δ_B (ppm): 27.2 (br. s, N*B*).

Hydroboration of tert-butyl isocyanate

97. *N,N-methyl-{B(OCMe$_2$)$_2$}-tert-butylamine*

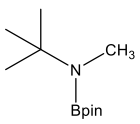

NMR scale: 22.8 µL of *tert*-butyl isocyanate. ^{1}H NMR (500 MHz, C_6D_6, 300 K) δ_H (ppm): 2.69 (3H, s, NC*H*$_3$), 1.28 (9H, s, C(C*H*$_3)_3$), 1.09 (12H, s, OC(C*H*$_3)_2$). ^{13}C{^{1}H} NMR (125.8 MHz, C_6D_6, 300 K) δ_C (ppm): 83.5 (O*C*$(CH_3)_2$), 52.2

($C(CH_3)_3$), 30.2 ($C(CH_3)_3$), 25.1 ($OC(CH_3)_2$). ^{11}B NMR (160.4 MHz, C_6D_6, 300 K) δ_B (ppm): 24.3 (br. s, N*B*).

Hydroboration of cyclohexyl isocyanate

98. ***N,N-methyl-{B(OCMe$_2$)$_2$}-cyclohexylamine***

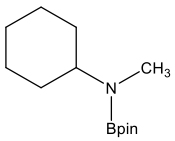

NMR scale: 25.5 µL of cyclohexyl isocyanate. ^{1}H NMR (500 MHz, C_6D_6, 300 K) δ_H (ppm): 3.29 (1H, m, NC*H*), 2.63 (3H, s, NCH_3), 1.62 (4H, m, NCH(CH_2)$_2$), 1.45 (4H, m, NCH(CH_2)$_2$(CH_2)$_2$), 1.12 (12H, s, OC(CH_3)$_2$), 0.88 (2H, m, (CH_2)$_2$CH_2). ^{13}C{^{1}H} NMR (125.8 MHz, C_6D_6, 300 K) δ_C (ppm): 83.5 ($OC(CH_3)_2$), 55.7 (N*C*H), 32.3 (N*C*H_3), 29.1 (NCH(CH_2)$_2$), 26.8 (NCH(CH_2)$_2$(CH_2)$_2$), 25.9 (OC(CH_3)$_2$), 14.7 ((CH_2)$_2$*C*H_2). ^{11}B NMR (160.4 MHz, C_6D_6, 300 K) δ_B (ppm): 27.4 (br. s, N*B*).

Hydroboration of 1-adamantyl isocyanate

99. ***N,N-methyl-{B(OCMe$_2$)$_2$}-adamantylamine***

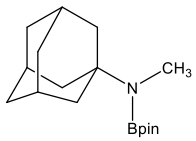

NMR scale: 35 mg of adamantyl isocyanate. ^{1}H NMR (500 MHz, C_6D_6, 300 K) δ_H (ppm): 2.73 (3H, s, NCH_3), 1.65 – 1.06 (15H, m, Ad-*H*), 1.10 (12H, s, OC(CH_3)$_2$). ^{13}C{^{1}H} NMR (125.8 MHz, C_6D_6, 300 K) δ_C (ppm): 83.5 ($OC(CH_3)_2$), 42.6 (N*C*H_3), 37.4 (Ad-*C*), 30.8 (Ad-*C*), 25.3 (OC(CH_3)$_2$), 25.1 (Ad-*C*). ^{11}B NMR (160.4 MHz, C_6D_6, 300K) δ_B (ppm): 27.5 (br. s, N*B*).

100. ***N-2,4,6-trimethylphenyl imine***

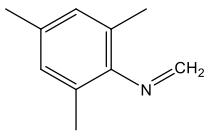

^{1}H NMR (500 MHz, C_6D_6, 300 K) δ_H (ppm): 7.24 (1H, d, J_{HH} = 12 Hz, NCH_2), 6.82 (1H, d, J_{HH} = 12 Hz, NCH_2), 6.76 (2H, s, *m*-*H*), 2.25 (6H, s, *o*-CH_3), 2.09 (3H, s, *p*-CH_3). ^{13}C{^{1}H} NMR (75.5 MHz, C_6D_6, 300 K) δ_C (ppm): 138.2 (*ipso*-*C*), 135.2 (*o*-*C*), 133.4 (*p*-*C*), 129.4 (NCH_2), 124.7 (*m*-*C*), 23.4 (*o*-*C*H_3), 18.6 (*p*-*C*H_3).

101. ***N-2,6-di-iso-propylphenyl imine***

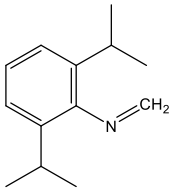

^{1}H NMR (500 MHz, C_6D_6, 300 K) δ_H (ppm): 7.25 (1H, d, J_{HH} = 20 Hz, NCH_2), 7.10 (2H, d, J_{HH} = 5 Hz, *m*-*H*), 7.07 (1H, t, J_{HH} = 5 Hz, *p*-*H*), 6.90 (1H, d, J_{HH} = 20 Hz, NCH_2), 2.98 (2H, sept, J_{HH} = 10 Hz, C*H*(CH_3)$_2$), 1.31 (6H, d, J_{HH} = 10 Hz, CH(CH_3)$_2$), 1.23 (6H, d, J_{HH} = 10 Hz, CH(CH_3)$_2$). ^{13}C{^{1}H} NMR (75.5 MHz, C_6D_6, 300 K) δ_C (ppm): 154.3 (*ipso*-*C*), 147.3 (*o*-*C*), 138.5 (*p*-*C*), 124.2 (*m*-*C*), 127.8 (N*C*H_2), 28.3 (*C*H(CH_3)$_2$), 25.4 (CH(*C*H_3)$_2$).

102. ***LMgOBpin***

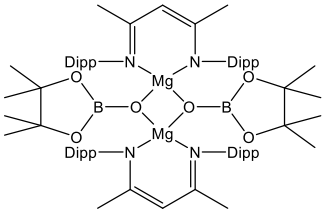

Due to insoluble nature of this compound, no NMR data could be obtained.

7.7 X-Ray Crystallographic Data

Table 7-1. X-Ray crystallographic data for Chapter 2

Compound	2	12	13	14	16	32
Molecular formula	C_{52} H_{69} Mg N_5 O	C_{40} H_{57} Mg N_3 O	C_{48} H_{69} Mg N_5 O	C_{98} H_{128} Mg_2 N_8 O_2	C_{51} H_{63} Mg N_5 O	$C_{69.50}$ H_{94} Mg N_6
Molecular weight	804.43	620.20	756.39	1498.70	786.37	1037.82
Space group	$P2_1/c$	C2/m	$P2_1nb$	P 1 2_1/c 1	P-1	P 21/n
a (Å)	13.3560(3)	17.9823(4)	11.4752(1)	12.35220(10)	9.7610(1)	11.1770(1)
b (Å)	17.4416(2)	19.5182(6)	20.0367(2)	29.6250(3)	11.5270 (4)	25.6120(3)
c (Å)	20.6267(4)	13.2619(4)	20.6247(2)	23.9944(2)	20.7970(4)	22.8890(3)
α °	90	90	90	90	96.877(1)	90
β °	91.014(1)	129.804(1)	90	96.1040(10)	93.202(1)	96.622(1)
γ °	90	90	90	90	92.212(1)	90
D_C Mg m^{-3}	1.112	1.152	1.059	1.140	1.127	1.059
μ (mm^{-1})	0.078	0.084	0.075	0.081	0.080	0.070
Reflections collected	78826	30713	83094	118585	42714	85482
Unique reflections	10989	4215	10838	19910	10557	11437
Parameters varied	545	258	514	1019	534	716
R_{int}	0.0679	0.0697	0.0678	0.0702	0.0594	0.0709
R_1	0.0520	0.0492	0.0435	0.0521	0.0519	0.0534
wR_2	0.1314	0.1286	0.0907	0.1136	0.1135	0.1173

Table 7-2. X-Ray Crystallographic Data for Chapters 3 & 4

Compound	46	53	69	70	71	73
Molecular formula	$C_{21}H_{32}B_2NO_5$	$C_{15}H_{31}B_2NO_4$	$C_{37}H_{49}MgN_3O$	$C_{74}H_{98}Mg_2N_6O_2$	$C_{40}H_{64}MgBN_3O_2$	$C_{102}H_{132}BMg_2N_6O_2$
Molecular weight	400.10	311.03	576.10	1152.20	654.06	1533.57
Space group	C 2/c	P $\bar{1}$	P 2_1/n	P 2_1/n	P 2_1/c	C_c
a (Å)	10.2451(3)	6.30720(10)	12.7410(2)	22.7470 (2)	13.7058(2)	12.3279(5)
b (Å)	11.5707(4)	12.4643(3)	12.9480(2)	13.2640(1)	13.1659(2)	30.1877(9)
c (Å)	19.7004(6)	12.5184(3)	20.7600(3)	24.9170 (2)	22.9509(3)	26.5175(11)
α °	90	101.1406(10)	90	90	90	90
***β* °**	103.599(2)	100.1735(10)	92.575 (1)	115.512(1)	96.1775(6)	102.622(2)
γ °	90	103.8021(12)	90	90	90	90
D_C Mg m^{-3}	1.171	1.133	1.118	1.128	1.055	1.058
μ (mm-^{1})	0.080	0.078	0.083	0.084	0.077	0.074
Reflections collected	20219	16086	58058	113992	76184	35062
Unique reflections	2567	3190	7818	15492	9431	14729
Parameters varied	155	208	391	779	445	1061
R_{int}	0.0862	0.0465	0.0658	0.0685	0.0814	0.1401
R_1	0.0865	0.0495	0.0569	0.0561	0.0498	0.0804
wR_2	0.1531	0.1087	0.1247	0.1192	0.1103	0.1714

Table 7-3. X-Ray Crystalographic Data for Chapters 5 & 6

Compound	80	81	84	90	102
Molecular formula	$C_{74.10}H_{109.20}Mg_2N_6$	$C_{13}H_{27}BN_2O_2$	$C_{31}H_{47}BN_2O_2$	$C_{84}H_{138}B_2Mg_2N_8O_4$	$C_{76}H_{112}B_2Mg_2N_4O_6$
Molecular weight	1132.69	254.18	490.52	1394.26	1247.94
Space group	$P2_1/c$	P-1	P-1	$Pc2_1n$	P 1 2_1/a 1
a (Å)	18.9579(8)	6.1250(2)	9.7280(2)	17.5990(2)	23.9571(3)
b (Å)	19.7413(9)	10.7140(5)	9.8860(2)	18.1910(2)	13.2163(3)
c (Å)	18.7107(8)	12.8050(5)	17.6310(4)	26.4980(4)	24.4044(4)
α °	90	107.001(2)	80.384(1)	90	90
β °	99.765(4)	98.855(2)	86.488(1)	90	109.7774(10)
γ °	90	92.034(2)	62.486(1)	90	90
D_C Mg m^{-3}	1.090	1.067	1.099	1.092	1.140
μ (mm-^{1})	1.563	0.070	0.067	0.079	0.086
Reflections collected	50997	13285	30569	115793	133249
Unique reflections	12177	7818	8551	17241	12741
Parameters varied	840	171	338	938	839
R_{int}	0.0901	0.0356	0.0690	0.0983	0.1228
R_1	0.0810	0.0447	0.0554	0.0675	0.0543
wR_2	0.2100	0.1175	0.1124	0.1312	0.1250

Notes:

Compound 16 - Methyl hydrogens attached to C1 and C5 are disordered

Compound 32 - In addition to one molecule of the magnesium complex, the asymmetric unit was noted to contain half of a toluene molecule. This solvent moiety lies close to a crystallographic inversion centre which serves to generate the remainder. As such, the methyl group is present at 50% occupancy, due to symmetry imposed disorder. H5 was located and refined at a distance of 0.98Å from N5. The methyl hydrogens attached to C1, C5 and C32 were included as being disordered, at calculated positions. Dif fraction was noted to decline at higher Bragg angles and, hence, data were truncated to a theta value of 25 degrees.

Compound 80 - The asymmetric unit comprises two independent dimer halves, each proximate to a crystallographic inversion centre (which is exploited to generate the molecule remainders) plus half of a toluene molecule with 60% occupancy. The latter, which also straddles an inversion centre, necessarily means that the associated methyl substituent is disordered by symmetry. Consequently, the hydrogen attached to C75 for the 50% of time when the solvent methyl group is absent from the asymmetric unit was omitted from the refinement. H30 and H66 were located and refined at a distance of 0.98Å from the parent carbons. 60:40 disorder was modelled for the cyclohexyl group based on C67. C_1-C_2 and $C_1 \ldots C_3$ distances were restrained in the minor disordered position of this ring, to assist convergence. Some ADP restraints were also included for the same reason.

Compound 81 - 2 molecules the asymmetric unit

Chapter 8. References

1. R. W. Hoffmann, *Chemical Society Reviews*, 2003, **32**, 225-230.

2. F. Bickelhaupt, *Chemical Society Reviews*, 1999, **28**, 17-23.

3. T. Satoh, *Chemical Society Reviews*, 2007, **36**, 1561-1572.

4. S. P. Green, C. Jones and A. Stasch, *Science*, 2007, **318**, 1754-1757.

5. S. Krieck, H. Goerls, L. Yu, M. Reiher and M. Westerhausen, *Journal of the American Chemical Society*, 2009, **131**, 2977-2985.

6. M. Westerhausen, *Angewandte Chemie-International Edition*, 2008, **47**, 2185-2187.

7. R. D. Shannon, *Acta Crystallographica Section A*, 1976, **32**, 751-767.

8. M. H. Chisholm, J. Gallucci and K. Phomphrai, *Chemical Communications*, 2003, 48-49.

9. M. H. Chisholm, J. C. Gallucci and K. Phomphrai, *Inorganic Chemistry*, 2004, **43**, 6717-6725.

10. S. Sarish, S. Nembenna, S. Nagendran, H. W. Roesky, A. Pal, R. Herbst-Irmer, A. Ringe and J. Magull, *Inorganic Chemistry*, 2008, **47**, 5971-5977.

11. A. G. M. Barrett, I. J. Casely, M. R. Crimmin, M. S. Hill, J. R. Lachs, M. F. Mahon and P. A. Procopiou, *Inorganic Chemistry*, 2009, **48**, 4445-4453.

12. A. G. M. Barrett, C. Brinkmann, M. R. Crimmin, M. S. Hill, P. Hunt and P. A. Procopiou, *Journal of the American Chemical Society*, 2009, **131**, 12906-12907.

13. C. Jones, S. J. Bonyhady, S. Nembenna and A. Stasch, *European Journal of Inorganic Chemistry*, 2012, 2596-2601.

14. J. F. Dunne, J. Su, A. Ellern and A. D. Sadow, *Organometallics*, 2008, **27**, 2399-2401.

15. J. F. Dunne, S. R. Neal, J. Engelkemier, A. Ellern and A. D. Sadow, *Journal of the American Chemical Society*, 2011, **133**, 16782-16785.

16. M. Arrowsmith, M. S. Hill and G. Kociok-Köhn, *Organometallics*, 2011, **30**, 1291.

17. J. S. Wixey and B. D. Ward, *Dalton Transactions*, 2011, **40**, 7693-7696.

18. S. Datta, P. W. Roesky and S. Blechert, *Organometallics*, 2007, **26**, 4392-4394.

19. S. Datta, M. T. Gamer and P. W. Roesky, *Organometallics*, 2008, **27**, 1207-1213.

20. A. G. M. Barrett, M. R. Crimmin, M. S. Hill, P. B. Hitchcock, G. Kociok-Köhn and P. A. Procopiou, *Inorganic Chemistry*, 2008, **47**, 7366-7376.

21. B. Liu, T. Roisnel, J.-F. Carpentier and Y. Sarazin, *Angewandte Chemie (International ed. in English)*, 2012, **51**, 4943-4946.

22. B. A. Vaartstra, J. C. Huffman, W. E. Streib and K. G. Caulton, *Inorganic Chemistry*, 1991, **30**, 121-125.

23. M. Westerhausen, M. Hartmann, N. Makropoulos, B. Wieneke, M. Wieneke, W. Schwarz and D. Stalke, *Zeitschrift Fur Naturforschung Section B-a Journal of Chemical Sciences*, 1998, **53**, 117-125.

24. M. Arrowsmith, M. S. Hill and G. Kociok-Köhn, *Organometallics*, 2010, **29**, 4203-4206.

25. M. R. Crimmin, A. G. M. Barrett, M. S. Hill, D. J. MacDougall, M. F. Mahon and P. A. Procopiou, *Chemistry-a European Journal*, 2008, **14**, 11292-11295.

26. S. Hong and T. J. Marks, *Accounts of Chemical Research*, 2004, **37**, 673-686.

27. R. Anwander, *Lanthanide Amides*, Springer, Berlin Heidelberg, 1996.

28. Y. W. Li and T. J. Marks, *Organometallics*, 1996, **15**, 3770-3772.

29. G. A. Molander and J. A. C. Romero, *Chemical Reviews*, 2002, **102**, 2161-2185.

30. S. W. Hong, S. Tian, M. V. Metz and T. J. Marks, *Journal of the American Chemical Society*, 2003, **125**, 14768-14783.

31. B. D. Stubbert and T. J. Marks, *Journal of the American Chemical Society*, 2007, **129**, 4253-4271.

32. S. Hong, A. M. Kawaoka and T. J. Marks, *Journal of the American Chemical Society*, 2003, **125**, 15878-15892.

33. A. M. Seyam, B. D. Stubbert, T. R. Jensen, J. J. O'Donnell, C. L. Stern and T. J. Marks, *Inorganica Chimica Acta*, 2004, **357**, 4029-4035.

34. A. Motta, I. L. Fragala and T. J. Marks, *Organometallics*, 2006, **25**, 5533-5539.

35. V. M. Arredondo, S. Tian, F. E. McDonald and T. J. Marks, *Journal of the American Chemical Society*, 1999, **121**, 3633-3639.

36. Y. W. Li and T. J. Marks, *Journal of the American Chemical Society*, 1998, **120**, 1757-1771.

37. J. S. Ryu, T. J. Marks and F. E. McDonald, *Journal of Organic Chemistry*, 2004, **69**, 1038-1052.

38. J. S. Ryu, G. Y. Li and T. J. Marks, *Journal of the American Chemical Society*, 2003, **125**, 12584-12605.

39. X. Yu and T. J. Marks, *Organometallics*, 2007, **26**, 365-376.

40. S. D. Wobser, C. J. Stephenson, M. Delferro and T. J. Marks, *Organometallics*, 2013, **32**, 1317-1327.

41. X. Yu, S. Seo and T. J. Marks, *Journal of the American Chemical Society*, 2007, **129**, 7244-7245.

42. A. Dzudza and T. J. Marks, *Organic Letters*, 2009, **11**, 1523-1526.

43. S. Seo, X. Yu and T. J. Marks, *Journal of the American Chemical Society*, 2009, **131**, 263-276.

44. S. Seo and T. J. Marks, *Chemistry-a European Journal*, 2010, **16**, 5148-5162.

45. P. W. Roesky, U. Denninger, C. L. Stern and T. J. Marks, *Organometallics*, 1997, **16**, 4486-4492.

46. G. Jeske, H. Lauke, H. Mauermann, H. Schumann and T. J. Marks, *Journal of the American Chemical Society*, 1985, **107**, 8111-8118.

47. A. Motta, I. L. Fragala and T. J. Marks, *Organometallics*, 2005, **24**, 4995-5003.

48. A. M. Kawaoka, M. R. Douglass and T. J. Marks, *Organometallics*, 2003, **22**, 4630-4632.

49. M. R. Douglass, C. L. Stern and T. J. Marks, *Journal of the American Chemical Society*, 2001, **123**, 10221-10238.

50. C. J. Weiss, S. D. Wobser and T. J. Marks, *Organometallics*, 2010, **29**, 6308-6320.

51. C. J. Weiss and T. J. Marks, *Dalton Transactions*, 2010, **39**, 6576-6588.

52. A. Dzudza and T. J. Marks, *Journal of Organic Chemistry*, 2008, **73**, 4004-4016.

53. S. Seo and T. J. Marks, *Organic Letters*, 2008, **10**, 317-319.

54. A. M. Kawaoka and T. J. Marks, *Journal of the American Chemical Society*, 2005, **127**, 6311-6324.

55. L. Jia, X. M. Yang, A. M. Seyam, I. D. L. Albert, P. F. Fu, S. T. Yang and T. J. Marks, *Journal of the American Chemical Society*, 1996, **118**, 7900-7913.

56. S. Seo, X. Yu and T. J. Marks, *Tetrahedron Letters*, 2013, **54**, 1828-1831.

57. G. Jeske, H. Lauke, H. Mauermann, P. N. Swepston, H. Schumann and T. J. Marks, *Journal of the American Chemical Society*, 1985, **107**, 8091-8103.

58. A. S. Dudnik, V. L. Weidner, A. Motta, M. Delferro and T. J. Marks, *Nature Chemistry*, 2014, **6**, 1100-1107.

59. M. Westerhausen, S. Schneiderbauer, A. N. Kneifel, Y. Soltl, P. Mayer, H. Noth, Z. Y. Zhong, P. J. Dijkstra and J. Feijen, *European Journal of Inorganic Chemistry*, 2003, 3432-3439.

60. Y. Sarazin, R. H. Howard, D. L. Hughes, S. M. Humphrey and M. Bochmann, *Dalton Transactions*, 2006, 340-350.

61. M. G. Davidson, C. T. O'Hara, M. D. Jones, C. G. Keir, M. F. Mahon and G. Kociok-Köhn, *Inorganic Chemistry*, 2007, **46**, 7686-7688.

62. W. Vargas and K. Ruhlandt-Senge, *European Journal of Inorganic Chemistry*, 2003, 3472-3479.

63. D. J. Burkey and T. P. Hanusa, *Organometallics*, 1996, **15**, 4971-4976.

64. D. C. Green, U. Englich and K. Ruhlandt-Senge, *Angewandte Chemie-International Edition*, 1999, **38**, 354-357.

65. A. G. M. Barrett, M. R. Crimmin, M. S. Hill, P. B. Hitchcock, S. L. Lomas, M. F. Mahon, P. A. Procopiou and K. Suntharalingam, *Organometallics*, 2008, **27**, 6300-6306.

66. A. G. Avent, M. R. Crimmin, M. S. Hill and P. B. Hitchcock, *Organometallics*, 2005, **24**, 1184-1188.

67. M. Westerhausen, M. H. Digeser, M. Krofta, N. Wiberg, H. Noth, J. Knizek, W. Ponikwar and T. Seifert, *European Journal of Inorganic Chemistry*, 1999, 743-750.

68. M. Westerhausen, M. H. Digeser, B. Wieneke, H. Noth and J. Knizek, *European Journal of Inorganic Chemistry*, 1998, 517-521.

69. M. Westerhausen, C. Birg, M. Krofta, P. Mayer, T. Seifert, H. Noth, A. Pfitzner, T. Nilges and H. J. Deiseroth, *Zeitschrift Fur Anorganische Und Allgemeine Chemie*, 2000, **626**, 1073-1080.

70. M. Westerhausen, M. H. Digeser, H. Noth and J. Knizek, *Zeitschrift Fur Anorganische Und Allgemeine Chemie*, 1998, **624**, 215-220.

71. S. E. Baillie, V. L. Blair, T. D. Bradley, W. Clegg, J. Cowan, R. W. Harrington, A. Hernan-Gomez, A. R. Kennedy, Z. Livingstone and E. Hevia, *Chemical Science*, 2013, **4**, 1895-1905.

72. M. Westerhausen, M. H. Digeser and W. Schwarz, *Inorganic Chemistry*, 1997, **36**, 521-527.

73. M. Westerhausen, M. H. Digeser, H. Noth, W. Ponikwar, T. Seifert and K. Polborn, *Inorganic Chemistry*, 1999, **38**, 3207-3214.

74. M. Westerhausen, M. H. Digeser, C. Guckel, H. Noth, J. Knizek and W. Ponikwar, *Organometallics*, 1999, **18**, 2491-2496.

75. M. Westerhausen, H. D. Hausen and W. Schwarz, *Zeitschrift Fur Anorganische Und Allgemeine Chemie*, 1992, **618**, 121-130.

76. M. Westerhausen and H. D. Hausen, *Zeitschrift Fur Anorganische Und Allgemeine Chemie*, 1992, **615**, 27-34.

77. A. Weeber, S. Harder, H. H. Brintzinger and K. Knoll, *Organometallics*, 2000, **19**, 1325-1332.

78. F. Feil and S. Harder, *Organometallics*, 2000, **19**, 5010-5015.

79. F. Feil and S. Harder, *Organometallics*, 2001, **20**, 4616-4622.

80. S. Harder, F. Feil and A. Weeber, *Organometallics*, 2001, **20**, 1044-1046.

81. M. R. Crimmin, I. J. Casely and M. S. Hill, *Journal of the American Chemical Society*, 2005, **127**, 2042-2043.

82. C. Brinkmann, A. G. M. Barrett, M. S. Hill and P. A. Procopiou, *Journal of the American Chemical Society*, 2012, **134**, 2193-2207.

83. J. R. Lachs, A. G. M. Barrett, M. R. Crimmin, G. Kociok-Köhn, M. S. Hill, M. F. Mahon and P. A. Procopiou, *European Journal of Inorganic Chemistry*, 2008, 4173-4179.

84. A. G. M. Barrett, T. C. Boorman, M. R. Crimmin, M. S. Hill, G. Kociok-Köhn and P. A. Procopiou, *Chemical Communications*, 2008, 5206-5208.

85. A. G. M. Barrett, M. R. Crimmin, M. S. Hill and P. A. Procopiou, *Proceedings of the Royal Society a-Mathematical Physical and Engineering Sciences*, 2010, **466**, 927-963.

86. M. R. Crimmin, A. G. M. Barrett, M. S. Hill, P. B. Hitchcock and P. A. Procopiou, *Organometallics*, 2007, **26**, 2953-2956.

87. M. R. Crimmin, A. G. M. Barrett, M. S. Hill, P. B. Hitchcock and P. A. Procopiou, *Organometallics*, 2008, **27**, 497-499.

88. Y. K. Kim, T. Livinghouse and J. E. Bercaw, *Tetrahedron Letters*, 2001, **42**, 2933-2935.

89. M. Arrowsmith, M. R. Crimmin, A. G. M. Barrett, M. S. Hill, G. Kociok-Köhn and P. A. Procopiou, *Organometallics*, 2011, **30**, 1493-1506.

90. M. R. Crimmin, M. Arrowsmith, A. G. M. Barrett, I. J. Casely, M. S. Hill and P. A. Procopiou, *Journal of the American Chemical Society*, 2009, **131**, 9670-9685.

91. M. E. Jung and G. Piizzi, *Chemical Reviews*, 2005, **105**, 1735-1766.

92. M. R. Gagne, C. L. Stern and T. J. Marks, *Journal of the American Chemical Society*, 1992, **114**, 275-294.

93. T. M. A. Al-Shboul, H. Goerls and M. Westerhausen, *Inorganic Chemistry Communications*, 2008, **11**, 1419-1421.

94. B. Liu, T. Roisnel, J.-F. Carpentier and Y. Sarazin, *Chemistry-a European Journal*, 2013, **19**, 13445-13462.

95. B. Liu, J.-F. Carpentier and Y. Sarazin, *Chemistry-a European Journal*, 2012, **18**, 13259-13264.

96. A. G. M. Barrett, M. R. Crimmin, M. S. Hill, P. B. Hitchcock, S. L. Lomas, M. F. Mahon and P. A. Procopiou, *Dalton Transactions*, 2010, **39**, 7393-7400.

97. L. Orzechowski and S. Harder, *Organometallics*, 2007, **26**, 2144-2148.

98. S. Haerling, J. Greiser, T. M. A. Al-Shboul, H. Goerls, S. Krieck and M. Westerhausen, *Australian Journal of Chemistry*, 2013, **66**, 1264-1273.

99. M. S. Hill, D. J. Liptrot, D. J. MacDougall, M. F. Mahon and T. P. Robinson, *Chemical Science*, 2013, **4**, 4212-4222.

100. P. Bellham, M. S. Hill, G. Kociok-Köhn and D. J. Liptrot, *Dalton Transactions*, 2013, **42**, 737-745.

101. P. Bellham, M. S. Hill, G. Kociok-Köhn and D. J. Liptrot, *Chemical Communications*, 2013, **49**, 1960-1962.

102. P. Bellham, M. S. Hill and G. Kociok-Köhn, *Organometallics*, 2014, **33**, 5716-5721.

103. D. J. Liptrot, M. S. Hill, M. F. Mahon and D. J. MacDougall, *Chemistry-a European Journal*, 2010, **16**, 8508-8515.

104. P. Bellham, M. S. Hill, D. J. Liptrot, D. J. MacDougall and M. F. Mahon, *Chemical Communications*, 2011, **47**, 9060-9062.

105. M. S. Hill, M. Hodgson, D. J. Liptrot and M. F. Mahon, *Dalton Transactions*, 2011, **40**, 7783-7790.

106. F. Buch and S. Harder, *Organometallics*, 2007, **26**, 5132-5135.

107. M. S. Hill, M. F. Mahon and T. P. Robinson, *Chemical Communications*, 2010, **46**, 7587-7589.

108. S. Harder and J. Brettar, *Angewandte Chemie-International Edition*, 2006, **45**, 3474-3478.

109. D. J. Gallagher, K. W. Henderson, A. R. Kennedy, C. T. O'Hara, R. E. Mulvey and R. B. Rowlings, *Chemical Communications*, 2002, 376-377.

110. P. C. Andrikopoulos, D. R. Armstrong, A. R. Kennedy, R. E. Mulvey, C. T. O'Hara and R. B. Rowlings, *European Journal of Inorganic Chemistry*, 2003, 3354-3362.

111. J. Spielmann and S. Harder, *Chemistry-a European Journal*, 2007, **13**, 8928-8938.

112. S. Harder, *Chemical Reviews*, 2010, **110**, 3852-3876.

113. S. Harder, *Chemical Communications*, 2012, **48**, 11165-11177.

114. J. Spielmann and S. Harder, *European Journal of Inorganic Chemistry*, 2008, 1480-1486.

115. P. Jochmann, J. P. Davin, T. P. Spaniol, L. Maron and J. Okuda, *Angewandte Chemie-International Edition*, 2012, **51**, 4452-4455.

116. A. G. M. Barrett, M. R. Crimmin, M. S. Hill, P. B. Hitchcock and P. A. Procopiou, *Organometallics*, 2007, **26**, 4076-4079.

117. S. J. Bonyhady, S. P. Green, C. Jones, S. Nembenna and A. Stasch, *Angewandte Chemie-International Edition*, 2009, **48**, 2973-2977.

118. S. J. Bonyhady, C. Jones, S. Nembenna, A. Stasch, A. J. Edwards and G. J. McIntyre, *Chemistry-a European Journal*, 2010, **16**, 938-955.

119. A. Sidiropoulos, C. Jones, A. Stasch, S. Klein and G. Frenking, *Angewandte Chemie-International Edition*, 2009, **48**, 9701-9704.

120. C. Jones, A. Sidiropoulos, N. Holzmann, G. Frenking and A. Stasch, *Chemical Communications*, 2012, **48**, 9855-9857.

121. W. D. Woodul, E. Carter, R. Mueller, A. F. Richards, A. Stasch, M. Kaupp, D. M. Murphy, M. Driess and C. Jones, *Journal of the American Chemical Society*, 2011, **133**, 10074-10077.

122. S. J. Bonyhady, D. Collis, G. Frenking, N. Holzmann, C. Jones and A. Stasch, *Nature Chemistry*, 2010, **2**, 865-869.

123. M. S. Hill, D. J. MacDougall and M. F. Mahon, *Dalton Transactions*, 2010, **39**, 11129-11131.

124. M. S. Hill, G. Kociok-Köhn, D. J. MacDougall, M. F. Mahon and C. Weetman, *Dalton Transactions*, 2011, **40**, 12500-12509.

125. M. Arrowsmith, M. S. Hill, D. J. MacDougall and M. F. Mahon, *Angewandte Chemie-International Edition*, 2009, **48**, 4013-4016.

126. D. J. Liptrot, M. S. Hill and M. F. Mahon, *Chemistry-a European Journal*, 2014, **20**, 9871-9874.

127. S. Harder, J. Spielmann, J. Intemann and H. Bandmann, *Angewandte Chemie-International Edition*, 2011, **50**, 4156-4160.

128. J. Intemann, J. Spielmann, P. Sirsch and S. Harder, *Chemistry-a European Journal*, 2013, **19**, 8478-8489.

129. F. Buch, H. Brettar and S. Harder, *Angewandte Chemie-International Edition*, 2006, **45**, 2741-2745.

130. V. Leich, T. P. Spaniol, L. Maron and J. Okuda, *Chemical Communications*, 2014, **50**, 2311-2314.

131. P. Andersson and I. Munslow, *Modern Reduction Methods*, Wiley, 2008.

132. H.-J. Grutzmacher, *Catalytic Heterofunctionization*, Wiley-VCH, 2001.

133. H. C. Brown, H. I. Schlesinger and A. B. Burg, *Journal of the American Chemical Society*, 1939, **61**, 673-680.

134. H. I. Schlesinger, H. C. Brown and A. E. Finholt, *Journal of the American Chemical Society*, 1953, **75**, 205-209.

135. H. I. Schlesinger, H. C. Brown, H. R. Hoekstra and L. R. Rapp, *Journal of the American Chemical Society*, 1953, **75**, 199-204.

136. H. C. Brown and B. C. S. Rao, *Journal of the American Chemical Society*, 1956, **78**, 2582-2588.

137. H. C. Brown and B. C. S. Rao, *Journal of the American Chemical Society*, 1956, **78**, 5694-5695.

138. H. C. Brown and B. C. S. Rao, *Journal of Organic Chemistry*, 1957, **22**, 1136-1137.

139. D. Mannig and H. Noth, *Angewandte Chemie-International Edition in English*, 1985, **24**, 878-879.

140. K. Burgess and M. J. Ohlmeyer, *Chemical Reviews*, 1991, **91**, 1179-1191.

141. K. Oshima, T. Ohmura and M. Suginome, *Journal of the American Chemical Society*, 2012, **134**, 3699-3702.

142. K. N. Harrison and T. J. Marks, *Journal of the American Chemical Society*, 1992, **114**, 9220-9221.

143. J. F. Zhang, B. L. Lou, G. H. Guo and L. X. Dai, *Journal of Organic Chemistry*, 1991, **56**, 1670-1672.

144. T. Hayashi, Y. Matsumoto and Y. Ito, *Journal of the American Chemical Society*, 1989, **111**, 3426-3428.

145. D. A. Evans, G. C. Fu and B. A. Anderson, *Journal of the American Chemical Society*, 1992, **114**, 6679-6685.

146. S. A. Westcott, N. J. Taylor, T. B. Marder, R. T. Baker, N. J. Jones and J. C. Calabrese, *Journal of the Chemical Society-Chemical Communications*, 1991, 304-305.

147. S. Duttwyler, S. Chen, C. Lu, B. Q. Mercado, R. G. Bergman and J. A. Ellman, *Angewandte Chemie-International Edition*, 2014, **53**, 3877-3880.

148. D. V. Gutsulyak, A. van der Est and G. I. Nikonov, *Angewandte Chemie-International Edition*, 2011, **50**, 1384-1387.

149. S. B. Amin and T. J. Marks, *Angewandte Chemie-International Edition*, 2008, **47**, 2006-2025.

150. S. Kozuch and S. Shaik, *Accounts of Chemical Research*, 2011, **44**, 101-110.

151. S. Kozuch, *Wiley Interdisciplinary Reviews-Computational Molecular Science*, 2012, **2**, 795-815.

152. T. J. Hadlington, M. Hermann, G. Frenking and C. Jones, *Journal of the American Chemical Society*, 2014, **136**, 3028-3031.

153. S. Harder and J. Spielmann, *Journal of Organometallic Chemistry*, 2012, **698**, 7-14.

154. M. Arrowsmith, T. J. Hadlington, M. S. Hill and G. Kociok-Köhn, *Chemical Communications*, 2012, **48**, 4567-4569.

155. M. Arrowsmith, M. S. Hill and G. Kociok-Köhn, *Chemistry-a European Journal*, 2013, **19**, 2776-2783.

156. J. Intemann, M. Lutz and S. Harder, *Organometallics*, 2014, **33**, 5722-5729.

157. D. Mukherjee, A. Ellern and A. D. Sadow, *Chemical Science*, 2014, **5**, 959-964.

158. M. D. Anker, M. Arrowsmith, P. Bellham, M. S. Hill, G. Kociok-Köhn, D. J. Liptrot, M. F. Mahon and C. Weetman, *Chemical Science*, 2014, **5**, 2826-2830.

159. A. Berkefeld, W. E. Piers, M. Parvez, L. Castro, L. Maron and O. Eisenstein, *Chemical Science*, 2013, **4**, 2152-2162.

160. J. M. Berg, J. L. Tymoczko and L. Stryer, *Biochemistry*, Freeman, New York, 2002.

161. U. Eisner and J. Kuthan, *Chemical Reviews*, 1972, **72**, 1-42.

162. A. Hantzsch, *Justus Liebigs Annalen der Chemie*, 1882, **215**, 1-82.

163. F. Bossert, H. Meyer and E. Wehinger, *Angewandte Chemie-International Edition in English*, 1981, **20**, 762-769.

164. M. F. Gordeev, D. V. Patel, B. P. England, S. Jonnalagadda, J. D. Combs and E. M. Gordon, *Bioorganic & Medicinal Chemistry*, 1998, **6**, 883-889.

165. V. M. Briukhanov, I. Zverev and V. I. Elkin, *Eksp. Klin. Farmakol*, 1994, **57**, 47-49.

166. J. M. Tusell, S. Barron and J. Serratosa, *Neurotoxicology*, 1993, **15**, 751-756.

167. G. A. Wachter, M. C. Davis, A. R. Martin and S. G. Franzblau, *Journal of Medicinal Chemistry*, 1998, **41**, 2436-2438.

168. B. Desai, D. Sureja, Y. Naliapara, A. Shah and A. K. Saxena, *Bioorganic & Medicinal Chemistry*, 2001, **9**, 1993-1998.

169. A. R. Pape, K. P. Kaliappan and E. P. Kundig, *Chemical Reviews*, 2000, **100**, 2917-2940.

170. J. G. Keay, *Advances in Heterocyclic Chemistry*, 1986, **39**, 1-77.

171. R. A. Sulzbach, *Journal of Organometallic Chemistry*, 1970, **24**, 307-314.

172. K. Ziegler and H. Zeiser, *Berichte der deutschen chemischen Gesellschaft (A and B Series)*, 1930, **63**, 1847-1851.

173. D. R. Armstrong, R. E. Mulvey, D. Barr, R. Snaith and D. Reed, *Journal of Organometallic Chemistry*, 1988, **350**, 191-205.

174. W. Clegg, L. Dunbar, L. Horsburgh and R. E. Mulvey, *Angewandte Chemie-International Edition in English*, 1996, **35**, 753-755.

175. D. D. Tanner and C. M. Yang, *Journal of Organic Chemistry*, 1993, **58**, 1840-1846.

176. K. Hensen, A. Lemke, T. Stumpf, M. Bolte, H. Fleischer, C. R. Pulham, R. O. Gould and S. Harris, *Inorganic Chemistry*, 1999, **38**, 4700-4704.

177. P. T. Lansbury and J. O. Peterson, *Journal of the American Chemical Society*, 1963, **85**, 2236-2242.

178. P. T. Lansbury and J. O. Peterson, *Journal of the American Chemical Society*, 1961, **83**, 3537-3538.

179. P. T. Lansbury and J. O. Peterson, *Journal of the American Chemical Society*, 1962, **84**, 1756-1757.

180. C. T. Carver, D. Benitez, K. L. Miller, B. N. Williams, E. Tkatchouk, W. A. Goddard, III and P. L. Diaconescu, *Journal of the American Chemical Society*, 2009, **131**, 10269-10278.

181. P. L. Diaconescu, *Accounts of Chemical Research*, 2010, **43**, 1352-1363.

182. C. T. Carver and P. L. Diaconescu, *Journal of the American Chemical Society*, 2008, **130**, 7558-7559.

183. M. H. Chisholm, J. C. Huffman and K. Phomphrai, *Journal of the Chemical Society-Dalton Transactions*, 2001, 222-224.

184. I. L. Fedushkin, A. A. Skatova, G. K. Fukin, M. Hummert and H. Schumann, *European Journal of Inorganic Chemistry*, 2005, 2332-2338.

185. C. C. Chang, B. Srinivas, M. L. Wu, W. H. Chiang, M. Y. Chiang and C. S. Hsiung, *Organometallics*, 1995, **14**, 5150-5159.

186. C. C. Chang and M. S. Ameerunisha, *Coordination Chemistry Reviews*, 1999, **189**, 199-278.

187. S. J. Connon, *Organic & Biomolecular Chemistry*, 2007, **5**, 3407-3417.

188. K. L. Miller, B. N. Williams, D. Benitez, C. T. Carver, K. R. Ogilby, E. Tkatchouk, W. A. Goddard, III and P. L. Diaconescu, *Journal of the American Chemical Society*, 2010, **132**, 342-355.

189. K. Schwetlick, R. Noack and F. Stebner, *Journal of the Chemical Society-Perkin Transactions 2*, 1994, 599-608.

190. C. N. Rowley, T.-G. Ong, J. Priem, T. K. Woo and D. S. Richeson, *Inorganic Chemistry*, 2008, **47**, 9660-9668.

191. R. Matsubara and S. Kobayashi, *Accounts of Chemical Research*, 2008, **41**, 292-301.

192. G. Stork, R. Terrell and J. Szmuszkovicz, *Journal of the American Chemical Society*, 1954, **76**, 2029-2030.

193. B. M. Day, N. E. Mansfield, M. P. Coles and P. B. Hitchcock, *Chemical Communications*, 2011, **47**, 4995-4997.

194. B. M. Day, W. Knowelden and M. P. Coles, *Dalton Transactions*, 2012, **41**, 10930-10933.

195. R. J. Schwamm and M. P. Coles, *Organometallics*, 2013, **32**, 5277-5280.

196. L. J. Hao, J. F. Harrod, A. M. Lebuis, Y. Mu, R. H. Shu, E. Samuel and H. G. Woo, *Angewandte Chemie-International Edition*, 1998, **37**, 3126-3129.

197. W. Clegg, A. J. Scott, C. Y. Dai, G. Lesley, T. B. Marder, N. C. Norman and L. J. Farrugia, *Acta Crystallographica Section C-Crystal Structure Communications*, 1996, **52**, 2545-2547.

198. K. C. Jantunen, B. L. Scott, P. J. Hay, J. C. Gordon and J. L. Kiplinger, *Journal of the American Chemical Society*, 2006, **128**, 6322–6323.

199. F. Ullman, *Ullmann's Encyclopedia of Industrial Chemistry*, Wiley-VCH, Weinheim, Germany, 2008.

200. H. U. Blaser, C. Malan, B. Pugin, F. Spindler, H. Steiner and M. Studer, *Advanced Synthesis & Catalysis*, 2003, **345**, 103-151.

201. F. E. Gould, G. S. Johnson and A. F. Ferris, *Journal of Organic Chemistry*, 1960, **25**, 1658-1660.

202. L. Hegedus and T. Mathe, *Applied Catalysis a-General*, 2005, **296**, 209-215.

203. L. Hegedus, T. Mathe and T. Karpati, *Applied Catalysis a-General*, 2008, **349**, 40-45.

204. Y. Y. Huang and W. M. H. Sachtler, *Journal of Catalysis*, 1999, **188**, 215-225.

205. S. Laval, W. Dayoub, A. Favre-Reguillon, M. Berthod, P. Demonchaux, G. Mignani and M. Lemaire, *Tetrahedron Letters*, 2009, **50**, 7005-7007.

206. L. H. Amundsen and L. S. Nelson, *Journal of the American Chemical Society*, 1951, **73**, 242-244.

207. J. Z. Saavedra, A. Resendez, A. Rovira, S. Eagon, D. Haddenham and B. Singaram, *Journal of Organic Chemistry*, 2012, **77**, 221-228.

208. A. S. B. Prasad, J. V. B. Kanth and M. Periasamy, *Tetrahedron*, 1992, **48**, 4623-4628.

209. D. Haddenham, L. Pasumansky, J. DeSoto, S. Eagon and B. Singaram, *Journal of Organic Chemistry*, 2009, **74**, 1964-1970.

210. P. A. Chase, G. C. Welch, T. Jurca and D. W. Stephan, *Angewandte Chemie-International Edition*, 2007, **46**, 8050-8053.

211. P. A. Chase, T. Jurca and D. W. Stephan, *Chemical Communications*, 2008, 1701-1703.

212. H. I. Schlesinger and B. A. Burg, *Chemical Reviews*,1942, **31**, 1-41.

213. Y. Chujo, I. Tomita and T. Saegusa, *Macromolecules*, 1994, **27**, 6714-6717.

214. D. Jaganyi and A. Mzinyati, *Polyhedron*, 2006, **25**, 2730-2736.

215. A. Y. Khalimon, P. Farha, L. G. Kuzmina and G. I. Nikonov, *Chemical Communications*, 2012, **48**, 455-457.

216. W. Uhl and M. Matar, *Zeitschrift Fur Naturforschung Section B-a Journal of Chemical Sciences*, 2004, **59**, 1214-1222.

217. J. Kaneti, P. V. Schleyer, T. Clark, A. J. Kos, G. W. Spitznagel, J. G. Andrade and J. B. Moffat, *Journal of the American Chemical Society*, 1986, **108**, 1481-1492.

218. P. Binger, F. Sandmeyer and C. Kruger, *Organometallics*, 1995, **14**, 2969-2976.

219. A. C. Hillier, T. Fox, H. W. Schmalle and H. Berke, *Journal of Organometallic Chemistry*, 2003, **669**, 14-24.

220. J. R. Galsworthy, C. E. Housecroft, J. S. Humphrey, X. J. Song, A. J. Edwards and A. L. Rheingold, *Journal of the Chemical Society-Dalton Transactions*, 1994, 3273-3277.

221. I. L. Fedushkin, A. G. Morozov, V. A. Chudakova, G. K. Fukin and V. K. Cherkasov, *European Journal of Inorganic Chemistry*, 2009, 4995-5003.

222. J. F. Hartwig, S. Bhandari and P. R. Rablen, *Journal of the American Chemical Society*, 1994, **116**, 1839-1844.

223. D. R. Edwards, Y. B. Hleba, C. J. Lata, L. A. Calhoun and C. M. Crudden, *Angewandte Chemie-International Edition*, 2007, **46**, 7799-7802.

224. E. V. Anslyn and D. A. Dougherty, *Modern Physical Organic Chemistry*, University Science Books, Sausalito, California, 2006.

225. R. A. Michelin, M. Mozzon and R. Bertani, *Coordination Chemistry Reviews*, 1996, **147**, 299-338.

226. R. Cini, P. A. Caputo, F. P. Intini and G. Natile, *Inorganic Chemistry*, 1995, **34**, 1130-1137.

227. N. A. Bokach, V. Y. Kukushkin, M. L. Kuznetsov, D. A. Garnovskii, G. Natile and A. J. L. Pombeiro, *Inorganic Chemistry*, 2002, **41**, 2041-2053.

228. K. V. Luzyanin, M. Haukka, N. A. Bokach, M. L. Kuznetsov, V. Y. Kukushkin and A. J. L. Pombeiro, *Journal of the Chemical Society-Dalton Transactions*, 2002, 1882-1887.

229. R. Ros, J. Renaud and R. Roulet, *Journal of Organometallic Chemistry*, 1976, **104**, 271-279.

230. F. A. Cotton, L. M. Daniels, C. A. Murillo and X. P. Wang, *Polyhedron*, 1998, **17**, 2781-2793.

231. F. A. Cotton and F. E. Kuhn, *Journal of the American Chemical Society*, 1996, **118**, 5826-5827.

232. V. Y. Kukushkin, I. V. Ilichev, G. Wagner, J. da Silva and A. J. L. Pombeiro, *Journal of the Chemical Society-Dalton Transactions*, 1999, 3047-3052.

233. V. Y. Kukushkin, I. V. Ilichev, M. A. Zhdanova, G. Wagner and A. J. L. Pombeiro, *Journal of the Chemical Society-Dalton Transactions*, 2000, 1567-1572.

234. M. L. Kuznetsov, *Journal of Molecular Structure-Theochem*, 2004, **674**, 33-42.

235. R. M. Oballa, J.-F. Truchon, C. I. Bayly, N. Chauret, S. Day, S. Crane and C. Berthelette, *Bioorganic & Medicinal Chemistry Letters*, 2007, **17**, 998-1002.

236. O. Castano, R. Notario, K. Hori and J. L. M. Abboud, *Structural Chemistry*, 1996, **7**, 321-327.

237. O. Exner, S. Bohm, M. Decouzon, J. F. Gal and P. C. Maria, *Journal of the Chemical Society-Perkin Transactions 2*, 2002, 168-172.

238. R. H. Staley, J. E. Kleckner and J. L. Beauchamp, *Journal of the American Chemical Society*, 1976, **98**, 2081-2085.

239. C. Colominas, M. Orozco, F. J. Luque, J. I. Borrell and J. Teixido, *Journal of Organic Chemistry*, 1998, **63**, 4947-4953.

240. R. Tillner-Roth and D. G. Friend, *Journal of Physical and Chemical Reference Data*, 1998, **27**, 45-61.

241. S. Chakrabarty, S. Choudhary, A. Doshi, F.-Q. Liu, R. Mohan, M. P. Ravindra, D. Shah, X. Yang and F. F. Fleming, *Advanced Synthesis & Catalysis*, 2014, **356**, 2135-2196.

242. I. Ugi, *Angewandte Chemie-International Edition*, 1959, **71**, 386-386.

243. M. Lazar and R. J. Angelici, *Isocyanide Binding Modes on Metal Surfaces and in Metal Complexes, in:Modern Surface Organometallic Chemistry*, WileyVCH, Weinham, 2009.

244. V. P. Boyarskiy, N. A. Bokach, K. V. Luzyanin and V. Y. Kukushkin, *Chemical reviews*, 2015, **115**, 2698-2779.

245. B. R. Barnett, C. E. Moore, A. L. Rheingold and J. S. Figueroa, *Chemical Communications*, 2015, **51**, 541-544.

246. R. J. Wehmschulte and P. P. Power, *Polyhedron*, 2000, **19**, 1649-1661.

247. W. J. Zheng, A. Stasch, J. Prust, H. W. Roesky, F. Cimpoesu, M. Noltemeyer and H. G. Schmidt, *Angewandte Chemie-International Edition*, 2001, **40**, 3461-3464.

248. R. C. Weast, M. J. Astle and W. H. Beyer, *CRC Handbook of Chemistry and Physics*, 1984.

249. B. Neumueller, *Zeitschrift Fur Anorganische Und Allgemeine Chemie*, 2007, **633**, 193-204.

250. A. G. M. Barrett, M. R. Crimmin, M. S. Hill, P. B. Hitchcock and P. A. Procopiou, *Dalton Transactions*, 2008, 4474-4481.

251. T. M. A. Al-Shboul, G. Volland, H. Goerls and M. Westerhausen, *Zeitschrift Fur Anorganische Und Allgemeine Chemie*, 2009, **635**, 1568-1572.

252. S. Bontemps, L. Vendier and S. Sabo-Etienne, *Angewandte Chemie-International Edition*, 2012, **51**, 1671-1674.

253. M. H. Holthausen, M. Colussi and D. W. Stephan, *Chemistry-a European Journal*, 2015, **21**, 2193-2199.

254. R. Boese, R. Koster and M. Yalpani, *Zeitschrift Fur Naturforschung Section B-a Journal of Chemical Sciences*, 1994, **49**, 1453-1458.

255. A. J. Bur and L. J. Fetters, *Chemical Reviews*, 1976, **76**, 727-746.

256. J. Shi, Z. Guo, X. Wei, D. Liu and M. F. Lappert, *Synlett*, 2011, 1937-1939.

257. H. Abeliovich, *Biophysical Journal*, 2005, **89**, 76-79.

258. L. A. M. Harris, E. C. Y. Tam, M. P. Coles and J. R. Fulton, *Dalton Transactions*, 2014, **43**, 13803-13814.

259. A. R. Kennedy, R. E. Mulvey, C. L. Raston, B. A. Roberts and R. B. Rowlings, *Chemical Communications*, 1999, 353-354.

260. Z. Otwinowski and W. Minor, *Denzo-Scalepack "Processing of X-ray Diffraction Data Collected in Oscillation Mode"*, Academic Press, New York, 1997.

261. J. Feldman, S. J. McLain, A. Parthasarathy, W. J. Marshall, J. C. Calabrese and S. D. Arthur, *Organometallics*, 1997, **16**, 1514-1516.

262. A. P. Dove, V. C. Gibson, P. Hormnirun, E. L. Marshall, J. A. Segal, A. J. P. White and D. J. Williams, *Dalton Transactions*, 2003, 3088-3097.